frontiers | Research Topics

# Functional response of aquatic plants to environmental stressors

**Edited by**
Jun Xu and Qiang Yang

**Published in**
Frontiers in Plant Science

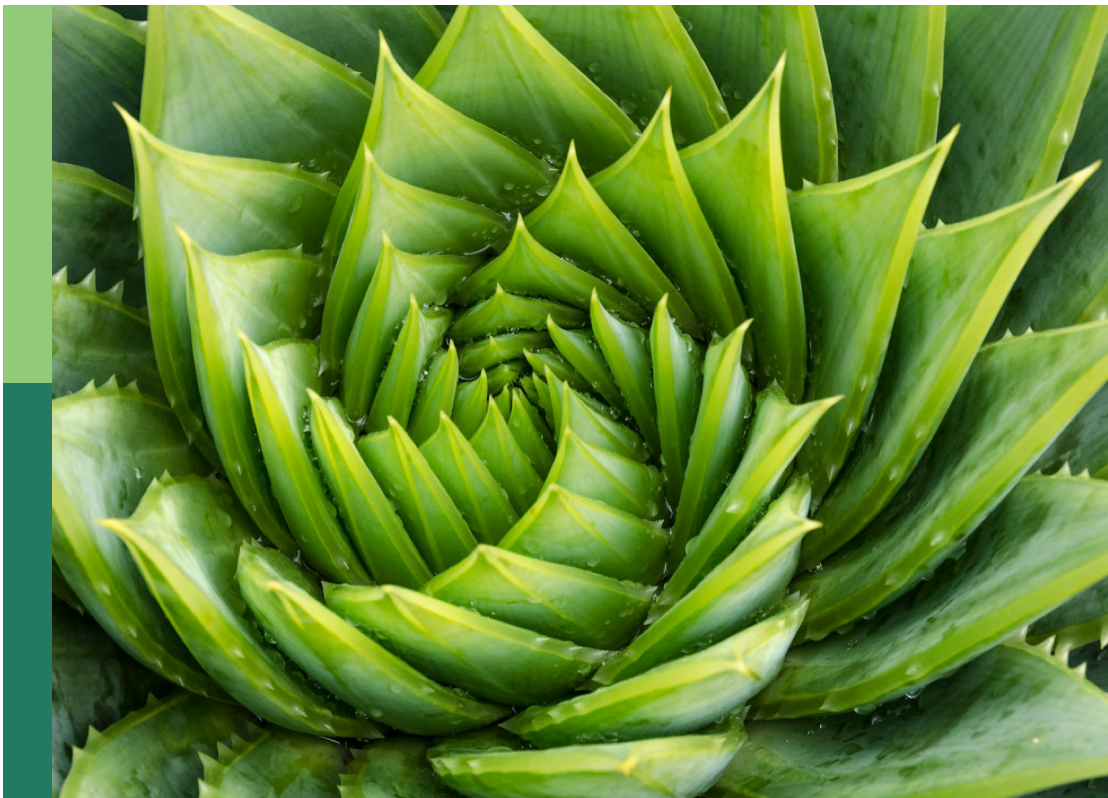

ISSN 1664-8714
ISBN 978-2-8325-6253-6
DOI 10.3389/978-2-8325-6253-6

## About Frontiers

Frontiers is more than just an open access publisher of scholarly articles: it is a pioneering approach to the world of academia, radically improving the way scholarly research is managed. The grand vision of Frontiers is a world where all people have an equal opportunity to seek, share and generate knowledge. Frontiers provides immediate and permanent online open access to all its publications, but this alone is not enough to realize our grand goals.

## Frontiers journal series

The Frontiers journal series is a multi-tier and interdisciplinary set of open-access, online journals, promising a paradigm shift from the current review, selection and dissemination processes in academic publishing. All Frontiers journals are driven by researchers for researchers; therefore, they constitute a service to the scholarly community. At the same time, the *Frontiers journal series* operates on a revolutionary invention, the tiered publishing system, initially addressing specific communities of scholars, and gradually climbing up to broader public understanding, thus serving the interests of the lay society, too.

## Dedication to quality

Each Frontiers article is a landmark of the highest quality, thanks to genuinely collaborative interactions between authors and review editors, who include some of the world's best academicians. Research must be certified by peers before entering a stream of knowledge that may eventually reach the public - and shape society; therefore, Frontiers only applies the most rigorous and unbiased reviews. Frontiers revolutionizes research publishing by freely delivering the most outstanding research, evaluated with no bias from both the academic and social point of view. By applying the most advanced information technologies, Frontiers is catapulting scholarly publishing into a new generation.

## What are Frontiers Research Topics?

Frontiers Research Topics are very popular trademarks of the *Frontiers journals series*: they are collections of at least ten articles, all centered on a particular subject. With their unique mix of varied contributions from Original Research to Review Articles, Frontiers Research Topics unify the most influential researchers, the latest key findings and historical advances in a hot research area.

Find out more on how to host your own Frontiers Research Topic or contribute to one as an author by contacting the Frontiers editorial office: frontiersin.org/about/contact

# Functional response of aquatic plants to environmental stressors

**Topic editors**

Jun Xu — Institute of Hydrobiology, Chinese Academy of Sciences (CAS), China

Qiang Yang — German Centre for Integrative Biodiversity Research (iDiv), Germany

**Citation**

Xu, J., Yang, Q., eds. (2025). *Functional response of aquatic plants to environmental stressors*. Lausanne: Frontiers Media SA. doi: 10.3389/978-2-8325-6253-6

# Table of contents

frontiers | Frontiers in Plant Science

TYPE Original Research
PUBLISHED 28 February 2024
DOI 10.3389/fpls.2024.1367773



OPEN ACCESS

EDITED BY
Qiang Yang,
German Centre for Integrative Biodiversity Research (iDiv), Germany

REVIEWED BY
Yun Li,
Chinese Academy of Sciences (CAS), China
Jing Chen,
Wuhan Polytechnic University, China

*CORRESPONDENCE
Huan Wang
wanghuan@hainanu.edu.cn

RECEIVED 09 January 2024
ACCEPTED 14 February 2024
PUBLISHED 28 February 2024

CITATION
Niu X, Ren W, Xu C, Wang R, Zhang J and Wang H (2024) Taxonomic and functional β-diversity patterns reveal stochastic assembly rules in microbial communities of seagrass beds. *Front. Plant Sci.* 15:1367773. doi: 10.3389/fpls.2024.1367773



# Taxonomic and functional β-diversity patterns reveal stochastic assembly rules in microbial communities of seagrass beds

Xiaofeng Niu[1,2], Wenjing Ren[1], Congjun Xu[2], Ruilong Wang[2], Jingwei Zhang[2] and Huan Wang[1,2*]

[1]School of Marine Biology and Fisheries, State Key Laboratory of Marine Resource Utilization in South China Sea, Hainan University, Haikou, Hainan, China, [2]Institute of Hydrobiology, Chinese Academy of Sciences, Wuhan, Hubei, China

Microorganisms are important members of seagrass bed ecosystems and play a crucial role in maintaining the health of seagrasses and the ecological functions of the ecosystem. In this study, we systematically quantified the assembly processes of microbial communities in fragmented seagrass beds and examined their correlation with environmental factors. Concurrently, we explored the relative contributions of species replacement and richness differences to the taxonomic and functional β-diversity of microbial communities, investigated the potential interrelation between these components, and assessed the explanatory power of environmental factors. The results suggest that stochastic processes dominate community assembly. Taxonomic β-diversity differences are governed by species replacement, while for functional β-diversity, the contribution of richness differences slightly outweighs that of replacement processes. A weak but significant correlation ($p < 0.05$) exists between the two components of β-diversity in taxonomy and functionality, with almost no observed significant correlation with environmental factors. This implies significant differences in taxonomy, but functional convergence and redundancy within microbial communities. Environmental factors are insufficient to explain the β-diversity differences. In conclusion, the assembly of microbial communities in fragmented seagrass beds is governed by stochastic processes. The patterns of taxonomic and functional β-diversity provide new insights and evidence for a better understanding of these stochastic assembly rules. This has important implications for the conservation and management of fragmented seagrass beds.

KEYWORDS

**stochastic assembly, β-diversity, replacement, attached microbial communities, seagrass bed, habitat fragmentation**

# 1 Introduction

Assembly mechanisms are closely linked to changes in community structure, diversity, and the ecological functions they support (Fukami, 2015). This phenomenon has been extensively studied in various ecosystems, such as soil microbes (Wang et al., 2022; Cao et al., 2023), bacterioplankton (Dai et al., 2017), intertidal communities (Loke and Chisholm, 2023), and plants (Peter and Harrington, 2018; Tanunchai et al., 2023). Assembly processes are influenced by various environmental factors, with community turnover cycles limiting exploration. Microorganisms, which are often the most abundant group within systems, play a crucial role in material and energy cycling (Tarquinio et al., 2019; Lemay et al., 2021; Nguyen et al., 2022). Due to their short life cycles, rapid community turnover, and sensitivity to the environment, they are excellent subjects for investigating community assemblage (Vogel et al., 2021a, Vogel et al., 2021b). Seagrass bed ecosystems are known for their highly diverse habitats and host abundant microbial communities, providing habitats for various marine organisms and numerous ecosystem services (Yarnall et al., 2022; Han et al., 2023). These characteristics make seagrass beds an ideal environment for studying microbial community assembly mechanisms (Santos et al., 2016; Du et al., 2020). However, due to factors like climate change, pollution influx, and commercial fishing, seagrass beds in China are rapidly declining (Santos et al., 2016; Xu et al., 2022), resulting in significant losses of ecosystem services they provide (Xiao et al., 2020; Li et al., 2022). Despite ongoing attention and research on related issues, our comprehension of microbial community assembly in fragmented seagrass beds remains limited (Du et al., 2020; Hu et al., 2021), constraining our ability to develop applications for seagrass bed conservation and restoration.

The widely embraced null model method, which quantifies community assembly using beta-mean nearest taxon distance (β-NTI) based on phylogenetic distance and species abundance (Stegen et al., 2012), is designed to elucidate spatial alterations in phylogenetic β-diversity (Zhou and Ning, 2017). Assembly processes, which encompass deterministic and stochastic components, provide insights into variations in community structure composition and diversity dynamics (Prosser et al., 2007). Currently, the latter has garnered significant attention and research focus in seagrass habitats (Crump et al., 2018; Liu et al., 2022; Kardish and Stachowicz, 2023). However, investigations into community assembly, particularly concerning microbial communities, remain relatively limited (Leibold et al., 2017; Zhou and Ning, 2017; Fahrig, 2019). Understanding changes in microbial communities is crucial for seagrass growth (Milbrandt et al., 2008), health (Vandenkoornhuyse et al., 2015), and the ecological functions they provide (Liu et al., 2017; Zhang et al., 2023). Additionally, related research indicates that microbial communities are seldom uniformly distributed in the environment and their spatial variation is primarily dependent on diffusion (Vincent et al., 2021). However, it is currently unknown how microbial function varies as a result.

β-diversity refers to the variations in species composition between different communities, delineated by the processes of species replacement and richness differences. Methods for partitioning β-diversity aim to discern the roles of these processes in total β-diversity, investigating their collective impact on species distribution patterns across diverse spatiotemporal dimensions (Baselga, 2010; Podani and Schmera, 2011). Both taxonomic and functional β-diversity can be quantified between communities, offering valuable insights into the rules governing micro-community assembly (Luo et al., 2023). However, analysis of taxonomic data is inherently limited as it does not provide information about the ecological roles of species (McGill et al., 2006). The use of functional data aids in obtaining a more nuanced comprehension of biodiversity patterns and processes (Swenson et al., 2012; Villéger et al., 2012), which is a well-established application in related research (Swenson et al., 2011; Cardoso et al., 2014).

Since the introduction of β-diversity patterns (Williams, 1996; Lennon et al., 2001), the diversity patterns of plant and animal species have been extensively studied, resulting in various hypotheses (Shen et al., 2020). More recently, attention has also been given to microbial communities, particularly in soils (Li et al., 2020), with fewer investigations in aquatic environments (Sun et al., 2024). However, there is still a lack of understanding regarding fragmented seagrass bed habitats. These patches may resemble individual islands, but their dynamics are significantly influenced by the ebb and flow of seawater. Therefore, classical island ecology theories, such as the area-diversity theory, may not be directly applicable to seagrass bed patches (Chisholm et al., 2016). Additionally, some studies suggest that ecological and evolutionary processes, rather than island biogeography theories, primarily govern species assembly on islands (HilleRisLambers et al., 2012; Mittelbach and Schemske, 2015). Research on microbial communities in seawater indicates that species replacement significantly contributes to β-diversity patterns (Lyu et al., 2023).

This work randomly selected seagrass patches of varying sizes, inculding *Enhalus acoroides* and *Thalassia hemprichi*. Microorganisms attached to the leaves and those present in the surrounding seawater, were systematically sampled. The study analyzed the patterns of β-diversity, considering both taxonomic and functional aspects, and used null models to investigate the mechanisms of microbial community assembly in fragmented seagrass beds. The hypotheses are as follows: (1) The phylogenetic relationships of metapopulation provide a more comprehensive background for community assembly within fragmented seagrass bed habitats. Stochastic processes predominantly shape the constitution of local species pools, thereby influencing on community assembly. (2) Replacement processes are the primary driver of β-diversity differences in microbial communities. (3) Microbial functions play a significant role in community assembly through mechanisms that involve environmental adaptation and niche differentiation. Despite taxonomic differences, functional convergence suggests functional redundancy.

# 2 Materials and methods

## 2.1 Sampling

Microbial samples were collected in July 2022 from a fragmented seagrass bed area located between Nanhai Village and

Baozhi Village (19.4741°N – 19.4784°N, 110.8096°E – 110.8192°E) in Wenchang City, within the South China Sea. A total of 43 seagrass patches were selected, with 27 patches dominated by *Enhalus acoroides*, 13 patches dominated by *Thalassia hemprichii*, and 3 patches co-dominated by both seagrasses. Each patch had designated sampling points at the center and the edge, where microbial samples were collected from seagrass leaf and the surrounding seawater (Figure 1A). Specifically, microbial samples from the seawater and seagrass leaves were collected at the center and edge of *E. acoroides* patches (including patches with both seagrasses). For *T. hemprichii* patches, also including 3 patches with both seagrasses, microbial samples were collected from seagrass leaves at the center and edge. In total, we obtained 60 seawater microbial samples, 60 microbial samples attached to *E.*

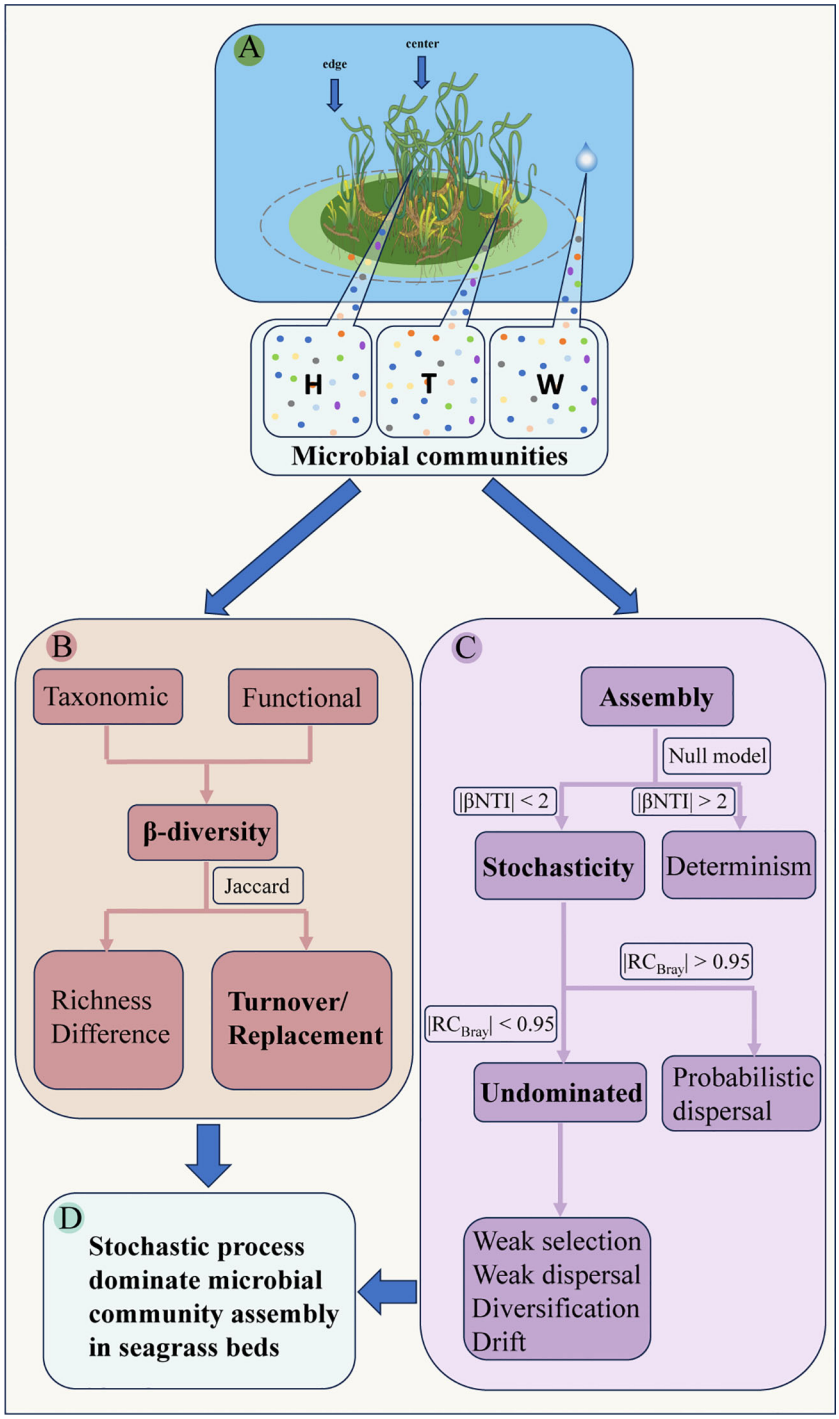


FIGURE 1
Schematic diagram of microbial community assembly and β-diversity patterns in seagrass beds. (**A**, conceptual diagram of sampling; **B**, anaylsis of β-diversity; **C**, anaylsis of assembly process; **D**, the main conclusion; W, surrounding seawater; H, *E. acoroides*; T, *T. hemprichii*).

*acoroides*, and 32 microbial samples attached to *T. hemprichii*, with half at the center and half at the edge of patches. Environmental variables, such as total nitrogen (TN), total phosphorus (TP), and phosphate ($PO_4^{3-}$), as well as patch characteristics, such as seagrass biomass, patch area, and isolation, were measured. Both environmental variables and patch characteristics are classified as environmental factors.

Microbial samples were filtered onto 0.22 μm diameter filter membranes, with seawater initially filtered through a 5 μm before further filtration to 0.22 μm, with a volume of 1 L. Microorganisms from seagrass leaves were gently brushed into distilled water and subsequently filtered onto the filter membranes. The membranes were stored at -80°C until genomic DNA extraction. Another 1 L seawater sample was collected and transported promptly to the laboratory for measuring TN, TP, and $PO_4^{3-}$ concentrations, using spectrophotometer and molybdenum blue methods (Murphy and Riley, 1962). Seagrass biomass, including both aboveground and belowground parts, was weighted at wet and dry conditions. Patch morphological assessments and patch areas measurements were conducted using unmanned aerial vehicles (DJI Mini 4 Pro) and GPS markers.

## 2.2 DNA sequencing

Microbial DNA was extracted from the filter membranes using a Thermo genomic DNA extraction kit. A biological company was contracted for high-throughput sequencing services. The OD260/280 values of the DNA samples were within the range of 1.8 to 2.0. The concentration, determined using a Nanodrop 2000 spectrophotometer, exceeded 50 μg/μL, with a total amount surpassing 2 μg. The DNA samples mentioned above were diluted to 1 ng/μL with sterile water and used as a template for PCR amplification of the 16S rRNA target gene. High-fidelity enzymes and primers with barcode tags were used for the amplification. After amplification, PCR products of equal volumes were mixed based on their concentration, and 2% agarose gel electrophoresis was conducted for detection. Subsequently, the target bands were purified using gel extraction kits from QIAGEN. Finally, the raw sequencing data was obtained though sequencing with the Hiseq2500 platform and library preparation using Illumina kits.

The processes of assembly, quality control, and filtering are necessary to convert data into valid data. Subsequently, the Uparse software (Edgar, 2013) was used with a sequence similarity threshold of 97% (Schloss and Handelsman, 2005) to obtain operational taxonomic units (OTUs). After taxonomic annotation based on representative sequences and normalization of OTUs abundance information (Green et al., 2017) based on the minimum sequence count, a total of 4320 OTUs were obtained from seawater, 6739 from *E. acoroides*, and 3157 from *T. hemprichii*, respectively. The taxa, classified at the Family level by OTUs, were used for data analysis in this study. All sequences utilized in this study are publicly accessible at the NCBI Sequence Read Archive (http://www.ncbi.nlm.nih.gov/Traces/sra) under accession PRJNA1048314.

## 2.3 Analysis of microbial community assembly

The microbial community assembly was quantified using a well-accepted null model (Chase et al., 2011) that evaluates the deterministic and stochastic processes based on the abundance of microbial taxonomic groups and their phylogenetic evolutionary distances. This analysis involved 999 randomizations. The phylogenetic relatedness of taxa within the community was evaluated using nearest taxon index (NTI) and its calculation was performed using the "picante" package (Webb et al., 2008). A homogeneous assembly is indicated by NTI values >2 or mean NTI > 0 (at the regional level), while heterogeneous assembly is suggested by NTI values < -2 or mean NTI < 0 (at the regional level) (Kembel, 2009; Stegen et al., 2013).

The β-NTI (Webb et al., 2008; Kembel et al., 2011) and $RC_{Bray}$ (Stegen et al., 2013) values were used to quantify deterministic and stochastic processes. These values were calculated using the "pNST" function in the "NST" package. Assembly of community is considered deterministic if |β-NTI| > 2, while stochastic processes dominate assembly if |β-NTI| < 2 (Kembel et al., 2011). The $RC_{Bray}$ value provides a more precise understanding of stochastic processes. If $|RC_{Bray}|$ is greater than 0.95, it is likely that community assembly is dominated by probabilistic dispersal. On the other hand, if $|RC_{Bray}|$ is less than 0.95, community assembly can be attributed to undominated processes such as weak selection, weak dispersal, diversification, and drift (Stegen et al., 2015) (Figure 1C). Stegen et al. (2013) developed a statistical framework to describe the ecological processes of community assembly (Figure 1C).

To explore the impact of environmental factors on community assembly, the mantel test based on matrix data was employed to observe the correlation between the two. Euclidean distances for both environmental variables and patch characteristics were calculated using the "dist" function of the "vegan" R package, resulting in matrix data. The significance threshold was set at $p < 0.05$. The patch isolation was calculated based on the coordinates between sampling sites using the "distm" function in the "geosphere" R package.

## 2.4 Analysis of microbial community β-diversity patterns

A β-diversity partitioning approach based on the Jaccard dissimilarity index (Podani and Schmera, 2011; Carvalho et al., 2012; Cardoso et al., 2014) was used to calculate three paired β-diversity metrics for both microbial taxonomy and ecological functional groups (referred to as "functional"): total diversity (Total), turnover or replacement (Repl), and richness differences (RichDiff) (Figure 1B). Ternary plots were utilized to illustrate the varying contributions of different metrics to β-diversity differences. The differences between taxonomic and functional were compared for each diversity metric, and their correlation was explored using the mantel test. Additionally, the mantel test was used to indicate the relationship between the β-diversity metrics and environmental factors.

The β-diversity analysis in microbial taxonomy employed the data obtained from the classification of OTUs at the Family level, which yielded 416 taxa in seawater, 464 taxa in *E. acoroides*, and 364 taxa in *T. hemprichii*. Ecological function groups of microbial communities in seagrass beds were obtained by comparing OTUs classification tables with the functional annotation of prokaryotic taxa (FAPROTAX) (http://www.zoology.ubc.ca/louca/FAPROTAX/) using Python scripts. These functional groups effectively explained and predicted the functions related to the cycling of elements such as carbon (C), nitrogen (N), phosphorus (P), and sulfur (S) (Louca et al., 2016; Kumar et al., 2018; Picazo et al., 2021). A total of 57 ecological functional groups were identified from microbial communities of seawater and *E. acoroides*, and 48 in *T. hemprichii*. These data were used for β-diversity analysis in microbial functionality.

The analyses were conducted using the R software (Team, 2023). The β-diversity calculation used the "adespatial" package, the mantel test used the "vegan" package, and functional annotations were based on the Linux system and accomplished using the "FAPROTAX" package.

# 3 Results

## 3.1 Stochasticity, undominated process specifically, determines microbial community assembly

The average NTI values of microbial communities in both seagrass species are higher than those in the surrounding seawater, and both are greater than zero (Supplementary Figure S1). This suggests a homogeneous assembly of communities in seagrass beds and a closer phylogenetic relationship in the microbial communities attached to seagrasses. The assembly of microbial communities in seagrass beds is primarily governed by stochastic processes, accounting for over 75%, as evidenced by β-NTI values (Supplementary Figure S2; Figure 2A). The contribution of deterministic processes in seawater and *T. hemprichii* patches is higher at the edge than at the center, while the opposite is observed in *E. acoroides* patches (Figure 2A). Further identification revealed that determinism is primarily attributed to heterogeneous selection, whereas stochasticity is mainly attributed to undominated processes, including weak selection, weak dispersal, diversification, and drift (Figure 2B).

Mantel test results (Supplementary Table S1) indicate a significant correlation between the assembly processes of microbial communities (β-NTI) at the centers ($p < 0.05$) of *E. acoroides* patches with seagrass biomass and a partially significant correlation ($p < 0.08$) at the edges. At the centers of *T. hemprichii* patches, community assembly is partially correlated with TN and isolation, while at the edges, it is significantly correlated with $PO_4^{3-}$ (Supplementary Table S1). We analyzed whether there were patterns of variation in dominant taxa, defined as taxa with abundances exceeding 1% across all sampling sites, within the community in fragmented seagrass bed patches (Supplementary Figure S3). The results showed no discernible patterns, suggesting that dominant taxa do not dictate the assembly of microbial communities in fragmented seagrass beds.

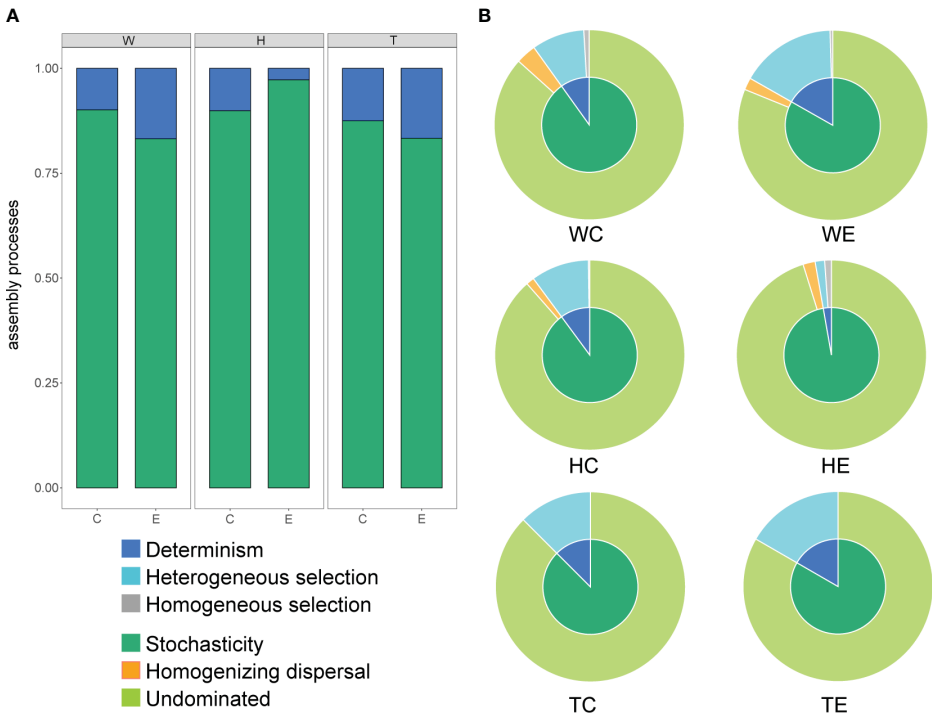


FIGURE 2
The proportion of different assembly processes of microbial communities in seagrass beds (**A**, the proportion of deterministic and stochastic processes; **B**, the proportion of components of deterministic and stochastic processes; W, surrounding seawater; H, *E. acoroides*; T, *T. hemprichii*; C, center of the patch; E, edge of the patch).

## 3.2 Replacement is responsible for the β-diversity difference of microbial communities

The analysis of β-diversity partition indicates that the differences in microbial community composition are primarily driven by species replacement, which contributes significantly more to β-diversity than richness differences (Figure 3; Table 1). Furthermore, no significant differences were observed between seawater and the two seagrass species, nor between the center and edge of patches. In seawater microbial communities, species replacement processes accounted for an average of 73.96%, while richness differences processes accounted for 26.04% (Table 1). In the microbial communities attached to *E. acoroides*, species replacement processes were 73.42% and richness differences processes were 26.58%. For the microbial communities attached to *T. hemprichii*, species replacement processes accounted for 71.65% and richness differences processes accounted for 28.35% (Table 1). The mantel test revealed that the species replacement processes of most communities did not exhibit significant correlation with environmental factors (Supplementary Table S2). Specifically, the replacement process was significantly and positively correlated with patch area, isolation, and $PO_4^{3-}$ in the central community of *E. acoroides* patches. TP and TN were significantly and positively correlated with the replacement process at the edge of *T. hemprichii* patches (Supplementary Table S2).

Among the top 15 most abundant ecological function groups, the majority are associated with the C cycle (Supplementary Figure S4). However, their relative abundance varies. Chemoheterotrophy and aerobic_chemoheterotrophy are most abundant in the microbial communities of seawater and *T. hemprichii*, whereas the opposite is true for *E. acoroides* (Supplementary Figure S4). In contrast to differences in community composition, microbial functional differences in seawater are mainly contributed by replacement processes, whereas in seagrass richness differences play a predominant role (Figure 4; Table 1). Specifically (Table 1), in seawater microbial communities, replacement processes contribute an average of 54.27%, while richness difference processes contribute 45.73%. For the communities attached to *E. acoroides*, replacement processes contribute an average of 43.47% and richness differences processes contribute 56.53%. In the microbial communities attached to *T. hemprichii*, replacement processes were 37%, and richness differences processes contributed 63%. Replacement processes of most communities were not significantly correlated with environmental factors, except for a significant positive correlation with $PO_4^{3-}$ and patch isolation in seawater at the edge of patches (Supplementary Table S3). There was no significant correlation between all richness difference processes and environmental factors (Supplementary Table S4).

A comparison was conducted between taxonomy and functionality for the three components of β-diversity: total β-diversity, replacement, and richness differences. The results indicate that both total β-diversity and replacement exhibit higher values in taxonomy than in functionality, while richness differences are relatively similar between the two (Figure 5). Mantel analyses were performed to examine the relationship between taxonomic

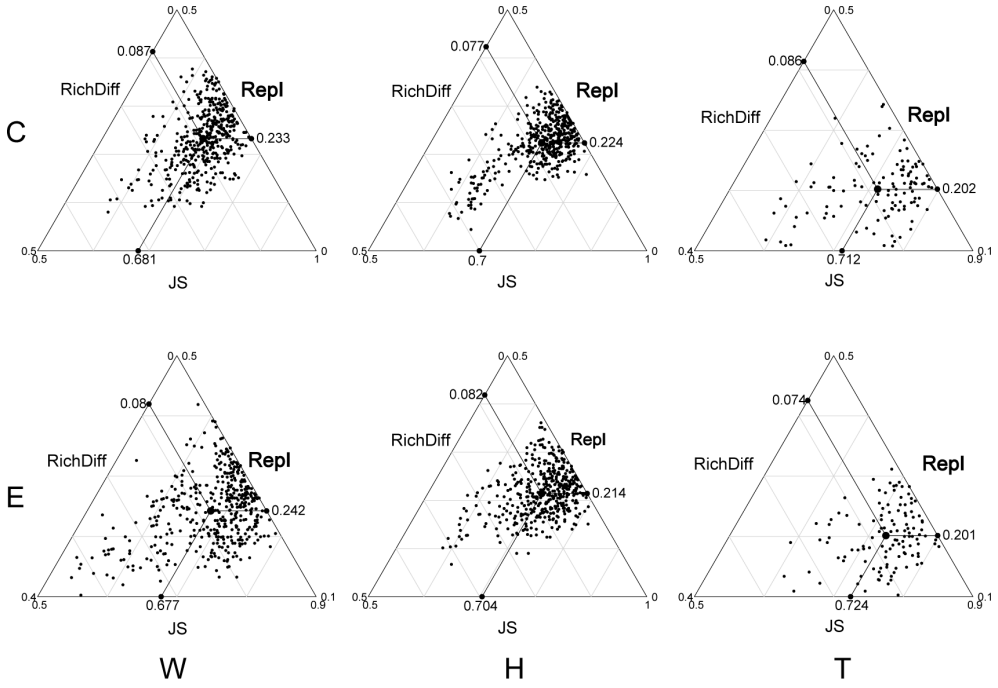


FIGURE 3
Triangular plots of taxonomic β-diversity comparisons (using Jaccard dissimilarity index) in seagrass beds among all sites (Its position is determined by a triplet of values from the JS (Jaccard Similarity), Repl (replacement) and RichDiff (richness difference) matrices. The mean values of JS, Repl and RichDiff are shown. Each point represents a pair of sites with 435 pairs sites in the W and H, 120 pairs sites in the T. W, surrounding seawater; H, *E. acoroides*; T, *T. hemprichii*; C, center of the patch; E, edge of the patch.).

TABLE 1 The contribution of replacement and richness differences to β-diversity differences (W, surrounding seawater; H, *E. acoroides*; T, *T. hemprichii*; C, center of the patch; E, edge of the patch).

| | | W-C | W-E | H-C | H-E | T-C | T-E |
|---|---|---|---|---|---|---|---|
| Taxonomy | Replacement | 0.7281 | 0.7511 | 0.7446 | 0.7238 | 0.7025 | 0.7304 |
| | Richness difference | 0.2719 | 0.2489 | 0.2554 | 0.2762 | 0.2975 | 0.2696 |
| Function | Replacement | 0.5742 | 0.5111 | 0.4108 | 0.4585 | 0.4269 | 0.3121 |
| | Richness difference | 0.4258 | 0.4889 | 0.5892 | 0.5415 | 0.5731 | 0.6879 |

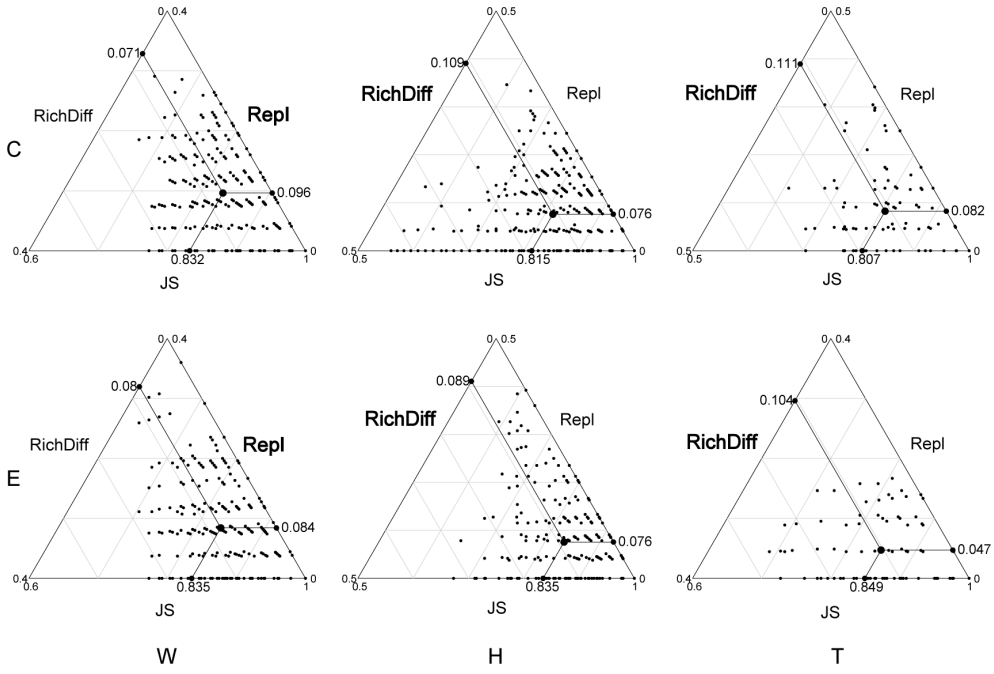


FIGURE 4
Triangular plots of functional β-diversity comparisons (using Jaccard dissimilarity index) for microbes in seagrass beds among all sites. (Its position is determined by a triplet of values from the JS (Jaccard Similarity), Repl (replacement) and RichDiff (richness difference) matrices. The mean values of JS, Repl and RichDiff are shown. Each point represents a pair of sites with 435 pairs sites in the W and H, 120 pairs sites in the T. W, surrounding seawater; H, *E. acoroides*; T, *T. hemprichii*; C, center of the patch; E, edge of the patch.).

and functional β-diversity. Significant positive correlations were found for total β-diversity in seawater, including both the center and edge. Only at the edge of *E. acoroides* patches, total β-diversity exhibited a significant positive correlation. At the center and edge of *T. hemprichii* patches, significant positive correlations of total β-diversity and richness difference were observed. However, replacement processes existed a partially significant positive correlation at the center (Table 2).

# 4 Discussion

While it is widely recognized that both deterministic and stochastic processes impact community assembly (Ofiţeru et al., 2010; Chase and Myers, 2011; Zhou and Ning, 2017), there is an ongoing debate regarding their relative importance in governing community variations (Zhou et al., 2013; Vellend et al., 2014). Notably, the significance of stochastic processes has historically been understated in this discourse (Zhou and Ning, 2017; Li and Gao, 2023). The study highlights the significant role of stochastic processes in microbial community assembly in fragmented seagrass beds, in contrast to traditional island ecology perspectives. Additionally, the study reveals differences in the patterns of functional and taxonomic β-diversity, including the relative contributions of replacement and richness difference processes and their responses to environmental factors. This aids in a better understanding and elucidation of these stochastic rules. On the basis of the dominant factor of stochastic assembly, perhaps focusing on community function in future management and restoration is an ingenious perspective.

## 4.1 The stochastic assembly processes in microbial communities

The NTI results reflect the phylogenetic clustering relationships within communities. An average NTI across multiple communities at

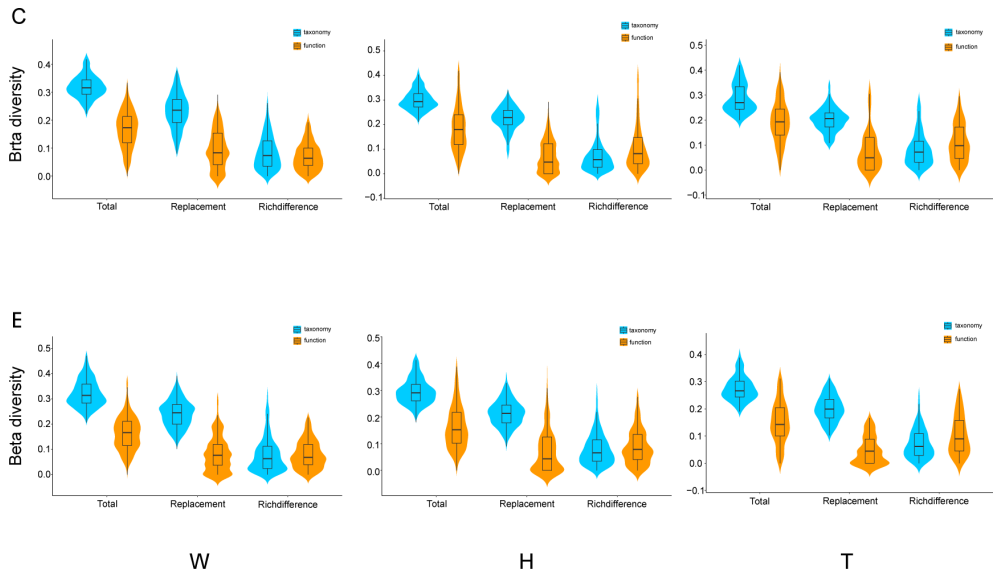


FIGURE 5
Comparisons of β-diversity components (total, replacement and richness difference) for taxonomy and ecological function groups of microorganisms in seagrass beds (W, surrounding seawater; H, *E. acoroides*; T, *T. hemprichii*; C, center of the patch; E, edge of the patch.).

TABLE 2 Mantel test between the β-diversity components (total, replacement and richness difference) and taxonomy, ecological function groups of microorganisms in seagrass beds (Bold numbers indicates significant correlation, $p < 0.05$.

| | W-C | | W-E | | H-C | | H-E | | T-C | | T-E | |
|---|---|---|---|---|---|---|---|---|---|---|---|---|
| | r | *p* | r | *p* | r | *p* | r | *p* | r | *p* | r | *p* |
| Total | 0.3975 | **1e-04** | 0.3654 | **1e-04** | 0.0393 | 0.3594 | 0.2873 | **0.0165** | 0.4033 | **0.0171** | 0.4873 | **0.0053** |
| Replacement | 0.1261 | 0.1319 | 0.0827 | 0.2113 | -0.1672 | 0.9596 | 0.0154 | 0.4349 | 0.1997 | 0.062 | 0.0129 | 0.4781 |
| Richness Difference | -0.0455 | 0.7204 | 0.0423 | 0.2709 | -0.0252 | 0.5471 | 0.0662 | 0.1983 | 0.3285 | **0.0085** | 0.3097 | **0.0183** |

W, surrounding seawater; H, *E. acoroides*; T, *T. hemprichii*; C, center of the patch; E, edge of the patch).

the regional level demonstrates the homogeneous assembly of microbial communities across the region, rather than relying on a single NTI. In other words, the phylogenetic relationships of metapopulation provide background information for the microbial community assembly in seagrass beds. According to Stegen et al. (2013), undominant processes in stochasticity, such as weak selection, weak dispersal, diversification, and drift, are responsible for the assembly of microbial communities. The mantel results indicate a lack of significant correlation between β-NTI and environmental factors, supporting this notion. The findings suggest that community assembly in seagrass bed patches is minimally explained by environmental variables and patch characteristics, which is consistent with previous research on microbes (Ramette and Tiedje, 2007; Zhou et al., 2008; Graham et al., 2016).

Generally, diversification and dispersal are often considered components of stochastic processes, especially in microbial communities (Chase and Myers, 2011), as microbial dispersal is typically passive (Nemergut et al., 2013) and passive dispersal is regarded as random (Vellend et al., 2014). Drift refers to the random changes in the relative abundance of different species within a community over time, driven by inherent stochastic processes such as birth and death (Vellend, 2010; Nemergut et al., 2013). It is undeniably stochastic (Vellend et al., 2014). The challenge lies in the inability to directly measure these stochastic processes in community ecology. Furthermore, in microbial communities, drift is likely associated with functional redundancy and plays a crucial role in shaping community structure (Ofiţeru et al., 2010; Zhou et al., 2013), as the common functional redundancy in microbial communities can induce drift by increasing neutrality (Allison and Martiny, 2008; Delgado-Baquerizo et al., 2016). It is clear that there are dynamic exchanges between microorganisms attached to seagrass and the species pool in the surrounding seawater (Fahimipour et al., 2017). Seagrasses prevent or selectively filter microbial colonization for various reasons. Combining our results, it can be inferred that stochastic processes have a significant impact on the assembly of attached microbial communities by predominantly shaping the formation of local species pools.

## 4.2 Microbial community assembly from a β-diversity patterns perspective

Understanding the contributions of the two components of β-diversity is crucial for comprehending how communities change,

and provides a new perspective on community assembly (Carvalho et al., 2012). From a taxonomic standpoint, differences in microbial community β-diversity are mainly driven by species replacement. From a functional perspective, replacement processes contribute slightly more than richness differences in seawater microbial communities, which is contrary to the observed pattern in communities attached to seagrasses. These findings align with related research on seawater microbial communities (Sun et al., 2024). Furthermore, we observed that the proportion of dominant taxa did not exhibit consistent patterns with increasing or decreasing patch area of seagrass beds. This statement contrasts with the area-diversity theory in island ecology, which suggests that species diversity is proportional to island size (Li et al., 2020). The area-diversity theory is not applicable to fragmented seagrass bed patches; instead, replacement processes dominate the β-diversity differences in microbial communities. Previous studies suggest that species dispersal may cause species turnover among communities (Swenson et al., 2011). Dispersal is common in microbial communities (Wu et al., 2021).

Taxonomically, β-diversity is primarily influenced by replacement processes, while the contribution of richness differences to functional β-diversity slightly surpasses that of replacement. This implies a significant convergence of functional traits among communities (Carvalho et al., 2020), reinforcing the concept of heightened functional redundancy within microbial communities. The taxonomic dissimilarity and functional convergence suggest turnover among microbial taxa with similar functions (Wu et al., 2021). There is a weak yet significant correlation between taxonomic and function-based β-diversity components, indicating that these two facets provide complementary ecological information (Devictor et al., 2010). This pattern has been observed across diverse biological groups, including fish, planktonic plants, and zooplankton, as well as various habitats, encompassing different types of water bodies (Gianuca et al., 2018; Wu et al., 2018; Hill et al., 2019). Furthermore, there is limited correlation between β-diversity components from both taxonomic and functional perspectives and environmental factors, including environmental variables and patch characteristics. These findings suggest that environmental factors play a minimal role in driving replacement processes within microbial communities. The collective findings demonstrate that the β-diversity patterns provide a new perspective and reference for better understanding the stochastic assembly rules of microbial communities in fragmented seagrass beds.

Research indicates a complex and intimate interaction between plants and their associated microorganisms, whether in the rhizosphere microbiome (Gabriel Nuto et al., 2023; Tang et al., 2023) or the phyllosphere microbiome (Lehnen et al., 2016; Ettinger et al., 2017). Seagrasses are no exception, as changes in the structure and diversity of attached microbial communities, along with their responses to the environment, significantly impact the health, growth, and functions of seagrasses (Chen et al., 2022; O'Connor et al., 2022). For instance, alterations in rhizosphere microbial communities play a pivotal role in the successful transplantation of seagrasses (Christiaen et al., 2013). Undoubtedly, the ecosystem services provided by seagrass beds, such as high productivity and a robust carbon sequestration capacity (Fourqurean et al., 2012; Han et al., 2023), predominantly rely on seagrasses. Therefore, delving into community assembly mechanisms is crucial for understanding of the intricate relationship between microbial communities and seagrasses. This knowledge can guide the development of targeted management strategies to protect and restore seagrass bed ecosystems.

## 5 Conclusion

The assembly processes of microbial communities attached to seagrass play a crucial role in the growth and health of seagrasses and, consequently, the stability, diversity, and multifunctionality of seagrass bed ecosystems. We emphasize the dominance of stochastic rules, particularly undominant processes such as weak selection, weak dispersal, diversification, and drift, in the assembly of these communities (Figure 1D). The taxonomic-based differences in β-diversity are driven by replacement processes, whereas in functional β-diversity, the contribution of richness differences slightly surpasses that of replacement processes. Although there are significant taxonomic distinctions among microbial communities in seagrass beds, functional convergence and redundancy are observed. Environmental factors, indicative of deterministic processes, provide minimal explanation for the patterns of β-diversity. In summary, stochastic processes govern the assembly of microbial communities in fragmented seagrass beds. The taxonomic and functional β-diversity patterns provide a new perspective and support for better comprehending these stochastic assembly rules. This study provides foundational evidence for the mechanisms of microbial community assembly in fragmented seagrass beds, offering novel insights for the conservation and management of seagrass beds.

## Data availability statement

The datasets presented in this study can be found in online repositories. The names of the repository/repositories and accession number(s) can be found in the article/Supplementary Material.

## Ethics statement

The manuscript presents research on animals that do not require ethical approval for their study.

## Author contributions

XN: Conceptualization, Formal analysis, Writing – original draft, Visualization. WR: Formal analysis, Methodology, Writing – review & editing. CX: Data curation, Methodology, Writing – review & editing. RW: Data curation, Methodology, Writing – review & editing. JZ: Formal analysis, Methodology, Writing – review & editing. HW: Conceptualization, Data curation, Funding acquisition, Methodology, Project administration, Supervision, Writing – review & editing.

## Funding

The author(s) declare financial support was received for the research, authorship, and/or publication of this article. This research was supported by the National Natural Science Foundation of China (Grant No. 32001151 and 42377469) and Hainan University Start-up Funding for Scientific Research (KYQD (ZR)-23, 086) and Hainan University Start-up Funding for Scientific Research (KYQD (ZR)-23, 087).

## Conflict of interest

The authors declare that the research was conducted in the absence of any commercial or financial relationships that could be construed as a potential conflict of interest.

## Publisher's note



## Supplementary material

The Supplementary Material for this article can be found online at: https://www.frontiersin.org/articles/10.3389/fpls.2024.1367773/full#supplementary-material

## References

Allison, S. D., and Martiny, J. B. H. (2008). Resistance, resilience, and redundancy in microbial communities. *Proc. Natl. Acad. Sci.* 105, 11512–11519. doi: 10.1073/pnas.0801925105

Baselga, A. (2010). Partitioning the turnover and nestedness components of beta diversity. *Global Ecol. Biogeography* 19, 134–143. doi: 10.1111/j.1466-8238.2009.00490.x

Cao, J., Zhang, Y., Dai, G., Cui, K., Wu, X., Qin, F., et al. (2023). The long-acting herbicide mesosulfuron-methyl inhibits soil microbial community assembly mediating nitrogen cycling. *J. Hazard Mater* 443, 130293. doi: 10.1016/j.jhazmat.2022.130293

Cardoso, P., Rigal, F., Carvalho, J. C., Fortelius, M., Borges, P. A. V., Podani, J., et al. (2014). Partitioning taxon, phylogenetic and functional beta diversity into replacement and richness difference components. *J. Biogeography* 41, 749–761. doi: 10.1111/jbi.12239

Carvalho, J. C., Cardoso, P., and Gomes, P. (2012). Determining the relative roles of species replacement and species richness differences in generating beta-diversity patterns. *Global Ecol. Biogeography* 21, 760–771. doi: 10.1111/j.1466-8238.2011.00694.x

Carvalho, J. C., Malumbres-Olarte, J., Arnedo, M. A., Crespo, L. C., Domenech, M., and Cardoso, P. (2020). Taxonomic divergence and functional convergence in Iberian spider forest communities: Insights from beta diversity partitioning. *J. Biogeography* 47, 288–300. doi: 10.1111/jbi.13722

Chase, J. M., Kraft, N. J. B., Smith, K. G., Vellend, M., and Inouye, B. D. (2011). Using null models to disentangle variation in community dissimilarity from variation in α-diversity. *Ecosphere* 2(2):art24. doi: 10.1890/ES10-00117.1

Chase, J. M., and Myers, J. A. (2011). Disentangling the importance of ecological niches from stochastic processes across scales. *Philos. Trans. R Soc. Lond B Biol. Sci.* 366, 2351–2363. doi: 10.1098/rstb.2011.0063

Chen, J., Zang, Y., Yang, Z., Qu, T., Sun, T., Liang, S., et al. (2022). Composition and functional diversity of epiphytic bacterial and fungal communities on marine macrophytes in an intertidal zone. *Front. Microbiol.* 13. doi: 10.3389/fmicb.2022.839465

Chisholm, R. A., Fung, T., Chimalakonda, D., and O'dwyer, J. P. (2016). Maintenance of biodiversity on islands. *Proc. R. Soc. B: Biol. Sci.* 283, 20160102. doi: 10.1098/rspb.2016.0102

Christiaen, B., Mcdonald, A., Cebrian, J., and Ortmann, A. C. (2013). Response of the microbial community to environmental change during seagrass transplantation. *Aquat. Bot.* 109, 31–38. doi: 10.1016/j.aquabot.2013.03.008

Crump, B. C., Wojahn, J. M., Tomas, F., and Mueller, R. S. (2018). Metatranscriptomics and amplicon sequencing reveal mutualisms in seagrass microbiomes. *Front. Microbiol.* 9. doi: 10.3389/fmicb.2018.00388

Dai, W., Zhang, J., Tu, Q., Deng, Y., Qiu, Q., and Xiong, J. (2017). Bacterioplankton assembly and interspecies interaction indicating increasing coastal eutrophication. *Chemosphere* 177, 317–325. doi: 10.1016/j.chemosphere.2017.03.034

Delgado-Baquerizo, M., Giaramida, L., Reich, P. B., Khachane, A. N., Hamonts, K., Edwards, C., et al. (2016). Lack of functional redundancy in the relationship between microbial diversity and ecosystem functioning. *J. Ecol.* 104, 936–946. doi: 10.1111/1365-2745.12585

Devictor, V., Mouillot, D., Meynard, C., Jiguet, F., Thuiller, W., and Mouquet, N. (2010). Spatial mismatch and congruence between taxonomic, phylogenetic and functional diversity: the need for integrative conservation strategies in a changing world. *Ecol. Lett.* 13, 1030–1040. doi: 10.1111/j.1461-0248.2010.01493.x

Du, J., Hu, W., Nagelkerken, I., Sangsawang, L., Loh, K. H., Ooi, J. L.-S., et al. (2020). Seagrass meadows provide multiple benefits to adjacent coral reefs through various microhabitat functions. *Ecosystem Health Sustainability* 6, 1812433. doi: 10.1080/20964129.2020.1812433

Edgar, R. C. (2013). UPARSE: highly accurate OTU sequences from microbial amplicon reads. *Nat. Methods* 10, 996–998. doi: 10.1038/nmeth.2604

Ettinger, C. L., Voerman, S. E., Lang, J. M., Stachowicz, J. J., and Eisen, J. A. (2017). Microbial communities in sediment from Zostera marina patches, but not the Z. marina leaf or root microbiomes, vary in relation to distance from patch edge. *PeerJ* 5, e3246. doi: 10.7717/peerj.3246

Fahimipour, A. K., Kardish, M. R., Lang, J. M., Green, J. L., Eisen, J. A., and Stachowicz, J. J. (2017). Global-scale structure of the eelgrass microbiome. *Appl. Environ. Microbiol.* 83 (12), e03391-16. doi: 10.1128/AEM.03391-16

Fahrig, L. (2019). Habitat fragmentation: A long and tangled tale. *Global Ecol. Biogeography* 28, 33–41. doi: 10.1111/geb.12839

Fourqurean, J. W., Duarte, C. M., Kennedy, H., Marbà, N., Holmer, M., Mateo, M. A., et al. (2012). Seagrass ecosystems as a globally significant carbon stock. *Nat. Geosci.* 5, 505–509. doi: 10.1038/ngeo1477

Fukami, T. (2015). Historical contingency in community assembly: integrating niches, species pools, and priority effects. *Annu. Rev. Ecology Evolution Systematics* 46, 1–23. doi: 10.1146/annurev-ecolsys-110411-160340

Gabriel Nuto, N., Pedro Avelino Maia De, A., Hermano Melo, Q., Arthur Prudncio De Arajo, P., Margareth Da Silva, C., Daniel, G., et al. (2023). Bridging soil biogeochemistry and microbial communities (archaea and bacteria) in tropical seagrass meadows. *Front. Mar. Sci.* 10. doi: 10.3389/fmars.2023.1190497

Gianuca, A. T., Engelen, J., Brans, K. I., Hanashiro, F. T. T., Vanhamel, M., Van Den Berg, E. M., et al. (2018). Taxonomic, functional and phylogenetic metacommunity ecology of cladoceran zooplankton along urbanization gradients. *Ecography* 41, 183–194. doi: 10.1111/ecog.02926

Graham, E. B., Knelman, J. E., Schindlbacher, A., Siciliano, S., Breulmann, M., Yannarell, A., et al. (2016). Microbes as engines of ecosystem function: when does community structure enhance predictions of ecosystem processes? *Front. Microbiol.* 7. doi: 10.3389/fmicb.2016.00214

Green, S. J., Wen, C., Wu, L., Qin, Y., Van Nostrand, J. D., Ning, D., et al. (2017). Evaluation of the reproducibility of amplicon sequencing with Illumina MiSeq platform. *PloS One* 12 (4), e0176716. doi: 10.1371/journal.pone.0176716

Han, Q., Qiu, C., Zeng, W., Chen, S., Zhao, M., Shi, Y., et al. (2023). Sediment carbon sequestration and driving factors in seagrass beds from Hainan island and the Xisha islands. *Processes* 11, 456. doi: 10.3390/pr11020456

Hill, M. J., Heino, J., White, J. C., Ryves, D. B., and Wood, P. J. (2019). Environmental factors are primary determinants of different facets of pond macroinvertebrate alpha and beta diversity in a human-modified landscape. *Biol. Conserv.* 237, 348–357. doi: 10.1016/j.biocon.2019.07.015

HilleRisLambers, J., Adler, P. B., Harpole, W. S., Levine, J. M., and Mayfield, M. M. (2012). Rethinking community assembly through the lens of coexistence theory. *Annu. Rev. Ecology Evolution Systematics* 43, 227–248. doi: 10.1146/annurev-ecolsys-110411-160411

Hu, W., Zhang, D., Chen, B., Liu, X., Ye, X., Jiang, Q., et al. (2021). Mapping the seagrass conservation and restoration priorities: coupling habitat suitability and anthropogenic pressures. *Ecol. Indic.* 129, 107960. doi: 10.1016/j.ecolind.2021.107960

Kardish, M. R., and Stachowicz, J. J. (2023). Local environment drives rapid shifts in composition and phylogenetic clustering of seagrass microbiomes. *Sci. Rep.* 13, 3673. doi: 10.1038/s41598-023-30194-x

Kembel, S. W. (2009). Disentangling niche and neutral influences on community assembly: assessing the performance of community phylogenetic structure tests. *Ecol. Lett.* 12, 949–960. doi: 10.1111/j.1461-0248.2009.01354.x

Kembel, S. W., Eisen, J. A., Pollard, K. S., and Green, J. L. (2011). The phylogenetic diversity of metagenomes. *PloS One* 6, e23214. doi: 10.1371/journal.pone.0023214

Kumar, A., Ng, D. H. P., Wu, Y., and Cao, B. (2018). Microbial community composition and putative biogeochemical functions in the sediment and water of tropical granite quarry lakes. *Microbial Ecol.* 77, 1–11. doi: 10.1007/s00248-018-1204-2

Lehnen, N., Marchant, H. K., Schwedt, A., Milucka, J., Lott, C., Weber, M., et al. (2016). High rates of microbial dinitrogen fixation and sulfate reduction associated with the Mediterranean seagrass Posidonia oceanica. *Systematic Appl. Microbiol.* 39, 476–483. doi: 10.1016/j.syapm.2016.08.004

Leibold, M. A., Chase, J. M., and Ernest, S. K. M. (2017). Community assembly and the functioning of ecosystems: how metacommunity processes alter ecosystems attributes. *Ecology* 98, 909–919. doi: 10.1002/ecy.1697

Lemay, M. A., Chen, M. Y., Mazel, F., Hind, K. R., Starko, S., Keeling, P. J., et al. (2021). Morphological complexity affects the diversity of marine microbiomes. *ISME J.* 15, 1372–1386. doi: 10.1038/s41396-020-00856-z

Lennon, J. J., Koleff, P., Greenwood, J. J. D., and Gaston, K. J. (2001). The geographical structure of British bird distributions: diversity, spatial turnover and scale. *J. Anim. Ecol.* 70, 966–979. doi: 10.1046/j.0021-8790.2001.00563.x

Li, Q., Jin, R., Ye, Z., Gu, J., Dan, L., He, J., et al. (2022). Mapping seagrass meadows in coastal. *Geocarto Int.* 37, 12602–12617. doi: 10.1080/10106049.2022.2070672

Li, S.-P., Wang, P., Chen, Y., Wilson, M. C., Yang, X., Ma, C., et al. (2020). Island biogeography of soil bacteria and fungi: similar patterns, but different mechanisms. *ISME J.* 14, 1886–1896. doi: 10.1038/s41396-020-0657-8

Li, T. Q., and Gao, J. Y. (2023). Attribution of dispersal limitation can better explain the assembly patterns of plant microbiota. *Front. Plant Sci.* 14. doi: 10.3389/fpls.2023.1168760

Liu, S., Jiang, Z., Zhang, J., Wu, Y., Huang, X., and Macreadie, P. I. (2017). Sediment microbes mediate the impact of nutrient loading on blue carbon sequestration by mixed seagrass meadows. *Sci. Total Environ.* 599-600, 1479–1484. doi: 10.1016/j.scitotenv.2017.05.129

Liu, S., Trevathan-Tackett, S. M., Jiang, Z., Cui, L., Wu, Y., Zhang, X., et al. (2022). Nutrient loading decreases blue carbon by mediating fungi activities within seagrass meadows. *Environ. Res.* 212, 113280. doi: 10.1016/j.envres.2022.113280

Loke, L. H. L., and Chisholm, R. A. (2023). Unveiling the transition from niche to dispersal assembly in ecology. *Nature* 618, 537–542. doi: 10.1038/s41586-023-06161-x

Louca, S., Parfrey, L. W., and Doebeli, M. (2016). Decoupling function and taxonomy in the global ocean microbiome. *Science* 353, 1272–1277. doi: 10.1126/science.aaf4507

Luo, W., Wang, Y., Cahill, J. F., Luan, F., Zhong, Y., Li, Y., et al. (2023). Root-centric β diversity reveals functional homogeneity while phylogenetic heterogeneity in a subtropical forest. *Ecology* 105 (1), e4189. doi: 10.1002/ecy.4189

Lyu, Y., Zhang, J., Chen, Y., Li, Q., Ke, Z., Zhang, S., et al. (2023). Distinct diversity patterns and assembly mechanisms of prokaryotic microbial sub-community in the water column of deep-sea cold seeps. *J. Environ. Manage.* 348, 119240. doi: 10.1016/j.jenvman.2023.119240

McGill, B. J., Enquist, B. J., Weiher, E., and Westoby, M. (2006). Rebuilding community ecology from functional traits. *Trends Ecol. Evol.* 21, 178–185. doi: 10.1016/j.tree.2006.02.002

Milbrandt, E. C., Greenawalt-Boswell, J., and Sokoloff, P. D. (2008). Short-term indicators of seagrass transplant stress in response to sediment bacterial community disruption. *Botanica Marina* 51, 103–111. doi: 10.1515/BOT.2008.020

Mittelbach, G. G., and Schemske, D. W. (2015). Ecological and evolutionary perspectives on community assembly. *Trends Ecol. Evol.* 30, 241–247. doi: 10.1016/j.tree.2015.02.008

Murphy, J., and Riley, J. P. (1962). A modified single solution method for the determination of phosphate in natural waters. *Anal. Chim. Acta* 27, 678–681. doi: 10.1016/S0003-2670(00)88444-5

Nemergut, D. R., Schmidt, S. K., Fukami, T., O'neill, S. P., Bilinski, T. M., Stanish, L. F., et al. (2013). Patterns and processes of microbial community assembly. *Microbiol. Mol. Biol. Rev.* 77, 342–356. doi: 10.1128/MMBR.00051-12

Nguyen, X. V., Phan, T. T. H., Cao, V. L., Nhat, N. T. N., Nguyen, T. H., Nguyen, X. T., et al. (2022). Current advances in seagrass research: a review from Viet Nam. *Front. Plant Sci.* 13. doi: 10.3389/fpls.2022.991865

O'Connor, M., Griffiths, G., Smith, R., Hessing-Lewis, M., Davis, K., Forbes, C., et al. (2022). A reciprocal transplant experiment sheds new light on a classic marine seagrass-algal symbiosis and suggests influence of epiphytic symbiont on seagrass microbiota. *Aquat. Bot.* 179, 103511. doi: 10.1016/j.aquabot.2022.103511

Ofiţeru, I. D., Lunn, M., Curtis, T. P., Wells, G. F., Criddle, C. S., Francis, C. A., et al. (2010). Combined niche and neutral effects in a microbial wastewater treatment community. *Proc. Natl. Acad. Sci.* 107, 15345–15350. doi: 10.1073/pnas.1000604107

Peter, D. H., and Harrington, T. B. (2018). Effects of forest harvesting, logging debris, and herbicides on the composition, diversity and assembly of a western Washington, USA plant community. *For. Ecol. Manage.* 417, 18–30. doi: 10.1016/j.foreco.2018.01.045

Picazo, A., Villaescusa, J. A., Rochera, C., Miralles-Lorenzo, J., Quesada, A., and Camacho, A. (2021). Functional metabolic diversity of bacterioplankton in maritime Antarctic lakes. *Microorganisms* 9 (10), 2077. doi: 10.3390/microorganisms9102077

Podani, J., and Schmera, D. (2011). A new conceptual and methodological framework for exploring and explaining pattern in presence – absence data. *Oikos* 120, 1625–1638. doi: 10.1111/j.1600-0706.2011.19451.x

Prosser, J. I., Bohannan, B. J. M., Curtis, T. P., Ellis, R. J., Firestone, M. K., Freckleton, R. P., et al. (2007). The role of ecological theory in microbial ecology. *Nat. Rev. Microbiol.* 5, 384–392. doi: 10.1038/nrmicro1643

Ramette, A., and Tiedje, J. M. (2007). Multiscale responses of microbial life to spatial distance and environmental heterogeneity in a patchy ecosystem. *Proc. Natl. Acad. Sci.* 104, 2761–2766. doi: 10.1073/pnas.0610671104

Santos, R. O., Lirman, D., and Pittman, S. J. (2016). Long-term spatial dynamics in vegetated seascapes: fragmentation and habitat loss in a human-impacted subtropical lagoon. *Mar. Ecol.* 37, 200–214. doi: 10.1111/maec.12259

Schloss, P. D., and Handelsman, J. (2005). ). Introducing DOTUR, a computer program for defining operational taxonomic units and estimating species richness. *Appl. Environ. Microbiol.* 71, 1501–1506. doi: 10.1128/AEM.71.3.1501-1506.2005

Shen, C., Gunina, A., Luo, Y., Wang, J., He, J. Z., Kuzyakov, Y., et al. (2020). Contrasting patterns and drivers of soil bacterial and fungal diversity across a mountain gradient. *Environ. Microbiol.* 22, 3287–3301. doi: 10.1111/1462-2920.15090

Stegen, J. C., Lin, X., Fredrickson, J. K., Chen, X., Kennedy, D. W., Murray, C. J., et al. (2013). Quantifying community assembly processes and identifying features that impose them. *ISME J.* 7, 2069–2079. doi: 10.1038/ismej.2013.93

Stegen, J. C., Lin, X., Fredrickson, J. K., and Konopka, A. E. (2015). Estimating and mapping ecological processes influencing microbial community assembly. *Front. Microbiol.* 6, 370. doi: 10.3389/fmicb.2015.00370

Stegen, J. C., Lin, X., Konopka, A. E., and Fredrickson, J. K. (2012). Stochastic and deterministic assembly processes in subsurface microbial communities. *ISME J.* 6, 1653–1664. doi: 10.1038/ismej.2012.22

Sun, Y., Li, H., Zhang, J., Wang, H., Cui, X., Gao, X., et al. (2024). Assembly mechanisms of microbial communities in plastisphere related to species taxonomic types and habitat niches. *Mar. Pollut. Bull.* 198, 115894. doi: 10.1016/j.marpolbul.2023.115894

Swenson, N. G., Anglada-Cordero, P., and Barone, J. A. (2011). Deterministic tropical tree community turnover: evidence from patterns of functional beta diversity along an elevational gradient. *Proc. R. Soc. B: Biol. Sci.* 278, 877–884. doi: 10.1098/rspb.2010.1369

Swenson, N. G., Stegen, J. C., Davies, S. J., Erickson, D. L., Forero-Montaña, J., Hurlbert, A. H., et al. (2012). Temporal turnover in the composition of tropical tree communities: functional determinism and phylogenetic stochasticity. *Ecology* 93, 490–499. doi: 10.1890/11-1180.1

Tang, L. Y., Zhan, L., Han, Y. A., Wang, Z. R., Dong, L., and Zhang, Z. (2023). Microbial community assembly and functional profiles along the soil-oot continuum of salt-tolerant *Suaeda glauca* and *Suaeda salsa*. *Front. Plant Sci.* 14. doi: 10.3389/fpls.2023.1301117

Tanunchai, B., Ji, L., Schroeter, S. A., Wahdan, S. F. M., Thongsuk, K., Hilke, I., et al. (2023). Tree mycorrhizal type regulates leaf and needle microbial communities, affects microbial assembly and co-occurrence network patterns, and influences litter decomposition rates in temperate forest. *Front. Plant Sci.* 14. doi: 10.3389/fpls.2023.1239600

Tarquinio, F., Hyndes, G. A., Laverock, B., Koenders, A., and Säwström, C. (2019). The seagrass holobiont: understanding seagrass-bacteria interactions and their role in seagrass ecosystem functioning. *FEMS Microbiol. Lett.* 366 (6), fnz057. doi: 10.1093/femsle/fnz057

Team, R. C. (2023). *A language and environment for statistical computing* (Vienna, Austria: R foundation for statistical computing).

Vandenkoornhuyse, P., Quaiser, A., Duhamel, M., Le Van, A., and Dufresne, A. (2015). The importance of the microbiome of the plant holobiont. *New Phytol.* 206, 1196–1206. doi: 10.1111/nph.13312

Vellend, M. (2010). Conceptual synthesis in community ecology. *Q Rev. Biol.* 85, 183–206. doi: 10.1086/652373

Vellend, M., Srivastava, D. S., Anderson, K. M., Brown, C. D., Jankowski, J. E., Kleynhans, E. J., et al. (2014). Assessing the relative importance of neutral stochasticity in ecological communities. *Oikos* 123, 1420–1430. doi: 10.1111/oik.01493

Villéger, S., Miranda, J. R., Hernandez, D. F., and Mouillot, D. (2012). Low functional β-Diversity despite high taxonomic β-Diversity among tropical estuarine fish communities. *PloS One* 7, e40679. doi: 10.1371/journal.pone.0040679

Vincent, S. G. T., Jennerjahn, T., and Ramasamy, K. (2021). "Chapter 3 - Environmental variables and factors regulating microbial structure and functions," in *Microbial communities in coastal sediments*. Eds. S. G. T. Vincent, T. Jennerjahn and K. Ramasamy (Elsevier), 79–117. doi: 10.1016/B978-0-12-815165-5.00003-0

Vogel, M. A., Mason, O. U., and Miller, T. E. (2021a). Composition of seagrass phyllosphere microbial communities suggests rapid environmental regulation of community structure. *FEMS Microbiol. Ecol.* 97 (3), fiab013. doi: 10.1093/femsec/fiab013

Vogel, M. A., Mason, O. U., and Miller, T. E. (2021b). Environmental stressors alter the composition of seagrass phyllosphere microbial communities. *Climate Change Ecol.* 2, 100042. doi: 10.1016/j.ecochg.2021.100042

Wang, X. D., Li, Y., Yan, Z. Q., Hao, Y. B., Kang, E. Z., Zhang, X. D., et al. (2022). The divergent vertical pattern and assembly of soil bacterial and fungal communities in response to short-term warming in an alpine peatland. *Front. Plant Sci.* 13. doi: 10.3389/fpls.2022.986034

Webb, C. O., Ackerly, D. D., and Kembel, S. W. (2008). Phylocom: software for the analysis of phylogenetic community structure and trait evolution. *Bioinformatics* 24, 2098–2100. doi: 10.1093/bioinformatics/btn358

Williams, P. H. (1996). Mapping variations in the strength and breadth of biogeographic transition zones using species turnover. *Proc. R. Soc. B: Biol. Sci.* 263, 579–588. doi: 10.1098/rspb.1996.0087

Wu, N., Qu, Y., Guse, B., Makarevičiūtė, K., To, S., Riis, T., et al. (2018). Hydrological and environmental variables outperform spatial factors in structuring species, trait composition, and beta diversity of pelagic algae. *Ecol. Evol.* 8, 2947–2961. doi: 10.1002/ece3.3903

Wu, N., Zhou, S., Zhang, M., Peng, W., Guo, K., Qu, X., et al. (2021). Spatial and local environmental factors outweigh geo-climatic gradients in structuring taxonomically and trait-based β-diversity of benthic algae. *J. Biogeography* 48, 1842–1857. doi: 10.1111/jbi.14108

Xiao, X., Huang, Y., and Holmer, M. (2020). Current trends in seagrass research in China, (2010-2019). *Aquat. Bot.* 166, 103266. doi: 10.1016/j.aquabot.2020.103266

Xu, C., Su, G., Zhao, K., Xu, X., Li, Z., Hu, Q., et al. (2022). Current status of greenhouse gas emissions from aquaculture in China. *Water Biol. Secur.* 1, 100041. doi: 10.1016/j.watbs.2022.100041

Yarnall, A. H., Byers, J. E., Yeager, L. A., and Fodrie, F. J. (2022). Comparing edge and fragmentation effects within seagrass communities: A meta-analysis. *Ecology* 103, e3603. doi: 10.1002/ecy.3603

Zhang, J., Yang, Q., Yue, W., Yang, B., Zhou, W., Chen, L., et al. (2023). Seagrass Thalassia hemprichii and associated bacteria co-response to the synergistic stress of ocean warming and ocean acidification. *Environ. Res.* 236, 116658. doi: 10.1016/j.envres.2023.116658

Zhou, J., Kang, S., SChadt, C. W., and Garten, C. T. (2008). Spatial scaling of functional gene diversity across various microbial taxa. *Proc. Natl. Acad. Sci.* 105, 7768–7773. doi: 10.1073/pnas.0709016105

Zhou, J., Liu, W., Deng, Y., Jiang, Y.-H., Xue, K., He, Z., et al. (2013). Stochastic assembly leads to alternative communities with distinct functions in a bioreactor microbial community. *mBio* 4 (2), e00584-12. doi: 10.1128/mbio.00584-00512

Zhou, J., and Ning, D. (2017). Stochastic community assembly: does it matter in microbial ecology? *Microbiol. Mol. Biol. Rev.* 81 (4), e00002-17. doi: 10.1128/MMBR.00002-17

frontiers | Frontiers in Plant Science

TYPE Correction
PUBLISHED 06 August 2024
DOI 10.3389/fpls.2024.1470123



OPEN ACCESS

APPROVED BY
Frontiers Editorial Office,
Frontiers Media SA, Switzerland

*CORRESPONDENCE
Huan Wang
wanghuan@hainanu.edu.cn

RECEIVED 25 July 2024
ACCEPTED 26 July 2024
PUBLISHED 06 August 2024

CITATION
Niu X, Ren W, Xu C, Wang R, Zhang J and Wang H (2024) Corrigendum: Taxonomic and functional β-diversity patterns reveal stochastic assembly rules in microbial communities of seagrass beds.
*Front. Plant Sci.* 15:1470123.
doi: 10.3389/fpls.2024.1470123



# Corrigendum: Taxonomic and functional β-diversity patterns reveal stochastic assembly rules in microbial communities of seagrass beds

Xiaofeng Niu[1,2], Wenjing Ren[1], Congjun Xu[2], Ruilong Wang[2], Jingwei Zhang[2] and Huan Wang[1,2]*

[1]School of Marine Biology and Fisheries, State Key Laboratory of Marine Resource Utilization in South China Sea, Hainan University, Haikou, Hainan, China, [2]Institute of Hydrobiology, Chinese Academy of Sciences, Wuhan, Hubei, China

KEYWORDS

**stochastic assembly, β-diversity, replacement, attached microbial communities, seagrass bed, habitat fragmentation**

A Corrigendum on

Taxonomic and functional β-diversity patterns reveal stochastic assembly rules in microbial communities of seagrass beds

By Niu X, Ren W, Xu C, Wang R, Zhang J and Wang H (2024) T. *Front. Plant Sci.* 15:1367773. doi: 10.3389/fpls.2024.1367773.

In the published article, there was an error in the Funding statement. For the Hainan University Start-up Funding for Scientific Research, "KYOD (ZR)-23, 086" and "KYOD (ZR)-23, 087" were incorrectly used instead of "KYQD (ZR)-23, 086" and "KYQD (ZR)-23, 087". The correct Funding statement appears below.

**FUNDING**

The author(s) declare financial support was received for the research, authorship, and/or publication of this article. This research was supported by the National Natural Science Foundation of China (Grant No. 32001151 and 42377469) and Hainan University Start-up Funding for Scientific Research (KYQD (ZR)-23, 086) and Hainan University Start-up Funding for Scientific Research (KYQD (ZR)-23, 087).

The authors apologize for this error and state that this does not change the scientific conclusions of the article in any way. The original article has been updated.

## Publisher's note

All claims expressed in this article are solely those of the authors and do not necessarily represent those of their affiliated organizations, or those of the publisher, the editors and the reviewers. Any product that may be evaluated in this article, or claim that may be made by its manufacturer, is not guaranteed or endorsed by the publisher.

frontiers | Frontiers in Plant Science

TYPE Original Research
PUBLISHED 05 March 2024
DOI 10.3389/fpls.2024.1367205



OPEN ACCESS

EDITED BY
Qiang Yang,
German Centre for Integrative Biodiversity Research (iDiv), Germany

REVIEWED BY
Qijia Cai,
South China Institute of Environmental Sciences, China
Pei Hong,
Anhui Normal University, China

*CORRESPONDENCE
Tiantian Yang
ttyang@ihb.ac.cn

RECEIVED 08 January 2024
ACCEPTED 07 February 2024
PUBLISHED 05 March 2024

CITATION
Pan J, Yang Z, Hu N, Xiao B, Wang C, Wu X and Yang T (2024) Effect of extracellular polymeric substances on the colony size and morphological changes of *Microcystis*. *Front. Plant Sci.* 15:1367205. doi: 10.3389/fpls.2024.1367205



# Effect of extracellular polymeric substances on the colony size and morphological changes of *Microcystis*

Jiaxin Pan[1,2], Zhongyong Yang[1], Nan Hu[2,3], Bangding Xiao[2,4], Chunbo Wang[2,4], Xingqiang Wu[2,4] and Tiantian Yang[2,4]*

[1]College of Hydraulic and Envrionmental Engineering, China Three Gorges University, Yichang, China, [2]Key Laboratory of Algal Biology of Chinese Academy of Sciences, Institute of Hydrobiology, Chinese Academy of Sciences, Wuhan, China, [3]School of Envrionmental Studies, China University of Geosciences, Wuhan, China, [4]Kunming Dianchi and Plateau Lakes Institute, Dianchi Lake Ecosystem Observation and Research Station of Yunnan Province, Kunming, China

Surface blooms of colony-forming *Microcystis* are increasingly occurring in aquatic ecosystems on a global scale. Recent studies have found that the *Microcystis* colonial morphology is a crucial factor in the occurrence, persistence, and dominance of *Microcystis* blooms, yet the mechanism driving its morphological dynamics has remained unknown. This study conducted a laboratory experiment to test the effect of extracellular polymeric substances on the morphological dynamics of *Microcystis*. Ultrasound was used to disaggregate colonies, isolating the cells and of the *Microcystis* suspension. The single cells were then re-cultured under three homologous EPS concentrations: group CK, group Low, and group High. The size, morphology, and EPS [including tightly bound EPS (TB-EPS), loosely bound EPS (LB-EPS), bound polysaccharides (B-polysaccharides), and bound proteins (B-proteins)] changes of colonies were closely monitored over a period of 2 months. It was observed that colonies were rapidly formed in group CK, with median colony size ($D_{50}$) reaching 183 μm on day 12. The proportion of colonies with a size of 150–500 μm increased from 1% to more than 50%. Colony formation was also observed in both groups Low and High, but their $D_{50}$ increased at a slower rate and remained around 130 μm after day 17. Colonies with a size of 50–150 μm account for more than 50%. Groups CK and Low successively recovered the initial *Microcystis* morphology, which is a ring structure formed of several small colonies with a $D_{50}$ of 130 μm. During the recovery of the colony morphology, the EPS per cell increased and then decreased, with TB-EPS and B-polysaccharides constituting the primary components. The results suggest that colony formation transitioned from adhesion driven to being division driven over time. It is suggested that the homologous EPS released into the ambient environment due to the disaggregation of the colony is a chemical cue that can affect the formation of a colony. This plays an important but largely ignored role in the dynamics of *Microcystis* and surface blooms.

KEYWORDS

**extracellular polymeric substances, *Microcystis*, colony formation, colony size, morphology**

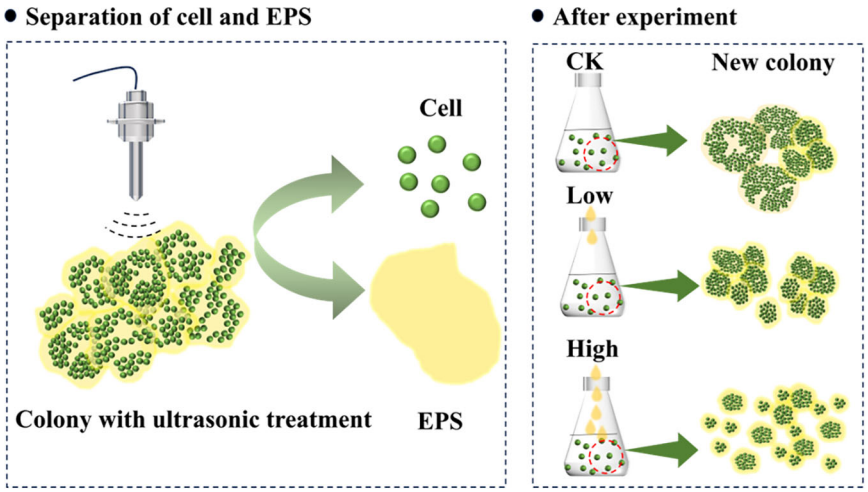


GRAPHICAL ABSTRACT

## Highlights

- The TB-EPS and B-polysaccharides primarily contribute to colony formation.
- *Microcystis* unicell forms a colony by cell adhesion.
- *Microcystis* achieves specific morphotypes by rapid cell division.
- Homologous EPS has an inhibitory effect on the morphological recovery of *Microcystis*.

## 1 Introduction

*Microcystis* spp. are widespread, harmful bloom-forming cyanobacteria (Sun et al., 2016; Chen et al., 2020; Kondo et al., 2023). Its colonies, characterized by individual cells embedded within extracellular matrices rich in extracellular polymeric substances (EPS) (Xiao et al., 2018), are ecologically significant for *Microcystis* enhancing persistence of individual cells in dynamic environments. Through cell aggregation, colonies provide protection, efficient resource uptake, and create unique microenvironments (Stal, 2017; Xiao et al., 2018). These advantages bolster ecological success and shape community structure (Visser et al., 2005; Yamamoto et al., 2011).

Under natural conditions, *Microcystis* mainly exists in colonies. But in typical laboratory cultures, it exists as single cells. Laboratory *Microcystis* strains can form colonies due to various biotic and abiotic factors. Biotic factors, such as EPS (Omori et al., 2019; Wei et al., 2020, 2021), *Microcystin* (Gan et al., 2012), allelopathy (Li et al., 2020), and zooplankton (Yang and Kong, 2012), are commonly involved. Abiotic factors include $Ca^{2+}$ (Chen and Lurling, 2020; Huang et al., 2022), $Mg^{2+}$ (Omori et al., 2019), temperature (Wei et al., 2020), and light (Wei et al., 2021). For *Microcystis* in the field, colony size may become larger under the disturbance caused by different wind and wave conditions (Duan et al., 2019). However, under some environmental stresses, colonies may also disaggregate to adapt to the novel environment. Strong turbulence can cause the disaggregation of a colony (Wu et al., 2019b). In late autumn and winter, as light decreases and water temperatures drop, *Microcystis* colonies in the lake may disaggregate resulting in a decreasing size (Tsujimura et al., 2000).

Colony formation is achieved through the mechanisms of cell division and adhesion, and these two mechanisms are often interactive (Xiao et al., 2017) posing a challenge in evaluating their respective roles. Division and adhesion are usually quantified by comparing colony cell growth with total cell number growth (Xiao et al., 2017; Duan et al., 2018). Studies have shown that after colony-induced culturing of laboratory *Microcystis* strains and field isolated single-celled *Microcystis* strains, the newly formed colonies did not exhibit specific types of morphology in a few months (Duan et al., 2018; Chen and Lurling, 2020). When future cell division events take place, the arbitrary arrangement of cells within the colony becomes regular (Otsuka et al., 2000; Sun et al., 2016). It helps to form colonies with distinct morphological characteristics.

The formation of a colony is seemingly associated with EPS. For example, EPS has been found to contribute to the adhesion, cohesion, and aggregation of *Microcystis* cells providing the foundation for the development of multi-cellular structures (Karampatzakis et al., 2017; Liu et al., 2018). This matrix is excreted by *Microcystis* into their surrounding environment (Duan et al., 2018), where it functions as a critical scaffold for colony formation. EPS can be categorized as soluble EPS (SL-EPS) and binding EPS (B-EPS) according to the degree of tight binding with a colony, and B-EPS is further divided into loosely bound EPS (LB-EPS) and tightly bound EPS (TB-EPS) (Omori et al., 2019; Tan et al., 2020). The main constituents of *Microcystis* EPS are polysaccharides and proteins, and many humic acid-like components have been identified recently (Xiao et al., 2019; Van Le et al., 2022). In natural water bodies, EPS can be released by

disaggregation of a colony and death of a cell (Sigee et al., 2007). However, how EPS affect the colony dynamics of *Microcystis* has remained unclear.

To enhance the understanding of colony formation and dynamics, the single-celled *Microcystis* was used to culture a colony with homologous EPS in the laboratory. In the present study, ultrasound was used to simulate the natural forces that cause the disaggregation of a colony and to isolate the cells and EPS. By incubating the single cells with varied amount homologous EPS, we aim to (i) explore the effect of EPS on the morphological characteristics of *Microcystis* and (ii) investigate the mechanism of colony formation during this process. This study is expected to contribute to a better understanding of the differences between single-celled and colonial morphologies of *Microcystis*, the strategies involved in community formation, and the role of EPS in *Microcystis* colony formation and morphological changes.

# 2 Materials and methods

## 2.1 *Microcystis* colony culture and collection

On 20 March 2023, a phytoplankton net with a mesh size of 63 μm was used to collect a thin layer of surface scum composed of cyanobacteria that was collected during the early stages of a spring bloom in Guanqiao fish pond located in Wuhan, China. The collected cyanobacterial colonies were quickly transported to the laboratory. They were immediately filtered through a 300-μm mesh filter followed by a 45-μm mesh filter to eliminate coarse impurities. The filtered and concentrated cyanobacterial colonies were subjected to a pre-culturing process in 10% BG11 medium, at a temperature of 25°C, under a light/dark cycle of 12 h/12 h with light exposure of 25 μmol photons $m^{-2}$ $s^{-2}$, for a duration of 3 days (Zhao et al., 2019; Gao et al., 2020; Xu et al., 2023). Morphological identification was conducted, which revealed the predominance of *Microcystis* species (Supplementary Figure S1C).

## 2.2 Acquisition of cells and homologous EPS of *Microcystis*

To isolate cells from *Microcystis* colonies, the *Microcystis* colonies were subjected to pretreatment using an Ultrasonic Processor (VCX150, Sonics & Materials Inc., USA). The colonies were dispersed into individual cells (Supplementary Figures S2B and S3B) through the application of ultrasonic waves (Wu et al., 2012; Zhang et al., 2021). The ultrasonic amplitude was set at 50%, and a total energy of 108–112 J was released over a 4-min duration. The single cells obtained from ultrasonic dispersion were stained with fluorescein diacetate (FDA) at 100 μg $mL^{-1}$ and subsequently kept in darkness for 5 min (Chen et al., 2005). Upon exposure to an excitation light source, the cells exhibited a vibrant green fluorescence (Supplementary Figure S3B) confirming that the ultrasonic treatment employed did not induce cellular mortality (Yang et al., 2021). Both the cells and EPS were isolated by centrifugation at 9,000 rpm for 10 min. The experimental cells were obtained by subjecting them to three rounds of resuspension and centrifugation in 10% sterile BG-11 medium.

The resulting supernatant from centrifugation at 9,000 rpm was collected and subsequently filtered using GF/F membranes (0.22 μm; Waterman, UK) to obtain *Microcystis* EPS that was devoid of cells. This collected EPS is called homologous EPS. To prevent the EPS from rapidly deteriorating at ambient temperature, the separated homologous EPS was promptly refrigerated and stored for later use.

## 2.3 Experiment design

The homologous EPS collected during pre-treatment was added to cells at different concentrations, determined by the dissolved organic carbon (DOC) concentration. This resulted in EPS concentrations of 0 mg $L^{-1}$ (CK), 0.66 mg $L^{-1}$ (Low), and 12 mg $L^{-1}$ (High) within the culture system (Supplementary Table S1). During the collection of *Microcystis* in the field, the pond's DOC content was measured to be 12 mg $L^{-1}$ at a depth of 0.1 m below the water surface.

All groups were cultured in Erlenmeyer flasks containing 10% sterile BG11 medium. In all groups, the starting cell density was consistent at $6.5\times10^8$ cell $L^{-1}$. The experiments were conducted in an Illuminated Incubator (PGX-100A-LED, Jiangsu Tianling Instrument Co., Ltd., Yancheng, China). Culture conditions mirrored those of wild *Microcystis* colonies, with gentle agitation provided by manual shaking two to three times per day (Gao et al., 2020; Xu et al., 2023). Other culturing conditions were the same as those in Section 2.1. Samples were collected every 3 days during the initial phase when cells reaggregated into microcolonies and every 5 days when the size of reaggregated colonies stabilized. Nutrient concentrations within the culture system were monitored throughout the sampling period to ensure adequate nutrient availability. All experimental groups were conducted in quadruplicate, and the results were reported as averages.

## 2.4 Growth parameters and morphology

The *Microcystis* population is enumerated after the alkaline hydrolysis using an optical microscope (BX43, Olympus Corporation). The relative growth rate (ν) of *Microcystis* was calculated as follows (Xu et al., 2023):

$$\nu = (C_{tj} - C_{ti})/C_{ti}$$

where $C_{ti}$ and $C_{tj}$ (cells $L^{-1}$) are the cell densities of *Microcystis* at two consecutive sampling times.

Chlorophyll a (Chl*a*) was measured using a 4.8-mL sample. The Phytoplankton Analyzer (Phyto-PAM, Walz Co., Erlangen, Germany) was utilized for the assessment of *Microcystis* photosynthetic activity (Ye et al., 2023). The Fv/Fm parameter represents the potential maximum conversion efficiency of *Microcystis* photosystem II, as it is overwhelmingly dominant (Wang et al., 2018). Photos were taken using software (HaoKangBioImaging) on a microscope.

## 2.5 Zeta potential, pH, and dissolved oxygen

The zeta potential of *Microcystis* was measured with a Malvern Zetasizer (Malvern-Nano-ZSMalvern, UK) (Tattibayeva et al., 2022). The pH was determined with a pH meter (pH100A, EcoSence, China). Additionally, the dissolved oxygen (DO) in the *Microcystis* fluid was quantified using a YSI instrument (YSI Pro ODO, USA).

## 2.6 Colony size and compactness

The study utilized a Laser *In-Situ* Scattering and Transmissometer instrument (LISST-200X, Sequoia Scientific Inc., Bellevue, WA, USA) to measure colony size, cell size, and biovolume concentration. The median colony size ($D_{50}$), representing the median biovolume concentration location, was used to characterize the diameter of *Microcystis* cells and colonies. Before measuring, the *Microcystis* sample was appropriately diluted with distilled water. Then, 10 mL of the diluted sample was used to determine the size distribution and biovolume concentration ($V_{colony}$ in μL $L^{-1}$) of the original *Microcystis* colony. After the measurements, the *Microcystis* fluid was retrieved, and the colonies were disaggregated into single cells through alkaline hydrolysis at 85 °C for 6–8 min (Wang et al., 2015). The size distribution and biovolume concentration ($V_{cell}$ in μL $L^{-1}$) of *Microcystis* cells were subsequently assessed using the LISST-200X. The volume ratio (VR) of the cells to colonies was calculated according to established laboratory protocols from prior studies (Wu et al., 2020; Xu et al., 2023), and it indicates the relative compactness of colonies:

$$VR = V_{cell}/V_{colony}$$

where $V_{cell}$ (μL $L^{-1}$) and $V_{colony}$ (μL $L^{-1}$) are the mean biovolume concentrations of single cells and of colonies in a sample.

## 2.7 EPS and DOC measuring

Coomassie Brilliant Blue G-250 and phenol-sulfuric acid were used to measure polysaccharides and proteins, respectively (Wang and Xing, 2009; Ma et al., 2021; Duan et al., 2022) in this study. The sample was first centrifuged at 5,000 rpm for 15 min. After removing the supernatant, the remaining sediment was resuspended using a 0.05% NaCl solution. The suspended algae solution was then centrifuged at 5,000 rpm for LB-EPS measurement (Xiao et al., 2018). The residual sediment was re-suspended with a 0.05% NaCl solution at an adjusted pH of 10 and heated at 45°C for 4 h. Subsequently, centrifugation was performed at 11,000 rpm for 15 min, and the resulting supernatant was collected for the measurement of polysaccharides and proteins (Yang et al., 2008; Xiao et al., 2012, 2019). LB-EPS encompasses loosely bound proteins and polysaccharides. TB-EPS comprises tightly bound proteins and polysaccharides.

The content of dissolved polymeric substances (S-EPS) was represented by DOC in this study. The DOC in liquid samples filtered through GF/F membranes was quantified using a Total Organic Carbon Analyzer (TOC-VCPH, Shimadzu Co., Kyoto, Japan).

## 2.7 Statistical analysis

SPSS statistics software (version 27, Chicago, IL, USA) was used to determine the differences in physiological regulation of *Microcystis* at different periods of colony formation and the differences in colony formation caused by homologous EPS. Values with $p< 0.05$ were considered significant, while those with $p< 0.01$ were considered very significant. All data images were produced using Origin 2021 software (OriginLab, Northampton, MA, USA).

# 3 Results

## 3.1 Growth of *Microcystis* under different EPS concentrations

As shown in Figure 1A, there was no significant difference in *Microcystis* cell density during the first 0–6 days. However, the cell density in group High remained consistently higher than the other two groups for the following 42 days. In Figure 1B, the growth rate of group CK had a small peak of 0.46 $day^{-1}$ during 3–6 days followed by a small decrease and a rise to the second peak of 1.05 $day^{-1}$ during 27–32 days. This pattern repeated, reaching the third peak of 1.05 $day^{-1}$ during 42–47 days. During the final 20 days of the experiment, the rapid increase in growth rate of group CK ceased and then decreased to a stagnant growth state. It showed a relatively stable and low cell density curve in Figure 1A. The growth rate of group Low rose and fell during the experiment in general. But it decreased to 0.25 $day^{-1}$ between days 27 and 32 before peaking at 0.84 $day^{-1}$ in the following 5 days. Group High had higher growth rate at the beginning and end of experiment. Specifically, the peak values observed were 0.69 and 1.17 $day^{-1}$ on days 6–9 and 42–47. At the same time, it was observed that the dissolved total phosphorus (DTP) in this set of systems was almost depleted by the end of day 12, and the medium was replenished in a timely manner (Supplementary Figure S4). The growth rate of group High reached a second small peak of 1.7 on days 22–27. A third peak in growth rate was observed after 47 days. The growth rate of group Low reached a small peak on day 22 and increased rapidly to 7.4 on days 32–52. In the long term, the addition of homologous EPS is beneficial to *Microcystis* population.

The Chl*a* per cell in group CK was significantly lower than that in group Low ($p< 0.05$). In comparison to group Low, the difference in Chl*a* content in group High was much more significant ($p< 0.01$). The Chl*a* content per cell increased during the initial 6 days, followed by a decrease as the days progressed, and eventually stabilizing at a relatively constant value. The Chl*a* content was similar among the different treatment groups (Figure 1D).

During the first 6 days, the photochemical efficiency of PSII (Fv/Fm) significantly decreased in all treatment groups. The magnitude of the decrease was directly proportional to the amount of added

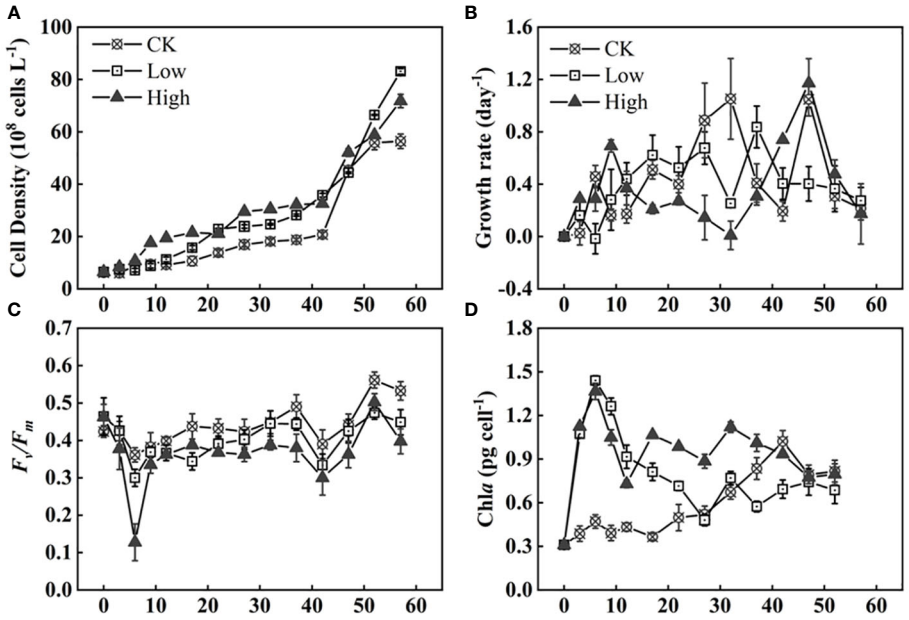


FIGURE 1
Time series of cell density **(A)**, growth rate **(B)**, photochemical efficiency of PSII (Fv/Fm) **(C)**, and Chl*a* concentration **(D)** of *Microcystis* under three homologous EPS concentrations (Supplementary Table S1 for explanation of the experimental groups).

homologous EPS. The group with high homologous EPS addition showed a reduction of 0.34, which was two to five times lower than the low addition group and group CK (Figure 1C). Overall, group CK had the highest Fv/Fm value, while the group with high homologous EPS addition had the lowest value.

## 3.2 Changes in physicochemical parameters of the *Microcystis*

It was observed that the absolute value of the Zeta potential in group CK increased in the first 0–3 days before decreasing. Groups Low and High experienced a decrease in the absolute value of Zeta potential until 12 days (Figure 2A). From days 10 to 40, the absolute value of the Zeta potential of group CK remained at 20 to 24, which was lower than that of the other two groups. There is no significant difference in the Zeta potential between group Low and group High. The concentration of DO and pH of group High were higher than those in group Low. Similarly, group Low had higher DO and pH than group CK in the first 20 days (Figures 2B, C).

## 3.3 The impact of EPS concentration on colony size and morphology

### 3.1.1 Dynamics of colony morphology

As shown in Figure 3, the addition of homologous EPS had a lasting and profound effect on the restoration of colony morphology. Both groups CK and group Low successfully returned to the original *Microcystis novacekii* form by the end of the experiment (Figures 3A4, B4). However, the colonies of group High consist of small spherical or nearly spherical colonies (diameter<50 μm) forming loose large colonies (Figure 3C4). For group CK, some large colonies were observed on day 6. On day 12, many gaps appeared between the colonies, which were then divided into distinct and tiny blocks (Figure 3A2). By day 27, the colonies had taken on the classic form of *Microcystis novacekii*, with three to five small colonies connected in rings (Figure 3A3). The differences between group Low and group CK were that there were fewer large colonies in the process of morphological recovery in group Low (Supplementary Figure S5), and the ring form formed by connecting small groups does not appear until day 32 (Figures 3B1–B3).

### 3.1.2 The impact of EPS on colony size and compactness

During the first three days of the experiment, $D_{50}$ increased at the same rate in all groups. However, after that, group CK exhibited a greater growth trend in $D_{50}$, reaching its first peak on the 12th day and gradually decreasing thereafter. In contrast, $D_{50}$ under different initial EPS concentrations remained relatively stable at approximately 120 μm on day 17 (Figure 4A). The maximum $D_{50}$ values of groups Low and High were 166 and 187 μm, respectively. The two groups of colonies were similar in size. $D_{50}$ of group CK and two EPS addition groups were significantly different ($p< 0.05$).

Simultaneously, it was discovered that different concentrations of EPS influenced the formation of *Microcystis* colonies. The colony size in group CK quickly recovered to the size of the original colonies (Figure 4A). Meanwhile, the cell density remained relatively constant during this period. The recovery speed of colony size in groups Low and High was slower than that of group CK, requiring 17 and 27 days, respectively. During the

10.3389/fpls.2024.1367205

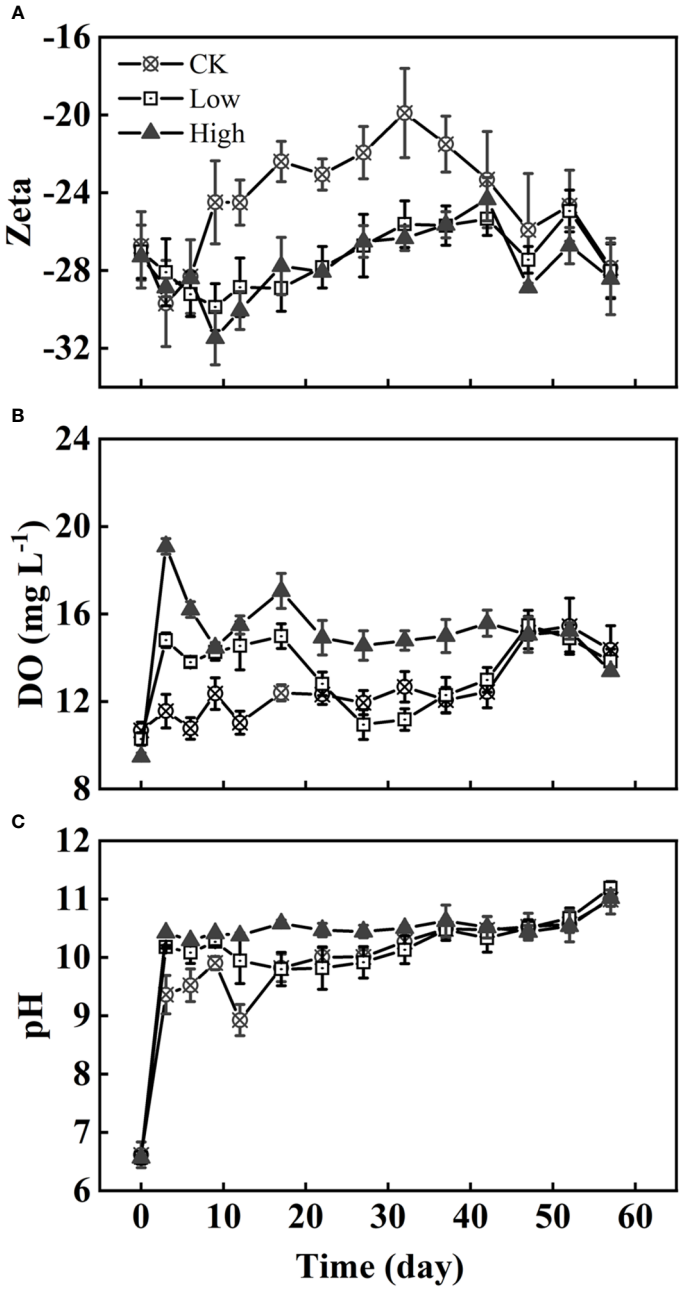


FIGURE 2
The variation of the Zeta potential **(A)**, DO **(B)**, and pH **(C)** of algae under three homologous EPS concentrations over time. Difference between group CK and two EPS addition groups on Zeta potential and DO were very significant and significant ($p< 0.01$, $p< 0.05$).

initial stages of the experiment, the colonies VR decreased due to loose cell adhesion (Figure 4B). In Supplementary Figure S5, the proportion of the VC for 0–50, 50–150, and 150–500 μm in the total VC was roughly the same on day 0. Specifically, the VC proportion for 0–50 μm was 72% ± 4%, the VC proportion for 50–150 μm was 27.5% ± 3.5%, and the VC proportion for 150–500 μm was 1%. After 3 days, the VC proportion for 0–50 μm decreased in each group, while the VC proportion for 50–150 μm increased significantly, and the VC proportion for 150–500 μm increased slightly. After 12 days, the VC proportion for 150–500 μm in group CK remained stable at over 50%. The VC proportion for 50–150 μm also remained stable at more than 38% ± 4%, while the VC proportion of 0–50 μm accounted for only a very small percentage of 3%–5%. Compared with group CK, colonies measuring 150–500 μm accounted for the majorities of the proportion. Two groups with added homologous EPS accounted for more colonies of 50-150 μm proportion. Additionally, the proportion of 50–150 μm in group High was higher than that in group Low.

Group High exhibited the lowest $D_{50}$ indicating that a high concentration of homologous EPS had an inhibitory effect on the process of colony formation when compared with no and low concentrations of homologous EPS. After 12 days, there was a significant increase in cell density, with a rise of $(10.4 \pm 2.4) \times 10^8$

10.3389/fpls.2024.1367205

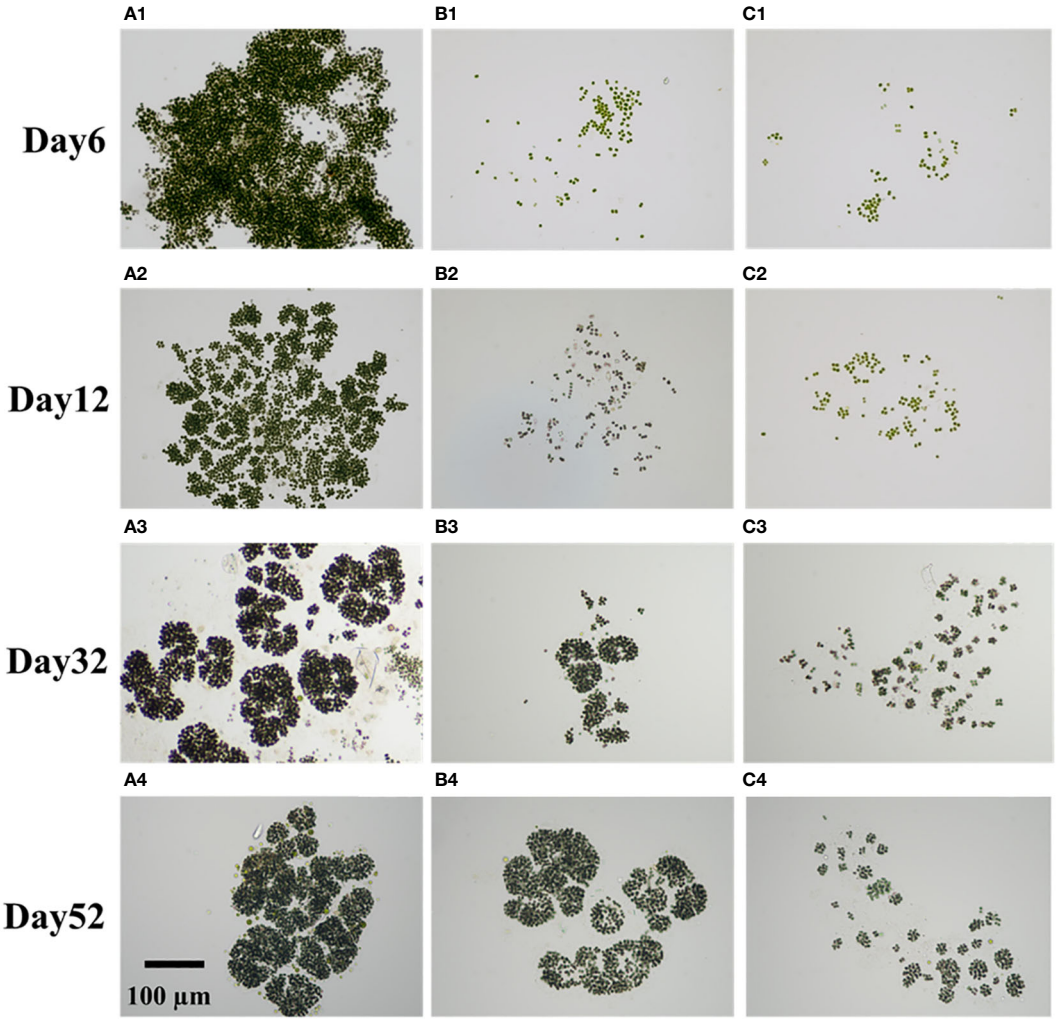


FIGURE 3
Different colony forms formed over time. They are microphotographs taken at ×20 magnification [group CK: groups **(A1–A4)**; group Low: **(B1–B4)**; High: **(C1–C4)**]. Row 1: day 6; row 2: day 12; row 3: day 32; row 4: day 52.

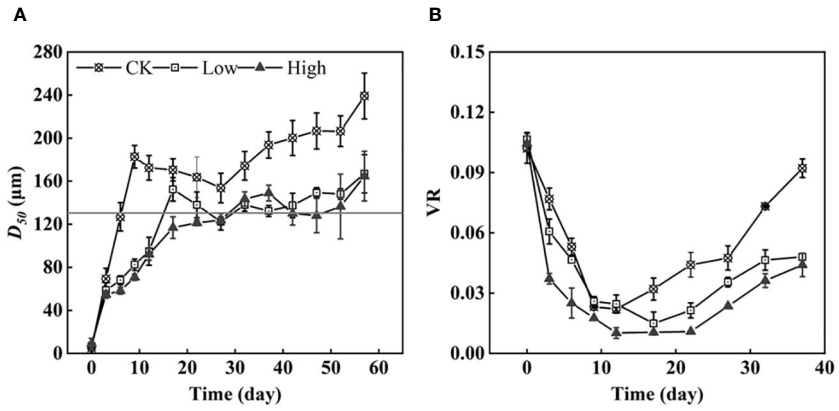


FIGURE 4
The medium-sized colonies under three homologous EPS concentrations and the original colonies (horizontal solid line: 130 μm) **(A)** and the colony volume ratio (VR) **(B)**.

cells $L^{-1}$, and the cell density began to increase. Although group CK had the lowest cell density, it exhibited the fastest VR growth. This indicates that the EPS produced by cells during cultivation was more effective in promoting cell density than the added homologous EPS.

## 3.4 Changes in EPS of *Microcystis* colonies

In this experiment, the EPS of *Microcystis* were analyzed by their content of polysaccharides and proteins as representative structural EPS. The ultrasonic treatment used to extract the EPS was not entirely thorough, as evidenced by the incomplete extraction of TB-EPS (Figure 5B). The addition of homologous EPS resulted in a rapid response from *Microcystis* cells, as indicated by the production of LB-EPS. The strength of the positive response was directly proportional to the amount of homologous EPS added (Figure 5A). Initially, the added homologous EPS mainly consisted of soluble EPS, with a smaller proportion of LB-EPS. Among them, proteinaceous substances had a higher proportion than polysaccharides (Figures 5A, B, D, F). During the experiment, the LB-EPS on individual cells in both groups Low and High first decreased from 0 to 6 days and then increased. In groups CK, Low, and High, the LB-EPS content on individual cells reached its highest levels at approximately 32 days, with values of 0.045, 0.048, and 0.065 pg $cell^{-1}$, respectively (Figure 5A). In contrast to the immediate decrease in LB-EPS content in groups CK and Low, group High maintained its peak levels for 10 days. Over the course of 0–20 days, the TB-EPS on individual cells in group Low was significantly higher than in groups CK and High. In Figure 5B, the TB-EPS peak values were 0.092, 0.111, and 0.139 pg $cell^{-1}$ for groups Low, CK, and High, respectively. The peak order of B-polysaccharides on cells was similar to that of TB-EPS, with only group High showing a peak of up to 0.114 pg $cell^{-1}$ at 32 days. According to the trend of extracellular substances on cells from 0 to 6 days, polysaccharides are suggested to be mainly TB-EPS, while proteins are suggested to be mainly LB-EPS (Figures 5A–D). The trends in B-EPS on individual cells in each group were generally similar, with group CK maintaining lower B-EPS levels than the other two groups (Figure 5A), resulting in the formation of denser *Microcystis* colonies in group CK. The DOC level in group CK consistently remained low, with a slight decrease after a gradual increase (Figure 5F). In group Low, the DOC level was above 0.003 pg $cell^{-1}$ after the ninth day and continued to decline after approximately 20 days. The DOC level in group High rapidly decreased from 0.018 to 0.003 pg $cell^{-1}$ within the first 3 days and has since fluctuated between 0 and 0.003 pg $cell^{-1}$.

# 4 Discussion

Under no and low homologous EPS addition, *Microcystis* cells isolated from field strains can recover to the colonies with original morphological level, including colony size and morphology. Based on VR, it suggests that the formation of *Microcystis* colonies from single cells to stable shapes involves two main stages. Stage 1: Cells aggregate into small colonies through adhesion (decreasing VR). Stage 2: Colonies become more compact (increasing VR) and eventually form a specific colony morphology.

At the beginning of stage 1, the Chl*a* content of cell and DO all increased (Figures 1, 2). The pH rapidly increased to 9–10 within 3 days (Figure 2). Such alkaline condition could be created by the photosynthesis of cyanobacteria. The colony's photosynthesis is promoted by the elevated pH, which increases until it surpasses 10 (Fang et al., 2018). This could facilitate colony formation (Bano and Siddiqui, 2004; Fang et al., 2018). At stage 1, which lasted for about 12 days, the cell densities of all three groups did not increase significantly (Figure 1A), while colonies were observed in all groups. Particularly, in group CK, the colony size of *Microcystis* on the sixth day is comparable to original colonies (Figure 4A). Therefore, this process of cell aggregation is most likely caused by adhesion. Although adhesion has been considered as one of the mechanisms for the formation of colonies (Duan et al., 2019), the involved processes have not been fully clarified. Colonies formed in all groups suggest that the cell adhesion is not caused by homologous EPS. Contrarily, the results suggest that homologous EPS can inhibit this process. The more homologous the EPS added, the stronger the inhibition observed (Figure 3). Under different homologous EPS additions, the rate of change in $D_{50}$ in the first 12 days was group CK > group Low > group High (Figure 3). At the same time, counterintuitively, it was found that the VR of colonies did not become dense with the decrease in $D_{50}$. Group CK with a larger size had the largest colony VR (Figure 3). The TB-EPS on cells was not completely removed (Figure 5B). Most *Microcystis* (>85%) have a layer of hydrophobic proteins outside the cell wall named S-layer, which is important for cell adhesion and surface recognition (Šmarda et al., 2002; Schachtsiek et al., 2004; Zu et al., 2020). This structure may overlap with TB-EPS, which allows cells in group CK to directly recognize and adhere to special substances between TB-EPS, thus forming larger and relatively denser colonies. A recent study (Duan et al., 2022) shows that few perssads of LB-EPS in *Microcystis novacekii* are enhanced in favor of colony adhesion. Cells with low and high EPS concentrations first face the binding of TB-EPS to homologous EPS, then resulting in looser colonies. Besides, due to the larger physiological differences between different strains (Zhang et al., 2007; Wu and Song, 2008; Du et al., 2023), adhesion of *Microcystis* occurs in the same morphological type relating to different EPS components (Duan et al., 2022).

Stage 2 occurred after 12 days. Contrary to single-celled *Microcystis* strains forming colonies in the laboratory, colony B-EPS secretion capacity was inversely related to colony size (Xu et al., 2016). The organic matter synthesized by cells is first used for proliferation rather than self-protection especially during the last period of rapid cell growth. Consequently, a reciprocal limitation is observed between cell growth and the produce of EPS. Generally, group CK exhibited significantly larger colony sizes, although with the lowest recorded cell density and absolute Zeta potential values. It is easier to form a bloom with a lower absolute value of cell surface potential resulting in larger colony size of the bloom (Cao and Yang, 2010; Liu et al., 2016). In all groups, the absolute value of Zeta potential increases first and decreases, which is roughly consistent with the time of B-EPS change (Figures 2A, 5E). It

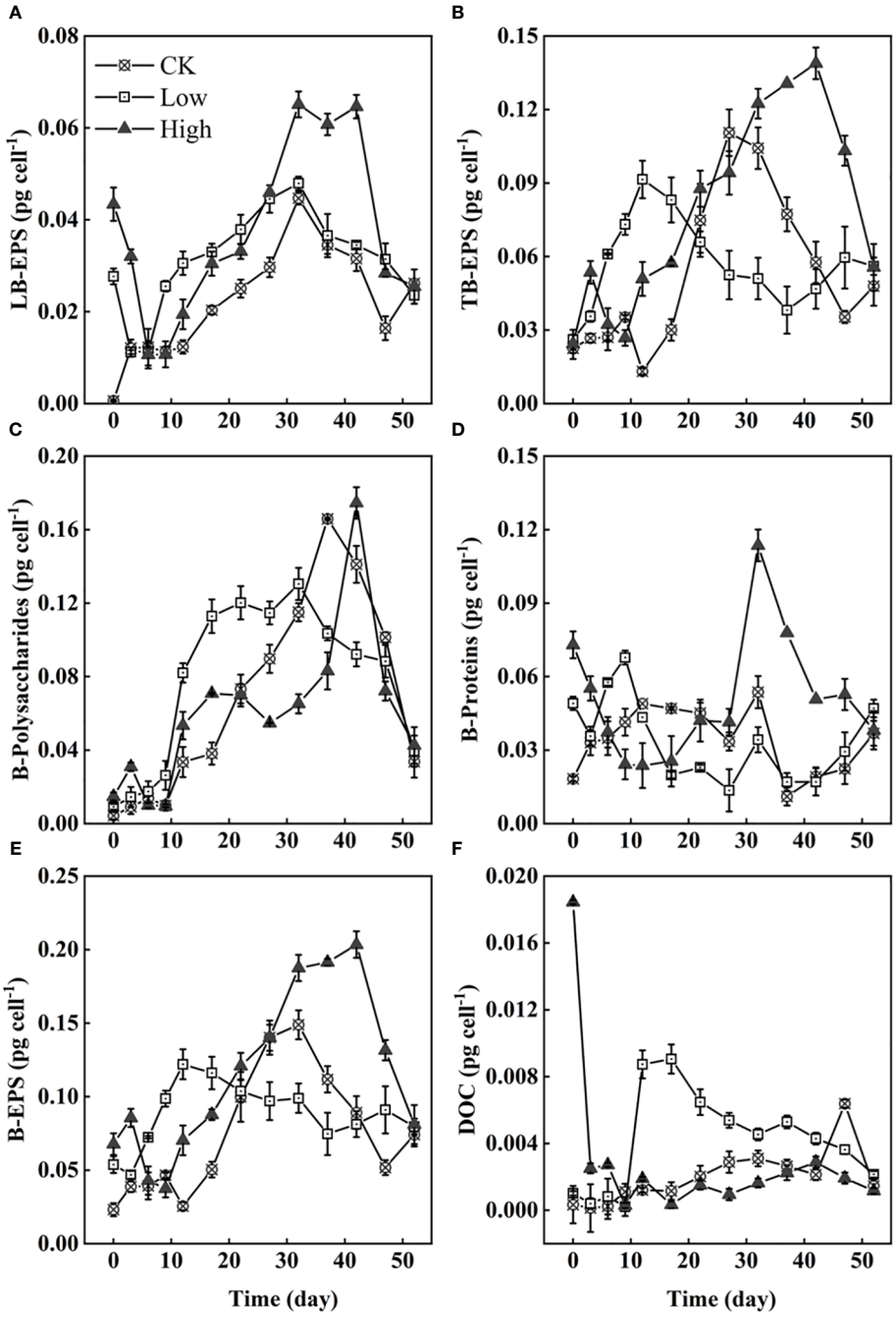


FIGURE 5
The content of LB-EPS **(A)**, TB-EPS **(B)**, B-polysaccharides **(C)**, B-protein **(D)**, bound extracellular polymers (B-EPS) **(E)**, and DOC **(F)**. All on individual *Microcystis* cells.

suggests that the change in surface zeta potential over time may be caused by changes in the composition and content of B-EPS (Bernhardt et al., 1985; Liu et al., 2016).The colony of *Microcystis novacekii* has an orderly arrangement of cells, and it is spherical or nearly spherical, and three to five small colonies are connected into a ring structure (Yu et al., 2007). Through microscopic observation, we found that the colonies appeared to have a more obvious morphological type in the period of rapid growth of cell density, which we identified as *Microcystis novacekii* (groups CK and High) (Figure 3). Cell division results in the orderly arrangement of cells within the colony (Xiao et al., 2017). Group High may take longer to exhibit this pattern. Based on this finding, we hypothesize that in the natural environment, the homologous EPS, which is often accompanied by colony disaggregation, is a signaling important chemical cue that transmits environmental stress to *Microcystis* inhibiting the formation of new colonies.

It is reported that co-occurring microorganisms isolated from *Microcystis* blooms from Lake Taihu can increase or decrease *Microcystis aeruginosa* colony size (e.g., *Chryseobacterium* sp. and *Bacillus cereus*) (Wu et al., 2019a). In this experiment, the possible

role of the co-occurring microorganisms in the formation of the colony remains uncertain. In the process of colony formation, EPS on cells always increases and then decreases. The TB-EPS and B-polysaccharides were more abundant (Figure 5) indicating that they may contribute to colony maintenance more than LB-EPS, S-EPS, and B-proteins. It is undeniable that more EPS is conducive to colony formation, but the colony that has formed a morphological structure seems to maintain the morphological structure with a low EPS presence (Figure 5). The vital role of EPS in the dynamics of *Microcystis* colonial morphology, as revealed by this study, implies that monitoring the EPS content in lakes may be another potential means for early warning of harmful cyanobacterial blooms.

## 5 Conclusion

The colony-forming process of *Microcystis* from single cells' specific morphological characteristics is helpful to further understand the early development process of *Microcystis* blooms. During the colony formation, adhesion contributed more. Then cell division took over, accompanied by the increase in EPS on *Microcystis*. The EPS decreased when the *Microcystis* was divided into a morphologically distinct structure. The homologous EPS has a certain influence on the development of colony morphology features. This study provides new insights into the single-cell to colonial transformation of *Microcystis* and the processes associated with colony morphological changes.

## Data availability statement

The original contributions presented in the study are included in the article/Supplementary Material. Further inquiries can be directed to the corresponding author.

## Author contributions

JP: Data curation, Formal analysis, Methodology, Software, Supervision, Visualization, Writing – original draft, Conceptualization, Investigation, Project administration, Validation, Writing – review & editing. ZY: Funding acquisition, Writing – review & editing. NH: Investigation, Writing – review & editing. BX: Resources, Writing – review & editing. CW: Funding acquisition, Writing – review & editing. XW: Supervision, Writing – review & editing. TY: Conceptualization, Data curation, Formal analysis, Funding acquisition, Investigation, Methodology, Project administration, Supervision, Writing – original draft, Writing – review & editing.

## Funding

The author(s) declare financial support was received for the research, authorship, and/or publication of this article. This study was financially supported by the Hubei Province Postdoctoral Innovation Research Position (Letter No. 153 of Hubei Human Resources and Social Security. Additional support was provided by the China's National Key R&D Programmes (2022YFC3203601), National Natural Science Foundation of China (42061134013), the Key Project of Hubei Province Natural Science Foundation (2021CFA092), and the Yunnan Province-Kunming City Major Science and Technology Project (202202AH210006). In addition, the Three Gorges Innovation and Development Joint Fund (2023AFD201) and the Natural Science Foundation of Hubei Province (2022CFB207) also supported this article.

## Conflict of interest

The authors declare that the research was conducted in the absence of any commercial or financial relationships that could be construed as a potential conflict of interest.

## Publisher's note



## Supplementary material

The Supplementary Material for this article can be found online at: https://www.frontiersin.org/articles/10.3389/fpls.2024.1367205/full#supplementary-material

## References

Bano, A., and Siddiqui, P. J. A. (2004). Characterization of five marine cyanobacterial species with respect to their pH and salinity requirements. *Pakistan J. Bot.* 36, 133–143.

Bernhardt, H., Hoyer, O., Schell, H., and Lusse, B. (1985). Reaction-mechanisms involved in the influence of algogenic organic-matter on flocculation. *Z. Wasser. Abwasser. Forsch.* 18, 18–30.

Cao, H., and Yang, Z. (2010). Variation in Colony Size of *Microcystis aeruginosa* in a Eutrophic Lake during Recruitment and Bloom Formation. *J. Freshw. Ecol.* 25, 331–335. doi: 10.1080/02705060.2010.9664375

Chen, H., and Lurling, M. (2020). Calcium promotes formation of large colonies of the cyanobacterium *Microcystis* by enhancing cell-adhesion. *Harmful. Algae.* 92, 101768. doi: 10.1016/j.hal.2020.101768

Chen, L., Liang, W., Qu, J., Xie, M., Lei, P., and Liu, H. (2005). Study on the detection of cyanobacteria cell activity by FDA-PI two-color fluorescence method. *Environ. Chem.* 05), 554–557. doi: 10.3321/j.issn:0254-6108.2005.05.014

Chen, X.-D., Liu, Y., Yang, L.-M., Hu, X.-Y., and Jia, A.-Q. (2020). Hydrogen sulfide signaling protects chlamydomonas reinhardtii against allelopathic damage from cyanobacterial toxin microcystin-LR. *Front. Plant Sci.* 1105. doi: 10.3389/fpls.2020.01105

Du, X., Song, D., Wang, H., Yang, J., Liu, H., and Huo, T. (2023). The combined effects of filter-feeding bivalves (Cristaria plicata) and submerged macrophytes (Hydrilla verticillate) on phytoplankton assemblages in nutrient-enriched freshwater mesocosms. *Front. Plant Sci.* 14, 1069593. doi: 10.3389/fpls.2023.1069593

Duan, Z., Tan, X., Parajuli, K., Upadhyay, S., Zhang, D., Shu, X., et al. (2018). Colony formation in two *Microcystis* morphotypes: Effects of temperature and nutrient availability. *Harmful. Algae.* 72, 14–24. doi: 10.1016/j.hal.2017.12.006

Duan, Z., Tan, X., Parajuli, K., Zhang, D., and Wang, Y. (2019). Characterization of *Microcystis* morphotypes: Implications for colony formation and intraspecific variation. *Harmful. Algae.* 90, 101701. doi: 10.1016/j.hal.2019.101701

Duan, Z., Tan, X., and Zeng, Q. (2022). Key physiological traits and chemical properties of extracellular polymeric substances determining colony formation in a cyanobacterium. *J. Oceanol. Limnol.* 40, 1720–1731. doi: 10.1007/s00343-022-1353-5

Fang, F., Gao, Y., Gan, L., He, X., and Yang, L. (2018). Effects of different initial pH and irradiance levels on cyanobacterial colonies from Lake Taihu, China. *J. Appl. Phycol.* 30, 1777–1793. doi: 10.1007/s10811-018-1394-5

Gan, N., Xiao, Y., Zhu, L., Wu, Z., Liu, J., Hu, C., et al. (2012). The role of microcystins in maintaining colonies of bloom-forming *Microcystis* spp. *Environ. Microbiol.* 14, 730–742. doi: 10.1111/j.1462-2920.2011.02624.x

Gao, Y., Fu, Q., Lu, J., Yang, H., Orr, P. T., Zhang, F., et al. (2020). Enhanced pyrogallol toxicity to cyanobacterium *Microcystis aeruginosa* with increasing alkalinity. *J. Appl. Phycol.* 32, 1827–1835. doi: 10.1007/s10811-020-02096-2

Huang, X., Gu, P., Wu, H., Wang, Z., Huang, S., Luo, X., et al. (2022). Shift of calcium-induced *Microcystis aeruginosa* colony formation mechanism: From cell adhesion to cell division. *Environ. pollut.* 313, 119997. doi: 10.1016/j.envpol.2022.119997

Karampatzakis, A., Song, C. Z., Allsopp, L. P., Filloux, A., Rice, S. A., Cohen, Y., et al. (2017). Probing the internal micromechanical properties of *Pseudomonas aeruginosa* biofilms by Brillouin imaging. *NPJ Biofilms. Microbiomes.* 3, 20. doi: 10.1038/s41522-017-0028-z

Kondo, M., Aoki, M., Hirai, K., Sagami, T., Ito, R., Tsuzuki, M., et al. (2023). slr2103, a homolog of type-2 diacylglycerol acyltransferase genes, for plastoquinone-related neutral lipid synthesis and NaCl-stress acclimatization in a cyanobacterium, Synechocystis sp. PCC 6803. *Front. Plant Sci.* 14, 1181180. doi: 10.3389/fpls.2023.1181180

Li, L., Jing, X.-l., Wang, L., Zeng, Z.-g., Chen, W.-h., Zhai, J.-h., et al. (2020). The extract of aquatic macrophyte Carex cinerascens induced colony formation in bloom-forming cyanobacterium *Microcystis aeruginosa*. *Environ. Sci. pollut. Res.* 27, 42276–42282. doi: 10.1007/s11356-020-08651-1

Liu, L., Huang, Q., and Qin, B. (2018). Characteristics and roles of *Microcystis* extracellular polymeric substances (EPS) in cyanobacterial blooms: a short review. *J. Freshw. Ecol.* 33, 183–193. doi: 10.1080/02705060.2017.1391722

Liu, L., Huang, Q., Qin, B., Zhu, G., Wu, P., and Wu, Y. (2016). Characterizing cell surface of blooming *Microcystis* in Lake Taihu, China. *Water Sci. Technol.* 73, 2731–2738. doi: 10.2166/wst.2016.069

Ma, X., Li, M., Jiang, E., Pan, B., and Gao, L. (2021). Humic acid inhibits colony formation of the cyanobacterium *Microcystis* at high level of iron. *Chemosphere* 281, 130742. doi: 10.1016/j.chemosphere.2021.130742

Omori, K., Datta, T., Amano, Y., and Machida, M. (2019). Effects of different types of extracellular polysaccharides isolated from cyanobacterial blooms on the colony formation of unicellular *Microcystis aeruginosa*. *Environ. Sci. pollut. Res.* 26, 3741–3750. doi: 10.1007/s11356-018-3892-z

Otsuka, S., Suda, S., Li, R. H., Matsumoto, S., and Watanabe, M. M. (2000). Morphological variability of colonies of *Microcystis* morphospecies in culture. *J. Gen. Appl. Microbiol.* 46, 39–50. doi: 10.2323/jgam.46.39

Schachtsiek, M., Hammes, W. P., and Hertel, C. (2004). Characterization of *Lactobacillus coryniformis* DSM 20001$^T$ surface protein Cpf mediating coaggregation with and aggregation among pathogens. *Appl. Environ. Microbiol.* 70, 7078–7085. doi: 10.1128/AEM.70.12.7078-7085.2004

Sigee, D. C., Selwyn, A., Gallois, P.Phycologia, A.P.D.J (2007). Patterns of cell death in freshwater colonial cyanobacteria during the late summer bloom. *Phycologia* 46, 284–292. doi: 10.2216/06-69.1

Stal, L. J. (2017). Gregarious cyanobacteria. *Environ. Microbiol.* 19, 2105–2109. doi: 10.1111/1462-2920.13739

Sun, Q., Zhu, W., Li, M., and Tan, X. (2016). Morphological changes of *Microcystis aeruginosa* colonies in culture. *J. Limnol.* 75, 14–23. doi: 10.4081/jlimnol.2015.1225

Šmarda, J., Šmajs, D., and Komrska, J. (2002). S-layers on cell walls of cyanobacteria. *Micron* 33, 257–277. doi: 10.1016/S0968-4328(01)00031-2

Tan, X., Shu, X., Duan, Z., and Parajuli, K. (2020). Two types of bound extracellular polysaccharides and their roles in shaping the size and tightness of *Microcystis* colonies. *J. Appl. Phycol.* 32, 255–262. doi: 10.1007/s10811-019-01937-z

Tattibayeva, Z. ,. C. A., Tazhibayeva, S., Kujawski, W., Zayadan, B., and Musabekov, K. (2022). Peculiarities of adsorption of Cr (VI) ions on the surface of Chlorella vulgaris ZBS1 algae cells. *Heliyon* 8, e10468. doi: 10.1016/j.heliyon.2022.e10468

Tsujimura, S., Tsukada, H., Nakahara, H., Nakajima, T., and Nishino, M. (2000). Seasonal variations of *Microcystis* populations in sediments of Lake Biwa, Japan. *Hydrobiologia* 434, 183–192. doi: 10.1023/A:1004077225916

Van Le, V., Srivastava, A., Ko, S.-R., Ahn, C.-Y., and Oh, H.-M. (2022). *Microcystis* colony formation: Extracellular polymeric substance, associated microorganisms, and its application. *Bioresour. Technol.* 360, 127610. doi: 10.1016/j.biortech.2022.127610

Visser, P. M., Ibelings, B. W., Mur, L. R., and Walsby, A. E. (2005). The ecophysiology of the harmful cyanobacterium *Microcystis*: Features explaining its success and measures for its control. *Harmful. Cyanobacteria.* 3, 109–142.

Wang, C., Wu, X., Tian, C., Li, Q., Tian, Y., Feng, B., et al. (2015). A quantitative protocol for rapid analysis of cell density and size distribution of pelagic and benthic *Microcystis* colonies by FlowCAM. *J. Appl. Phycol.* 27, 711–720. doi: 10.1007/s10811-014-0352-0

Wang, X., and Xing, S. (2009). Determination of protein guantitation using the method of coomassie brilliant blue. *Tianjin. Chem. Industry.* 3), 3.

Wang, H., Zhu, R., Zhang, J., Ni, L., Shen, H., and Xie, P. (2018). A novel and convenient method for early warning of algal cell density by chlorophyll fluorescence parameters and its application in a highland lake. *Front. Plant Sci.* 9. doi: 10.3389/fpls.2018.00869

Wei, K., Amano, Y., and Machida, M. (2020). Impacts of different extracellular polysaccharides on colony formation and buoyancy of *Microcystis aeruginosa*. *Annales. Limnologic-International. J. Limnol.* 56, 8. doi: 10.1051/limn/2020026

Wei, K., Amano, Y., and Machida, M. (2021). The Effect of pH and Light on the Colony Formation and Buoyancy of *Microcystis aeruginosa* UTEX-2061. *Water Air. Soil pollut.* 232. doi: 10.1007/s11270-021-05066-7

Wu, X., Joyce, E. M., and Mason, T. (2012). Evaluation of the mechanisms of the effect of ultrasound on *Microcystis aeruginosa* at different ultrasonic frequencies. *Water Res.* 46, 2851–2858. doi: 10.1016/j.watres.2012.02.019

Wu, X., Noss, C., Liu, L., and Lorke, A. (2019b). Effects of small-scale turbulence at the air-water interface on *microcystis* surface scum formation. *Water Res.* 167, 115091. doi: 10.1016/j.watres.2019.115091

Wu, Z.-X., and Song, L.-R. (2008). Physiological comparison between colonial and unicellular forms of *Microcystis aeruginosa* Kutz. (Cyanobacteria). *Phycologia* 47, 98–104. doi: 10.2216/07-49.1

Wu, H., Yang, T., Wang, C., Tian, C., Donde, O. O., Xiao, B., et al. (2020). Co-regulatory role of *Microcystis* colony cell volume and compactness in buoyancy during the growth stage. *Environ. Sci. pollut. Res.* 27, 42313–42323. doi: 10.1007/s11356-020-08250-0

Wu, Q., Zhang, X., Jia, S., Li, J., and Li, P. (2019a). Effects of the cultivable bacteria attached to *Microcystis* colonies on the colony size and growth of *Microcystis*. *J. Freshw. Ecol.* 34, 663–673. doi: 10.1080/02705060.2019.1665115

Xiao, Y., Gan, N., Liu, J., Zheng, L., and Song, L. (2012). Heterogeneity of buoyancy in response to light between two buoyant types of cyanobacterium *Microcystis*. *Hydrobiologia* No.1), 297–311. doi: 10.1007/s10750-011-0894-y

Xiao, M., Li, M., Duan, P., Qu, Z., and Wu, H. (2019). Insights into the relationship between colony formation and extracellular polymeric substances (EPS) composition of the cyanobacterium *Microcystis* spp. *Harmful. Algae.* 83, 34–41. doi: 10.1016/j.hal.2019.02.006

Xiao, M., Li, M., and Reynolds, C. S. (2018). Colony formation in the cyanobacterium *Microcystis*. *Biol. Rev.* 93, 1399–1420. doi: 10.1111/brv.12401

Xiao, M., Willis, A., Burford, M. A., and Li, M. (2017). Review: a meta-analysis comparing cell-division and cell-adhesion in *Microcystis* colony formation. *Harmful. Algae.* 67, 85–91. doi: 10.1016/j.hal.2017.06.007

Xu, G., Zhang, Y., Yang, T., Wu, H., Lorke, A., Pan, M., et al. (2023). Effect of light-mediated variations of colony morphology on the buoyancy regulation of *Microcystis* colonies. *Water Res.* 235, 119839. doi: 10.1016/j.watres.2023.119839

Xu, F., Zhu, W., Xiao, M., and Li, M. (2016). Interspecific variation in extracellular polysaccharide content and colony formation of *Microcystis* spp. cultured under different light intensities and temperatures. *J. Appl. Phycol.* 28, 1533–1541. doi: 10.1007/s10811-015-0707-1

Yamamoto, Y., Shiah, F.-K., and Chen, Y.-L. (2011). Importance of large colony formation in bloom-forming cyanobacteria to dominate in eutrophic ponds. *Annales. Limnologie-International. J. Limnol.* 47, 167–173. doi: 10.1051/limn/2011013

Yang, R., He, X. Q., Niu, G. L., Meng, F. F., Lu, Q., Liu, Z. Q., et al. (2021). A single fluorescent pH probe for simultaneous two-color visualization of nuclei and mitochondria and monitoring cell apoptosis. *ACS Sensors.* 6, 1552–1559. doi: 10.1021/acssensors.0c02372

Yang, Z., and Kong, F. (2012). Formation of large colonies: a defense mechanism of *Microcystis aeruginosa* under continuous grazing pressure by flagellate Ochromonas sp. *J. Phycol.* 71, 61–66. doi: 10.4081/jlimnol.2012.e5

Yang, Z., Kong, F., Shi, X., Zhang, M., Xing, P., and Cao, H. (2008). Changes in the morphology and polysaccharide content of *Microcystis aeruginosa* (cyanobacteria) during flagellate grazing. *J. Phycol.* No.3), 716–720. doi: 10.1111/j.1529-8817.2008.00502.x

Ye, Z.-P., Stirbet, A., An, T., Robakowski, P., Kang, H.-J., Yang, X.-L., et al. (2023). Investigation on absorption cross-section of photosynthetic pigment molecules based on a mechanistic model of the photosynthetic electron flow-light response in C3, C4 species and cyanobacteria grown under various conditions. *Front. Plant Sci.* 14, 1234462. doi: 10.3389/fpls.2023.1234462

Yu, G., Song, L., and Li, L. (2007). Discussion on taxonomy of common freshwater *microcystis* in China: A case study of Dianchi Lake. *J. Syst. Evol.* 45, 727–741.

Zhang, M., Kong, F., Tan, X., Yang, Z., Cao, H., and Xing, P. (2007). Biochemical, morphological, and genetic variations in *Microcystis aeruginosa* due to colony disaggregation. *World J. Microbiol. Biotechnol.* 23, 663–670. doi: 10.1007/s11274-006-9280-8

Zhang, L., Yang, J., Liu, L., Wang, N., Sun, Y., Huang, Y., et al. (2021). Simultaneous removal of colonial *Microcystis* and microcystins by protozoa grazing coupled with ultrasound treatment. *J. Hazardous. Mater.* 420, 126616. doi: 10.1016/j.jhazmat.2021.126616

Zhao, W., Zhao, P., Tian, Y., Shen, C., Li, Z., and Jin, C. (2019). Transport and retention of *Microcystis aeruginosa* in porous media: Impacts of ionic strength, flow rate, media size and pre-oxidization. *Water Res.* 162, 277–287. doi: 10.1016/j.watres.2019.07.001

Zu, Y., Hong, S., Xu, C., Li, W., Chen, S., and Li, J. (2020). Cell wall surface layer (S-layer) promotes colony formation in *Microcystis*: comparison of S-layer characteristics between colonial and unicellular forms of *Microcystis* and function conformation. *Environ. Sci. pollut. Res.* 27, 42254–42263. doi: 10.1007/s11356-020-08254-w

frontiers | Frontiers in Plant Science

TYPE Original Research
PUBLISHED 11 March 2024
DOI 10.3389/fpls.2024.1370874



OPEN ACCESS

EDITED BY
Qiang Yang,
German Centre for Integrative Biodiversity Research (iDiv), Germany

REVIEWED BY
Ming Li,
Northwest A&F University, China
Jihai Shao,
Hunan Agricultural University, China
Qichao Zhou,
Yunnan University, China
Zhe Lu,
Chinese Academy of Sciences (CAS), China

*CORRESPONDENCE
Huaming Wu
wu.h@rptu.de
Xingqiang Wu
xqwu@ihb.ac.cn

RECEIVED 15 January 2024
ACCEPTED 28 February 2024
PUBLISHED 11 March 2024

CITATION
Wu H, Wu X, Rovelli L and Lorke A (2024) Dynamics of *Microcystis* surface scum formation under different wind conditions: the role of hydrodynamic processes at the air-water interface. *Front. Plant Sci.* 15:1370874. doi: 10.3389/fpls.2024.1370874



# Dynamics of *Microcystis* surface scum formation under different wind conditions: the role of hydrodynamic processes at the air-water interface

Huaming Wu[1]*, Xingqiang Wu[2]*, Lorenzo Rovelli[1,3] and Andreas Lorke[1]

[1]Institute for Environmental Sciences, University of Kaiserslautern-Landau (RPTU), Landau, Germany, [2]Key Laboratory of Algal Biology of Chinese Academy of Sciences, Institute of Hydrobiology, Chinese Academy of Sciences, Wuhan, China, [3]Now at the Department of Ecology, Federal Institute of Hydrology - BfG, Koblenz, Germany

Due to climate change, *Microcystis* blooms occur at increasing frequencies in aquatic ecosystems worldwide. Wind-generated turbulence is a crucial environmental stressor that can vertically disperse the *Microcystis* surface scum, reducing its light availability. Yet, the interactions of *Microcystis* scum with the wind-generated hydrodynamic processes, particularly those at the air-water interface, remain poorly understood. Here, we explore the response of *Microcystis* (including colony size and migration dynamics) to varying magnitudes and durations of intermittent wind disturbances in a mesocosm system. The flow velocities, size of *Microcystis* colonies, and the areal coverage of the water surface by scum were measured through video observations. Our results demonstrate that low wind speeds increase colony size by providing a stable condition where *Microcystis* forms a scum layer and aggregates into large colonies at the air-water interface. In contrast, wind disturbances disperse scum and generate turbulence, resulting in smaller colonies with higher magnitudes of wind disturbance. We observed that surface scum can form rapidly following a long period (6 h) of high-magnitude (4.5 m $s^{-1}$) wind disturbance. Furthermore, our results indicate reduced water surface tension caused by the presence of *Microcystis*, which can decrease surface flow velocity and counteract wind-driven mixing. The reduced surface tension may also drive lateral convection at the water surface. These findings suggest that *Microcystis* reduces surface tension, likely by releasing surface-active materials, as an adaptive response to various wind conditions. This could result in an increased rate of surface scum re-formation under wind conditions and potentially facilitate the lateral expansion of scum patches during weak wind periods. This study reveals new insights into how *Microcystis* copes with different wind conditions and highlights the importance of the air-water interface for *Microcystis* scum dynamics.

KEYWORDS

**aquatic ecosystems, cyanobacterial blooms, wind disturbance, surface tension, biological-physical interactions, capillary force**

## Highlights

- Larger colony size of *Microcystis* at low wind speed
- Rapid formation of scum after strong wind disturbances
- Increasing re-formation rate of surface scum during recurring disturbances
- Increasing biomass of *Microcystis* leads to reduction of water surface tension
- Reduced surface tension can be advantageous for *Microcystis* surface scum

## 1 Introduction

Cyanobacterial blooms have been becoming a globally relevant threat to the ecological integrity of inland and coastal waters (Huisman et al., 2018; Ho et al., 2019). As one of the most common and ubiquitous cyanobacterial genera, *Microcystis* spp. can float upward to the water surface and form dense surface scum, i.e., visible mucilaginous cyanobacteria accumulating at the water surface (Oliver, 1994), disrupting the functioning of aquatic ecosystems.

Buoyancy regulation is an important cellular feature that enables *Microcystis* spp. to maintain their position at the water surface and form surface scum (Reynolds, 1987; Oliver, 1994). The buoyancy of *Microcystis* can be modulated by (i) the carbon-reserve metabolism, i.e., the accumulation of intracellular carbohydrates (Visser et al., 1997), (ii) the synthesis and collapse of gas-vesicles in the cells (Dunton and Walsby, 2005), (iii) the formation of colonies, i.e., aggregations of *Microcystis* cells embedded in a mucilaginous matrix, and (iv) trapping of gas bubbles within the colonies (Dervaux et al., 2015; Aparicio Medrano et al., 2016). The colony size of *Microcystis* is considered an important factor for surface scum formation as their floatation velocity increases with increasing colony size (Xiao et al., 2018; Wu et al., 2020).

Disturbances induced by wind are among the most important stressors that counteract scum formation (George and Edwards, 1976). Wind-generated turbulence can vertically disperse surface scum to deeper depths and reduce the light availability for *Microcystis* when the wind speed exceeds a critical value (2.6-3 m $s^{-1}$) (Cao et al., 2006; Wu et al., 2015). Below the critical wind speed, wind-generated flow leads to the accumulation of *Microcystis* in downwind areas of the basin (Chen et al., 2023). Although the flows generated by wind, including basin-scale circulation, waves and turbulent eddies exceed the size of *Microcystis* colonies by far, these motions are coupled through the turbulent cascade to the small-scale viscous environment of cells and colonies (Regel et al., 2004). Although wind disturbances at appropriate magnitudes can promote the aggregation of *Microcystis* colonies, continuous wind disturbances act as stressors by inhibiting growth and their aggregation through shear forces (O'Brien et al., 2004; Liu et al., 2019; Zhao et al., 2020).

The above studies have primarily focused on bulk water, without considering the presence of a free-water surface, i.e., the air-water interface. The physicochemical and biological properties at the water surface are measurably distinct from those in the underlying water, and various physical processes, such as momentum transfer from wind to water, wind-generated wave, and capillary effect can occur (Vella and Mahadevan, 2005; Cunliffe et al., 2013). For example, current knowledge focuses on how wind-generated turbulence in the water column affects colony size dynamics, but often overlooks the frequent aggregation of *Microcystis* at the water surface during low wind periods. This is due to a lack of understanding of aggregation mechanisms at the water surface and their role in colony size dynamics. Neglecting the aggregation of colonies at the water surface may lead to an overestimation of the role of colony size in surface scum formation, as larger colonies in the epilimnion are often considered as a cause (Zhu et al., 2014), instead of being the consequence of surface scum formation.

Current understandings of the interactions between *Microcystis* and wind-generated hydrodynamic processes are largely one-way, neglecting the potential feedback of *Microcystis* on hydrodynamics. Studies have revealed that phytoplankton can affect the physical properties of water; Dervaux et al. (2015) observed non-Newtonian behavior of algal suspensions at low shear stress, with viscosity increasing by three orders of magnitude. Additionally, proteins extracted from algae can reduce interfacial tension at the air-water interface, even at relatively low bulk concentrations (Chronakis et al., 2000). They attributed these findings to the release of extracellular polymeric substances (EPSs) by phytoplankton. The alteration in physical properties of water resulting from the released EPSs could be a response of phytoplankton to stressors, constituting two-way interactions between *Microcystis* and wind-generated hydrodynamic processes. However, these interactions have rarely been studied.

As a result of climate change, wind speeds are expected to decrease in some regions under future climates (Vautard et al., 2010; Ranjbar et al., 2022), necessitating the testing of how *Microcystis* responds to different magnitudes and durations of intermittent wind disturbances. In this study, we conducted laboratory experiments in annular flumes, in which wind-driven flow was simulated by controlled air circulation above the water surface. Different magnitudes of wind forcing (0.5, 1.5, 3.8, and 4.5 m $s^{-1}$) and durations of their periodic occurrence (3 and 6 h) were used to simulate the periodic formation, development, dissipation and re-formation of surface scum over a period of seven days. We hypothesized that *Microcystis* surface scum can interact with the hydrodynamic processes at the air-water interface by affecting the physical properties of water, i.e., water surface tension. The experiments aimed at (i) studying the response of colony size and surface scum dynamics of *Microcystis* to wind-generated turbulence, and (ii) exploring the effect of *Microcystis* surface scum on hydrodynamic processes mediated by surface tension. The results of this study are expected to be instrumental in the mechanistic and process-based understanding of surface scum dynamics.

# 2 Materials and methods

## 2.1 Source of material

A stock of phytoplankton (approximately 90% of the phytoplankton was *Microcystis aeruginosa* by microscopic observation) was collected from the Moselle River in southwest Germany on 9 August 2022 during a heavy *Microcystis* bloom. Colonies were collected from the water surface using a silk plankton net with a 40 µm mesh size. To select predominantly *Microcystis* colonies, the samples were first filtered through a 500 µm sieve to remove large particles and then through a 40 µm sieve. The filtered *Microcystis* colonies with sizes between 40 and 500 µm were stored and cultured at 20 ± 1°C and photosynthetically active radiation (PAR) of 15 µmol photons $s^{-1}$ $m^{-2}$.

## 2.2 Experimental design

### 2.2.1 Flume experiments

The dynamics of *Microcystis* colonies under different wind conditions were studied in five annular flumes with outer and inner diameters of 700 and 560 mm (Supplementary Figure S1). The light intensity and wind speed were varied in individual flumes. Flow velocities and *Microcystis* colonies were observed in video recordings with digital cameras (Raspberry Pi HQ Camera, United Kingdom, 1080p, 30 fps) at the water surface and at three different depths (near the water surface at 0 – 6 cm depth, in a middle layer at 12 – 18 cm depth and close to the flume bottom at 24 – 30 cm depth). All operations, including environmental settings (i.e., wind and light) and video recordings (i.e., cameras and laser light sheet for underwater illumination) were fully automated and computer-controlled (see Supplementary Figure S1 for details).

Before the experiment, all flumes were sterilized for 30 min using an ozone generator. The flumes were then filled with distilled water (volume: ~ 41.5 L, water height: ~ 30 cm) before a nutrient stock solution (BG-11, see Supplementary Table S1 for details) and *Microcystis* colonies were added to the five flumes. The final concentration of nutrients in the flumes was 10% (v/v) of BG-11 medium. Optical density at a wavelength of 680 nm ($OD_{680}$) was used as a proxy for *Microcystis* biomass (Lv et al., 2018; Wu et al., 2019) and measured by a spectrophotometer (Novaspec II, Amersham Pharmacia Biotech Inc, UK). The initial optical density (at 680 nm) of *Microcystis* in the flumes was 0.05 ± 0.01, which corresponds to an approximate cell density of 7.9 ×$10^5$ cells $mL^{-1}$ (Lv et al., 2018).

During the following 7-day experimental period, different magnitudes (0.5, 1.5, 3.8, 4.5 m $s^{-1}$) and durations (3 and 6 h) of intermittent wind forcing were applied in the flumes at a constant water temperature of 22.3 ± 1.0°C. The chosen temperature is within the range of water temperatures for which *Microcystis* blooms were observed under field conditions (18 - 24°C, Feng et al., 2019). No temperature difference between the water surface, the middle layer and the bottom of the flume was observed. Two different wind forcing (high wind speed and low wind speed) were applied alternately for two different durations. The wind speed was measured 2 cm above the water surface at a location between the two fans using a hot-wire anemometer (Testo 425, Germany). The high wind speed in the flumes F1 – F5 was 4.5, 4.5, 3.8, 1.5, and 1.5 m $s^{-1}$, respectively, whereas a wind speed of 0.5 m $s^{-1}$ was used in all flumes during the low wind periods (Figure 1). The high wind speed periods were defined as wind disturbances. Due to **a** technical issue, the experiment in F4 started at 11:00 on Day 2. Surface waves were observed in our experiment during wind disturbances; the amplitudes of the waves were determined to be < 8 mm through visual estimates using video footage. Due to the differing aerodynamic characteristics between the flume and the atmosphere, it is not easy to directly compare the airflow generated in the flumes with wind velocities measured in the atmospheric boundary layer above water surfaces. We estimated an equivalent wind speed in the atmospheric boundary layer at a standard height of 10 m ($U_{10}$) from observed surface flow velocities ($U_0$, described below) using a fixed wind factor (the ratio of wind speed at 10 m to the surface flow velocity of water, $f$ = 0.01 [Wu, 1975)] as $U_{10}=U_0/f$.

We applied a diurnal light cycle (12:12 h light: dark periods) to all flumes. To simulate the light conditions in the field, the irradiance at the water surface was modulated as a sinusoidal function with a maximum irradiance of 800 µmol photons $m^{-2}$ $s^{-1}$ and truncated to zero for the nights (18:00 – 6:00) in induvial flumes (Figure 1). We defined the period 0:00 – 12:00 as stage I and the period 12:00 – 24:00 as stage II.

Videos were recorded at hourly intervals for estimating the surface flow velocity and areal coverage of the water surface with *Microcystis*. In addition, flow velocities and size of *Microcystis* colonies were observed at three different depths in the bulk water. The biomass of *Microcystis* colonies at the water surface and in the

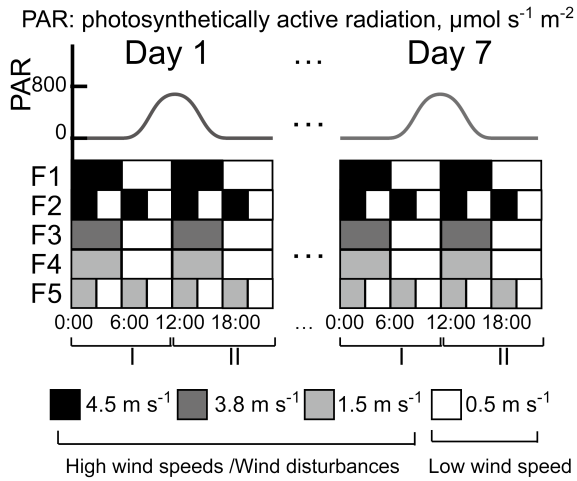


FIGURE 1
Diurnal variations of photosynthetically active radiation (PAR, upper panel) and wind speed (lower panel) in the five flumes (F1 – F5) during the 7-day experiment. The morning period (0:00 to 12:00) was defined as stage I and the afternoon (12:00 to 24:00) was defined as stage II. The wind speeds of 4.5, 3.8 and 1.5 m $s^{-1}$ were defined as high wind speeds and the wind speed of 0.5 m $s^{-1}$ was defined as low wind speed.

bulk water (~15 cm depth) were daily measured during 9:00- 11:00 am (low wind periods).

### 2.2.2 Supplementary experiment

Due to the sampling difficulties caused by strong heterogeneity in the surface scum layer and dispersal of surfactant molecules during sampling, surface tension measurements could not be conducted under the prevailing flow conditions in the flume experiment. Consequently, we conducted an additional experiment to investigate the relationship between surface tension and *Microcystis* biomass. We measured the $OD_{680}$ (as described above) and surface tension (using the Wilhelmy plate method with a tensiometer (TC1, Lauda Scientific, Germany)) of various *Microcystis* samples at different dilution factors (0%,1.5%, 3%, 6%, 9%, 15%, 75% and 100%). To ensure the $OD_{680}$ did not exceed the detection limit of the spectrophotometer, the $OD_{680}$ of algal samples higher than 0.3 were diluted 10 – 50 times, and then the $OD_{680}$ of algal samples was calculated from $OD_{680}$ of the diluted samples multiplied by the dilution factor.

## 2.3 Parameters of *Microcystis* and hydrodynamics measurements

Time-resolved observations of *Microcystis* colonies were obtained from video observations of the water surface using a down-looking digital camera (for the observation of surface scum and velocities of *Microcystis*) and of the bulk water (at depths of 0 – 4 cm, 12 – 16 cm and 26 – 30 cm) using side-looking cameras (for the observation of colony size and velocities of *Microcystis*). Videos of 90 s duration were hourly recorded. During the recordings at the water surface, illumination was provided by an LED spotlight, while during the recordings of the side-looking cameras, illumination in the bulk water was provided by a vertically oriented laser light sheet, which illuminated a central plane of the flow channel using a continuous-wave line laser (InLine HP, MediaLas, Germany; output power: 500 mW, green, 532 nm). Colonies within the approximately 3 mm thick light sheet were observed using three digital cameras in a perpendicular arrangement (Supplementary Figure S1). The resolution and field of view of the videos recorded by the cameras used in the experiments are shown in Supplementary Table S2.

Individual *Microcystis* colonies were detected in each image based on intensity thresholds during automated image processing. The analysis provided surface areal coverage of *Microcystis* (SAC, calculated as the percentage of water surface that was covered by colonies) for down-looking cameras, the equivalent spherical diameter of colonies for side-looking cameras, as well as colony velocities estimated using particle tracking velocimetry (Kelley and Ouellette, 2011). We estimated and summed up the area covered by the colonies for each frame, which was then divided by the camera's field of view to calculate the SAC. The change rate of surface areal coverage (dSAC/dt) during low wind periods, representing the reformation rate of surface scum, was estimated by the difference of mean SAC between subsequent recordings. The volumetric median colony diameter ($D_{v50}$, i.e., the colony size corresponding to the 50$^{th}$ percentile of observed colony volumes) was used to characterize the average colony size as described in Wu et al. (2019) and Wu et al. (2020). More than 300 colonies on each of the videos were used to estimate $D_{v50}$. The rate of change of colony size ($dD_{v50}$/dt) was used to characterize the aggregation or disaggregation of colonies. Since surface scum formed during low wind periods and was dispersed during wind disturbances, the $D_{v50}$ near the water surface at the beginning of a wind disturbance, when the surface scum layer was dispersed, was considered as a representative colony size at the water surface. To compare the colony size dynamics at the water surface and in the bulk water, $dD_{v50}$/dt in the bulk water was estimated as the difference of mean $D_{v50}$ near the water surface during wind disturbances between subsequent recordings. The $dD_{v50}$/dt at the water surface was estimated by the ratio of the difference of mean $D_{v50}$ near the water surface between the beginning of the wind disturbance and the end of the preceding wind disturbance to the duration of the wind disturbance.

The mean velocities of colonies at the water surface and in the bulk water were estimated by observing the displacement of identified colonies via particle tracking velocimetry, using the predictive tracking algorithm described by Kelley and Ouellette (2011).

We did not observe a consistent size-dependence of colony velocities (Supplementary Figure S2) and therefore considered the observed colony velocities as a proxy for flow velocity.

We use root-mean-square velocity fluctuations ($U_{rms}$) as the measure of the intensity of turbulence, which scales with the square root of turbulence kinetic energy, and is calculated as:

$$U_{rms} = \sqrt{\frac{1}{2}(\overline{(u')^2} + \overline{(v')^2})} \quad (1)$$

where the fluctuating velocity components of the horizontal ($u'$) and vertical ($v'$) flow velocities are the difference between the instantaneous and the temporarily averaged velocities (Reynolds decomposition: $u' = u - \bar{u}$ and $v' = v - \bar{v}$). The temporarily averaged velocity was calculated by averaging the velocities of all colonies in each video.

## 2.4 Statistical analyses

Shapiro-Wilk test was used to assess the normality of data. A *post hoc* LSD (least significant difference) test with one-way ANOVA was used to compare the surface areal coverage (SAC) and the flow velocity during low wind periods at different depths at both stages among the different flumes if the data were normally distributed with homogeneous variance, otherwise, Kruskal-Wallis tests were used. The differences in $D_{v50}$ of colonies among different flumes as well as the difference between the rate of colony size change ($dD_{v50}$/dt) at the water surface and in the bulk water were compared using the student *t*-test. The relationships between mean SAC and $D_{v50}$, mean SAC and $dD_{v50}$/d*t*, normalized flow velocity and SAC as well as between rate of change in SAC and time were fitted by linear regressions. All statistical analyses were performed using the software package SPSS 27.0 (IBM Corp, USA). Data are

presented as mean ± standard deviation and were tested for statistical significance at a significance level ($p$) of 0.05 unless stated otherwise.

# 3 Results

## 3.1 Dynamics of *Microcystis* surface scum formation

Surface scum layers developed during low wind periods and disappeared during wind disturbance over the seven-day experimental period (Figure 2). During wind disturbances (1.5 – 4.5 m $s^{-1}$), the areal coverage of the water surface with *Microcystis* colonies was generally < 1%, whereas it increased during low wind period (0.5 m $s^{-1}$) gradually from 0.1 to 25% from Day 1 to Day 7. The observed rates of change in SAC (dSAC/dt) and rates of change in SAC per unit biomass (dSAC/($OD_{680}$ dt)) during low wind speed linearly increased over time ($p$ < 0.05, Figure 3), suggesting that the surface scum recovered from wind disturbances at increasing rates. Similar to surface coverage, the biomass of *Microcystis* colonies in the thin surface layer showed a 2 - 6 fold increase from Day 1 to Day 7 (Supplementary Figure S3A).

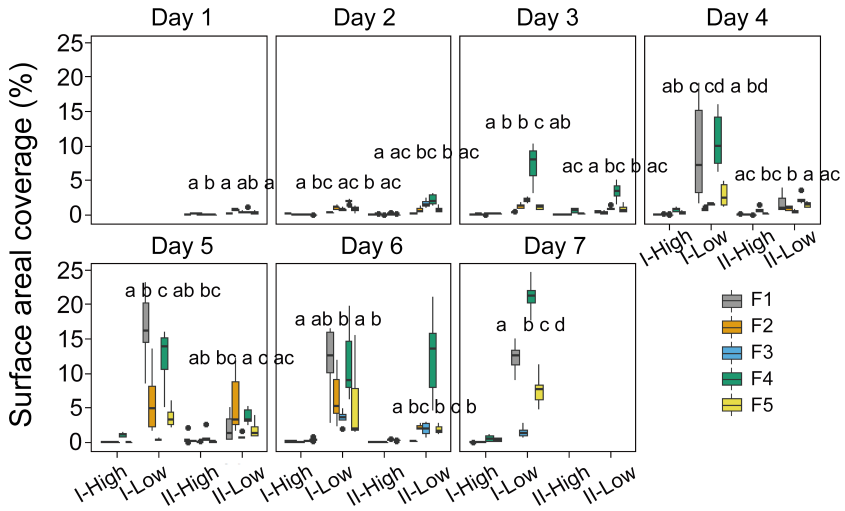


FIGURE 2
Temporal dynamics of the surface areal coverage of *Microcystis* colonies in different stages (I and II) and experimental flumes (F1 – F5, see legend for color assignment). High and Low represent the periods of high wind speed (wind disturbances, 4.5 m $s^{-1}$ for F1 and F2, 3.8 m $s^{-1}$ for F3, 1.5 m $s^{-1}$ for F4 and F5) and low wind speed (0.5 m $s^{-1}$), respectively. Different panels denote the time (day) after the start of the experiment. Each box plot shows the mean surface areal coverage observed in the hourly video observations ($n$=6). Different letters on top of the box plots indicate significant differences ($p$ < 0.05) in surface areal coverage during low wind periods between different groups at each stage, while the same or no letter indicates no significant difference (Kruskal-Wallis tests). F1: 6 h of high-magnitude (4.5 $m^{-1}$) wind disturbance; F2: 3 h of high-magnitude wind disturbance; F3: 6 h of moderate-magnitude (3.8 $m^{-1}$) wind disturbance; F4: 6 h of low-magnitude (1.5 $m^{-1}$) wind disturbance; F5: 3 h of low-magnitude wind disturbance.

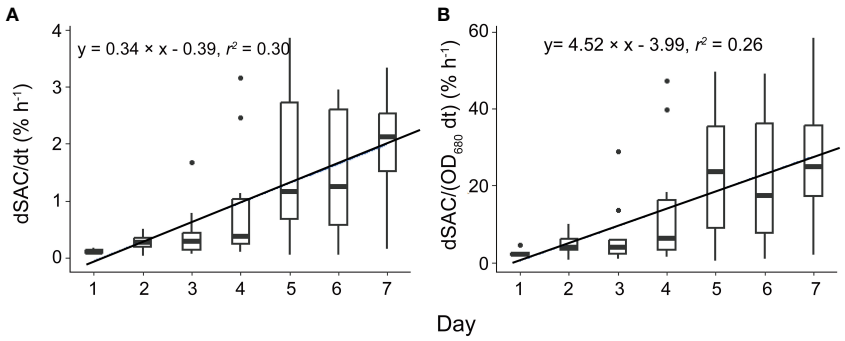


FIGURE 3
The temporal change of the rate of change in scum areal coverage (**A**, dSAC/dt) and the rate of change in scum areal coverage per unit biomass [**B**, dSAC/($OD_{680}$ dt)]. Significant linear relationships between dSAC/dt as well as dSAC/($OD_{680}$ dt) and time were observed ($p$ < 0.05). Each box plot shows the dSAC/dt or dSAC/($OD_{680}$ dt). Both solid lines represent linear regressions based on the equations provided in the legend, with a significance level of $p$ < 0.05. F1: 6 h of high-magnitude (4.5 $m^{-1}$) wind disturbance; F2: 3 h of high-magnitude wind disturbance; F3: 6 h of moderate-magnitude (3.8 $m^{-1}$) wind disturbance; F4: 6 h of low-magnitude (1.5 $m^{-1}$) wind disturbance; F5: 3 h of low-magnitude wind disturbance.

The formation of surface scum followed a diurnal pattern with the average surface coverage during low wind periods in the afternoon (stage II) being reduced by 87.7%, 36.6%, 31.3%, 44.5% and 51.1% (for F1 – F5) in comparison to that in the morning (stage I) (Figure 2).

The dynamics of surface scum formation varied in dependence on wind conditions (Figure 2). The prolonged duration of low wind periods promoted scum formation: the surface coverage in flumes F1 and F4 was significantly higher than that in F2 and F5 in most cases ($p < 0.05$). Wind magnitudes of 4.5 and 1.5 m $s^{-1}$ promoted the subsequent surface scum formation, in comparison to the intermediate magnitude of 3.8 m $s^{-1}$: In most cases, the surface areal coverage in F1 and F4 was higher than that in F3 ($p < 0.05$).

## 3.2 Dynamics of *Microcystis* colony size

The colony size showed temporal trends during the 7-day experiment (Figure 4). In the upper layer near the water surface, $Dv_{50}$ increased from the beginning to Day 7 by a factor of 2.4, 3.1, 2.4, 4.4 and 2.7 in F1- F5, respectively. During the increase of $Dv_{50}$, we observed the peaks in $Dv_{50}$ of *Microcystis* colonies near the water surface at times when the wind speed changed from low to high from Day 3 – Day 7 (Figure 4). Through visual observations, we found that such larger colonies suddenly appearing in the bulk water resulted from wind-induced entrainment of surface scum patches forming during preceding low wind periods.

The mean rate of change in colony size ($dDv_{50}/dt$) at the water surface and in the bulk water is -0.12 and 0.14 mm $h^{-1}$, respectively. In each flume, the $dDv_{50}/dt$ at the water surface is significantly higher than that in the bulk water ($p < 0.05$, Figure 5). At the beginning of wind disturbances, both $Dv_{50}$ and $dDv_{50}/dt$ increased linearly with increasing SAC during the preceding low wind period (Figure 6).

The median diameter of *Microcystis* colonies ($Dv_{50}$) was affected by the different wind conditions (Figure 4). $Dv_{50}$ increased with decreasing magnitude of wind disturbances regardless of their duration (Figure 4). The response of $Dv_{50}$ to the duration of the wind disturbance was dependent on its magnitude, with longer duration of high-magnitude wind disturbances leading to decreased $Dv_{50}$ (F1 < F2, Figure 4), whereas $Dv_{50}$ increased for longer durations of low-magnitude wind disturbances (F4 > F5, Figure 4). The order of mean $Dv_{50}$ of *Microcystis* colonies near the water surface was F4>F5>F3>F2>F1 when combining all measurements ($p < 0.05$).

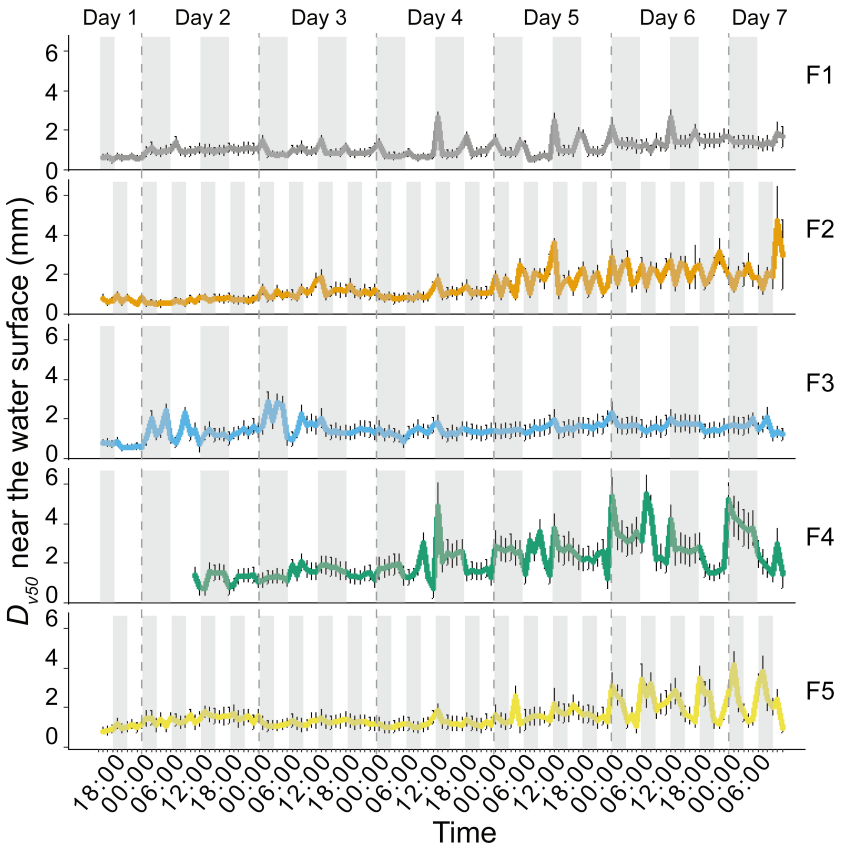


FIGURE 4
Temporal dynamics of the volume median diameter ($D_{v50}$) of *Microcystis* colonies near the water surface (0 - 6 cm depth) in different experimental flumes (F1 – F5, see legend for color assignment). Symbols show mean values and error bars are standard deviations. The periods of high wind speed (wind disturbances) were represented with gray shading. The initial lack of data in F4 was due to a technical issue. F1: 6 h of high-magnitude (4.5 $m^{-1}$) wind disturbance; F2: 3 h of high-magnitude wind disturbance; F3: 6 h of moderate-magnitude (3.8 $m^{-1}$) wind disturbance; F4: 6 h of low-magnitude (1.5 $m^{-1}$) wind disturbance; F5: 3 h of low-magnitude wind disturbance.

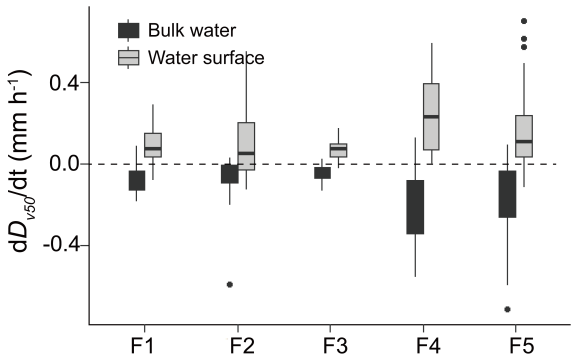


FIGURE 5
Rates of change in colony size ($dD_{v50}$/dt) at the water surface (grey-filled box plots) and in the bulk water (black-colored box plots) in different flumes (F1 – F5). The dashed horizontal line indicates the $dD_{v50}$/dt of 0 mm $h^{-1}$. Significant differences between $dD_{v50}$/dt at the water surface and in the bulk water were observedin all flumes (*t*-test, df=21 and 44, $p < 0.001$). F1: 6 h of high-magnitude (4.5 $m^{-1}$) wind disturbance; F2: 3 h of high-magnitude wind disturbance; F3: 6 h of moderate-magnitude (3.8 $m^{-1}$) wind disturbance; F4: 6 h of low-magnitude (1.5 $m^{-1}$) wind disturbance; F5: 3 h of low-magnitude wind disturbance.

## 3.3 Hydrodynamics under different wind conditions

At the beginning of the experiment, the surface flow velocities increased nearly linearly with the applied wind speed resulting in equivalent wind speeds in the atmospheric boundary layer ($U_{10}$) of 2.0 m $s^{-1}$ under low wind speed conditions and 2.8 to 5.3 m $s^{-1}$ during the simulated disturbances (Table 1).

The surface flow velocity and underwater flow velocities (at three depths) observed at a particular wind speed generally decreased from Day 1 to Day 7 (Supplementary Figure S4). The normalized flow velocity (defined as the ratio of flow velocity to wind speed) at the water surface and in the bulk water generally decreased linearly over time ($p < 0.05$, Supplementary Figure S5, Supplementary Table S3). In all flumes, the surface flow velocity and underwater flow velocities during low wind periods decreased to approximately 1 mm $s^{-1}$ on Day 7 (Figure 7).

At the applied wind speed of 0.5 m $s^{-1}$ (low wind periods), significant differences in surface flow velocity among different flumes were observed ($p$ <0.05, Figure 7). No consistent dependence of surface flow velocity on the duration of the intermittent wind disturbance was observed, while surface flow velocity during low wind periods generally increased with increasing preceding magnitudes of wind disturbance: The order of surface flow velocity during low wind periods was F1>F3>F4, except for Day 6 stage I and Day 7. Unlike the surface flow velocity, the underwater flow velocities during low wind periods did not differ significantly between different flumes in most cases (Supplementary Figure S6).

## 3.4 Relationship between *Microcystis* and hydrodynamic parameters

Higher SAC was primarily observed at low surface flow velocities (< 5 mm $s^{-1}$). However, it is noteworthy that SAC at moderate surface flow velocities (5-12 mm $s^{-1}$) on Day 3 – Day 6 could also surpass some SAC at low surface flow velocities (Supplementary Figure S7). Neither $Dv_{50}$ of colonies nor ($dDv_5$/dt) were linearly related to the root-mean-square velocities of colonies in the bulk water ($U_{rms}$, calculated using Equation 1) when combining all measurements (Supplementary Figure S8). However, the proportion of $dDv_{50}$/dt being smaller than -1 mm

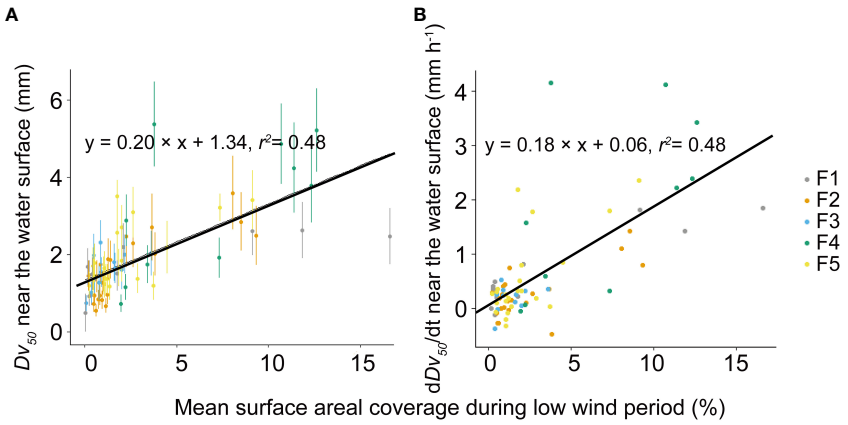


FIGURE 6
Relationship between the median diameter ($D_{v50}$) of *Microcystis* colonies near the water surface at the onset of high wind disturbances and mean surface areal coverage during the low wind period before the disturbance **(A)**. Relationship between the rate of change in the colony median diameter ($dD_{v50}$/dt) near the water surface at the onset of wind disturbances and mean surface areal coverage during low wind periods before the disturbance **(B)**. Symbols show mean values for different flumes (F1 – F5, see legend) and the error bars shown in **(A)** show the standard deviations. Both solid lines represent linear regressions based on the equations provided in the legend, with a significance level of $p < 0.05$. F1: 6 h of high-magnitude (4.5 $m^{-1}$) wind disturbance; F2: 3 h of high-magnitude wind disturbance; F3: 6 h of moderate-magnitude (3.8 $m^{-1}$) wind disturbance; F4: 6 h of low-magnitude (1.5 $m^{-1}$) wind disturbance; F5: 3 h of low-magnitude wind disturbance.

10.3389/fpls.2024.1370874

TABLE 1 Wind speed measured at 2 cm above the water surface in the flumes and the corresponding equivalent wind speed in the atmospheric boundary layer at 10 m height ($U_{10}$) derived from observed surface velocities at the beginning of the experiment using a wind factor of 0.01 (Wu, 1975).

| Wind speed measured in the flumes (m $s^{-1}$) | Calculated wind speed at 10 m height (m $s^{-1}$) | Magnitudes of wind disturbance |
|---|---|---|
| 0.5 | 2.0 ± 0.5 | No wind disturbance |
| 1.5 | 2.8 ± 0.2 | Low-magnitude |
| 3.8 | 3.9 ± 0.4 | Intermediate-magnitude |
| 4.5 | 5.3 ± 0.4 | High-magnitude |

$h^{-1}$ (indicating colony disaggregation) increased with increasing $U_{rms}$. Conversely, the proportion of $dDv_{50}/dt$ larger than 0.5 mm $h^{-1}$ (colony aggregation) decreased with increasing $U_{rms}$ when $U_{rms}$ exceeded 3 mm $s^{-1}$and increased with increasing $U_{rms}$ when $U_{rms}$ was smaller than 3 mm $s^{-1}$ (Supplementary Figure S9).

The presence of *Microcystis* affected the hydrodynamic parameters: In the flumes experiment, from Day 1 to Day 4, no linear relationships between the normalized flow velocity and SAC were found, but from Day 5 to Day 7, the normalized flow velocity decreased with increasing SAC ($p < 0.05$, Figure 8). The results of our supplementary dilution experiment showed that the surface tension decreased with the increasing optical density of *Microcystis* (Figure 9).

# 4 Discussion

## 4.1 The response of colony size and scum of *Microcystis* to wind-generated hydrodynamics

Our experiments successfully reproduced the periodical formation and dispersion of *Microcystis* surface scum under intermittent wind disturbances (Figure 2). During low wind periods (0.5 m $s^{-1}$), we observed gradually increased surface scum in all the flumes. Surprisingly, we found that scum was forming more rapidly following prolonged duration of high-magnitude wind disturbances compared to that following moderate magnitudes (F1, Figure 2). The differences in scum coverage in varying flumes can be attributed to the flow conditions, as they govern the migration of *Microcystis*. However, we found significant differences in flow velocities among flumes were only evident for the surface (Supplementary Figure S6; Figure 7), suggesting that the surface flow field likely played a pivotal role in modulating the response of scum formation to preceding wind disturbances.

Higher scum coverage can be observed at moderate surface flow velocities (5 - 12 mm $s^{-1}$) compared to lower surface flow velocities in some cases (Supplementary Figure S7). This result implies potential mechanisms for surface scum formation under moderate flow velocities, considering that surface scum is typically associated with lower flow conditions (Wu et al., 2015). Webster and Hutchinson (1994) suggested the trapping mechanisms of colonies by viscous sublayer. A possible explanation we proposed is the strong vertical velocity gradient

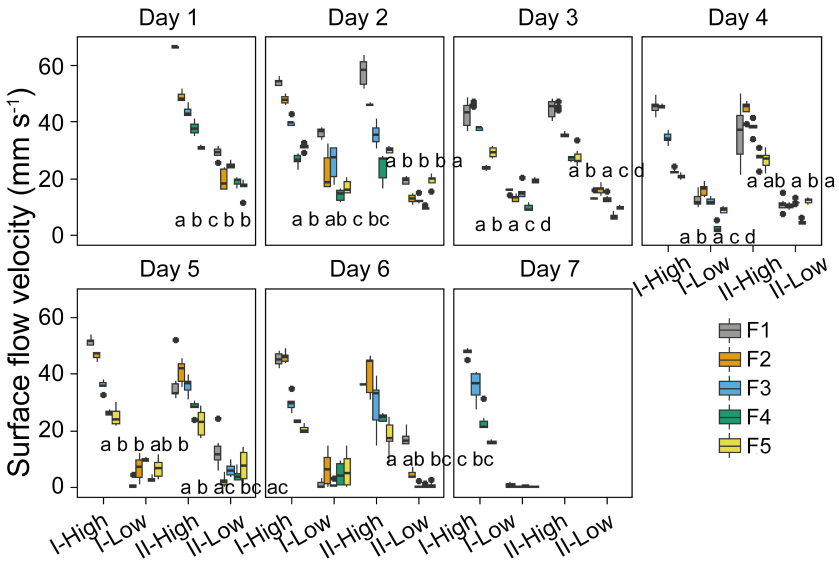


FIGURE 7
Temporal dynamics of the mean surface flow velocity in different stages (I and II) and experimental flumes (F1 – F5, see legend). High and Low represent periods of high wind speed (wind disturbances, 4.5 m $s^{-1}$ for F1 and F2, 3.8 m $s^{-1}$ for F3, 1.5 m $s^{-1}$ for F4 and F5) and low wind speed (0.5 m $s^{-1}$), respectively. Different panels denote the time (day) after the start of the experiment. Each box plot shows mean flow velocities observed in hourly video observations in the given stage in different flumes during the 7 days. Different lowercase letters indicate significant differences in flow velocity at different stages during low wind periods among different flumes, while the same letter, or the lack of a letter, indicates no significant differences. F1: 6 h of high-magnitude (4.5 $m^{-1}$) wind disturbance; F2: 3 h of high-magnitude wind disturbance; F3: 6 h of moderate-magnitude (3.8 $m^{-1}$) wind disturbance; F4: 6 h of low-magnitude (1.5 $m^{-1}$) wind disturbance; F5: 3 h of low-magnitude wind disturbance.

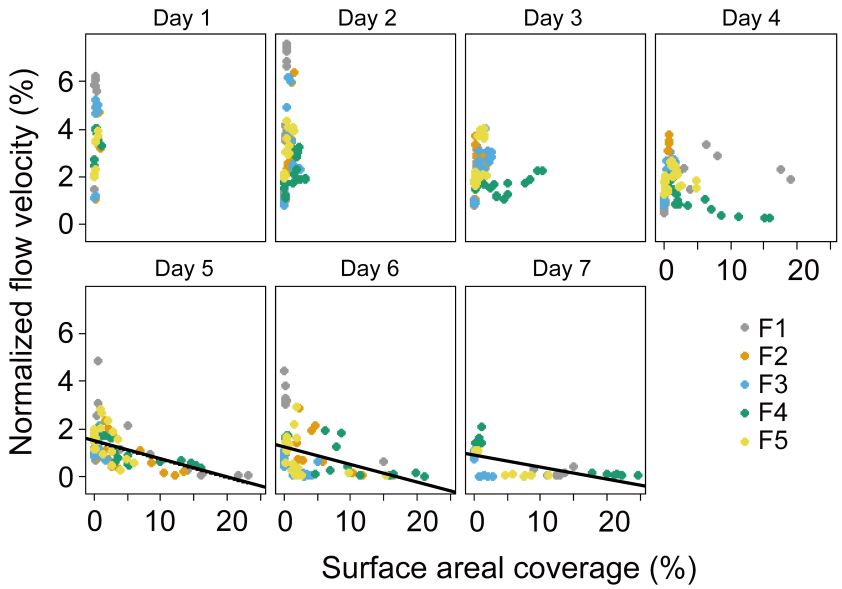


FIGURE 8
Normalized surface flow velocities (ratio of surface flow speed to wind speed) versus areal coverage of the water surface with algae. Symbols show mean values for different flumes F1 – F5, see legend. Different panels denote the time (day) during the experiment. No significant linear relationship was observed from Day 1 - 4 ($p > 0.05$), while significant linear relationship was observed from Day 5 to Day 7 (solid black lines, $p < 0.05$). F1: 6 h of high-magnitude (4.5 $m^{-1}$) wind disturbance; F2: 3 h of high-magnitude wind disturbance; F3: 6 h of moderate-magnitude (3.8 $m^{-1}$) wind disturbance; F4: 6 h of low-magnitude (1.5 $m^{-1}$) wind disturbance; F5: 3 h of low-magnitude wind disturbance.

within the viscous sublayer, where the higher flow velocities near the water surface result in lower static pressure and a net upward lift force on the colonies, of which the magnitudes depend on the colony size and morphology. Although this process was not resolved in our study due to the lack of small tracer particles, we speculate that these complex interactions may account for the higher scum coverage observed at moderate flow velocities following a prolonged period (6 h) of high-magnitude wind disturbance. Future studies should include a more detailed characterization of the hydrodynamic conditions at the water surface (e.g., adding additional small seeding particles to perform particle image velocimetry) to better understand this mechanism.

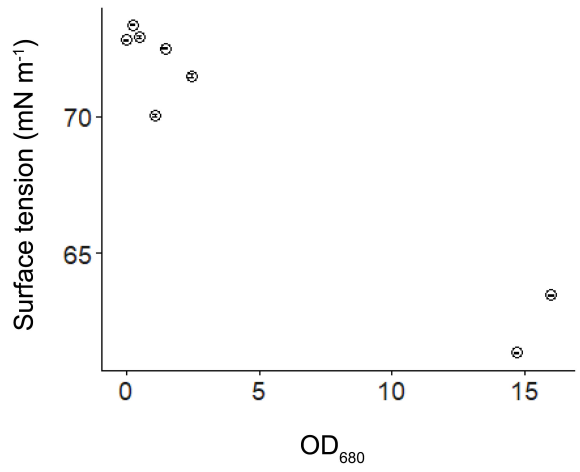


FIGURE 9
Water surface tension versus optical density of algal samples at 680 nm ($OD_{680}$). Error bars show the standard deviation of replicated surface tension measurements ($n$=3).

The observed increase in surface scum also led to more frequent aggregations among colonies at the air-water interface. The developing scum significantly increased the colony size (Figure 6), thereby explaining the higher rates of change in colony size at the surface compared to in the bulk water (Figure 5). Given the limited attention to these aggregations, the underlying mechanism is unclear. Here we proposed capillary forces could be a driver for the formation of *Microcystis* aggregations at the water surface. In the vicinity of immersed buoyant particles, attractive forces arise due to micro-deformation of the air-water interface (capillary immersion force, Kralchevsky and Nagayama, 2000; Paunov et al., 1993). The common phenomenon that floating objects such as bubbles tend to clump together or cling to the sides of the container is driven by capillary forces (Vella and Mahadevan, 2005). We speculate that capillary forces partly increase the encounter rate of *Microcystis* at the water surface during prolonged periods of low wind speed, which promotes their accumulation and aggregation.

During wind disturbance, surface scums were dispersed throughout the bulk water, in which the hydrodynamics was governed by turbulent flow. Our study showed that moderate wind-generated turbulence promoted the aggregation of *Microcystis* into larger colonies, whereas high wind-generated turbulence favored their disaggregation (Supplementary Figure S9). This dual effect can be explained by the opposing effects of turbulence in increasing the collision frequency of cells and colonies and by increasing shear forces (Liu et al., 2019; O'Brien et al., 2004; Njobuenwu and Fairweather, 2018; Yao and Capecelatro, 2021).

The latter likely limited the colony size in our experiments, which consistently decreased for increasing magnitudes of wind disturbances, regardless of disturbance duration (Figure 4). The duration of wind disturbances thus affects colony size by controlling the duration of interactions of colonies with turbulence, which may explain the magnitude-dependent effect of wind disturbance duration on colony size.

Periodic wind disturbances shifted the habitat of *Microcystis* between the air-water interface and the bulk water, during which the surface aggregation of *Microcystis* and the combination of their collision and disaggregation in the bulk water were alternating. In our experiments, such cycles constituted a positive feedback regulation between colony size and formation of surface scum, by which the size of suspended colonies and re-formation rate of scum continuously increased (Figure 3). It should be noted that colony size can also be affected by *Microcystis* growth (Xiao et al., 2018). However, the growth of *Microcystis* did not show notable differences among different flumes. In addition, the $D_{v50}$ changed in accordance with the wind conditions, with the peak in $D_{v50}$occurring after the start of the disturbances (Figure 4), suggesting that the colony size dynamics were likely governed by the hydrodynamic conditions rather than by growth.

## 4.2 The effect of *Microcystis* surface scum on hydrodynamics under different wind conditions

We found a pronounced reduction in water surface tension with increasing *Microcystis* biomass with our supplementary experiment (Figure 9), which can have important consequences for the hydrodynamic processes at the air-water interface. We found that the normalized flow velocity decreased with increasing scum coverage at the later phase of our experiment (Figure 8), suggesting that the dense scum layer suppressed the momentum transfer from wind to water. At low wind speed, the reduction in momentum transfer can be explained by low water surface roughness, which is a consequence of low water surface tension (suppression of capillary waves, Wüest and Lorke, 2003). The increasing scum layer explained the decrease in water flow velocity generated by a given wind speed over time in our experiments (Supplementary Figure S5) and in a previous study (Wu et al., 2019). These findings implied that floating *Microcystis* can promote the formation and persistence of surface scum by altering surface tension and counteracting wind-driven mixing. Such reduced flow velocity caused by the presence of scum layers additionally contributed to the increasing re-formation rate of surface scum (Figure 3). The lack of direct measurements of surface tension in the flumes does not negate the surface tension-mediated hydrodynamic interactions between *Microcystis* and the air-water interface during the flume experiments, as indicated by the observed reduction in flow velocity.

The reduced surface tension caused by *Microcystis* colonies can also directly generate surface flows being directed towards regions of high surface tension (Marangoni effect (Roché et al., 2014; Vinnichenko et al., 2018), i.e., a spreading towards *Microcystis*-free regions. Although we could not directly observe this flow in our experiment as the Marangoni flow was masked by the wind-driven flow, it is ubiquitously present in environmental flows (Scriven and Sternling, 1960). Similar to the 'soap boat' (a well-known visualization of Marangoni convection), we propose that the lateral gradient of surface tension in the vicinity of initial scum patches can drive their horizontal surface drift and reshape their distributions in the absence of external force (e.g., weak wind forcing).

## 4.3 The environmental relevance and limitations of the experiment

We scaled the wind speeds measured in the flumes to representative wind velocities at a standard measurement height of 10 m ($U_{10}$, see Supplementary Table S3). In our experiment, the low wind speed ($U_{10}$ of 2 m $s^{-1}$) corresponds to the wind magnitude during weak wind periods, while the wind disturbances ($U_{10}$ of 2.8 – 5.3 m $s^{-1}$) correspond to amplitudes of periodic wind forcing frequently observed over lakes (Saber et al., 2018; Fernández Castro et al., 2021). The chosen 6 h and 12 h periods of wind disturbances represent the lower and the upper range of field observations over lakes (Fernández Castro et al., 2021).

Surface scum formed during low wind periods and was dispersed during wind disturbances, which is in line with field investigation that showed an upper threshold of $U_{10}$ for scum persistence is 2.6 - 3 m $s^{-1}$ (George and Edwards, 1976; Cao et al., 2006; Qi et al., 2018). Moreover, light-induced changes in the buoyancy of *Microcystis*, commonly observed in the field (Ibelings et al., 1991), were successfully reproduced (Figure 2). These observations further demonstrate the validity of our experimental design.

The water depth in our study was limited by the dimensions of the flume to 30 cm, which is smaller than the amplitude of vertical migration of *Microcystis* in natural lakes. Consequently, the formation rates of surface scum that we observed in the flumes may be higher than those found in the field. In addition, the low water depth restricted vertical mixing at high wind speeds, exposing *Microcystis* in the bulk water to higher irradiance than in deeper water. However, the focus of this study was on the hydrodynamic interactions of surface scum with the air-water interface, which is not expected to be linked to the scale of the experimental setup or to water depth. As the light intensity affects both the growth and the buoyancy production of *Microcystis*, we utilized relatively high irradiance levels, as they often persist in surface waters in the field. Initially, our experiments also included the configuration of the low duration (3 h) and median-magnitude (3.8 m $s^{-1}$) wind disturbances. That data, however, had to be excluded due to technical issues with the flume operation. Future experiments should be conducted at higher resolutions (e.g., analyzing finer gradients of disturbance magnitude and duration) in order to provide a more comprehensive understanding of the partly non-linear interactions of wind with surface scum. Furthermore, buoyancy-driven migration could not be resolved in our measurements, as the flow velocity (generally exceeding 1 mm $s^{-1}$) surpasses the floatation velocity of most colonies (< 1 mm $s^{-1}$, Wallace et al., 2000).

Our study reveals the close connection between *Microcystis* dynamics and the air-water interface. The air-water interface emerges as a crucial habitat increasing colony size during scum formation (typically under low wind speeds), surpassing the impact of bulk water (Figure 5). Recent studies have shown that the wind has declined in some regions over the past few decades (Vautard et al., 2010; Ranjbar et al., 2022). Consequently, this study indicates that the projected decrease in wind speed under future climate conditions will result in larger colonies and facilitate the recovery of surface scum upon wind disturbance. Additionally, our finding of denser scum after prolonged periods of high wind speeds may have implications for early warning of blooms during windy conditions.

Our study also suggests that *Microcystis* reduces surface tension, likely through the excretion of surface-active substances. This process constitutes a dispersion-avoidance mechanism under wind conditions, allowing *Microcystis* to persist at well-lit depths. Furthermore, reduced surface tension potentially drives lateral convection, facilitating the expansion of *Microcystis* and mitigating competition for resources during weak wind periods. These processes may represent adaptive responses of *Microcystis* to wind stressors, suggesting that water surface tension, affected by *Microcystis*, may be an important mediator by which scum-forming cyanobacteria shape their habitat in favorable directions. Given the oversight of the aggregation of *Microcystis* at the air-water interface and their hydrodynamic interactions in current studies, it is important to consider these processes appropriately for a more accurate prediction of *Microcystis* scum dynamics in future climatic conditions.

## Data availability statement

The raw data supporting the conclusions of this article will be made available by the authors, without undue reservation.

## Author contributions

HW: Formal Analysis, Investigation, Writing – original draft. XW: Conceptualization, Funding acquisition, Writing – review & editing. LR: Methodology, Writing – review & editing. AL: Conceptualization, Funding acquisition, Methodology, Writing – review & editing.

## Funding

The author(s) declare that financial support was received for the research, authorship, and/or publication of this article. This study was financially supported by the German Research Foundation (grant no. LO 1150/18) and the National Natural Science Foundation of China (grant nos. 42061134013).

## Acknowledgments

We thank Christoph Bors (University of Kaiserslautern-Landau, Institute for Environmental Sciences) for his help with the experimental setup and measurements, and acknowledge the open-source scripts for particle tracking provided by the Environmental Complexity Lab (Stanford University, https://web.stanford.edu/~nto/software_tracking.shtml).

## Conflict of interest

The authors declare that the research was conducted in the absence of any commercial or financial relationships that could be construed as a potential conflict of interest.

## Publisher's note

All claims expressed in this article are solely those of the authors and do not necessarily represent those of their affiliated organizations, or those of the publisher, the editors and the reviewers. Any product that may be evaluated in this article, or claim that may be made by its manufacturer, is not guaranteed or endorsed by the publisher.

## Supplementary material

The Supplementary Material for this article can be found online at: https://www.frontiersin.org/articles/10.3389/fpls.2024.1370874/full#supplementary-material

## References

Aparicio Medrano, E., Uittenbogaard, R. E., Van De Wiel, B. J. H., Dionisio Pires, L. M., and Clercx, H. J. H. (2016). An alternative explanation for cyanobacterial scum formation and persistence by oxygenic photosynthesis. *Harmful Algae* 60, 27–35. doi: 10.1016/j.hal.2016.10.002

Cao, H. S., Kong, F. X., Luo, L. C., Shi, X. L., Yang, Z., Zhang, X. F., et al. (2006). Effects of wind and wind-induced waves on vertical phytoplankton distribution and surface blooms of *Microcystis* aeruginosa in Lake Taihu. *Freshw. Ecol.* 21, 231e238. doi: 10.1080/02705060.2006.9664991

Chen, H., Zhu, W., Wang, R., Feng, G., and Xue, Z. (2023). Rapid horizontal accumulation and bloom formation of the cyanobacterium *Microcystis* under wind stress. *Hydrobiologia* 850, 123–135. doi: 10.1007/s10750-022-05048-8

Chronakis, I. S., Galatanu, A. N., Nylander, T., and Lindman, B. (2000). The behaviour of protein preparations from blue-green algae (Spirulina platensis strain Pacifica) at the air/water interface. *Colloids Surf. A Physicochem. Eng. Asp.* 173, 181–192. doi: 10.1016/S0927-7757(00)00548-3

Cunliffe, M., Engel, A., Frka, S., Gašparović, B., Guitart, C., Murrell, J. C., et al. (2013). Sea surface microlayers: A unified physicochemical and biological perspective of the air–ocean interface. *Prog. Oceanogr.* 109, 104–116. doi: 10.1016/j.pocean.2012.08.004

Dervaux, J., Mejean, A., and Brunet, P. (2015). Irreversible collective migration of cyanobacteria in eutrophic conditions. *PloS One* 10, e0120906. doi: 10.1371/journal.pone.0120906

Dunton, P. G., and Walsby, A. E. (2005). The diameter and critical collapse pressure of gas vesicles in *Microcystis* are correlated with GvpCs of different length. *FEMS Microbiol. Lett.* 247, 37–43. doi: 10.1016/j.femsle.2005.04.026

Feng, B., Wang, C., Wu, X., Tian, C., Zhang, M., Tian, Y., et al. (2019). Spatiotemporal dynamics of cell abundance, colony size and intracellular toxin concentrations of pelagic and benthic *Microcystis* in Lake Caohai, China. *J. Environ. Sci.* 84, 184–196. doi: 10.1016/j.jes.2019.05.010

Fernández Castro, B., Sepúlveda Steiner, O., Knapp, D., Posch, T., Bouffard, D., and Wüest, A. (2021). Inhibited vertical mixing and seasonal persistence of a thin cyanobacterial layer in a stratified lake. *Aquat. Sci.* 83, 1–22. doi: 10.1007/s00027-021-00785-9

George, D., and Edwards, R. (1976). The effect of wind on the distribution of chlorophyll a and crustacean plankton in a shallow eutrophic reservoir. *J. Appl. Ecol.* 13, 667–690. doi: 10.2307/2402246

Ho, J. C., Michalak, A. M., and Pahlevan, N. (2019). Widespread global increase in intense lake phytoplankton blooms since the 1980s. *Nature* 574, 667–670. doi: 10.1038/s41586-019-1648-7

Huisman, J., Codd, G. A., Paerl, H. W., Ibelings, B. W., Verspagen, J. M. H., and Visser, P. M. (2018). Cyanobacterial blooms. *Nat. Rev. Microbiol.* 16, 471–483. doi: 10.1038/s41579-018-0040-1

Ibelings, B. W., Mur, L. R., and Walsby, A. E. (1991). Diurnal changes in buoyancy and vertical distribution in populations of *Microcystis* in two shallow lakes. *J. Plankton Res.* 13, 419–436. doi: 10.1093/plankt/13.2.419

Kelley, D. H., and Ouellette, N. T. (2011). Using particle tracking to measure flow instabilities in an undergraduate laboratory experiment. *Am. J. Phys.* 79, 267–273. doi: 10.1119/1.3536647

Kralchevsky, P. A., and Nagayama, K. (2000). Capillary interactions between particles bound to interfaces, liquid films and biomembranes. *Adv. Colloid Interface Sci.* 85, 145–192. doi: 10.1016/S0001-8686(99)00016-0

Liu, M., Ma, J., Kang, L., Wei, Y., He, Q., Hu, X., et al. (2019). Strong turbulence benefits toxic and colonial cyanobacteria in water: A potential way of climate change impact on the expansion of Harmful Algal Blooms. *Sci. Total. Environ.* 670, 613–622. doi: 10.1016/j.scitotenv.2019.03.253

Lv, L., Zhang, X., and Qiao, J. (2018). Flocculation of low algae concentration water using polydiallyldimethylammonium chloride coupled with polysilicate aluminum ferrite. *Environ. Technol.* 39, 83–90. doi: 10.1080/09593330.2017.1296028

Njobuenwu, D. O., and Fairweather, M. (2018). Large eddy simulation of particle agglomeration with shear breakup in turbulent channel flow. *Phys. Fluids* 30, 063303. doi: 10.1063/1.5037174

O'Brien, K. R., Meyer, D. L., Waite, A. M., Ivey, G. N., and Hamilton, D. P. (2004). Disaggregation of *Microcystis* aeruginosa colonies under turbulent mixing: laboratory experiments in a grid-stirred tank. *Hydrobiologia* 519, 143–152. doi: 10.1023/B:HYDR.0000026501.02125.cf

Oliver, R. L. (1994). Floating and sinking in gas-vacuolate cyanobacteria. *J.Phycol.* 30, 161–173. doi: 10.1111/j.0022-3646.1994.00161.x

Paunov, V. N., Kralchevsky, P. A., Denkov, N. D., and Nagayama, K. (1993). Lateral capillary forces between floating submillimeter particles. *J. Colloid Interface Sci.* 157, 100–112. doi: 10.1006/jcis.1993.1163

Qi, L., Hu, C., Visser, P. M., and Ma, R. (2018). Diurnal changes of cyanobacteria blooms in Taihu Lake as derived from GOCI observations. *Limnol. Oceanogr.* 63, 1711e1726. doi: 10.1002/lno.10802

Ranjbar, M. H., Hamilton, D. P., Etemad-Shahidi, A., and Helfer, F. (2022). Impacts of atmospheric stilling and climate warming on cyanobacterial blooms: An individual-based modelling approach. *Water Res.* 221, 118814. doi: 10.1016/j.watres.2022.118814

Regel, R. H., Brookes, J. D., Ganf, G. G., and Griffiths, R. W. (2004). The influence of experimentally generated turbulence on the Mash01 unicellular *Microcystis* aeruginosa strain. *Hydrobiologia* 517, 107–120. doi: 10.1023/B:HYDR.0000027341.08433.32

Reynolds, C. S. (1987). Cyanobacterial water-blooms. *Adv. Bot. Res.* 13, 67–143. doi: 10.1016/S0065-2296(08)60341-9

Roché, M., Li, Z., Griffiths, I. M., Le Roux, S., Cantat, I., Saint-Jalmes, A., et al. (2014). Marangoni flow of soluble amphiphiles. *Phys. Rev. Lett.* 112, 208302. doi: 10.1103/PhysRevLett.112.208302

Saber, A., James, D. E., and Hayes, D. F. (2018). Effects of seasonal fluctuations of surface heat flux and wind stress on mixing and vertical diffusivity of water column in deep lakes. *Adv. Water Resour.* 119, 150–163. doi: 10.1016/j.advwatres.2018.07.006

Scriven, L. E., and Sternling, C. V. (1960). The marangoni effects. *Nature* 187, 186–188. doi: 10.1038/187186a0

Vautard, R., Cattiaux, J., Yiou, P., Thépaut, J. N., and Ciais, P. (2010). Northern Hemisphere atmospheric stilling partly attributed to an increase in surface roughness. *Nat. Geosci.* 3, 756–761. doi: 10.1038/ngeo979

Vella, D., and Mahadevan, L. (2005). The "cheerios effect". *Am. J. Phys.* 73, 817–825. doi: 10.1119/1.1898523

Vinnichenko, N. A., Plaksina, Y. Y., Baranova, K. M., Pushtaev, A. V., and Uvarov, A. V. (2018). Mobility of free surface in different liquids and its influence on water striders locomotion. *Environ. Fluid Mech.* 18, 1045–1056. doi: 10.1007/s10652-018-9577-9

Visser, P. M., Passarge, J., and Mur, L. R. (1997). Modelling vertical migration of the cyanobacterium *Microcystis*. *Hydrobiologia* 349, 99–109. doi: 10.1023/A:1003001713560

Wallace, B. B., Bailey, M. C., and Hamilton, D. P. (2000). Simulation of vertical position of buoyancy regulating *Microcystis aeruginosa* in a shallow eutrophic lake. *Aquat. Sci.* 62, 320–333. doi: 10.1007/PL00001338

Webster, I. T., and Hutchinson, P. A. (1994). Effect of wind on the distribution of phytoplankton cells in lakes revisited. *Limnol. Oceanogr.* 39, 365e373. doi: 10.4319/lo.1994.39.2.0365

Wu, J. (1975). Wind-induced drift currents. *J. Fluid Mech.* 68, 49–70. doi: 10.1017/S0022112075000687

Wu, X., Noss, C., Liu, L., and Lorke, A. (2019). Effects of small-scale turbulence at the air-water interface on *Microcystis* surface scum formation. *Water Res.* 167, 115091. doi: 10.1016/j.watres.2019.115091

Wu, T., Qin, B., Brookes, J. D., Shi, K., Zhu, G., Zhu, M., et al. (2015). The influence of changes in wind patterns on the areal extension of surface cyanobacterial blooms in a large shallow lake in China. *Sci. Total Environ.* 518-519, 24–30. doi: 10.1016/j.scitotenv.2015.02.090

Wu, X., Yang, T., Feng, S., Li, L., Xiao, B., Song, L., et al. (2020). Recovery of *Microcystis* surface scum following a mixing event: Insights from a tank experiment. *Sci. Total. Environ.* 728, 138727. doi: 10.1016/j.scitotenv.2020.138727

Wüest, A., and Lorke, A. (2003). Small-scale hydrodynamics in lakes. *Annu. Rev. Fluid Mech.* 35, 373e412. doi: 10.1146/annurev.fluid.35.101101.161220

Xiao, M., Li, M., and Reynolds, C. S. (2018). Colony formation in the cyanobacterium *Microcystis*. *Biol. Rev. Camb. Philos. Soc* 93, 1399–1420. doi: 10.1111/brv.12401

Yao, Y., and Capecelatro, J. (2021). Deagglomeration of cohesive particles by turbulence. *J. Fluid Mech.* 911, A10. doi: 10.1017/jfm.2020.1020

Zhao, G., Gao, X., Zhang, C., and Sang, G. (2020). The effects of turbulence on phytoplankton and implications for energy transfer with an integrated water quality-ecosystem model in a shallow lake. *J. Environ. Manage.* 256, 109954. doi: 10.1016/j.jenvman.2019.109954

Zhu, W., Li, M., Luo, Y., Dai, X., Guo, L., Xiao, M., et al. (2014). Vertical distribution of *Microcystis* colony size in Lake Taihu: its role in algal blooms. *J. Gt. Lakes Res.* 40, 949–955. doi: 10.1016/j.jglr.2014.09.009

frontiers | Frontiers in Plant Science

TYPE Original Research
PUBLISHED 22 March 2024
DOI 10.3389/fpls.2024.1381798



OPEN ACCESS

EDITED BY
Qiang Yang,
German Centre for Integrative Biodiversity Research (iDiv), Germany

REVIEWED BY
Xiaoming Jiang,
Xi'an University of Technology, China
Zhiying Lu,
University of Alabama at Birmingham, United States

*CORRESPONDENCE
Lan Wang
wanglan@ihb.ac.cn
Qinghua Cai
qhcai@ihb.ac.cn

RECEIVED 04 February 2024
ACCEPTED 12 March 2024
PUBLISHED 22 March 2024

CITATION
Wang L, Tan L and Cai Q (2024) Distinct differences of vertical phytoplankton community structure in mainstream and a tributary bay of the Three Gorges Reservoir, China.
*Front. Plant Sci.* 15:1381798.
doi: 10.3389/fpls.2024.1381798



# Distinct differences of vertical phytoplankton community structure in mainstream and a tributary bay of the Three Gorges Reservoir, China

Lan Wang[1,2]*, Lu Tan[1] and Qinghua Cai[1]*

[1]State Key Laboratory of Freshwater Ecology and Biotechnology, Institute of Hydrobiology, Chinese Academy of Sciences, Wuhan, Hubei, China, [2]Hubei Key Laboratory of Wetland Evolution & Ecological Restoration, Wuhan Botanical Garden, Chinese Academy of Sciences, Wuhan, Hubei, China

The vertical distribution of phytoplankton plays a crucial role in shaping the dynamics and structure of aquatic communities. In highly dynamic reservoir systems, water level fluctuations significantly affect the physiochemical conditions and the phytoplankton community. However, the specific effects on the vertical characteristics of phytoplankton between the mainstream and the tributary bay of the reservoir remain unstudied. This study investigated the vertical aspects of phytoplankton density, biomass, α and β diversity through monthly sampling over two years in the mainstream (Chang Jiang, CJ) and a tributary bay (Xiang Xi, XX) of the Three Gorges Reservoir in China. Phytoplankton density and biomass were significantly higher in XX, indicating an increased risk of algal blooms in the tributary. The phytoplankton community in CJ showed more stable species-environment relationships, a lower Shannon index and a higher evenness index, suggesting a relatively simple structure and a more uniform distribution of phytoplankton among different water layers. Conversely, XX showed greater differences between water layers (higher β diversity), with significant negative correlations with water level and positive correlations with DO difference, dissolved silica (DSi) difference, and stratification. Peak phytoplankton density and biomass, as well as high β diversity in XX, occurred during periods of decreased water levels with strong stratification in spring and summer. A structural equation model complemented by path analysis revealed that a decrease in water level could increase β diversity either directly through internal processes with extended residence time or indirectly by modifying stratification and the vertical distribution of DSi in XX. Therefore, a proposed water quality management strategy for XX was to increase the water level or reduce β diversity by implementing artificial mixing during stratification periods. Overall, this study lies in its comprehensive investigation of the vertical characteristics of the phytoplankton community in both the mainstream and the tributary bay of the Three Gorges Reservoir, elucidating the significant impact of water level fluctuations and providing insights for targeted water quality management strategies in the tributary bay to mitigate potential ecological impacts.

KEYWORDS

vertical distribution, phytoplankton community, β diversity, water level, stratification

# 1 Introduction

River systems worldwide are increasingly affected by damming to meet growing demands for hydropower, flood control, and reliable water resources (Straškraba, 2005). The impoundment of reservoirs significantly alters river flows, shorelines, sediments, and aquatic organisms. These effects are particularly complex and profound in the tributaries of reservoirs, where hydrodynamics and water mass transport processes are significantly altered. Consider the Three Gorges Project, the world's largest hydraulic engineering project. With the implementation of the Three Gorges Dam Project in 2008, the reservoir water level fluctuated from 145 m above sea level in summer to 175 m above sea level in winter (first recorded on October 26, 2010). This resulted in a water level fluctuation zone of about 350 $km^2$ in the reservoir (New and Xie, 2008). Before the impoundment, the tributaries maintained a natural river state, with the water environment mainly determined by the characteristics of the tributary basin. However, after impoundment, the rising water level in the mainstream induces a flow back into the tributary (Liu et al., 2012). This results in a slowing of the flow velocity, a reduction in the aquatic environment capacity, and an influx of additional nutrients from the mainstream, further degrading the aquatic environment. As a result, the likelihood of algal blooms is significantly increased (Wang et al., 2011; Liu et al., 2012; Li et al., 2021).

Phytoplankton is widely recognized as the primary producer in aquatic ecosystems and plays a crucial ecological role. However, their abnormal proliferation, known as algal blooms, has negative impacts on the aquatic environment. Their sensitivity to environmental changes underscores their importance in understanding and mitigating environmental challenges. Therefore, it serves as a good indicator of water quality and ecosystem health (Phillips et al., 2013; Bellinger and Sigee, 2015). The vertical distribution of phytoplankton is fundamental to the dynamics and structure of aquatic communities (Ryabov et al., 2010). Increased mixing has been identified as a key strategy to mitigate algal blooms (Visser et al., 2016; Wen et al., 2022), and increasing mixing promotes uniformity in the vertical distribution of phytoplankton communities across different layers in terms of density, biomass, and compositional structure. This uniformity in the vertical distribution of phytoplankton has emerged as a reliable indicator of the effectiveness of water quality regulation under hydrodynamic conditions. Most related studies have traditionally focused on reporting vertical phytoplankton profiles based on total density (Ryabov et al., 2010; Ikram et al., 2017; Chen et al., 2021; Huang et al., 2022), total biomass (Ji et al., 2017; Xue et al., 2017; Sakharova and Korneva, 2018; Cordero-Bailey et al., 2021; Lu et al., 2023; Radchenko et al., 2023), or species composition (Ryabov et al., 2010; Mojica et al., 2015; Ikram et al., 2017; Sakharova and Korneva, 2018; Chen et al., 2021; Huang et al., 2022; Cui et al., 2023; Lu et al., 2023; Radchenko et al., 2023), with limited attention to diversity (Sakharova and Korneva, 2018; Cui et al., 2023). Diversity is also an important community attribute, and various reviews have concluded that diversity plays a major role in maintaining ecosystem productivity and stability (Cardinale et al., 2012; Tilman et al., 2014). Therefore, a comprehensive study of the vertical distribution patterns of phytoplankton in reservoir ecosystems serves as a valuable complement to current research and has practical implications for the development of effective human-driven regulation strategies in reservoirs.

The formation of vertical phytoplankton profiles is influenced by several primary factors. One factor is light intensity, which decreases with depth, making deep layers unfavorable for photosynthetic phytoplankton species. Another factor is the nutrient gradient, which supports diverse production for phytoplankton with different nutrient requirements. In addition, different water temperatures at different depths in a reservoir can directly affect phytoplankton, and the stratification of water quality conditions, along with changes in relative water column stability caused by thermal stratification, can indirectly affect phytoplankton dynamics (Cui et al., 2021). In many ecosystems, mixing and stratification play an essential role as key drivers of the distribution and segregation of different phytoplankton taxa (Mojica et al., 2015). In artificially regulated reservoirs, all of these factors can be influenced by hydrodynamic factors such as water level. Numerous studies have highlighted the potential to mitigate algal blooms by regulating hydrodynamic conditions such as water level fluctuations (Bakker and Hilt, 2015; Yang et al., 2016; Ji et al., 2017). The effect of hydrological factors on phytoplankton has become a research hotspot in recent years, as it is not only a key factor influencing phytoplankton growth, but also the most easily regulated factor in reservoirs (Cui et al., 2021). The effect of water level on phytoplankton biomass and composition in reservoir systems has been well studied (Naselli-Flores and Barone, 1997; Mac Donagh et al., 2009; Wang et al., 2011; Zhu et al., 2013; Yang et al., 2016). However, its influence on the vertical structure of phytoplankton and the underlying mechanisms are still lacking.

This study, conducted over two annual cycles with monthly sampling, examines the vertical distribution patterns of phytoplankton under the influence of different environmental factors and water levels. The primary objective is to explore potential differences in the vertical distribution of phytoplankton between the mainstream and the tributary of the Three Gorges Reservoir, and to understand how these differences variances respond to changes in hydrodynamic and environmental conditions. We hypothesized that the water level had both direct and indirect effects on the phytoplankton community and addressed the potential pathways of influence. The results will provide valuable scientific information for targeted management and conservation of the ecological systems within the mainstream and tributary of the Three Gorges Reservoir.

# 2 Materials and methods

## 2.1 Study site and sampling

The Three Gorges Reservoir (TGR) is located at 29°16'-31°25' N, 106°-110°50' E (Huang et al., 2006), with a subtropical monsoon climate prevails (Jiang et al., 2006). It has an average annual precipitation of 1,000-1,300 mm, characterized by warm winter and hot summer, early spring and cold autumn (Cai et al., 2010). It is more than 600 km long

and 1.1 km wide, with a surface area of 1,080 $km^2$ (Huang et al., 2006). The sampling site for the mainstream of TGR (Chang Jiang, CJ) is located near the dam, 31 km from the mouth of the Xiangxi River (Figure 1). The Xiangxi River is the largest tributary of the TGR in Hubei Province, with a mainstream length of 94 km and a watershed area of 3,099 $km^2$ (Wang et al., 1997). The lower 20-40 km section of Xiangxi River was named Xiangxi Bay after the impoundment of the TGR (Cai and Hu, 2006). The sampling site for the tributary of the TGR (Xiang Xi, XX) was located near the middle of Xiangxi Bay, 18 km from the mouth of the Xiangxi River (Figure 1). The CJ and XX sites have been sampled as a representative of the mainstream and tributary of the TGR since the early study by Kuang et al. (2005).

Sampling was performed monthly from September 2008 through August 2010. A 5 L Van Dorn sampler was used to collect water samples at depths of 0.5 m, 2 m, 5 m, 10 m, 15 m, and 20 m for both CJ and XX. 1 L samples for phytoplankton analysis were fixed with neutral Lugol's solution immediately after sampling. 250 ml samples for nutrient analysis were stored in a pre-cleaned plastic bottle and acidified with sulfuric acid for laboratory analysis.

## 2.2 Biotic and abiotic variable measurements

Phytoplankton was quantitatively analyzed in a Fuchs-Rosental slide using an Olympus CX21 microscope (Olympus Corporation, Japan) at 400× magnification. Previously, a sedimentation method was used to concentrate the phytoplankton (Huang et al., 2000; Cai, 2007). Taxonomic identification was performed according to the guidelines of Hu and Wei (2006) and John et al. (2002). Vertical profiles of water temperature (Temp, °C), conductivity (Cond, ms/cm), dissolved oxygen (DO, mg/L), pH, and turbidity (Turb, NTU) were measured using environmental monitoring systems (YSI 6600EDS, USA). Concentrations of total nitrogen (TN), nitrate-nitrogen ($NO_3$-N), total phosphorus (TP), phosphate-phosphorus ($PO_4$-P), and dissolved silicon (DSi) were measured with a segmented flow analyzer (Skalar San$^{++}$, Netherlands) according to the Protocols for Standard Observation and Measurement in Aquatic Ecosystems of the Chinese Ecosystem Research Network (CERN) (Huang et al., 2000; Cai, 2007).

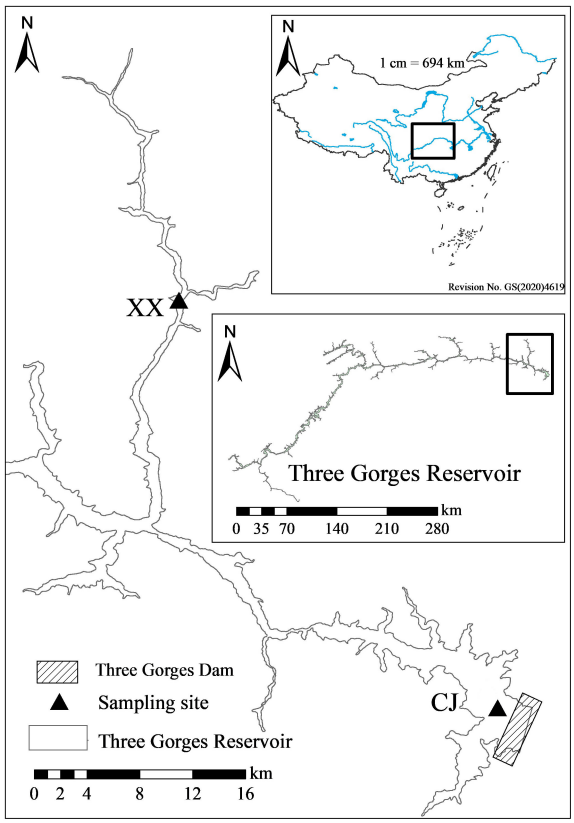


FIGURE 1
Map of sampling sites in this study.

## 2.3 Data analysis

Algal biovolume was calculated using formulas for geometric shapes, with the fresh weight unit expressed in mass, where 1 $mm^3$/L is equal to 1 mg/L (Huang et al., 2000; Wetzel and Likens, 2000). Real-time data on water level, inflow, and outflow data for the TGR were obtained from the China Three Gorges Corporation. Linear correlation between environmental variables was assessed using Pearson's correlation coefficient. To examine the relationship between phytoplankton community (density, biomass, and α diversity index Shannon and evenness) and environmental variables, we performed a Mantel test using the R package "LinkET".

Constrained ordination methods including Redundancy Analysis (RDA) and Canonical Correspondence Analysis (CCA), are used to examine the relationships between phytoplankton community structure and environmental factors. The decision to use either RDA (maximum DCA axis length below 3) or CCA (maximum DCA axis length above 4) ordination methods is based on Detrended Correspondence Analysis (DCA) applied to the species data, according to (Lepš and Šmilauer, 2003). In the RDA and CCA analysis, the significant environmental variables are identified using the "envfit" function.

The COSTATIS technique, which is based on Partial Triadic Analysis combined with Co-Inertia Analysis, was used to assess the stability of phytoplankton species-environment relationships using the R packages "ade4" and "adegraphics" (Slimani et al., 2017). COSTATIS brings to light the connections between two stable structures (a set of species data tables and a set of environmental parameter tables). The use of COSTATIS eliminates conflicting variation between the entire sequences are eliminated, thereby facilitating ease of interpretation (Thioulouse et al., 2004).

The Shannon index (Shannon) and Buzas and Gibson's evenness index (Evenness) were chosen to characterize α diversity. The Shannon index takes into account the number of individuals as well as the number of taxa and is calculated using the formula:

$$Shannon = -sum((n_i/n)ln(n_i/n))$$

where $n_i$ is the number of individuals of taxon i and n is the total number of individuals. The Buzas and Gibson's evenness index is calculated as:

$$\text{Evenness} = e^{\text{Shannon}}/S$$

where S is the number of taxa. The Friedman test was used to compare physical and chemical conditions, total density and biomass, and Shannon and evenness among different water layers for both CJ and XX. The Kruskal-Wallis H test was used to compare the physical and chemical conditions, total density and biomass, and Shannon and evenness between CJ and XX. Bray-Curtis dissimilarity was used to measure the β diversity among samples based on phytoplankton community, while Euclidean distance was used to assess the dissimilarity among samples with respect to environmental factors. Mantel test was performed to select significant environmental factors related to Bray-Curtis dissimilarity of the community. All the DCA, RDA, CCA, Shannon and evenness index, β diversity and Mantel test were calculated using the "vegan" package in R.

Two hydrodynamic factors were examined for their influence on the α and β diversity of the phytoplankton community: squared buoyancy frequency ($N^2$) and water level. Squared buoyancy frequency ($N^2$) can serve as an alternative indicator of stratification (Li et al., 2020) and is calculated using the formula:

$$N^2 = (g/\rho_0)/(d\rho/dz)$$

Where g is the gravitational acceleration (9.8092597 $m/s^2$), $\rho_0$ is the density of water at 3.98°C, and z is the water depth. In our study, $N^2$ is calculated for the entire water column, extending from the surface to a depth of 20 m, to assess the degree of stratification of the entire water column. A higher $N^2$ indicates a more stratified water column and a higher static stability. Eleven elementary indices were used to clarify the water level in three aspects: magnitude, frequency and rate of change of water level data, following the approach proposed by (Olden and Poff, 2003). These indices were calculated on the day of sampling and 1 to 30 days prior to sampling, with the aim of assessing the temporal effects of water level fluctuations on α and β diversity. The calculation of these indices was performed using the "SER" function within the R package "SER" (Guo et al., 2020). The univariate linear regression model was used to investigate the relationships between the β diversity and the Euclidean distance of environmental factors, as well as a single key environmental factor determined by the Mantel test. It was also used to investigate the response of α and β diversity to $N^2$ and water level over different time scales. In addition, a structural equation model (SEM) with path analysis was used to test the direct and indirect effects of the predictor variables (Shipley, 2002). Significant paths were retained while non-significant paths were removed from the developed model. The final model was validated using the Chi-square *p*-value, the goodness-of-fit index (GFI), the adjusted goodness-of-fit index (AGFI), and the root mean square error of approximation (RMSEA). Structural equation analysis was performed using the "lavaan" package in R.

# 3 Results

## 3.1 Hydrodynamic and environmental conditions

The main hydrodynamic conditions, including water level (Figure 2A), inflow and outflow of the TGR (Figure 2B), showed regular intra-annual variations during the two-year study period. The mean daily water level showed higher values from November to the following January and remained low from June to September. TGR inflow and outflow peaked from July to September and remained low from late November to the following March. From February to September, $N^2$ values in XX were significantly higher than those in CJ (Figure 2B). However, from October to the following January, the water column in both CJ and XX showed little stratification (indicating strong mixing).

Except for water temperature, pH and turbidity, significant differences were observed in most environmental conditions between CJ and XX (Table 1). Among water layers in CJ, TN, $NO_3$-N, $PO_4$-P, DSi and Turb showed no significant differences, while other environmental factors showed remarkable differences. In XX, most environmental factors showed significant differences among different water layers, except for Turb. TN, $NO_3$-N, TP, $PO_4$-P, DSi, and conductivity were significantly higher in CJ compared to XX, while XX showed significantly higher DO. The correlation analysis between environmental factors in Figure 3 showed that in both CJ and XX, TN and $NO_3$-N had relatively high positive correlations. In CJ, relatively high negative correlations were observed between Temp and Cond, and between Temp and DO. In XX, a relatively high negative correlation was observed between Temp and $PO_4$-P.

## 3.2 Phytoplankton community and response to environmental factors

Phytoplankton density and biomass varied significantly among the different water layers and were significantly lower in CJ than in XX (Table 1). Annual cycles showed two peaks in spring (March~April) and summer (July~August) for both CJ and XX (Supplementary Figure S1), and the vertical structure of phytoplankton density and biomass is shown in Supplementary Figures S2 and S3. Diatoms dominated in all layers for both sites. In the first year, the spring peak species were *Stephanodiscus* sp. in CJ and *Stephanodiscus* sp. and *Fragilaria* sp. in XX, while the summer peak in XX was more pronounced with *Stephanodiscus* sp., cyanophytes and cryptophytes. In the second year, density and biomass decreased in CJ, while the summer peak in XX exceeded that of the first year, dominated by *Stephanodiscus* sp., *Synedra acus* and some cyanophytes. Mantel test showed that more environmental factors were significantly correlated with phytoplankton density and biomass in XX compared to CJ, except pH and Turb (Figure 3). CJ showed significant relationships only with Temp and DO.

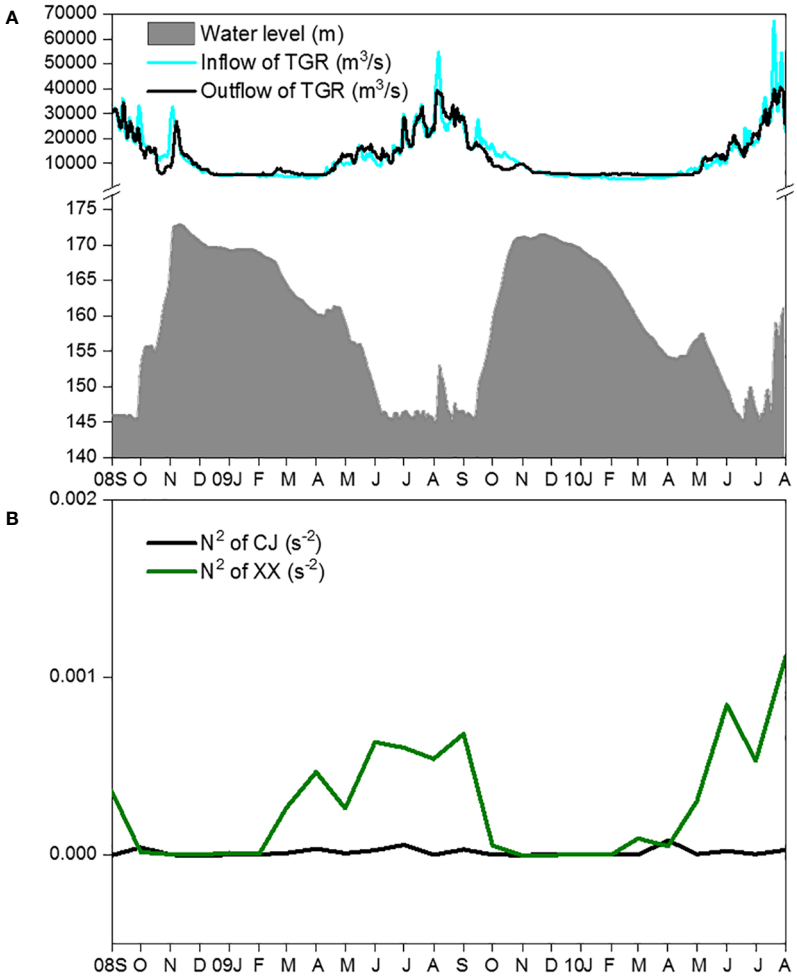


FIGURE 2
Changes of water level, inflow and outflow of TGR **(A)** and vertical stratification **(B)** during the study period.

RDA and CCA were selected for CJ and XX based on the maximum DCA axis length of 2.12 and 4.55, respectively. Figure 4 shows different patterns of phytoplankton community ordination between CJ and XX. In CJ, the primary RDA axis explained 21.47% of the variability in phytoplankton data, with significant correlations between phytoplankton species and environmental factors including DO ($r = -0.62$, $p = 0.001$) and Temp ($r = 0.54$, $p = 0.003$). In XX, the first two CCA axes together accounted for 25.21% of the variability in phytoplankton data (axis 1 = 16.57%, axis 2 = 8.64%), with significant correlations between phytoplankton species and environmental factors including Cond ($r = 0.72$, $p = 0.001$), Temp ($r = -0.57$, $p = 0.006$), and TP ($r = 0.52$, $p = 0.001$) on the first CCA axis. Monte Carlo simulation confirmed the significance of all CCA axes ($F = 3.638$, $p = 0.028$ for CJ, and $F = 7.796$, $p = 0.001$ for XX, 999 permutations). Notably, *Stephanodiscus* sp. (Stsp) stood out significantly in CJ, while few species were significantly different in XX.

COSTATIS is used to identify stable structures in phytoplankton species-environment relationships, ignoring temporal structures. The first eigenvalue is much more important than the following ones (97.0% and 2.8% of the total inertia for the first two axes). The COSTATIS co-inertia results for sampling sites are shown in Figure 5A, where the tip and the black bullet end of the arrow represent the site from the perspective of phytoplankton and environmental parameters, respectively. The lengths of the arrows are greater in XX than in CJ, indicating a greater discrepancy between phytoplankton and environmental factors. The closer proximity of the points in CJ compared to XX indicates that the water layers in CJ have a higher similarity in phytoplankton species-environment relationships. Figures 5B and C illustrates the intrastructure for the sampling sites overlaid with environmental parameters and species. Most of the environmental factors were in the direction of CJ, while DO pointed to XX. These results can be mutually corroborated with Table 1. Figure 5C indicates that the differentiation of phytoplankton species in different water layers of XX may be mainly due to a significant disparity of 0.5 m.

## 3.3 Phytoplankton diversity patterns and response to hydrodynamic and environmental conditions

Figures 6A and B show the Shannon and Evenness indices of different water layers. Similar temporal cycles were observed for both indices. While the Shannon index showed no significant

TABLE 1 Statistical summary of environmental conditions, phytoplankton density, biomass and diversity for CJ and XX.

| | CJ | | | XX | | | Differences between CJ and XX |
|---|---|---|---|---|---|---|---|
| | Mean | Min | Max | Mean | Min | Max | |
| TN (mg/L) | 1.73 | 0.94 | 2.54 | 1.38[a] | 0.56 | 2.54 | *** |
| $NO_3$-N (mg/L) | 1.49 | 0.85 | 2.11 | 1.21[c] | 0.45 | 1.98 | *** |
| TP (mg/L) | 0.115[a] | 0.02 | 0.73 | 0.093[c] | 0.01 | 0.55 | *** |
| $PO_4$-P (mg/L) | 0.085 | 0.01 | 0.26 | 0.064[c] | 0.01 | 0.15 | *** |
| DSi (mg/L) | 3.62 | 2.5 | 7.1 | 3.02[c] | 0.3 | 6.1 | ** |
| Temp (°C) | 18.67[c] | 10.76 | 25.47 | 19.22[c] | 10.27 | 30.71 | |
| Cond (ms/cm) | 0.372[c] | 0.312 | 0.416 | 0.347[c] | 0.277 | 0.429 | *** |
| DO (mg/L) | 7.86[c] | 5.46 | 10.25 | 9.55[c] | 4.67 | 21.19 | *** |
| pH | 7.98[c] | 7.51 | 8.65 | 7.99[c] | 6.30 | 9.63 | |
| Turb (NTU) | 18.26 | 0.10 | 115.55 | 7.64 | 0.02 | 82.96 | |
| Density (cells/L) | 4.26E6[b] | 1.93E5 | 2.26E8 | 1.70E7[b] | 7.89E4 | 2.28E8 | *** |
| Biomass (mg/L) | 0.163[b] | 0.012 | 5.768 | 1.450[b] | 0.006 | 18.327 | *** |
| Shannon | 1.032 | 0.188 | 1.772 | 1.207 | 0.077 | 2.266 | ** |
| Evenness | 0.399[a] | 0.093 | 0.756 | 0.334[a] | 0.077 | 0.961 | *** |

Significance level:
[a]denotes p<0.05,
[b]denotes p<0.01,
[c]denotes p<0.001, blank denotes p >0.05, from Friedman test.
*** denotes p<0.001, ** denotes p<0.01, blank denotes p >0.05, from Kruskal–Wallis H test.

variation among the water layers, a notable vertical variation was observed for the Evenness index (Table 1). Overall, XX had a higher Shannon index while CJ had a higher evenness index (Figures 6A, B; Table 1). In CJ, significant relationships were observed between the Shannon index and TN, DSi, Temp and DO, while the Evenness index showed significant relationships with DSi, Temp, Cond, DO and Turb (Figure 3). However, in XX, the Shannon index only showed significant relationships with Temp, while the evenness index showed significant relationships with $NO_3$-N, Temp, and DO.

The Shannon index showed a significant positive relationship with $N^2$ in XX, but no relationship with $N^2$ in CJ (Figure 6C). The evenness index showed no relationship with $N^2$ in either CJ or XX (Figure 6D). Among the 11 water level indices, the "mean of the daily data before sampling date" index showed significantly more and stronger correlations with the Shannon and Evenness indices. Therefore, it was selected to establish the correlations. The Shannon index showed a negative correlation with water level in XX, with a slight increase observed as the number of days in advance for water level increased (Figure 6E). Conversely, the Shannon index did not show a significant relationship with water level in CJ. The evenness index showed a negative correlation with water level in CJ, with a slight improvement observed as the number of days in advance for water level increased (Figure 6F). However, the evenness index did not show a significant relationship with water level in XX.

The β diversity for pairs of water layers over time is shown in Figure 7A, based on the Bray-Curtis dissimilarity of the community in CJ and XX. In most months, XX had higher β diversity compared to CJ, with exceptions in some spring months. During late autumn and winter, the disparity in pairs of water layers was remarkably low, indicating a uniform distribution of the phytoplankton community in both CJ and XX during these months. DSi (r=0.40, $p< 0.001$) and DO (r=0.39, $p< 0.001$) were identified by Mantel test as the most significant and influential environmental factors related to the differences in community structure between different water layers. The β diversity of the phytoplankton community in XX was found to be significantly positively correlated with the Euclidean distance of the total environmental factor matrix, DSi, and DO ($p< 0.001$, Figures 7B-D). However, in CJ, only the difference of DSi in different water layers was significantly positively correlated with β diversity ($p = 0.04$, Figure 7C).

The β diversity showed a positive correlation with $N^2$ in XX, while no significant relationship with $N^2$ was observed in CJ (Figure 7E). Among the 11 water level indices, the "mean of the daily data before sampling date" index showed significantly more and stronger correlations with β diversity. Therefore, it was chosen to establish the correlations. The β diversity showed a negative correlation with the water level in XX, and this effect showed a slight increase with an increase in the number of days in advance for the water level (Figure 7F). In contrast, no significant relationship was found between β diversity and water level in CJ.

Based on the above results, we constructed structural equation models to disentangle the complex interactions of direct and indirect effects of predicted variables on β diversity in XX (Figure 8). As hypothesized, both water level and stratification had significant direct and indirect effects on β diversity in XX. Water level had a direct negative effect (-0.37) and stratification had

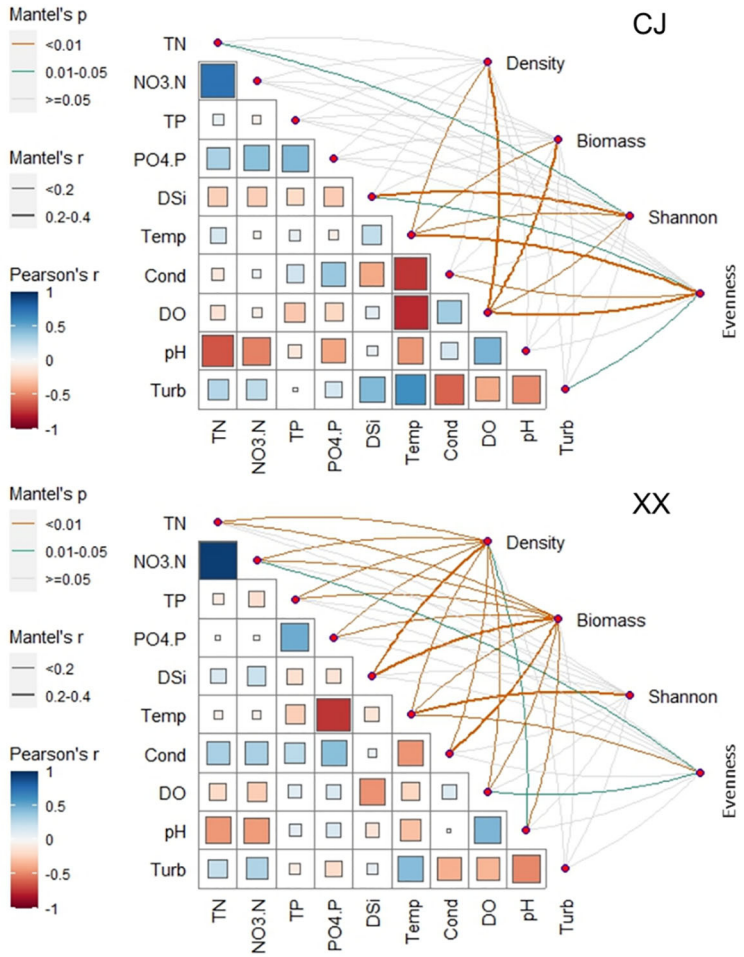


FIGURE 3
Relationship between environmental variables and phytoplankotn density, biomass, α diversity indices (Shannon and Evenness) through Mantel tests. Pairwise comparisons of different enviornmental variables are presented in the bottom-left section.

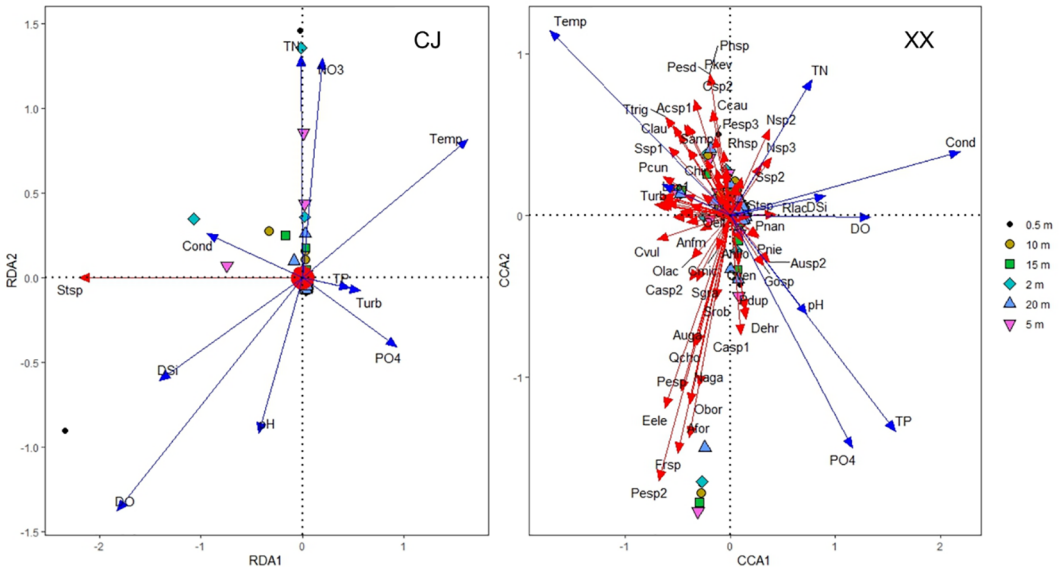


FIGURE 4
Phytoplankton community ordination based on RDA for CJ and CCA for XX.

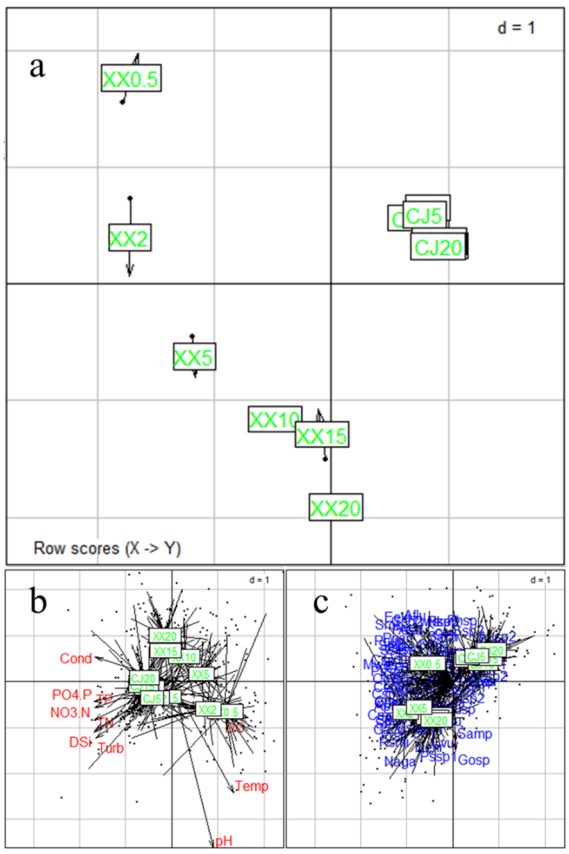


FIGURE 5
COSTATIS Co-inertia results for sampling locations **(A)**, and intrastructure plot of the COSTATIS method: projection of the sampling locations superimposed with environmental parameters **(B)** and species **(C)**, CJ0.5, CJ2, CJ5, CJ10, CJ15, and CJ20 indicate depths of 0.5 m, 2 m, 5 m, 10 m, 15 m, and 20 m for CJ, and XX0.5, XX2, XX5, XX10, XX15, and XX20 indicate depths of 0.5 m, 2 m, 5 m, 10 m, 15 m, and 20 m for XX.

a direct positive effect (0.14) on β diversity. Their indirect effects followed the path of water level → stratification → DSi difference → β diversity. The *p*-value of the Chi-squared test was 0.783, and the goodness-of-fit index (GFI) and adjusted goodness-of-fit index (AGFI) were 0.999 and 0.996, respectively. The root mean square error of approximation (RMSEA) was 0.000. The results indicated that the proposed models provided good interpretations of the original data (Schermelleh-Engel et al., 2003).

# 4 Discussion

## 4.1 Vertical divergences in phytoplankton total density, total biomass and community composition

The aquatic ecosystems in both CJ and XX experienced identical and highly dynamic water level fluctuations during the study period. However, the phytoplankton density in XX was found to be 4 times higher with almost 9 times higher biomass compared to CJ during the two-year study period. This observation highlights the increased risk of algal bloom in the tributary when compared to the mainstream of the reservoir. Kuang et al. (2005) conducted a study on phytoplankton density before the impoundment of TGR and found that phytoplankton density in the tributary was 3.8 times higher than that in the mainstream. After years of operation following the impoundment of TGR, the dynamics of phytoplankton in the tributary become more complicated. The results in Figure 3 show that phytoplankton density and biomass were only related to Temp and DO in CJ, while almost all the environmental factors influenced phytoplankton density and biomass in XX, supporting the above conclusion to some extent. Although XX had a significantly lower nutrient level as shown in Table 1, it had a higher phytoplankton density and biomass. This suggests that nutrient availability did not limit phytoplankton growth in XX.

On the other hand, even in a well-mixed water column, where phytoplankton and nutrients are homogenized throughout the water column, a light gradient is inevitable (Mellard et al., 2011). Therefore, phytoplankton will experience different local light levels and therefore different growth rates. In this study, the turbidity of CJ and XX was relatively low and didn't show significant differences, but the phytoplankton density and biomass were significantly higher in XX than in CJ and had distinct vertical variations, suggesting that phytoplankton growth is free from light limitation caused by high turbidity in both CJ and XX. This finding is consistent with a study by Liu et al. (2012), and is consistent with the characteristics of the phytoplankton composition. Diatoms are the primary phytoplankton group in the study area and have a low light requirement (Huisman et al., 2004). Both theoretical predictions and field experiments with artificial mixing have shown that diatoms are more efficient species at low light levels than Microcystis (Huisman et al., 2004). Phytoplankton growth was not limited by nutrients or light; therefore, the relatively lower mixing or stronger stratification in XX may facilitate favorable conditions with longer residence time for phytoplankton growth, even though the inflow and outflow of TGR reached their peak for the year during this period. Liu et al. (2012) showed that seasonal thermal stratification is strongly developed in the tributary, but weak in the mainstream of the TGR. Similar findings have been reported in a drinking water reservoir, where thermal intensity (water temperature and thermal stratification intensity) was found to be a key driver of spatiotemporal changes in phytoplankton (Lu et al., 2023).

Throughout the two-year study, phytoplankton density and biomass showed peak values in spring and summer, followed by low values in the autumn and winter, which occurred almost simultaneously for CJ and XX. Significant vertical differences in phytoplankton density and biomass were observed during the peak period, with the surface showing the highest values. A notable finding during this peak period was the significant evolution of phytoplankton from a diatom-dominated community to a chlorophyta/cyanophyta/cryptophyta/dinophyta-dominated community. Turbulence promoted diatom growth, but cyanophyta and dinoflagellates prefer stable water conditions (Rath et al., 2021). A significant disappearance of diatoms was strongly associated with the weakening of mixing. Interestingly, this peak period coincides

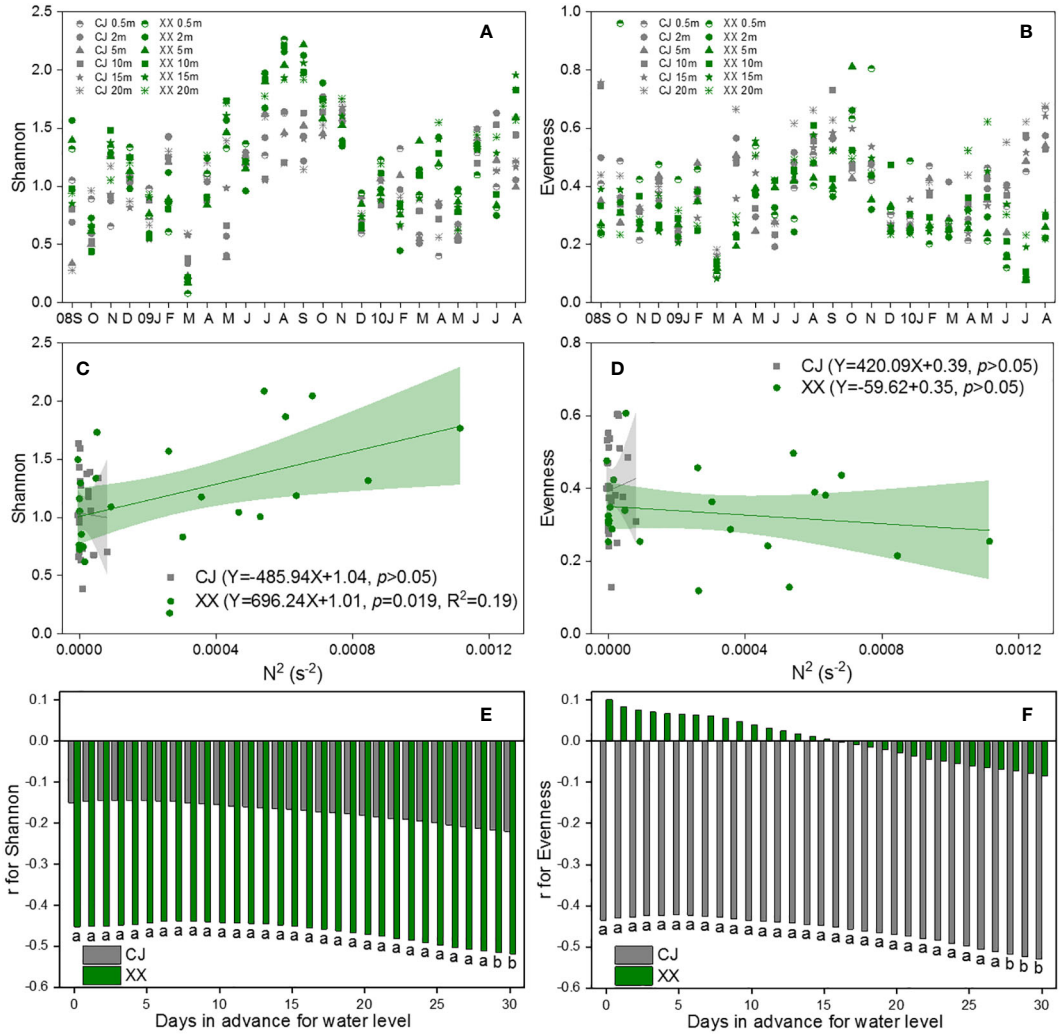


FIGURE 6
Vertical changes of Shannon **(A)** and Evenness **(B)**, their response to $N^2$ **(C, D)** and water level **(E, F)** in CJ and XX. Significance level: [a] denotes $p<0.05$, [b] denotes $p<0.01$, blank denotes $p>0.05$.

with the stratification period, which is characterized by relatively high $N^2$ values and medium to low water levels. Therefore, both water level and stratification level may influence the vertical differences in total density, total biomass, and the composition of phytoplankton. This conclusion, asserting that the vertical heterogeneity of the phytoplankton corresponds to its vertical hydrological structure, was also confirmed in a 6 m deep lagoon (Radchenko et al., 2023).

When analyzing the responses of phytoplankton community structure to environmental factors, excluding hydrodynamic conditions, it was observed that DO and Temp were significant factors influencing the phytoplankton community in CJ. In contrast, Cond, Temp and TP emerged as significant factors influencing the phytoplankton community in XX. The undeniable effect of temperature on phytoplankton is evident, and in this study, water temperature emerged as a key factor influencing the structure of the phytoplankton community in both CJ and XX. Similar results have been reported in other reservoir systems (Cai et al., 2020; Cui et al., 2023). In addition to water temperature, phytoplankton community structure was more strongly influenced by nutrients in XX compared to CJ. This suggests that nutrients played a more important role in shaping phytoplankton composition in the tributary. While most nutrients showed no vertical variation in CJ, they showed significant differences in the vertical direction in XX, resulting in different phytoplankton compositions in different water layers.

COSTATIS is preferred when species-environment relationships are strong, and temporal structures are not of primary importance (Thioulouse, 2011). In this study, it is applied to test whether stable species-environment relationships can be found in CJ and XX through multiple repeated sampling. The COSTATIS analysis showed that the sites representing the six water layers of CJ were aggregated, while those in XX were quite separated, indicating a more stable species-environment relationship in CJ compared to XX. This means that when considering temporal changes, the species-environment relationship varied significantly in XX, while it remained relatively unchanged in CJ. To some extent, this indicates that CJ

10.3389/fpls.2024.1381798

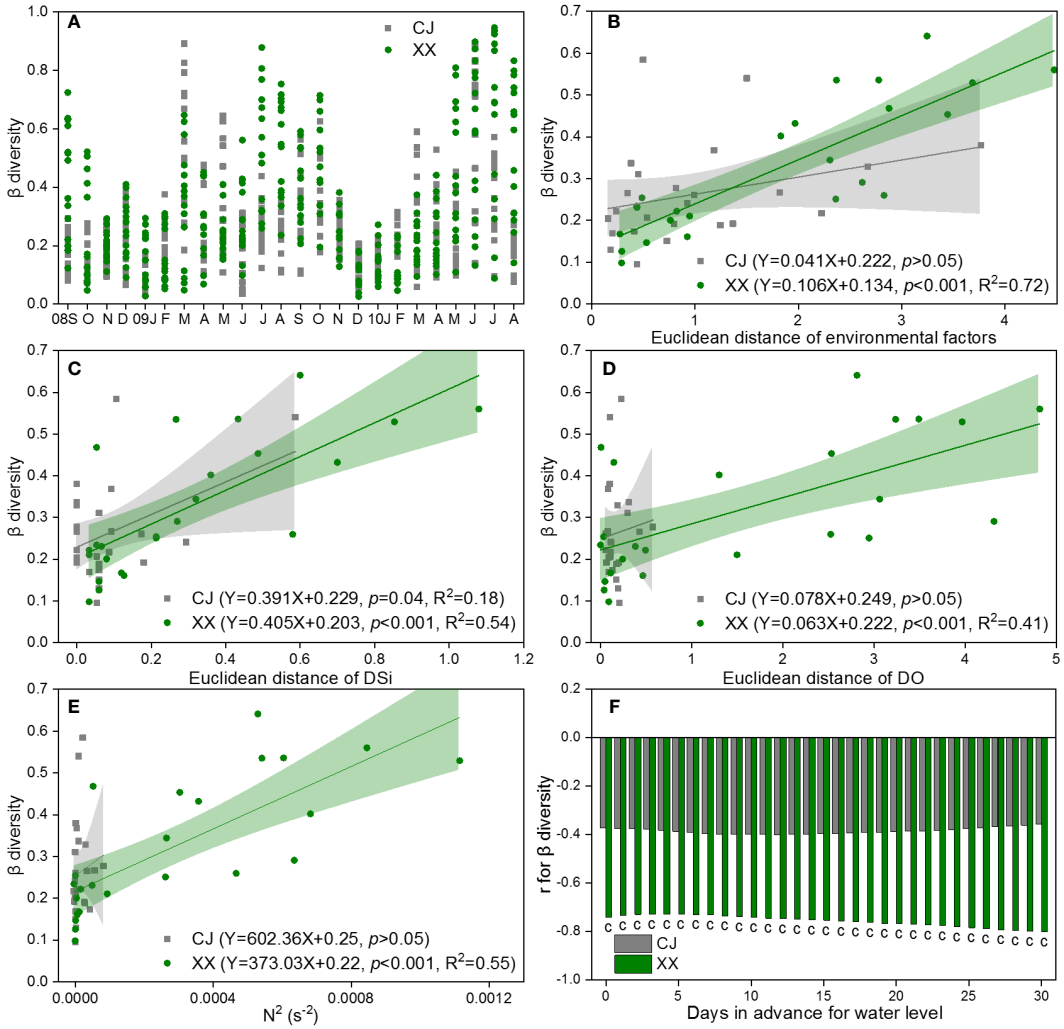


FIGURE 7
β diversity for pairs of water layers based on Bray-Curtis dissimilarity of community **(A)** and its response to Euclidean distance of environmental factors **(B)**, DSi **(C)** and DO **(D)**, as well as $N^2$ **(E)** and water level **(F)** in CJ and XX. Significance level: c denotes $p<0.001$, blank denotes $p>0.05$.

has a stronger resistance to external disturbances and the ability to maintain the system structure relatively unchanged. The relatively stable phytoplankton community structure in CJ was consistent with the temporal dynamics of phytoplankton composition in Supplementary Figures S2 and S3. A similar result was reported by Rodrigues et al. (2018), who found high stability of phytoplankton-environment relationships in all reservoir zones except the tributary in a reservoir in central Brazil.

## 4.2 Impact of water level on vertical disparities in phytoplankton diversity

The vertical differences in phytoplankton diversity between CJ and XX are evident in several aspects. As a representative of α diversity, the Shannon index was higher in XX, while the evenness index was higher in CJ, although both showed similar temporal patterns throughout the study period. This suggests that CJ had a more simplified and evenly distributed phytoplankton community structure compared to XX. The significant negative correlation between the evenness index and water level in CJ indicates that, even during the summer with low water levels, the water column in CJ remains relatively mixed, maintaining an evenly distributed phytoplankton community. In contrast, the phytoplankton community in XX exhibited high species diversity during the summer with low water level and strong stratification.

From the perspective of β diversity, CJ showed a much more similar phytoplankton community between different water layers, with a relatively aggregated pattern of low β diversity. The phytoplankton community in CJ maintained a higher level of independence compared to XX, as the β diversity in CJ showed only a weak correlation with DSi. In contrast, in XX, all the environmental factors, including the matrix and single key environmental factors (DSi and DO), as well as $N^2$, showed significant and high positive correlations with β diversity in XX. In addition, water level showed a significant and high negative correlation with β diversity in XX. Due to the multitude of factors associated with β diversity in XX, a structural equation model was

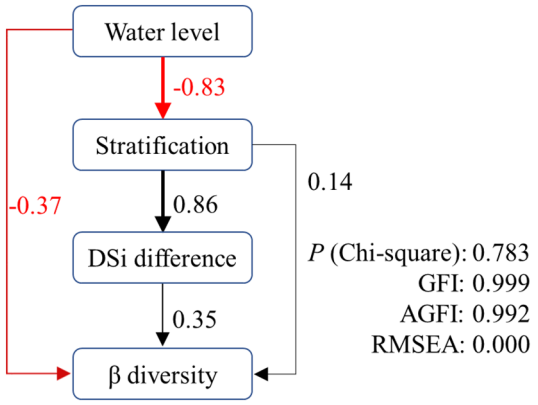


FIGURE 8
Path with structural equation model predicting direct and indirect effects of water level on β diversity in XX.

applied to elucidate the potential pathways through which these factors act. The results showed that both stratification and water level had direct and indirect effects on β diversity in XX, with the direct path involving the DSi difference in water layers.

Water level fluctuation is a complex variable that integrates various physical effects into a comprehensive descriptor (Li et al., 2018). It has been recognized as a key factor influencing phytoplankton biomass and composition in rivers, lakes, and reservoirs (Naselli-Flores and Barone, 1997; Mac Donagh et al., 2009; Wang et al., 2011; Zhu et al., 2013; Yang et al., 2016) through both direct and indirect pathways. Direct effects include biomass dilution and mixing effects during periods of high and low water, respectively. Indirect effects alter the physicochemical characteristics of water bodies, including nutrient variation and underwater light availability (Valdespino-Castillo et al., 2014; Fadel et al., 2015; Liu et al., 2019). These studies have provided valuable insights into how phytoplankton biomass and composition respond to water level effects. However, to the best of our knowledge, the effects of water level on the vertical β diversity of phytoplankton have not been reported.

The reduction of water level during the spring and summer in our study area leads to a more pronounced effect of internal processes with increased residence time. This explains to some extent the direct negative effect of water level on the β diversity of phytoplankton in XX. It also provides a plausible explanation for the occurrence of cyanobacterial blooms following water level drawdowns in certain reservoirs (Cooke, 1980; Yang et al., 2016). The indirect influence of water level acts through stratification and the difference in DSi. The critical role of seasonal stratification in shaping phytoplankton structure and dynamics has been established in reservoir systems (Fonseca and de Mattos Bicudo, 2011; Wang et al., 2011). Our study further confirms that stratification directly affects the variation of community structure throughout the water column, and this stratification is significantly negatively affected by water level (r = -0.83). Stratification promotes an uneven distribution of physiochemical factors in the water column, which in our study significantly increased the DSi difference between water layers (r = 0.86). Silicon is a crucial nutrient for diatom growth, as diatoms need it to build their siliceous cell walls. The high availability of silicon favors the growth of diatoms over non-siliceous phytoplankton (Tréguer and Pondaven, 2000). Consequently, a higher DSi difference induces an increased β diversity of phytoplankton in the vertical direction, thus closing the indirect pathway from water level to β diversity.

To date, numerous researchers have proposed potential strategies for XX under the influence of complex hydrodynamic conditions. Ji et al. (2017) found that the rising water level can lead to an increases or decreases in chlorophyll *a* depending on the water circulation patterns in XX, which were based on both the tributary inflow and the intrusion flow from the TGR. Ye et al. (2022) suggest that the rising water levels have a greater effect on phytoplankton blooms than falling water levels. Gai et al. (2023) suggest a potential dam operation strategy to mitigate blooms during stratification, which involves withdrawing the warm surface water from upstream reservoirs to increase horizontal flows in the surface layer. Through the analysis of vertical phytoplankton data, our study provides a compelling direction for formulating effective water quality management strategies, particularly for XX. Our results highlight the significant negative correlations between β diversity and water level through both direct and indirect effects. During stratification periods characterized by decreased water level, increased phytoplankton density and biomass, along with notable vertical differences of the phytoplankton community, manipulation of water level and application of artificial mixing emerge as promising strategies. The proposed approach involves raising the water level to facilitate dilution and implementing artificial mixing techniques to reduce the β diversity of phytoplankton in different water layers. This approach will not only promote water quality, but also provide a sustainable solution to maintain a balanced ecosystem in the tributary bay. Potential future research directions include: 1) investigating the long-term effects of water level fluctuations on phytoplankton dynamics to understand their ongoing impact on aquatic ecosystems, 2) incorporating advanced modeling techniques to simulate and predict the response of vertical phytoplankton communities to varying environmental conditions to aid in the development of more effective management strategies.

## 5 Conclusion

The study describes the vertical phytoplankton structure and highlights the complex responses of phytoplankton to water level fluctuations and environmental conditions. Monthly data were collected over 2 years in both the mainstream (CJ) and the tributary bay (XX) of the Three Gorges Reservoir. CJ exhibited a more uniform distribution of nutrients across water layers, but maintained a higher overall nutrient level compared to XX. Phytoplankton density and biomass were lower in CJ, which was influenced by water temperature and dissolved oxygen (DO). The phytoplankton community in CJ showed a more stable species-environment relationship, a lower Shannon index and a higher evenness index. This suggests a relatively simple community structure and a more uniform distribution of phytoplankton among different water layers in CJ.

XX had significantly higher phytoplankton density and biomass, influenced by a wide range of environmental factors. The phytoplankton community in XX showed diverse species-environment relationships across different water layers, higher Shannon diversity and a lower evenness. In particular, XX showed increased differences in phytoplankton community between water layers (higher β diversity). These differences showed significant negative correlations with water level and positive correlations with differences in DO, differences in dissolved silica (DSi) and stratification. Peak values of phytoplankton density and biomass, as well as high β diversity in XX, were observed during periods of low water level and strong stratification in spring and summer. A structural equation model complemented by path analysis revealed that a decrease in water level could increase β diversity either directly through internal processes with extended residence time or indirectly by modifying stratification and the vertical distribution of DSi in XX. The substantial disparity in phytoplankton structure characterization between CJ and XX underscores the key role of the tributary in the TGR ecosystem. A proposed water quality management strategy for XX includes raising water levels to facilitate dilution and implementing artificial mixing techniques to reduce the β diversity of phytoplankton across different water layers. The combination of these water quality management methods is expected to effectively control and mitigate algal blooms and help maintain a balanced ecosystem in the tributary bay.

## Data availability statement

The raw data supporting the conclusions of this article will be made available by the authors, without undue reservation.

## Author contributions

LW: Writing – review & editing, Writing – original draft, Visualization, Methodology, Investigation, Formal analysis, Conceptualization. LT: Writing – review & editing, Investigation, Data curation. QC: Writing – review & editing, Supervision, Resources, Project administration, Funding acquisition, Conceptualization.

## Funding

The author(s) declare that financial support was received for the research, authorship, and/or publication of this article. This study was supported by the Hubei Key Laboratory of Wetland Evolution & Ecological Restoration, the Strategic Priority Research Program of CAS (XDA23040500), the National Natural Science Foundation of China (30330140), and the National S&T Basic Work of China (2014FY120200).

## Acknowledgments

We thank Professor Li Wei of Tibet University for conceptualizing and suggesting data analysis, and we also thank the reviewers for their valuable comments and suggestions to improve this manuscript.

## Conflict of interest

The authors declare that the research was conducted in the absence of any commercial or financial relationships that could be construed as a potential conflict of interest.

## Publisher's note



## Supplementary material

The Supplementary Material for this article can be found online at: https://www.frontiersin.org/articles/10.3389/fpls.2024.1381798/full#supplementary-material

## References

Bakker, E., and Hilt, S. (2015). Impact of water-level fluctuations on cyanobacterial blooms: options for management. *Aquat. Ecol.* 50, 485–498. doi: 10.1007/s10452-015-9556-x

Bellinger, E., and Sigee, D. (2015). *Freshwater Algae: Identification, Enumeration and Use as Bioindicators. 2nd Edition* (UK: John Wiley & Sons, Ltd).

Cai, Q. (2007). *Protocols for Standard Observation and Measurement in Aquatic Ecosystems* (Beijing: Chinese Environmental Science Press).

Cai, Q., and Hu, Z. (2006). Studies on eutrophication problem and control strategy in the Three Gorges Reservoir. *Acta Hydrobiologica Sin.* 30, 7–11. doi: 10.3321/j.issn:1000-3207.2006.01.002

Cai, Q., Liu, M., He, Y., Zeng, X., and Jiang, T. (2010). *Climate Change Impact Assessment Report for the Three Gorges Reservoir Area of the Yangtze River* (Beijing: China Meteorological Press).

Cai, Y., Tang, C., and Cao, Y. (2020). Seasonal variation of physical and chemical factors and distribution characteristics of phytoplankton in a subtropical reservoir: a case study from Lianhe Reservoir, South China. *Acta Sci. Nat. Univ. Sunyatseni.* 59, 59–72. doi: 10.13471/j.cnki.acta.snus.2020.03.007

Cardinale, B. J., Duffy, J. E., Gonzalez, A., Hooper, D. U., Perrings, C., Venail, P., et al. (2012). Biodiversity loss and its impact on humanity. *Nature* 486, 59–67. doi: 10.1038/nature11148

Chen, Z., Sun, J., Gu, T., Zhang, G. C., and Wei, Y. Q. (2021). Nutrient ratios driven by vertical stratification regulate phytoplankton community structure in the oligotrophic western Pacific Ocean. *Ocean Sci.* 17, 1775–1789. doi: 10.5194/os-17-1775-2021

Cooke, G. (1980). Lake level drawdown as a macrophyte control technique. *JAWRA J. Am. Water Resour. Assoc.* 16, 317–322. doi: 10.1111/j.1752-1688.1980.tb02397.x

Cordero-Bailey, K., Bollozos, I. S. F., Palermo, J. D. H., Silvano, K. M., Escobar, M. T. L., Jacinto, G. S., et al. (2021). Characterizing the vertical phytoplankton distribution in the Philippine Sea off the northeastern coast of Luzon. *Estuar. Coast. Shelf Sci.* 254, 107322. doi: 10.1016/j.ecss.2021.107322

Cui, G. Y., Wang, B. L., Xiao, J., Qiu, X. L., Liu, C. Q., and Li, X. D. (2021). Water column stability driving the succession of phytoplankton functional groups in karst hydroelectric reservoirs. *J. Hydrology*. 592, 125607. doi: 10.1016/j.jhydrol.2020.125607

Cui, Z., Gao, W., Li, Y., Wang, W., Wang, H., Liu, H., et al. (2023). Dissolved oxygen and water temperature drive vertical spatiotemporal variation of phytoplankton community: Evidence from the largest diversion water source area. *Int. J. Environ. Res. Public Health* 20, 4307. doi: 10.3390/ijerph20054307

Fadel, A., Atoui, A., Lemaire, B., Vinçon-Leite, B., and Slim, K. (2015). Environmental factors associated with phytoplankton succession in a Mediterranean reservoir with a highly fluctuating water level. *Environ. Monit. Assess.* 187, 633. doi: 10.1007/s10661-015-4852-4

Fonseca, B., and de Mattos Bicudo, C. (2011). Phytoplankton seasonal and vertical variations in a tropical shallow reservoir with abundant macrophytes (Ninféias Pond, Brazil). *Hydrobiologia* 665, 229–245. doi: 10.1007/s10750-011-0626-3

Gai, B., Sun, J., Lin, B., Li, Y., Mi, C., and Shatwell, T. (2023). Vertical mixing and horizontal transport unravel phytoplankton blooms in a large riverine reservoir. *J. Hydrology* 627, 130430. doi: 10.1016/j.jhydrol.2023.130430

Guo, K., Wu, N., Manolaki, P., Baattrup-Pedersen, A., and Riis, T. (2020). Short-period hydrological regimes override physico-chemical variables in shaping stream diatom traits, biomass and biofilm community functions. *Sci. Total Environ.* 743, 140720. doi: 10.1016/j.scitotenv.2020.140720

Hu, H., and Wei, Y. (2006). *The Freshwater Algae of CHINA—Systematics, Taxonomy and Ecology* (Beijing: Science Press).

Huang, T., Wen, C., Wang, S., Wen, G., Li, K., Zhang, H., et al. (2022). Controlling spring Dinoflagellate blooms in a stratified drinking water reservoir via artificial mixing: Effects, mechanisms, and operational thresholds. *Sci. Total Environ.* 847, 157400. doi: 10.1016/j.scitotenv.2022.157400

Huang, X., Chen, W., and Cai, Q. (2000). *Survey, Observation and Analysis of Lake Ecosystem* (Beijing: China Standards Press).

Huang, Z., Li, Y., Chen, Y., Li, J., Xing, Z., Ye, M., et al. (2006). *Water quality prediction and water environmental carrying capacity calculation for Three Gorges Reservoir* (Beijing: China WaterPower Press).

Huisman, J., Sharples, J., Stroom, J. M., Visser, P. M., Kardinaal, W. E. A., Verspagen, J. M. H., et al. (2004). Changes in turbulent mixing shift competition for light between phytoplankton species. *Ecology* 85, 2960–2970. doi: 10.1890/03-0763

Ikram, H., Ouadiaa, T., Laila, S., Leila, E., Aziz, A., Said, C., et al. (2017). Vertical phytoplankton community distribution under seasonal fluctuations. *Elixir Biosci.* 110, 48239–48243.

Ji, D. B., Wells, S. A., Yang, Z. J., Liu, D. F., Huang, Y. L., Ma, J., et al. (2017). Impacts of water level rise on algal bloom prevention in the tributary of Three Gorges Reservoir, China. *Ecol. Eng.* 98, 70–81. doi: 10.1016/j.ecoleng.2016.10.019

Jiang, T., Zhang, Q., Zhu, D., and Wu, Y. (2006). Yangtze floods and droughts (China) and teleconnections with ENSO activities, (1470–2003). *Quaternary Int.* 144, 29–37. doi: 10.1016/j.quaint.2005.05.010

John, D., Whitton, B., and Brook, A. (2002). *The Freshwater Algal Flora of the British Isles—An Identification Guide to Freshwater and Terrestrial Algae* (UK: Cambridge University Press).

Kuang, Q., Bi, Y., Zhou, G., Cai, Q., and Hu, Z. (2005). Study on the phytoplankton in the Three Gorges Reservoir before and after sluice and the protection of water quality. *Acta Hydrobiologica Sin.* 29, 353–358. doi: 10.1111/j.1440-1789.2005.00601.x

Lepš, J., and Šmilauer, P. (2003). *Multivariate Analysis of Ecological Data Using CANOCO* (Cambridge: Cambridge University Press).

Li, G., Cheng, L., Zhu, J., Trenberth, K., Mann, M., and Abraham, J. (2020). Increasing ocean stratification over the past half-century. *Nat. Climate Change* 10, 1116–1123. doi: 10.1038/s41558-020-00918-2

Li, Q., Xiao, J., Ou, T., Han, M., Wang, J., Chen, J., et al. (2018). Impact of water level fluctuations on the development of phytoplankton in a large subtropical reservoir: implications for the management of cyanobacteria. *Environ. Sci. pollut. Res.* 25, 1306–1318. doi: 10.1007/s11356-017-0502-4

Li, P. Y., Yao, Y., Lian, J. J., and Ma, C. (2021). Effect of thermal stratified flow on algal blooms in a tributary bay of the Three Gorges reservoir. *J. Hydrology*. 601, 126648. doi: 10.1016/j.jhydrol.2021.126648

Liu, J., Chen, Y., Li, M., Liu, B., Liu, X., Wu, Z., et al. (2019). Water-level fluctuations are key for phytoplankton taxonomic communities and functional groups in Poyang Lake. *Ecol. Indic.* 104, 470–478. doi: 10.1016/j.ecolind.2019.05.021

Liu, L., Liu, D., Johnson, D. M., Yi, Z., and Huang, Y. (2012). Effects of vertical mixing on phytoplankton blooms in Xiangxi Bay of Three Gorges Reservoir: implications for management. *Water Res.* 46, 2121–2130. doi: 10.1016/j.watres.2012.01.029

Lu, Y., Tuo, Y., Zhang, L., Hu, X., Huang, B., Chen, M., et al. (2023). Vertical distribution rules and factors influencing phytoplankton in front of a drinking water reservoir outlet. *Sci. Total Environ.* 902, 166512. doi: 10.1016/j.scitotenv.2023.166512

Mac Donagh, M., Casco, M., and Claps, M. (2009). Plankton relationships under small water level fluctuations in a subtropical reservoir. *Aquat. Ecol.* 43, 371–381. doi: 10.1007/s10452-008-9197-4

Mellard, J. P., Yoshiyama, K., Litchman, E., and Klausmeier, C. A. (2011). The vertical distribution of phytoplankton in stratified water columns. *J. Theor. Biol.* 269, 16–30. doi: 10.1016/j.jtbi.2010.09.041

Mojica, K. D. A., van de Poll, W. H., Kehoe, M., Huisman, J., Timmermans, K. R., Buma, A. G. J., et al. (2015). Phytoplankton community structure in relation to vertical stratification along a north-south gradient in the Northeast Atlantic Ocean. *Limnology Oceanography* 60, 1498–1521. doi: 10.1002/lno.10113

Naselli-Flores, L., and Barone, R. (1997). Importance of water-level fluctuation on population dynamics of cladocerans in a hypertrophic reservoir (Lake Arancio, south-west Sicily, Italy). *Hydrobiologia* 360, 223–232. doi: 10.1007/978-94-011-4964-8_25

New, T., and Xie, Z. (2008). Impact of large dams on riparian vegetation: Applying global experience to the case of China's Three Gorges Dam. *Biodiversity Conserv.* 17, 3149–3163. doi: 10.1016/S0075-9511(03)80025-7

Olden, J., and Poff, N. (2003). Redundancy and the choice of hydrologic indices for characterizing streamflow regimes. *River Res. Applic.* 19, 101–121. doi: 10.1002/rra.700

Phillips, G., Lyche-Solheim, A., Skjelbred, B., Mischke, U., Drakare, S., Free, G., et al. (2013). A phytoplankton trophic index to assess the status of lakes for the Water Framework Directive. *Hydrobiologia* 704, 75–95. doi: 10.1007/s10750-012-1390-8

Radchenko, I. G., Aksenova, V. A., Voronov, D. A., Rostanets, D. V., and Krasnova, E. D. (2023). Annual dynamics of a layered phytoplankton structure in a meromictic lagoon partially isolated from the White Sea. *Diversity* 15, 1009. doi: 10.3390/d15091009

Rath, A. R., Mitbavkar, S., and Anil, A. C. (2021). Response of the phytoplankton community to seasonal and spatial environmental conditions in the Haldia port ecosystem located in the tropical Hooghly River estuary. *Environ. Monit Assess.* 193, 548. doi: 10.1007/s10661-021-09255-z

Rodrigues, L. C., Pivato, B. M., Vieira, L. C. G., Bovo-Scomparin, V. M., Bortolini, J. C., Pineda, A., et al. (2018). Use of phytoplankton functional groups as a model of spatial and temporal patterns in reservoirs: a case study in a reservoir of central Brazil. *Hydrobiologia* 805, 147–161. doi: 10.1007/s10750-017-3289-x

Ryabov, A. B., Rudolf, L., and Blasius, B. (2010). Vertical distribution and composition of phytoplankton under the influence of an upper mixed layer. *J. Theor. Biol.* 263, 120–133. doi: 10.1016/j.jtbi.2009.10.034

Sakharova, E. G., and Korneva, L. G. (2018). Phytoplankton in the littoral and pelagial zones of the rybinsk reservoir in years with different temperature and water-level regimes. *Inland Water Biol.* 11, 6–12. doi: 10.1134/S1995082918010157

Schermelleh-Engel, K., Moosbrugger, H., and Müller, H. (2003). Evaluating the fit of structural equation models: tests of significance and descriptive goodness-of-fit measures. *Mpr Online*. 8 (2), 23–74.

Shipley, B. (2002). *Cause and Correlation in Biology: A User's Guide to Path Analysis, Structural Equations and Causal Inference* (Cambridge: Cambridge University Press, Cambridge).

Slimani, N., Guilbert, E., Ayni, F., Jrad, A., Boumaiza, M., and Thioulouse, J. (2017). The use of STATICO and COSTATIS, two exploratory three-ways analysis methods: an application to the ecology of aquatic heteroptera in the Medjerda watershed (Tunisia). *Environ. Ecol. Stat* 24, 269–295. doi: 10.1007/s10651-017-0370-6

Straškraba, M. (2005). "Reservoirs and other artificial water bodies," in *The Lakes Handbook: Volume 2 Lake Restoration and Rehabilitation* (Oxford: Blackwell Publishing).

Thioulouse, J. (2011). Simultaneous analysis of a sequence of paired ecological tables: A comparison of several methods. *Ann. Appl. Stat.* 5, 2300–2325. doi: 10.1214/10-aoas372

Thioulouse, J., Simier, M., and Chessel, D. (2004). Simultaneous analysis of a sequence of paired ecological tables. *Ecology* 85, 272–283. doi: 10.1890/02-0605

Tilman, D., Isbell, F., and Cowles, J. M. (2014). Biodiversity and ecosystem functioning. *Annu. Rev. Ecol. Evol. Syst.* 45, 471–493. doi: 10.1146/annurev-ecolsys-120213-091917

Tréguer, P., and Pondaven, P. (2000). Silica control of carbon dioxide. *Nature* 406, 358–359. doi: 10.1038/35019236

Valdespino-Castillo, P. M., Merino-Ibarra, M., Jimenez-Contreras, J., Castillo-Sandoval, F. S., and Ramirez-Zierold, J. A. (2014). Community metabolism in a deep (stratified) tropical reservoir during a period of high water-level fluctuations. *Environ. Monit Assess.* 186, 6505–6520. doi: 10.1007/s10661-014-3870-y

Visser, P. M., Ibelings, B. W., Bormans, M., and Huisman, J. (2016). Artificial mixing to control cyanobacterial blooms: a review. *Aquat. Ecol.* 50, 423–441. doi: 10.1007/s10452-015-9537-0

Wang, L., Cai, Q., Xu, Y., Kong, L., Tan, L., and Zhang, M. (2011). Weekly dynamics of phytoplankton functional groups under high water level fluctuations in a subtropical reservoir-bay. *Aquat. Ecol.* 45, 197–212. doi: 10.1007/s10452-010-9346-4

Wang, J., Wang, B., and Luo, Z. (1997). *Glossary of the Yangtze River* (Wuhan: Wuhan Press).

Wen, C., Huang, T., Wen, G., Li, K., Yang, S., Zhang, H., et al. (2022). Controlling phytoplankton blooms in a canyon-shaped drinking water reservoir via artificial and induced natural mixing: Taxonomic versus functional groups. *Chemosphere* 287, 131771. doi: 10.1016/j.chemosphere.2021.131771

Wetzel, R., and Likens, G. (2000). *Limnological analyses* Vol. 3 (New York: Springer).

Xue, K., Zhang, Y. C., Ma, R. H., and Duan, H. T. (2017). An approach to correct the effects of phytoplankton vertical nonuniform distribution on remote sensing reflectance of cyanobacterial bloom waters. *Limnology Oceanography-Methods* 15, 302–319. doi: 10.1002/lom3.10158

Yang, J., Lv, H., Yang, J., Liu, L., Yu, X., and Chen, H. (2016). Decline in water level boosts cyanobacteria dominance in subtropical reservoirs. *Sci. Total Environ.* 557-558, 445–452. doi: 10.1016/j.scitotenv.2016.03.094

Ye, L., Tan, L., Wu, X., Cai, Q., and Li, B. L. (2022). Nonlinear causal analysis reveals an effective water level regulation approach for phytoplankton blooms controlling in reservoirs. *Sci. Total Environ.* 806, 150948. doi: 10.1016/j.scitotenv.2021.150948

Zhu, K., Bi, Y., and Hu, Z. (2013). Responses of phytoplankton functional groups to the hydrologic regime in the Daning River, a tributary of Three Gorges Reservoir, China. *Sci. Total Environ.* 450-451, 169–177. doi: 10.1016/j.scitotenv.2013.01.101

frontiers | Frontiers in Plant Science

TYPE Original Research
PUBLISHED 03 April 2024
DOI 10.3389/fpls.2024.1367680



OPEN ACCESS

EDITED BY
Qiang Yang,
German Centre for Integrative Biodiversity Research (iDiv), Germany

REVIEWED BY
Jiachao Zhang,
Hunan Agricultural University, China
Sha Wu,
Shenzhen University, China

*CORRESPONDENCE
Xingqiang Wu
xqwu@ihb.ac.cn

RECEIVED 09 January 2024
ACCEPTED 01 March 2024
PUBLISHED 03 April 2024

CITATION
Yang T, Pan J, Wu H, Tian C, Wang C, Xiao B, Pan M and Wu X (2024) Rapid flotation of *Microcystis wesenbergii* mediated by high light exposure: implications for surface scum formation and cyanobacterial species succession. *Front. Plant Sci.* 15:1367680. doi: 10.3389/fpls.2024.1367680



# Rapid flotation of *Microcystis wesenbergii* mediated by high light exposure: implications for surface scum formation and cyanobacterial species succession

Tiantian Yang[1,2], Jiaxin Pan[1,3], Huaming Wu[4], Cuicui Tian[1,2], Chunbo Wang[1,2], Bangding Xiao[1,2], Min Pan[2] and Xingqiang Wu[1,2]*

[1]Key Laboratory of Algal Biology of Chinese Academy of Sciences, Institute of Hydrobiology, Chinese Academy of Sciences, Wuhan, China, [2]Kunming Dianchi & Plateau Lakes Institute, Dianchi Lake Ecosystem Observation and Research Station of Yunnan Province, Kunming, China, [3]College of Hydraulic and Envrionmental Engineering, China Three Gorges University, Yichang, China, [4]Institute for Environmental Sciences, University of Koblenz-Landau, Landau, Germany

Increasing occurrences of *Microcystis* surface scum have been observed in the context of global climate change and the increase in anthropogenic pollution, causing deteriorating water quality in aquatic ecosystems. Previous studies on scum formation mainly focus on the buoyancy-driven floating process of larger *Microcystis* colonies, neglecting other potential mechanisms. To study the non-buoyancy-driven rapid flotation of *Microcystis*, we here investigate the floating processes of two strains of single-cell species (*Microcystis aeruginosa* and *Microcystis wesenbergii*), which are typically buoyant, under light conditions (150 µmol photons $s^{-1}$ $m^{-2}$). Our results showed that *M. wesenbergii* exhibited fast upward migration and formed surface scum within 4 hours, while *M. aeruginosa* did not form visible scum throughout the experiments. To further explore the underlying mechanism of these processes, we compared the dissolved oxygen (DO), extracellular polymeric substance (EPS) content, and colony size of *Microcystis* in different treatments. We found supersaturated DO and the formation of micro-bubbles (50–200 µm in diameter) in *M. wesenbergii* treatments. *M. aeruginosa* produces bubbles in small quantities and small sizes. Additionally, *M. wesenbergii* produced more EPS and tended to aggregate into larger colonies. *M. wesenbergii* had much more derived-soluble extracellular proteins and polysaccharides compared to *M. aeruginosa*. At the same time, *M. wesenbergii* contains abundant functional groups, which was beneficial to the formation of agglomerates. The surface scum observed in *M. wesenbergii* is likely due to micro-bubbles attaching to the surface of cell aggregates or becoming trapped within the colony. Our study reveals a species-specific mechanism for the rapid floatation of *Microcystis*, providing novel insights into surface scum formation as well as succession of cyanobacterial species.

KEYWORDS

***Microcystis*, surface scum formation, cell aggregation, micro-bubbles, extracellular polymeric substance**

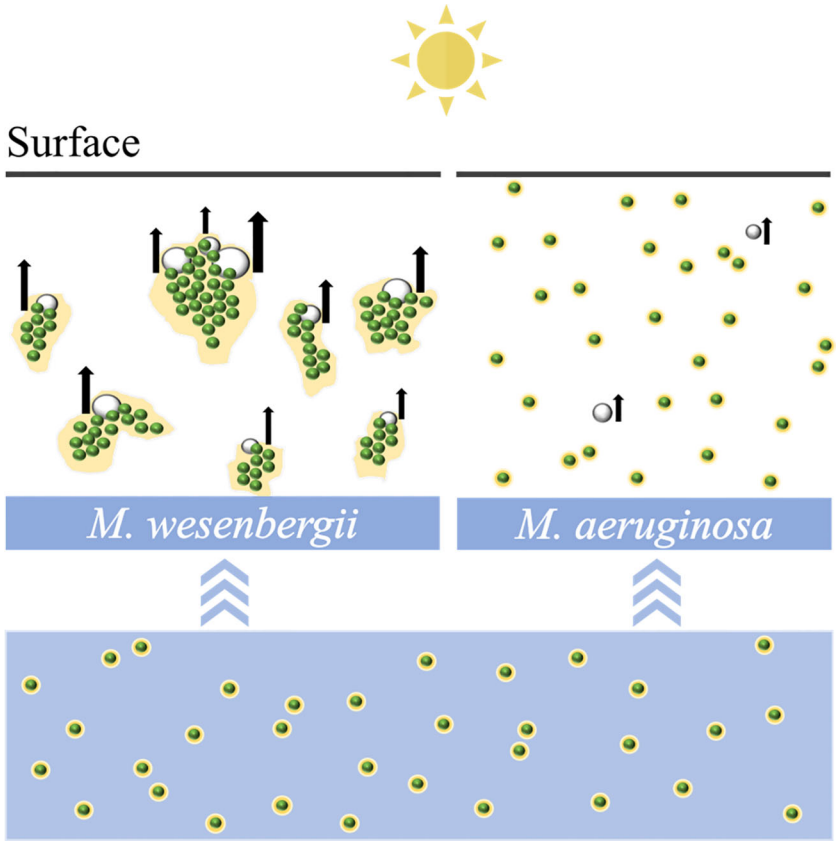


GRAPHICAL ABSTRACT

## Highlights

- EPS produced by *Microcystis wesenbergii* can contribute to the formation of large aggregates.
- The formation of aggregate and micro-bubble can drive the surface scum formation.
- Light and EPS contributed to the formation of the large algal aggregate.

## 1 Introduction

Cyanobacterial blooms exist in many freshwater bodies worldwide (Schindler, 1974). *Microcystis* spp., which can form colonies ranging in size from a few microns to a few millimeters, are the most common and ubiquitous toxic blooms (Paerl et al., 2014). Under warming and eutrophic conditions, *Microcystis* cells have the propensity to aggregate and float upward, giving rise to harmful *Microcystis* blooms (Luerling et al., 2017; Zhu et al., 2023). The extensive proliferation of harmful *Microcystis* has various negative effects on human health and environmental safety (Fiehn et al., 1998; Susanna et al., 2020). This phenomenon results in the depletion of dissolved oxygen in the water, causing disruptions to aquatic ecosystems (Paerl et al., 2011; Guo et al., 2022), in which the decay of biomass ultimately leads to oxygen depletion, causing a complete alteration of the aquatic environment (Hallegraeff, 1993). Microcystins are toxins produced by a variety of bloom-forming cyanobacteria that can cause hepatotoxicity in humans and animals (Zhou et al., 2021).

The formation of *Microcystis* blooms is affected by various biotic and abiotic factors, including nutrients, light, temperature (Andrew, 1991; Soranno, 1997; Hans and Valerie, 2012; Min et al., 2012), hydrodynamic conditions (Medrano et al., 2013; Chao et al., 2017), predation (Wang et al., 2010), and buoyancy of *Microcystis* colonies (Jacco and Luuc, 1984; Medrano et al., 2016). Due to the buoyancy regulation, *Microcystis* is capable of forming surface scum in eutrophic lakes (Chorus, 1999; Rainer et al., 2003). Many former studies suggest that buoyancy provides several competitive advantages for *Microcystis* over phytoplankton, including the capability to acquire light and carbon dioxide at the uppermost layer, and grazing avoidance (Reynolds and Walsby, 1975; Lovelock et al., 2008). *Microcystis* had a diurnal migration pattern, and migration causes were affected by multiple factors (Wu et al., 2019). This development will be rapid, probably on a characteristic timescale of approximately a day (Timothy et al., 2009). The sudden increases in biomass at the surface layer may lead to long-term proliferative cell interactions and mass migration of biomass. In many cases, this migration ends up forming thick scum on the surface of the water (Anne et al., 2016).

There is currently research evidence demonstrating that the regulation of gas buoyancy on vesicles and carbohydrate ballast is a crucial factor in the migration of *Microcystis* colony (Colin et al., 2002). The hypothesis posited suggests that the irreversible buoyancy of cyanobacterial colonies is induced by the growth of gas bubbles on or within the mucilage of the colonies (Medrano et al., 2016). They hypothesized that the irreversible buoyancy of cyanobacterial colonies is induced by the growth of bubbles on or inside the colony mucilage. These bubbles grow under conditions of oxygen supersaturation. Meanwhile, many abiotic factors can affect the buoyancy of *Microcystis* through these mechanisms (Hans and Jef, 2008; Paerl and Otten, 2013). For instance, light has been found to regulate buoyancy through the carbohydrate ballast mechanism. Specifically, *Microcystis* loses buoyancy under high light conditions, while it regains buoyancy under low light conditions. This allows *Microcystis* to exhibit a diel migration pattern, where it floats upward to the surface at night and sinks during the daytime. Although this migration pattern has been confirmed by many lake studies (Ma et al., 2015), there are exceptions where *Microcystis* forms scum on a shorter timescale of hours and can persist at the water surface even under high light conditions during the daytime. This may imply the existence of additional mechanisms for the rapid *Microcystis* flotation and the surface scum formation under strong light conditions.

To fill the knowledge gaps, the influence of high light on the floatation and surface scum formation of *Microcystis* was investigated in this study. We used two different strains of *Microcystis* species (*Microcystis wesenbergii* and *Microcystis aeruginosa*), which are neutrally buoyant, to study the non-buoyancy-driven floatation of *Microcystis* with laboratory experiments. We hypothesize that the bubbles generated from photosynthesis during high light exposure can felicitate the rapid floatation of *Microcystis*. We aim to study the mechanism of rapid floatation of *Microcystis* driven by bubble formation. This study is expected to provide new implications for the mechanism for the formation of *Microcystis* blooms as well as cyanobacterial species succession.

# 2 Materials and methods

## 2.1 *Microcystis* strains and culture conditions

Two different *Microcystis* strains (*M. wesenbergii*, FACHB-908, and *M. aeruginosa*, FACHB-905) used in this study were generously provided by the Freshwater Algae Culture Collection at the Institute of Hydrobiology, Chinese Academy of Sciences (FACHB-collection, Wuhan, China). The strains were cultured in BG11 medium (Supplementary Table 1) at 25°C with a 16-hour light/8-hour dark cycle of 32 μmol photons $s^{-1}$ $m^{-2}$ to obtain a cell density of ca. 800 μg/L (Lin et al., 2017).

## 2.2 Experimental design

To study the effect of light intensity on the *Microcystis* aggregation and their upward floating to the surface, *M. aeruginosa* and *M. wesenbergii* were diluted to the same initial Chl*a* concentration (ca. 800 μg/L). Two types of *Microcystis* were placed in separate 50-mL glass tubes (height, 20 cm) under strong light (150 μmol photons $s^{-1}$ $m^{-2}$) and dark conditions. The light source was derived from a LED lamp located on the side of the test tubes to provide light. Dark conditions were carried out in a closed cabinet. The room temperature was maintained at 25°C. Samples that float to the surface were mainly collected to measure the dissolved oxygen, electrolytic potential, and extracellular polysaccharides. All the treatments and controls were performed in triplicate. A Canon camera was used to capture images of *Microcystis* aggregation and floating to determine the state and size of the aggregation under light conditions.

## 2.3 Measurement and characterization of algal aggregate extracellular polymeric substances derived from *Microcystis*

To analyze the composition of special substances in extracellular polymeric substances (EPS) released by two different strains of *Microcystis* under light conditions, two treatments and two controls were prepared, as follows. To prepare surface aggregate samples, 50 mL of algal solution containing *M. wesenbergii* (A) and *M. aeruginosa* (B) was used. Light conditions were used as treatment and dark conditions as control, with the same density of *Microcystis* solution (L and D as abbreviations for light and dark, respectively). The samples were placed in a 50-mL centrifuge tube. Three parallel samples were analyzed for each group using the method described below.

### 2.3.1 EPS extraction and quantification

The extracellular polymeric substances were collected from the *M. aeruginosa* and *M. wesenbergii* cultures (stationary phase) according to the method of Xiao et al. (2019). Algae suspensions (10 mL) were centrifuged at 11,000 *g* and 4°C for 15 minutes, separating the supernatant and algal cells. The EPS fractions were then divided into soluble EPS (S-EPS) and bound EPS (B-EPS). The supernatant was used to determine the soluble EPS. The pH was adjusted to 10 using the 1 mol/L of sodium hydroxide. The samples were then placed in a water bath sonicator at intermediate power (25 kHz) and 45°C to separate cells from loosely bound EPS. The resulting EPS were classified as conjunction type and stored at −20°C until analysis. The total EPS content in the algal aggregate was calculated as the sum of polysaccharides and proteins. The protein content was determined using Coomassie brilliant blue (Marion, 1976). The polysaccharides were analyzed using the phenol-sulfuric acid method (Dubois et al., 1951).

### 2.3.2 EPS fluorescence staining and confocal laser scanning microscopy analysis

A modified fluorescence staining method according to Liu (Liu et al., 2020) was used to observe the components of EPS. The *Microcystis* samples were collected from the surface layer and washed three times with phosphate buffer (pH = 7) to remove the medium. They were then fixed with 2.5% glutaraldehyde. The SYTO63 stain (Thermo Fisher Scientific, Waltham, MA, USA), fluorescein isothiocyanate (FITC), and calcofluor white were used to stain bacterial cells, proteins, and polysaccharides, respectively. The spatial distribution of various components in EPS was observed using confocal laser scanning microscopy (CLSM) (TCS, Leica, Wetzlar, Germany). The excitation wavelengths for polysaccharides and proteins were 400 nm and 480 nm, with the emission wavelengths of 480 nm and 550 nm, respectively (Chen et al., 2007). After each staining procedure, samples were washed at least twice with phosphate-buffered saline (PBS) (pH = 7.2) to remove excess stains. The polysaccharides are represented by blue fluorescence, the proteins are represented by green fluorescence, and the bacteria are represented by red fluorescence (Badiaa et al., 2010). The sample preparation process should be carried out in a darkroom to avoid fluorescence.

### 2.3.3 Fourier transform infrared spectrum and fluorescence spectrometer analysis

The Fourier transform infrared (FT-IR) spectrum of EPS samples was analyzed using a Fourier transform infrared spectrometer (Nicolet 6700, Thermo Scientific Co., Ltd., USA). All samples were washed twice with PBS (pH = 7.2), then lyophilized, and stored at −20°C (Bo et al., 1996). Before FT-IR scanning, samples were ground with IR-grade KBr powder and molded into a disc. The infrared absorption spectra of transmittance or absorbance with wave number or wavelength were obtained by Fourier transform. The components of organic chemicals were analyzed using sub-peak spectra obtained from the original spectra through curve fitting.

The fluorescence intensity of the protein-like components and humic acid-like components in samples was measured using the fluorescence excitation–emission matrix (3D EEM) with a fluorescence spectrometer (Hitachi F4700, Hitachi, Tokyo, Japan) (Yunlin et al., 2014). The slit width was set to 5 nm, and the photomultiplier was set to a voltage of 720 V. The excitation scanning range was 250–450 nm, and the emission scanning range was 300–550 nm and 2 nm. The EEM data of deionized water were also subtracted to remove the effect of Raman scattering (Markus et al., 2010).

## 2.4 The *Microcystis* algae cell density

The cell density was counted three times in a hemocytometer using an optical microscope (BX43, Olympus Corporation, Tokyo, Japan) at ×40 magnification.

## 2.5 Statistical analysis

Variance analysis (ANOVA) was used to determine the difference in EPS content released from different strains of *Microcystis*. Statistical significance was set at $p < 0.05$. All significant differences between samples were determined using SPSS version 25 (IBM, USA). Graphs were generated using Origin 8.0 software (OriginLab, Northampton, MA, USA).

# 3 Results

## 3.1 Effect of light intensity on the surface *Microcystis* aggregates

As shown in Supplementary Video 1, *M. wesenbergii* suddenly produced bubbles under strong light intensity in the middle stage, causing the algal biomass to rise and reach a layer of foam at the air–water interface. Under suitable nutrient and light conditions, the dissolved oxygen (DO) in photosynthetic active cells was supersaturated to form bubbles. Bubbles were wrapped and expanded until buoyancy was sufficient to pull *M. wesenbergii* aggregates to the water surface and to form a stable surface bloom after 4 hours. However, this phenomenon was not observed in *M. aeruginosa*. *M. aeruginosa* only produced very few bubbles uniformly distributed in the water column.

Figure 1 illustrates the typical time evolution of the system. The culture kept in darkness remained homogeneous throughout the experiment. We observed a massive migration of the biomass toward the water surface in the sample exposed to high light exposure. The floating phenomena of *M. wesenbergii* and *M. aeruginosa* were distinct (Figure 1D). The migration and aggregation of *M. wesenbergii* resulted from the generation and floating migration of bubbles. At the same time, the bubbles cause *M. wesenbergii* to rise to the surface (Figure 1C). Approximately 1 hour after the start of the experiment, bubbles began to form gradually. For approximately 2 hours, the test tubes were filled with numerous stable bubbles (Figure 1A). When the test tubes were slightly shaken, the bubbles floated up quickly and did not adhere to the wall of the test tubes. This indicates that the *M. wesenbergii* is covering them, and these bubbles continued to increase until they were sufficiently supported to float. It should be noted that cyanobacteria under light conditions persist in the bacterial foam formed at the surface (Figure 1C) and did not sink even after 1 week. In contrast, the samples placed in darkness settled. Additionally, we observed supersaturated DO and the formation of micro-bubbles (50–200 μm in diameter) in *M. wesenbergii* treatments, while *M. aeruginosa* produced bubbles in small quantities and small sizes (Supplementary Figure 1).

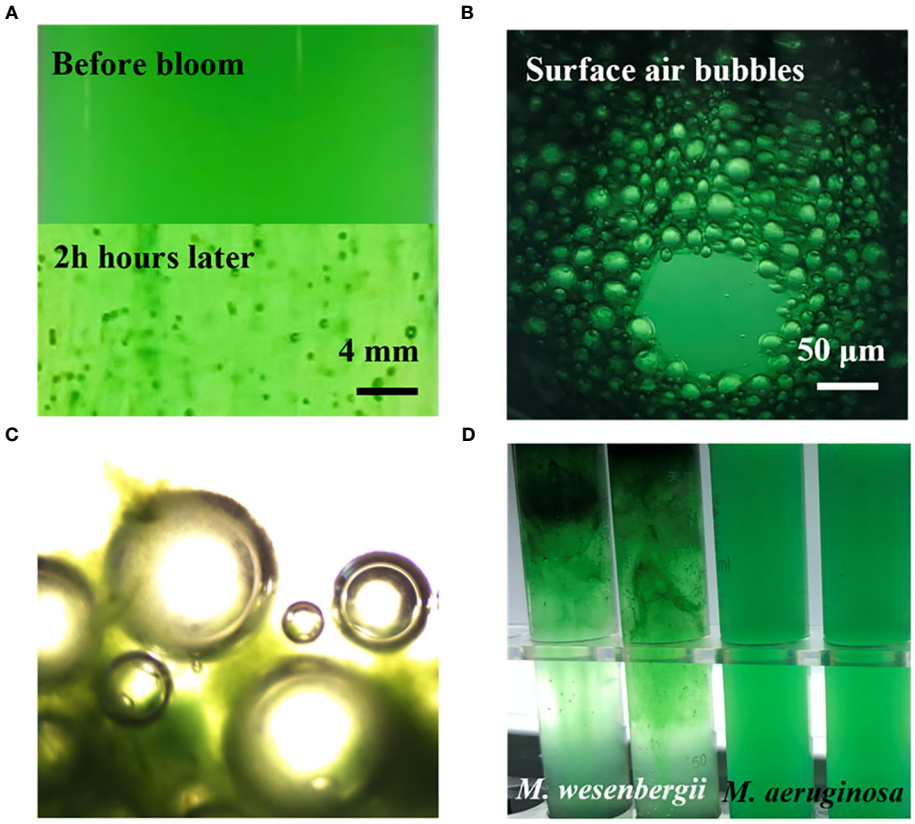


FIGURE 1
Contrast before and after the formation of cyanobacterial blooms. **(A)** Bubbles of *Microcystis wesenbergii* forming during experimentation. **(B)** Aggregation of the biomass and bubble production of *M. wesenbergii* during a bloom. **(C)** Microscopic bubbles and *Microcystis* aggregates. **(D)** Different experimental phenomena produced by *M. wesenbergii* and *Microcystis aeruginosa*.

## 3.2 Changes in physicochemical indexes of surface *Microcystis* aggregates (DO and zeta potential)

When the bloom in *M. wesenbergii* produced a large number of bubbles, we hypothesized that the gas was oxygen, a by-product of photosynthesis. We then measured the dynamic DO contents at the air–water interface under dark and light conditions. As shown in Figure 2A, the DO concentration of the two different strains of *Microcystis* was approximately 10.8 mg/L initially. The dissolved oxygen concentration of *M. wesenbergii* increased linearly at a rate of 5 mg $L^{-1}$ $h^{-1}$ over the next 4 hours under light conditions. Under dark conditions, the DO concentration decreased steadily and eventually fell below the equilibrium value of 8.1 mg/L, indicating active aerobic respiration in the system. In contrast, under light conditions, the DO concentration of *M. wesenbergii* increased linearly at a rate of 2 mg $L^{-1}$ $h^{-1}$ until the detection limit of the DO probe (42 mg/L) approximately 300 minutes after the start of the experiment. The rate of DO increase for *M. aeruginosa* was much lower. This was consistent with the experimental phenomenon (Figure 1D).

Zeta potential is usually used to monitor the electrostatic neutralization of particles to explain the relationship between particle instability and floc formation (Arya et al., 2019). The magnitude of the electrokinetic potential is associated with the stability of the solution. At the start of the experiment, the zeta potentials of *M. aeruginosa* and *M. wesenbergii* solution were similar below 30 mV. However, by the end of the experiment, the zeta potentials of the *M. wesenbergii* solution had significantly increased to a lower value of (−5 mV). The electric potential of *M. wesenbergii* changed noticeably before and after the experiment, indicating the neutralization of electrostatic particles by static electricity. This phenomenon was not observed in the other treatment groups, confirming the consistency of the experimental results.

## 3.3 Changes in the content of extracellular material in *Microcystis* aggregates

Polysaccharides and protein content were measured in mixed and surface samples of *M. wesenbergii* and *M. aeruginosa* under dark and light conditions. Figure 3 shows that under light conditions, the polysaccharides secreted by *M. wesenbergii* were significantly higher than those secreted by *M. aeruginosa* ($p < 0.05$), but there was little difference under dark conditions. Under light conditions, the polysaccharides secreted by the surface layer of *M. wesenbergii* were significantly higher than those in the water

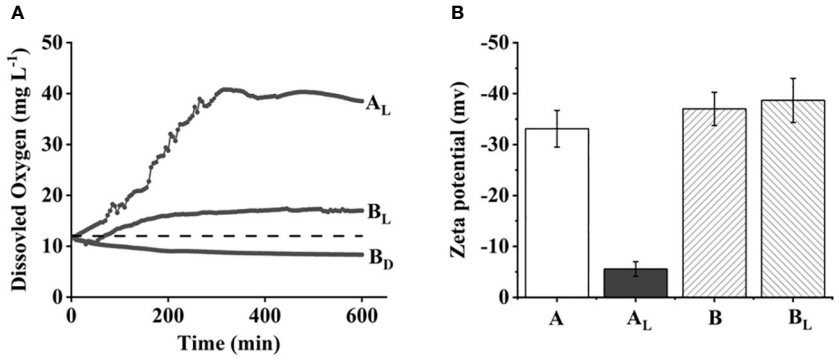


FIGURE 2
Surface dissolved oxygen (DO) concentration over time **(A)** and zeta potential of two different strains of *Microcystis* **(B)**. The dashed line in panel A indicates equilibrium value with air.

column ($p < 0.05$). Meanwhile, the content of polysaccharides secreted by *M. aeruginosa* on the surface and the water column was basically the same ($p > 0.05$). In the mixed samples of *M. wesenbergii*, the levels of dissolved polysaccharides and bound polysaccharides were 10.7 mg/L and 6.6 mg/L, respectively; the surface samples showed higher levels of polysaccharides, corresponding to 41.8 mg/L and 72.2 mg/L, respectively. The levels of dissolved proteins and loosely bound proteins increased from nearly zero at the beginning of the experiment to approximately 8 mg/L. In contrast, the mixed samples and surface samples of *M. aeruginosa* showed constant levels of polysaccharides and protein under both illuminated and dark conditions. The concentration of dissolved proteins increased from 0 mg/L to approximately 4 mg/L, while the level of bound proteins slightly decreased. Significant differences in the secretion of dissolved polysaccharides and bound polysaccharides were observed between *M. aeruginosa* and *M. wesenbergii* ($p < 0.01$). The polysaccharide content of *M. wesenbergii* decreased

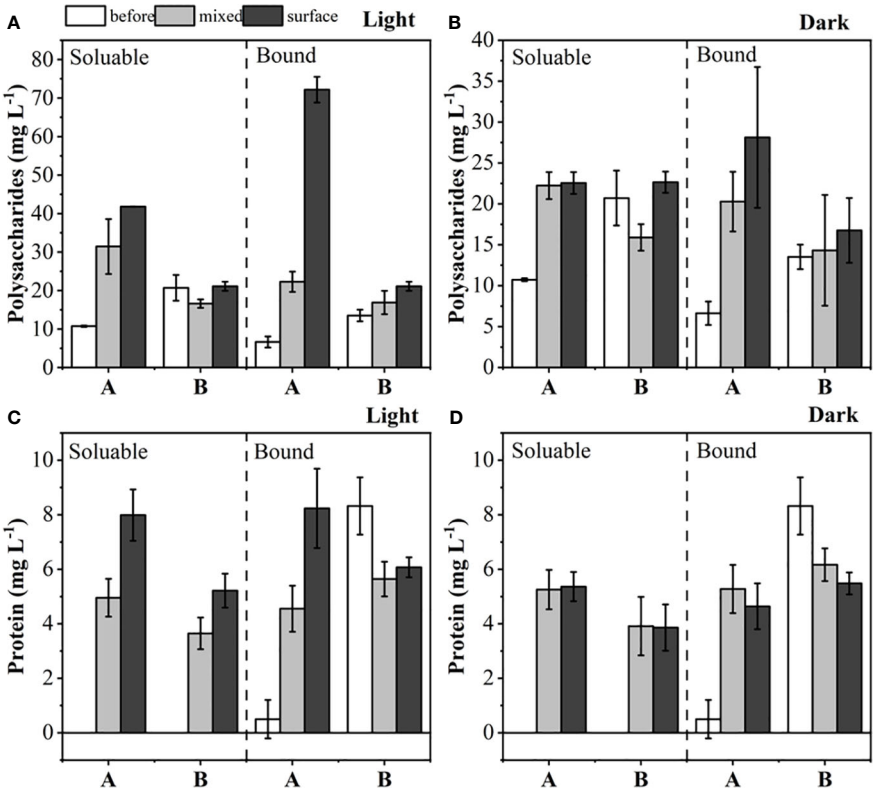


FIGURE 3
The content of polysaccharides in light **(A)** and darkness **(B)** before and after the experiment, and proteins in light **(C)** and darkness **(D)** before and after the experiment.

significantly under dark conditions, and both illumination and algal species had a significant impact on the concentration of dissolved polysaccharides ($p < 0.01$).

## 3.4 Qualitative analysis of extracellular species in *Microcystis* aggregates

### 3.4.1 CLSM picture of organic constituents in EPS

CLSM analysis was conducted to investigate the distribution of cells, proteins, and polysaccharides in the *Microcystis* aggregate (Figure 4). The results showed a significant increase in polysaccharides and protein of *M. wesenbergii* after illumination (Figures 4A, B), while no significant increase was observed in *M. aeruginosa* (Figures 4C, D). As shown in Figure 4, the membrane formed by the surface layer of *M. wesenbergii* samples has a network or membrane-like structure, which contains obvious polysaccharides and protein components. Additionally, *M. wesenbergii* cells formed large aggregates. As time increased, the protein and polysaccharide contents also increased significantly (Figure 3). It was worth noting that the content of both protein and polysaccharides was related to cell density (Figure 4B). However, the initial biomass remained consistent, and the protein surrounding the cells of *M. wesenbergii* was denser. This may be closely related to cell distribution and content.

### 3.4.2 Three-dimensional fluorescence in superficial surface *Microcystis* aggregates

The 3D EEM fluorescence spectra revealed three obvious fluorescent peaks in the EPS sample of strain FACHB 908 (Figure 5). Two of these peaks, observed at the excitation/emission wavelengths (Ex/Em) of 205/300 and 230/300, were identified as tyrosine protein-like. The third peak, observed at Ex/Em 235/350, was identified as tryptophan protein-like. No fluorescent peak was assigned for the presence of humic acid, suggesting that it may not be present in the EPS of laboratory trains.

### 3.4.3 FT-IR spectra in superficial surface *Microcystis* aggregates

FT-IR analysis was conducted on *M. wesenbergii* and *M. aeruginosa* to compare the composition of specific substances that produce surface blooms after light exposure. The functional groups were used to determine the type of compounds (Jingyun et al., 2010). The FT-IR results showed that there were no significant differences in most of the bands in *M. aeruginosa* before and after the experiment. As shown in Figure 6, the peak appeared at 1,726

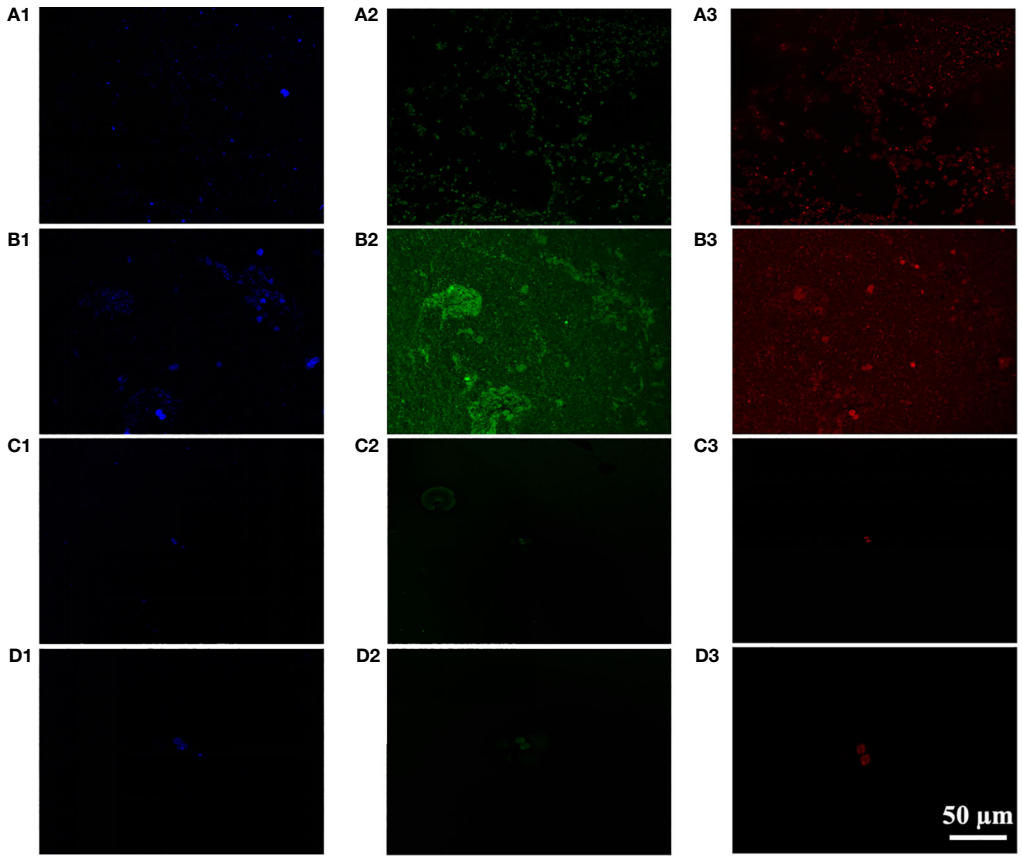


FIGURE 4
CLSM images of unicellular *Microcystis wesenbergii* before **(A)** after **(B)** and *Microcystis aeruginosa* before **(C)** after **(D)** floating up to the water surface (1, polysaccharides; 2, proteins; 3, bacteria). CLSM, confocal laser scanning microscopy.

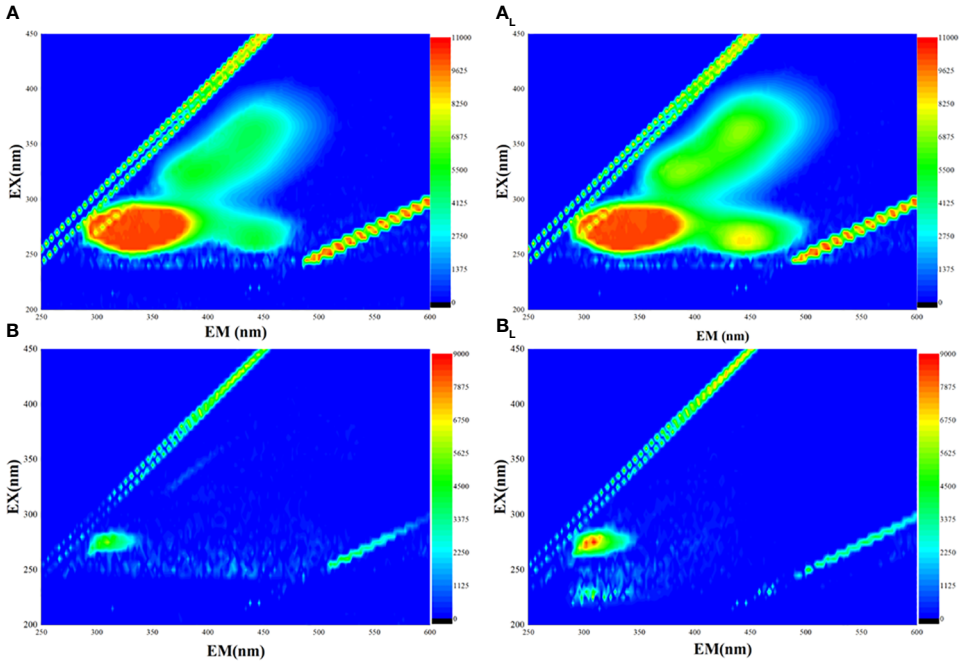


FIGURE 5
Three-dimensional fluorescence of two different strains of *Microcystis*. **(A)** *Microcystis wesenbergii* before light exposure. ($A_L$) *M. wesenbergii* under light. **(B)** *Microcystis aeruginosa* before light exposure. ($B_L$) *M. aeruginosa* under light.

$cm^{-1}$ after the experiment. At the spectral width of 1,537–1,652 $cm^{-1}$, the intensity of the bound amide group decreased, representing the NH in the peptide bond. The NH bond breaks with the CN bond. In the spectrum of *M. wesenbergii*, the NH stretch vibration at 3,382–3,338 $cm^{-1}$ significantly increased, indicating the full involvement of the NH bond in the process of surface water bloom formation and the creation of a surface film. The broad peak of 3,408–3,431 $cm^{-1}$ in the spectrum of *M. aeruginosa* was stronger than before the experiment, and the intensity of the spectrum of *M. wesenbergii* was stronger. These groups exhibited broad bands of polysaccharides (3,700–3,000 $cm^{-1}$ and 1,500–1,200 $cm^{-1}$) and proteins (1,700–1,600 $cm^{-1}$ and 1,200–1,050 $cm^{-1}$). Significant differences were observed in the bands of *M. wesenbergii* before and after the experiment, such as the polysaccharides (3,700–3,000 $cm^{-1}$), C–H characteristic peak (3,000–2,800 $cm^{-1}$), and the glycosidic bond (835 $cm^{-1}$). Strong

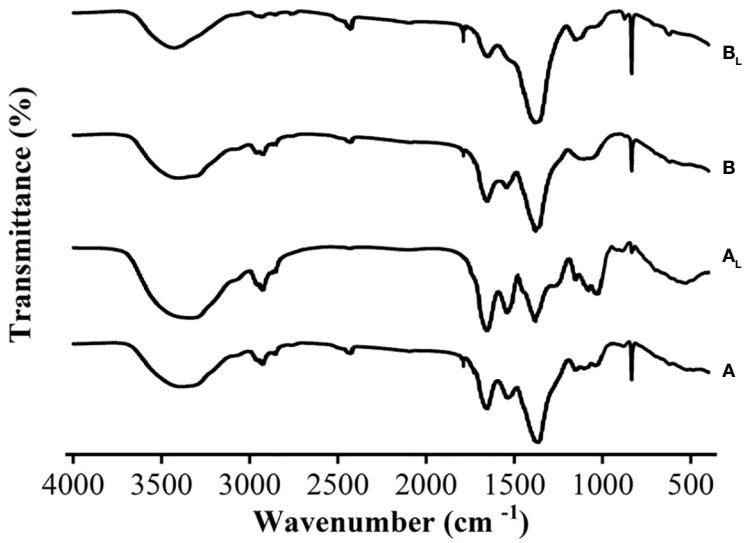


FIGURE 6
FT-IR spectra of two different strains of *Microcystis* before and after the experiment. **(A)** *Microcystis wesenbergii* before light exposure. ($A_L$) *M. wesenbergii* under light. **(B)** *Microcystis aeruginosa* before light exposure. ($B_L$) *M. aeruginosa* under light. FT-IR, Fourier transform infrared.

peaks near 3,400–3,500 $cm^{-1}$ bands were also observed, which belong to the stretch vibrations of N–H and O–H (Zongqian et al., 2019). These peaks were likely due to the presence of carboxylic acids, alcohols, and phenolic compounds (Mecozzi et al., 2001; Badiaa et al., 2010). The broad peak of 3,408–3,431 $cm^{-1}$ in the spectrum of *M. aeruginosa* was stronger than that before the experiment, and the intensity of the spectrum of *M. wesenbergii* was stronger. This peak was attributed to hydrogen bonds such as C–H, N–H, and O–H (Zongqian et al., 2019), indicating that there were compounds with the structure of R–$NH_2$ and R–CO–$NH_2$. The C═C stretching vibration at 1,657 $cm^{-1}$ was enhanced, and the C═C carboxylic acid (C═C skeleton vibration) at 1,367–1,384 $cm^{-1}$ was obvious. The peak at 836–1,081 $cm^{-1}$ represents the carbon–hydrogen bonds of polysaccharides that were converted from glycosides at 836 $cm^{-1}$ to polysaccharides (Christopher et al., 2011). The sharp increase in the intensity of the peak at 1,081 $cm^{-1}$ also indicates that polysaccharides are one of the important factors in the formation of surface blooms.

## 4 Discussion

Our study reveals a novel mechanism for the rapid flotation of *Microcystis* under light conditions, which is species-specific. Under such conditions, *M. wesenbergii* was capable of forming surface scum, while *M. aeruginosa* could not form visible scum throughout the experiments. This timescale is shorter than the observed timescale for scum formation in conventional bloom formation process. The timescale for the formation of cyanobacterial blooms in the wild is influenced by various factors, including the nutrient status of the water body, temperature, and light intensity. Generally, the formation of cyanobacterial blooms can range from several days to several weeks. In highly eutrophic waters, under warm and stable climatic conditions, blooms may develop rapidly (Christopher et al., 2011). Considering the difference in DO and EPS content between the treatments in our study, we speculated two possible reasons for the observed phenomenon: 1) exopolysaccharides may play an important role in algal cell adhesion and surface bloom formed, and 2) the rising process of $O_2$ bubbles accompanied by algal migration to the surface improves the biological amount leading to the formation of surface blooms. Under strong light conditions, the formation of bubbles can drive the formation of surface blooms.

For the first hypothesis, we analyzed the extracellular substances secreted by two *Microcystis* species. Light could affect the extracellular substances secreted by *Microcystis* and produce varying amounts of polysaccharides, thus affecting the aggregate formation. The SEM results confirmed the presence of significant secretions in the *M. wesenbergii* samples. These secretions can promote aggregate formation and upward migration to the water surface with the help of the micro-bubbles (Figure 1D). The S-EPS released from *M. wesenbergii* solution played an important role in the aggregation process (Figures 3A, B).

Studies have shown that proteins and polysaccharides are indispensable for maintaining the cross-linked structure of extracellular substances (Yang et al., 2008; Gan et al., 2012; Huiqun et al., 2018). The effect of EPS on the microbial aggregation process is mainly reflected in the bridging effect. However, the alteration of different types of EPS or the proportion of certain components can also affect this process. Meanwhile, the protein can promote the stability of maintaining the polymer structure (Badiaa et al., 2010). The protein in EPS contains more negatively charged amino acids (Figure 2). Compared with polysaccharides, the electrostatic bridging between EPS and divalent and polyvalent cations is more obvious. The existence of EPS and algal aggregates also contributes to better preservation of the integrity of colony algal cells. Furthermore, B-EPS, which tightly binds to the cell membrane of the algae, can serve as a binding molecule between algae cells, promoting the combination of *Microcystis* cells into a colony structure. CLSM results also confirmed that the large algal floc that rises to the surface was formed by large amounts of proteins and polysaccharides that adhere together tightly to form a "macroalgal collective" (Figure 1B). Indeed, EPS with multifunctional groups can promote the adsorption and chelation with various organic and inorganic matter to form aggregates in aqueous systems (Bai et al., 2016; Zhang et al., 2019).

The FT-IR spectroscopy of the *Microcystis* floating and migrating to the surface formed the surface film (Figure 6). This provides physical and chemical evidence for its formation and helps understand the occurrence of possible biomolecular groups or chemical changes. During the formation of surface blooms, the main functional groups in the extracellular substances secreted by *Microcystis*, such as hydroxyl and carboxyl groups, could have acted as binding sites and bridges with the high-molecular-weight adsorption sites of *Microcystis* S-EPS to form a network structure, which tightly packed single-celled *Microcystis*, and bubbles rise with photosynthesis (Figure 1). FT-IR analysis results showed that all samples contained a large number of hydrogen bonds, as evidenced by the broad peak of 3,500–3,400 $cm^{-1}$ and 3,431–3,408 $cm^{-1}$. There were noticeable changes in glycosidic bonds. The EPS was generally supported by a hydrogen bond system, and a higher ratio of hydrogen bonds resulted in stronger intermolecular interaction (Zhu et al., 2014). These findings were consistent with those of previous studies (Yang et al., 2016; Li et al., 2021).

For the second hypothesis, we analyzed the changes in oxygen quantity and electric potential during the formation of surface blooms. By modulating their buoyancy using internal gas vesicles, individual *Microcystis* can migrate along the water column at a speed of up to 1 mm/h (Walsby and Anthony, 1994). At the same time, the bubbles formed by the increase in sample oxygen are beneficial to the formation of water blooms on the surface of *Microcystis* (Johnk et al., 2008). This supports our conclusion that the rising process of $O_2$ bubbles is accompanied by algal migration to the surface, which improves the biological amount and forms surface blooms. The $O_2$ supersaturation is generally caused by concentrated photosynthesis, which in turn forms bubbles. The trapped $O_2$ bubbles provide lift and gather most of the biomass on the surface of the water column to form a denser foam layer. Also, this rapid migration process is irreversible. The foam will remain

stable for several weeks if the nutritional conditions are sufficient. According to literature reports, blooming occurs without a major increase in overall biomass, and the threshold for irreversible migration concentration is above $10^6$ cells/mL (Klemer et al., 1982). As cyanobacteria migrate toward the free surface, their effective concentration increases, and the system moves away from the critical point for blooming. The rate of oxygen production per unit biomass decreases under low light intensity or under weak photosynthetic mechanisms in harsh environments (Dervaux et al., 2015). Instead, light boosts photosynthesis and makes more bubbles. It is possible that oxygen production is the limiting factor for bloom formation.

The zeta potential is the potential of the shear plane in the double electric layer of charged particles in solution, which can reflect the stability of the colloidal system (Zhao et al., 2017). During the experimental stage (Figure 2B), the main force in *M. wesenbergii* solution is gravity rather than repulsion. The surface charge of protein molecules in the system is high, which maintains the stability of the system through electrostatic repulsion, making it difficult for protein molecules to accumulate (Bojorquez-Velazquez et al., 2016).

In addition, we performed a Fisher exact test bar plot on the species richness of *M. wesenbergii* before and after the experiment (Supplementary Figure 2). The results indicated a significant increase in species abundance at the level of *Microcystis* phylum after the experiment. Subsequently, individuals were randomly sampled from the specimens, and the dilution curve was based on the number of individuals and species (Supplementary Figure 3A). The species richness of *M. wesenbergii* before and after the experiment was compared by drawing dilution curves. Under the condition of extracting the same sequence, the number of operational taxonomic units (OTUs) of *M. wesenbergii* was higher after the experiment, indicating that the species richness of *M. wesenbergii* was higher. In this dilution graph (Supplementary Figure 3B), eventually, the curve tended to flatten out, further indicating that the number of samples taken was reasonable. Alpha diversity refers to the diversity within a specific region or ecosystem. The statistical t-test was used to detect significant differences between each of the two sets of index values (Supplementary Figure 3C).

Environmental isolates of *M. wesenbergii* form large colonies and exhibit complex vertical migration dynamics due to their dynamic glycan ballast ability to compete with oxygen-mediated upward migration. While similar experiments on indoor samples may still be qualitative, it would be interesting to test the mechanisms identified in this study using natural samples. Although the aggregation and binding of cyanobacteria EPS to form algal blooms have been reported (Parker et al., 2000; Micheletti et al., 2008), the underlying mechanisms were still poorly understood, and more work is needed to elucidate these binding processes. In this regard, similar experiments on algae with differences in EPS production can provide valuable data for further understanding the cell aggregation process. In future studies, we should also focus on effective and special substances that facilitate the aggregation process and identify the structure and properties of these substances. The dominant niche of high temperature-adapted cyanobacteria genera will be further reinforced with global warming and elevated carbon dioxide in the future. The cyanobacterial dominance and succession are inherently attributed to the distinctive traits of cyanobacteria including colony formation, gas vesicles, toxin release, and nitrogen fixation (Wang et al., 2021; Firsova et al., 2023). In the future, we will further explore the extracellular substances released by *Microcystis* and the physiological and biochemical effects of *Microcystis*.

## 5 Conclusion

The present study revealed that the two different species of *Microcystis* (*M. wesenbergii* and *M. aeruginosa*) ascended and gathered under light and dark conditions. It focused on the impact of the EPS and bubbles released by *Microcystis* on the formation of surface scum during the process of floating and gathering to the surface scum. The results showed the following:

(a) EPS produced by *M. wesenbergii* can contribute to the formation of large aggregates.
(b) The formation of aggregate and micro-bubble can drive the surface scum formation.
(c) Light and EPS contributed to the formation of the large algal aggregate.

## Data availability statement

The original contributions presented in the study are included in the article/Supplementary Material. Further inquiries can be directed to the corresponding author.

## Author contributions

TY: Conceptualization, Data curation, Formal Analysis, Validation, Visualization, Writing – original draft, Writing – review & editing. JP: Data curation, Methodology, Project administration, Visualization, Writing – review & editing. HW: Conceptualization, Writing – review & editing. CT: Supervision, Project administration, Resources, Writing – review & editing. CW: Supervision, Project administration, Resources, Writing – review & editing. BX: Supervision, Project administration, Resources, Writing – review & editing. MP: Supervision, Project administration, Resources, Writing – review & editing. XW: Funding acquisition, Project administration, Resources, Software, Supervision, Writing – review & editing.

## Funding

The author(s) declare financial support was received for the research, authorship, and/or publication of this article. This study was financially supported by China's National Key R&D Programmes (2022YFC3203601), Hubei Province Postdoctoral Innovation Research Position (Letter No. 153 of Hubei Human

Resources and Social Security). Additional support was provided by the National Natural Science Foundation of China (42061134013) and the Yunnan Province-Kunming City Major Science and Technology Project (202202AH210006). Additionally, the authors are indebted to Yuan Xiao, and Fang Zhou (Analysis and Testing Center, Institute of Hydrobiology, CAS), and the Laboratory for Downstream Process Technology and Engineering of Microalgae (LDPTEM) for lab equipment support.

## Conflict of interest

The authors declare that the research was conducted in the absence of any commercial or financial relationships that could be construed as a potential conflict of interest.

## Publisher's note



## Supplementary material

The Supplementary Material for this article can be found online at: https://www.frontiersin.org/articles/10.3389/fpls.2024.1367680/full#supplementary-material

## References

Andrew, R. K. (1991). Effects of nutritional status on cyanobacterial buoyancy, blooms, and dominance, with special reference to inorganic carbon. *Can. J. Bot.* 69, 1133–1138. doi: 10.1139/b91-145

Anne, W., Miki, H., and Michele, G. (2016). Effect of small-scale turbulence on the growth and metabolism of *Microcystis aeruginosa*. *Adv. Microbiol.* 06, 351–367. doi: 10.4236/aim.2016.65034

Arya, P., Vinayak, V. P., Richa, K., Paul, N. B., and Tyagi, V. V. (2019). Experimental studies on zeta potential of flocculants for harvesting of algae. *J. Of Environ. Manage.* 231, 562–569. doi: 10.1016/j.jenvman.2018.09.096

Badiaa, G., Djamel, G., and Ali, S. (2010). Algae and cyanotoxins removal by coagulation/flocculation: A review. *Desalination Water Treat.* 20, 133–143. doi: 10.5004/dwt.2010.1202

Bai, L., Xu, H., Wang, C., Deng, J., and Jiang, H. (2016). Extracellular polymeric substances facilitate the biosorption of phenanthrene on cyanobacteria *Microcystis aeruginosa*. *Chemosphere* 162, 172–180. doi: 10.1016/j.chemosphere.2016.07.063

Bo, F., Rikke, P., Kristian, K., and Per Halkjær, N. (1996). Extraction of extracellular polymers from activated sludge using a cation exchange resin. *Water Res.* 30, 1749–1758. doi: 10.1016/0043-1354(95)00323-1

Bojorquez-Velazquez, E., Lino-Lopez, G. J., Huerta-Ocampo, J. A., Barrera-Pacheco, A., Barba de la Rosa, A. P., Moreno, A., et al. (2016). Purification and biochemical characterization of 11S globulin from chan (*Hyptis suaveolens* L. Poit) seeds. *Food Chem.* 192, 203–211. doi: 10.1016/j.foodchem.2015.06.099

Chao, W., Tao, F., Peifang, W., Jun, H., and Jin, Q. (2017). Understanding the transport feature of bloom-forming *Microcystis* in a large shallow lake: A new combined hydrodynamic and spatially explicit agent-based modelling approach. *Ecol. Model.* 343, 25–38. doi: 10.1016/j.ecolmodel.2016.10.017

Chen, M.-Y., Lee, D.-J., Tay, J.-H., and Show, K.-Y. (2007). Staining of extracellular polymeric substances and cells in bioaggregates. *Appl. Microbiol. Biotechnol.* 75, 467–474. doi: 10.1007/s00253-006-0816-5

Chorus, I. (1999). *Toxic cyanobacteria in water: a guide to their public health consequences, monitoring, and management* (London; New York: E & FN Spon).

Christopher, M. P., William, T. B., Jamie, H. C., and Michael, A. M. (2011). Cellobiose dehydrogenase and a copper-dependent polysaccharide monooxygenase potentiate cellulose degradation by Neurospora crassa. *ACS Chem. Biol.* 6, 1399–1406. doi: 10.1021/cb200351y

Colin, S. R., Vera, H., Carla, K., Luigi, N.-F., and Sergio, M. (2002). Towards a functional classification of the freshwater phytoplankton. *J. Plankton Res.* 24, 417–428. doi: 10.1093/plankt/24.5.417

Dervaux, J., Mejean, A., and Brunet, P. (2015). Irreversible collective migration of cyanobacteria in eutrophic conditions. *PLoS One* 10, e0120906-. doi: 10.1371/journal.pone.0120906

Dubois, M., Gilles, K., Hamilton, J. K., Rebers, P. A., and Smith, F. (1951). A colorimetric method for the determination of sugars. *Nature* 168, 167. doi: 10.1038/168167a0

Fiehn, O., Wegener, G., Jochimsen, J., and Jekel, M. (1998). Analysis of the ozonation of 2-mercaptobenzothiazole in water and tannery wastewater using sum parameters, liquid- and gas chromatography and capillary electrophoresis. *Water Res.* 32, 1075–1084. doi: 10.1016/S0043-1354(97)00332-1

Firsova, A., Galachyants, Y., Bessudova, A., Titova, L., Sakirko, M., Marchenkov, A., et al. (2023). Environmental factors affecting distribution and diversity of phytoplankton in the Irkutsk reservoir ecosystem in June 2023. *Diversity*. 15, 1070. doi: 10.3390/d15101070

Gan, N., Xiao, Y., Zhu, L., Wu, Z., Liu, J., Hu, C., et al. (2012). The role of microcystins in maintaining colonies of bloom-forming *Microcystis* spp. *Environ. Microbiol.* 14, 730–742. doi: 10.1111/j.1462-2920.2011.02624.x

Guo, Y., Zhang, P., Chen, J., and Xu, J. (2022). Freshwater snail and shrimp differentially affect water turbidity and benthic primary producers. *Water Biol. Secur.* 1 (1), 100004. doi: 10.1016/j.watbs.2021.100004

Hallegraeff, G. M. (1993). A review of harmful algal blooms and their apparent global increase. *Phycologia*. 32, 79–99. doi: 10.2216/i0031-8884-32-2-79.1

Hans, W. P., and Jef, H. (2008). Blooms like it hot. *Science* 320, 57–58. doi: 10.1126/science.1155398

Hans, W. P., and Valerie, J. P. (2012). Climate change: Links to global expansion of harmful cyanobacteria. *Water Res.* 46, 1349–1363. doi: 10.1016/j.watres.2011.08.002

Huiqun, Z., Yanyan, J., Samir Kumar, K., Hui, L., Heting, F., and Qing, Z. (2018). Understanding the role of extracellular polymeric substances on ciprofloxacin adsorption in aerobic sludge, anaerobic sludge, and sulfate-reducing bacteria sludge systems. *Environ. Sci. Technol.* 52, 6476–6486. doi: 10.1021/acs.est.8b00568

Jacco, C. K., and Luuc, R. M. (1984). Buoyant density changes in the cyanobacterium *Microcystis aeruginosa* due to changes in the cellular carbohydrate content. *FEMS Microbiol. Lett.* 25, 105–109. doi: 10.1111/fml.1984.25.issue-1

Jingyun, F., Xin, Y., Jun, M., Chii, S., and Quan, Z. (2010). Characterization of algal organic matter and formation of DBPs from chlor(am)ination. *Water Res.* 44, 5897–5906. doi: 10.1016/j.watres.2010.07.009

Johnk, K. D., Huisman, J., Sharples, J., Sommeijer, B., Visser, P. M., and Stroom, J. M. (2008). Summer heatwaves promote blooms of harmful cyanobacteria. *Global Change Biol.* 14, 495–512. doi: 10.1111/j.1365-2486.2007.01510.x

Klemer, A. R., Feuillade, J., and Feuillade, M. (1982). Cyanobacterial blooms - carbon and nitrogen limitation have opposite effects on the buoyancy of oscillatoria. *Science*. 215, 1629–1631. doi: 10.1126/science.215.4540.1629

Li, Z., Wan, C., Liu, X., Wang, L., and Lee, D.-J. (2021). Understanding of the mechanism of extracellular polymeric substances of aerobic granular sludge against tetracycline from the perspective of fluorescence properties. *Sci. Total Environ.* 756, 144054. doi: 10.1016/j.scitotenv.2020.144054

Lin, Y., Chen, A., Wu, G., Peng, L., Xu, Z., and Shao, J. (2017). Growth, microcystins synthesis, and cell viability of *Microcystis aeruginosa* FACHB905 to dissolved organic matter originated from cattle manure. *Int. Biodeterioration Biodegrad.* 118, 126–133. doi: 10.1016/j.ibiod.2017.01.031

Liu, Y., Yang, Q., Zhu, M., Wang, L., Zhou, Q., Yang, Z., et al. (2020). Endocytosis in *microcystis aeruginosa* accelerates the synthesis of microcystins in the presence of lanthanum(III). *Harmful Algae*. 93, 101791. doi: 10.1016/j.hal.2020.101791

Lovelock, C. E., Clegg, E., Hurrey, L., Udy, J., and Moore, K. (2008). Growth and physiology of nuisance alga *Hincksia sordida* during a bloom in South East Queensland, Australia. *J. Exp. Mar. Biol. Ecol.* 363, 84–88. doi: 10.1016/j.jembe.2008.06.023

Luerling, M., Van Oosterhout, F., and Faassen, E. (2017). Eutrophication and warming boost cyanobacterial biomass and microcystins. *Toxins* 9, 64. doi: 10.3390/toxins9020064

Ma, X., Wang, Y., Feng, S., and Wang, S. (2015). Vertical migration patterns of different phytoplankton species during a summer bloom in Dianchi Lake, China. *Environ. Earth Sci.* 74, 3805–3814. doi: 10.1007/s12665-015-4279-9

Marion, M. B. (1976). A rapid and sensitive method for the quantitation of microgram quantities of protein utilizing the principle of protein-dye binding. *Analytical Biochem.* 72, 248–254. doi: 10.1016/0003-2697(76)90527-3

Markus, Z., Michael, A., Margit, M., and Fritz, H. F. (2010). Use of fluorescence fingerprints for the estimation of bloom formation and toxin production of *Microcystis aeruginosa*. *Water Res.* 44, 195–204. doi: 10.1016/j.watres.2009.09.035

Mecozzi, M., Pietrantonio, E., Amici, M., and Romanelli, G. (2001). Determination of carbonate in marine solid samples by FTIR-ATR spectroscopy. *Analyst*. 126, 144–146. doi: 10.1039/b009031j

Medrano, E. A., Uittenbogaard, R. E., de Wiel, B., Pires, L. M. D., and Clercx, H. J. H. (2016). An alternative explanation for cyanobacterial scum formation and persistence by oxygenic photosynthesis. *Harmful Algae*. 60, 27–35. doi: 10.1016/j.hal.2016.10.002

Medrano, E. A., Uittenbogaard, R. E., Pires, L. M. D., Wiel, B., and Clercx, H. J. H. (2013). Coupling hydrodynamics and buoyancy regulation in *Microcystis aeruginosa* for its vertical distribution in lakes. *Ecol. Model.* 248, 41–56. doi: 10.1016/j.ecolmodel.2012.08.029

Micheletti, E., Colica, G., Viti, C., Tamagnini, P., and De Philippis, R. (2008). Selectivity in the heavy metal removal by exopolysaccharide-producing cyanobacteria. *J. Appl. Microbiol.* 105, 88–94. doi: 10.1111/jam.2008.105.issue-1

Min, Z., Hongtao, D., Xiaoli, S., Yang, Y., and Fanxiang, K. (2012). Contributions of meteorology to the phenology of cyanobacterial blooms: Implications for future climate change. *Water Res.* 46, 442–452. doi: 10.1016/j.watres.2011.11.013

Paerl, H. W., Gardner, W. S., McCarthy, M. J., Peierls, B. L., and Wilhelm, S. W. (2014). Algal blooms: Noteworthy nitrogen. *Science*. 346, 175–175. doi: 10.1126/science.346.6206.175-a

Paerl, H. W., Hall, N. S., and Calandrino, E. S. (2011). Controlling harmful cyanobacterial blooms in a world experiencing anthropogenic and climatic-induced change. *Sci. Total Environ.* 409, 1739–1745. doi: 10.1016/j.scitotenv.2011.02.001

Paerl, H. W., and Otten, T. G. (2013). Harmful cyanobacterial blooms: causes, consequences, and controls. *Microbial Ecol.* 65, 995–1010. doi: 10.1007/s00248-012-0159-y

Parker, D. L., Mihalick, J. E., Plude, J. L., Plude, M. J., Clark, T. P., Egan, L., et al. (2000). Sorption of metals by extracellular polymers from the cyanobacterium *Microcystis aeruginosa* f. *flos-aquae* strain C3-40. *J. Appl. Phycology.* 12, 219–224. doi: 10.1023/A:1008195312218

Rainer, K., Guntram, C., and Ingrid, C. (2003). The abundance of microcystin-producing genotypes correlates positively with colony size in Microcystis sp. and determines its microcystin net production in lake Wannsee. *Appl. Environ. Microbiol.* 69, 787–795. doi: 10.1128/AEM.69.2.787-795.2003

Reynolds, C. S., and Walsby, A. E. (1975). Water-blooms. *Biol. Rev.* 50, 437–481. doi: 10.1111/j.1469-185X.1975.tb01060.x

Schindler, D. W. (1974). Eutrophication and recovery in experimental lakes: Implications for lake management. *Science*. 184, 897–899. doi: 10.1126/science.184.4139.897

Soranno, P. A. (1997). Factors affecting the timing of surface scums and epilimnetic blooms of blue-green algae in a eutrophic lake. *Can. J. Fisheries Aquat. Sci.* 54, 1965–1975. doi: 10.1139/cjfas-54-9-1965

Susanna, T. Y. T., Tiange, L., Shitian, W., and Richard, B. (2020). Harmful cyanobacterial blooms: a case study of a cool lake. *Water Environ. J.* 34, 490–502. doi: 10.1111/wej.12550

Timothy, W. D., Dianna, L. B., Gregory, L. B., and Christopher, J. G. (2009). The effects of temperature and nutrients on the growth and dynamics of toxic and non-toxic strains of *Microcystis* during cyanobacteria blooms. *Harmful Algae*. 8, 715–725. doi: 10.1016/j.hal.2009.02.004

Walsby, and Anthony, E. (1994). Gas vesicles. *Microbio. Rev* 58 (1), 94–144. doi: 10.1128/mr.58.1.94-144.1994

Wang, Z., Akbar, S., Sun, Y., Gu, L., and Yang, Z. (2021). Cyanobacterial dominance and succession: factors, mechanisms, predictions, and managements. *J. Environ. Manage.* 297, 113281. doi: 10.1016/j.jenvman.2021.113281

Wang, X., Qin, B., Gao, G., and Paerl, H. W. (2010). Nutrient enrichment and selective predation by zooplankton promote *Microcystis* (Cyanobacteria) bloom formation. *J. Plankton Res.* 32, 457–470. doi: 10.1093/plankt/fbp143

Wu, X., Noss, C., Liu, L., and Lorke, A. (2019). Effects of small-scale turbulence at the air-water interface on *microcystis* surface scum formation. *Water Res.* 167, 115091. doi: 10.1016/j.watres.2019.115091

Xiao, M., Li, M., Duan, P., Qu, Z., and Wu, H. (2019). Insights into the relationship between colony formation and extracellular polymeric substances (EPS) composition of the cyanobacterium *Microcystis* spp. *Harmful Algae*. 83, 34–41. doi: 10.1016/j.hal.2019.02.006

Yang, L., Guo, J., Yu, Y., An, Q., Wang, L., Li, S., et al. (2016). Hydrogen bonds of sodium alginate/Antarctic krill protein composite material. *Carbohydr. Polymers*. 142, 275–281. doi: 10.1016/j.carbpol.2016.01.050

Yang, Z., Kong, F., Shi, X., Zhang, M., Xing, P., and Cao, H. (2008). Changes in the morphology and polysaccharide content of Microcystis aeruginosa (cyanobacteria) during flagellate grazing. *J. Phycology*. 44 (3), 716–720. doi: 10.1111/j.1529-8817.2008.00502.x

Yunlin, Z., Guang, G., Kun, S., Cheng, N., Yongqiang, Z., Boqiang, Q., et al. (2014). Absorption and fluorescence characteristics of rainwater CDOM and contribution to Lake Taihu, China. *Atmospheric Environ.* 98, 483–491. doi: 10.1016/j.atmosenv.2014.09.038

Zhang, Z., Cao, R., Jin, L., Zhu, W., Ji, Y., Xu, X., et al. (2019). The regulation of N-acyl-homoserine lactones (AHLs)-based quorum sensing on EPS secretion via ATP synthetic for the stability of aerobic granular sludge. *Sci. Total Environ.* 673, 83–91. doi: 10.1016/j.scitotenv.2019.04.052

Zhao, C.-B., Zhang, H., Xu, X.-Y., Cao, Y., Zheng, M.-Z., Liu, J.-S., et al. (2017). Effect of acetylation and succinylation on physicochemical properties and structural characteristics of oat protein isolate. *Process Biochem.* 57, 117–123. doi: 10.1016/j.procbio.2017.03.022

Zhou, C., Chen, H., Zhao, H., and Wang, Q. (2021). Microcystin biosynthesis and toxic effects. *Algal Research-Biomass Biofuels Bioprod.* 55, 102277. doi: 10.1016/j.algal.2021.102277

Zhu, W., Dai, X., and Li, M. (2014). Relationship between extracellular polysaccharide (EPS) content and colony size of *Microcystis* is colonial morphology dependent. *Biochem. Syst. Ecol.* 55, 346–350. doi: 10.1016/j.bse.2014.04.009

Zhu, K., Zhang, H., Zhang, P., Wang, P., Li, H., Feng, M., et al. (2023). Interactive effects of warming and eutrophication on zooplankton could reverse the stoichiometric mismatch with phytoplankton. *Water Biol. Secur.* 2 (4), 100205. doi: 10.1016/j.watbs.2023.100205

Zongqian, W., Haiwei, Y., and Zun, Z. (2019). Study on the blends of silk fibroin and sodium alginate: Hydrogen bond formation, structure and properties. *Polymer*. 163, 144–153. doi: 10.1016/j.polymer.2019.01.004

frontiers | Frontiers in Plant Science

TYPE Original Research
PUBLISHED 16 April 2024
DOI 10.3389/fpls.2024.1390019



OPEN ACCESS

EDITED BY
Qiang Yang,
German Centre for Integrative Biodiversity Research (iDiv), Germany

REVIEWED BY
Yuan Niu,
Chinese Research Academy of Environmental Sciences, China
Wen Zhou,
Wuhan Botanical Garden, Chinese Academy of Sciences (CAS), China

*CORRESPONDENCE
Lan Wang
wanglan@ihb.ac.cn
Qinghua Cai
qhcai@ihb.ac.cn

RECEIVED 22 February 2024
ACCEPTED 01 April 2024
PUBLISHED 16 April 2024

CITATION
Tan L, Wang L and Cai Q (2024) Daily process and key characteristics of phytoplankton bloom during a low-water level period in a large subtropical reservoir bay.
*Front. Plant Sci.* 15:1390019.
doi: 10.3389/fpls.2024.1390019



# Daily process and key characteristics of phytoplankton bloom during a low-water level period in a large subtropical reservoir bay

Lu Tan[1], Lan Wang[1,2]* and Qinghua Cai[1]*

[1]State Key Laboratory of Freshwater Ecology and Biotechnology, Institute of Hydrobiology, Chinese Academy of Sciences, Wuhan, Hubei, China, [2]Hubei Key Laboratory of Wetland Evolution & Ecological Restoration, Wuhan Botanical Garden, Chinese Academy of Sciences, Wuhan, Hubei, China

Reservoirs, heavily influenced by artificial management, often harbor phytoplankton assemblages dominated by cyanobacteria or dinoflagellates, triggering significant changes in aquatic ecosystems. However, due to limited sampling frequency and insufficient attention to species composition, the bloom processes and key characteristics of phytoplankton community structure have not been systematically elucidated. During the low-water level period when blooms are most likely to occur (June to September) in a tributary bay of the Three Gorges Reservoir, daily sampling was conducted to investigate phytoplankton community composition, identify significant environmental factors, and evaluate important structure characteristics of phytoplankton community. The results showed that *Microcystis aeruginosa* maintained a clear dominance for almost a month in stage 1, with low Shannon and evenness but a high dominance index. Phytoplankton total density and biomass decreased drastically in stage 2, but *Microcystis aeruginosa* still accounted for some proportion. The highest Shannon and evenness but the lowest dominance index occurred in stage 3. *Peridiniopsis niei* occurred massively in stage 4, but its dominant advantages lasted only one to two days. $NH_4$-N was responsible for the dominance of *Microcystis aeruginosa*, while TP and $PO_4$-P was responsible for the dominance of *Peridiniopsis niei*; however, precipitation contributed to their drastic decrease or disappearance to some extent. The TN : TP ratio could be considered as an important indicator to determine whether *Microcystis aeruginosa* or *Peridiniopsis niei* dominated the phytoplankton community. Throughout the study period, physiochemical factors explained more variation in phytoplankton data than meteorological and hydrological factors. Pairwise comparisons revealed an increase in average β diversity with stage progression, with higher β diversities based on abundance data than those based on presence/absence data. Repl had a greater effect on β diversity differences based on presence/absence data, whereas RichDiff had a greater effect on β diversity differences based on species abundance data. Co-occurrence networks for stage 1 showed the most complex structure, followed by stage 4, while the

network for stage 3 was relatively sparse, although the overall community division remained compact. This study provides a useful attempt to explore the status and changes in phytoplankton community structure during the bloom process through high-resolution investigation.

KEYWORDS

phytoplankton, daily sampling, VPA, db-RDA, β diversity partition, network analysis, TN/TP

## 1 Introduction

Phytoplankton species are the most widespread and quantitatively relevant primary producers in aquatic ecosystems (Basset et al., 2008). A significant increase in phytoplankton biomass, known as a phytoplankton bloom, indicates an imbalance between phytoplankton growth and loss processes (Carstensen et al., 2007). It is widely accepted that global climate change and eutrophication have intensified phytoplankton blooms in lakes and reservoirs around the world (Ho et al., 2019; Griffith and Gobler, 2020; Liu et al, 2021). China has been severely threatened by water body eutrophication and frequent harmful phytoplankton bloom events during the past decade (Huang et al., 2020), which is one of the most challenging environmental problems (Huisman et al., 2018).

Reservoirs have become important frameworks within ecological studies of assemblage organization (Leitão et al., 2003), mainly due to the abiotic instability generated in their water bodies. Compared to lakes, reservoirs are subject to a greater degree of artificial management. Therefore, reservoirs can serve as a valuable water body type to study the ecological response of ecosystems to artificial interventions. Globally, reservoirs are inhabited by phytoplankton assemblages dominated by cyanobacteria such as *Microcystis* and *Dolichospermum*, or dinoflagellates such as *Ceratium*, forming either mixed or single blooms (see the literature cited by Bordet et al., 2017). Intense algal blooms can cause severe changes in the aquatic ecosystems (Reid et al., 2019), posing a significant threat to aquatic organisms and even humans using these water sources (Olokotum et al., 2020). Reservoir impoundment alters turbulence regimes, allowing the development of phytoplankton species that cannot thrive in fast-flowing waters, but gradually reach large populations in frequently stratified water columns with sufficient nutrients and light conditions (Bordet et al., 2017; Zeng et al., 2023). As the largest reservoir for water conservancy and hydropower projects in China, the Three Gorges Reservoir (TGR) has attracted widespread attention for its ecological impacts. Since the impoundment of the reservoir, the water level has risen significantly, the flow velocity has slowed down greatly, the water exchange has weakened, the artificial regulation has counteracted seasonal hydrological fluctuations (Ding et al., 2022; Ou et al., 2022), and the self-purification capacity of the water body has decreased (Liu et al., 2013). As a result, many tributary bays of the TGR have suffered from phytoplankton blooms of various sizes every year. In summer and early autumn (the low-water level period in the Three Gorges Reservoir), the light and water temperature conditions are good, which are favorable for algal growth, and algal blooms, especially cyanobacterial blooms, are prone to occur (Wang et al., 2011; Zhou et al., 2022). For example, a severe cyanobacterial bloom occurred in 2008 in Xiangxi Bay, a typical tributary of the Three Gorges Reservoir (Ministry of Environmental Protection of China, 2014), which seriously affected the safety of the water quality in the Three Gorges Reservoir area.

Research on phytoplankton bloom has primarily focused on the total amount of phytoplankton and the dominant species. However, the total algal abundance or biomass provides limited insight into the processes that govern their spatial and temporal distribution (Zhao et al., 2017). During blooms dominated by different species and at different stages of bloom development, the structure of phytoplankton communities can undergo significant changes with profound impacts on water quality. In addition, weekly sampling is essential for effective studies of phytoplankton blooms. This frequency is consistent with the timescale of population responses, as the generation time of phytoplankton varies from hours to a few days (Reynolds, 2006). While weekly dynamics of phytoplankton communities have been reported in Xiangxi Bay (Wang et al., 2011), changes in phytoplankton communities composition at higher sampling resolutions during the bloom process have not been documented. Therefore, more fine-scale and structured information on phytoplankton communities is urgently needed to fully understand the conceptual mechanisms driving bloom development.

The present study aimed to analyze phytoplankton communities during the bloom process using daily sampling data. Bloom stages were broadly defined based on total and relative abundance and biomass, as well as α diversity. We expected to identify differences in phytoplankton community structure within and between different bloom stages, and to explore the combined effects of environmental factors through a multifactorial investigation. The influence of environmental factors on the variation in phytoplankton community composition among sampling days (β diversity) was evaluated, and significant

environmental factors were identified. In addition, β diversity was decomposed into turnover and richness changes to assess their relative importance. Co-occurrence networks were constructed to compare the internal structure of the phytoplankton community in different bloom stages.

## 2 Materials and methods

### 2.1 Study site and sampling

The Three Gorges Reservoir (TGR), located at 29°16′~31°25′ N, 106°~110°50′ E, has a normal water level of 175 m above sea level and a summer flood protection level of 145 m, covers an area of 1080 $km^2$ with a volumetric capacity of $3.93 \times 10^{10}$ $m^3$, and extends over 600 km in length and an average width of 1.1 km (Huang et al., 2006). A subtropical monsoon climate dominates this region (Cai et al., 2010), characterized by an average annual precipitation of 1000 to 1300 mm. As the largest tributary of the TGR in Hubei Province, the Xiangxi River is located in 38 km upstream of the Three Gorges Dam. It extends for 94 km as a mainstream and drains a watershed area of 3099 $km^2$ (Wang et al., 1997). Notably, after the impoundment of the TGR, the lower 20~40 km stretch of the Xiangxi River was transformed into the Xiangxi Bay (Cai and Hu, 2006). 25 km upstream of the mouth of Xiangxi Bay, the sampling site in this study was located at the Xiangxi Ecosystem Station of the Institute of Hydrobiology, Chinese Academy of Sciences and China Three Gorges Corporation (Figure 1).

Daily sampling was conducted between June 18$^{th}$ and September 28$^{th}$, 2008, during a warm flood season characterized by small water level fluctuations around the low water level, i.e. 145 m a.s.l. Water samples were consistently collected at 10: 00 a.m., at a depth of 0.5 m below the water surface using a 5 L Van Dorn sampler. For nutrient analysis, samples were carefully stored in pre-

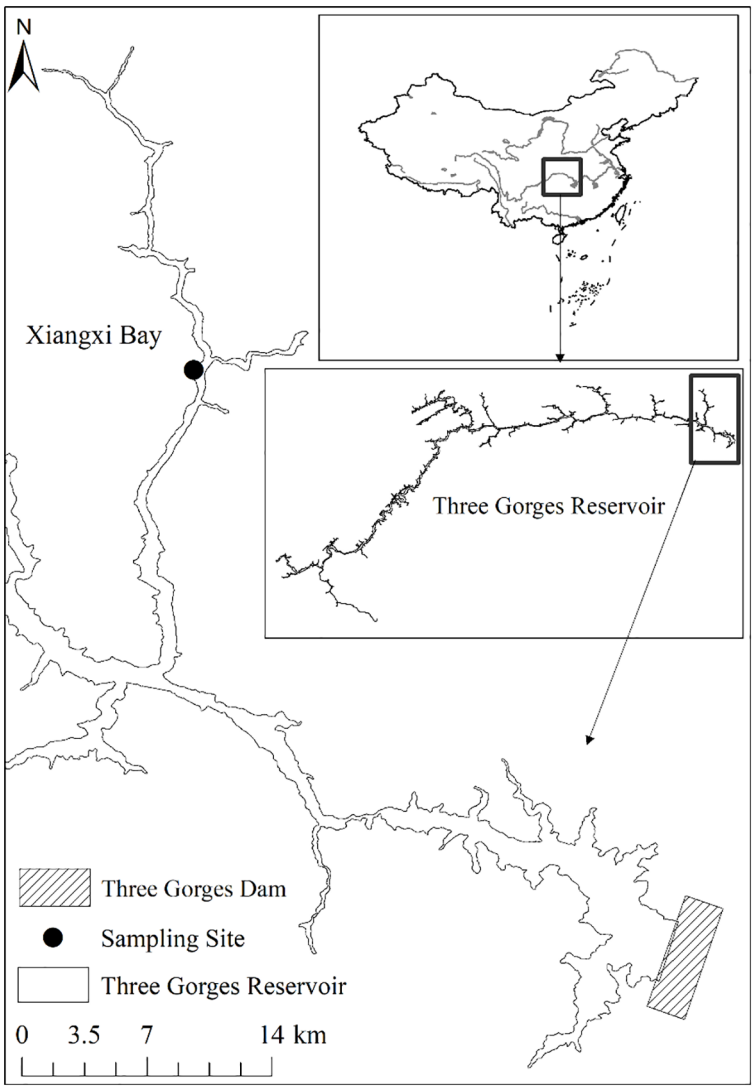


FIGURE 1
Location of the sampling site in Xiangxi Bay of the Three Gorges Reservoir, China.

cleaned plastic bottles and immediately acidified with sulfuric acid. Phytoplankton samples were preserved with neutral Lugol's solution immediately after collection.

## 2.2 Abiotic and biotic variable measurements and acquisition

Daily precipitation (Prep), vertical profiles of water temperature, and wind speed (Wind) were recorded using EcoTech monitoring stations (EcoTech Umwelt-Meßsysteme GmbH, Germany). Photosynthetic active radiation (PAR) in the air and vertical profiles of PAR through the water column were obtained using a quantum sensor (Li-192SA, USA). Real-time water level data of the TGR were obtained from China Three Gorges Corporation. In this study, the water level (WL) data were derived from the daily average water level, while the diurnal fluctuation of water level (DFWL) was calculated based on the daily fluctuation range of water level.

Surface water temperature (WT), conductivity (Cond), dissolved oxygen (DO), and pH were measured using environmental monitoring systems (YSI 6600EDS, USA). Total phosphorus (TP), total nitrogen (TN), phosphate phosphorus ($PO_4$-P), ammonia nitrogen ($NH_4$-N), nitrate nitrogen ($NO_3$-N), and dissolved silicon (DSi), were analyzed using a Continuous flow analyzer (Skalar San$^{++}$, Netherlands) according to the Standard Observation and Measurement Protocol for Aquatic Ecosystems of the Chinese Ecosystem Research Network (CERN) (Cai, 2007).

A sedimentation method was used prior to phytoplankton analysis (Cai, 2007). Taxonomic identification of phytoplankton species followed the procedures described by Hu and Wei (2006) and John, Whitton and Brook (2002). Algal enumeration was performed using Fuchs-Rosental slides and an Olympus CX21 model microscope (Olympus Corporation, Japan) at 400× magnification.

## 2.3 Data analysis

The Relative Water Column Stability (RWCS) indicates the thermal stratification conditions within a water body based on density variations throughout the water column (Padisák et al., 2003). This dimensionless parameter was calculated by comparing the density gradient across the water column with the difference in density of pure water at 4°C and 5°C, according to the formula described by Padisák et al. (2003):

$$RWCS = \frac{D_b - D_S}{D_4 - D_5}$$

where $D_b$, $D_s$, $D_4$, and $D_5$ represent the densities of the bottom water, surface water, and pure water at 4°C and 5°C, respectively. In this study, a depth of 1 m was considered the "surface layer", while the maximum depth was considered the "bottom layer" (with a water depth of approximately 10 m). The euphotic zone (Zeu) was defined as the depth at which 1% of the photosynthetically active radiation penetrates the surface (Naselli-Flores, 2000). Transparency, as indicated by the Secchi depth (SD), was measured using a Secchi disk.

Algal biomass was assessed using formulas applicable to geometric shapes, assuming the fresh weight unit expressed in mass, where 1 $mm^3$/L is equal to 1 mg/L (Wetzel and Likens, 2000). The Shannon index (Shannon), Pielou's evenness index (Evenness), and Dominance index (Dominance) were used to characterize α diversity. The Shannon index takes into account both the number of individuals and the number of taxa and is calculated using the formula:

$$\text{Shannon} = -\text{sum}((n_i/n)\ln(n_i/n))$$

where $n_i$ is the number of individuals of taxon i and n is the total number of individuals. Evenness is determined by dividing Shannon diversity by the logarithm of the number of taxa. Dominance is calculated as:

$$\text{Dominance} = -\text{sum}(n_i/n)^2$$

The Compositional dissimilarities of phytoplankton communities between different days (β diversity) were analyzed using both presence/absence data (using Podani family, Jaccard-based indices) and abundance data (using the Ruzicka index) in the R package "adespatial". This analysis allowed for the partitioning of dissimilarities into replacement and richness difference components, providing insight into the turnover and richness changes within the community over time. Correlation-based co-occurrence network analysis was used to explore the co-occurrence patterns among phytoplankton taxa. Pairwise Spearman's rank correlations (r) were calculated using the R package "psych". Only correlations with r greater than 0.8 or less than -0.8 and statistically significant with a *p*-value threshold of less than 0.01 were included in the network analyses. Network visualization and modular analysis were performed using Gephi (version 0.9.2). Topological characteristics including modularity, clustering coefficient, average degree, and average path length were calculated to provide quantitative insights into the structure and organization of the network.

Friedman's two-way analysis of variance by ranks was used to compare differences between phytoplankton bloom stages in abiotic and biotic parameters. Linear correlation between environmental variables was assessed using Pearson's correlation coefficient. To investigate the relationship between phytoplankton community (total density, total biomass, density of *Microcystis aeruginosa* and *Peridiniopsis niei*, and α diversity index Shannon, evenness, and dominance) and environmental variables, we performed a Mantel test using the R package "LinkET". The Variation Partitioning Analysisi (VPA) was performed based on the partitioning criterion of meteorological and hydrological (Prep, Wind, PAR, WL, DFWL, and RWCS), physical (Zeu, SD, WT, Cond), and chemical (DO, pH, TN, NH4-N, NO3-N, TP, PO4-P, DSi, and TN/TP) factors partition criterion. Distance-based redundancy analysis (db-RDA) is an ordination method similar to redundancy analysis (RDA), with the difference that non-Euclidean dissimilarity indices, such as the Bray-Curtis distance, can be considered (Oksanen et al., 2022). db-RDA successfully partitions data variability based on

complex designs or models, and applies an appropriate multivariate distance measure for ecological datasets, by computing principal coordinates and adjusting for negative eigenvalues when necessary, with a constant added to squared distances (Mcardle and Anderson, 2001). In this study, db-RDA was performed to explore relationships between phytoplankton species composition and environmental factors during daily processes using the R package "vegan".

# 3 Results

## 3.1 Daily phytoplankton bloom process

Euglenophyta (3 species). Daily changes in density and biomass are shown in Figure 2. *Microcystis aeruginosa* (Maer) and *Peridiniopsis niei* (Pnie) emerged as the most significant species when both density and biomass were considered simultaneously. *Microcystis aeruginosa* maintained a clear dominance for almost a month, with both its relative density and biomass exceeding 80% on most days. On July 2$^{nd}$, its density and biomass peaked at 5.23E8 cells/L and 34.22 mg/L, respectively. *Peridiniopsis niei* briefly dominated in mid-September. On September 15$^{th}$, its density and biomass peaked at 3.79E7 cells/L and 167.89 mg/L, respectively, representing 59.1% of the total density and 98.1% of the total biomass on that day. The α diversity indices Evenness, Shannon, and dominance showed clear temporal patterns (Figure 3). Evenness and Shannon followed a similar trend, with Shannon showing a wide range of variation. Both indices showed low values during the bloom periods of *Microcystis aeruginosa* and *Peridiniopsis niei*. Shannon reached its highest values around August and the second highest values from mid-July to early August. In contrast, Dominance showed opposite changes and was higher during the blooms of *Microcystis aeruginosa* and *Peridiniopsis niei*.

Based on the daily variation of density, biomass and α diversity indices, the study period was divided into four stages, designated S1 to S4 (Table 1). During S1, spanning from June 18$^{th}$ to July 11$^{th}$, the

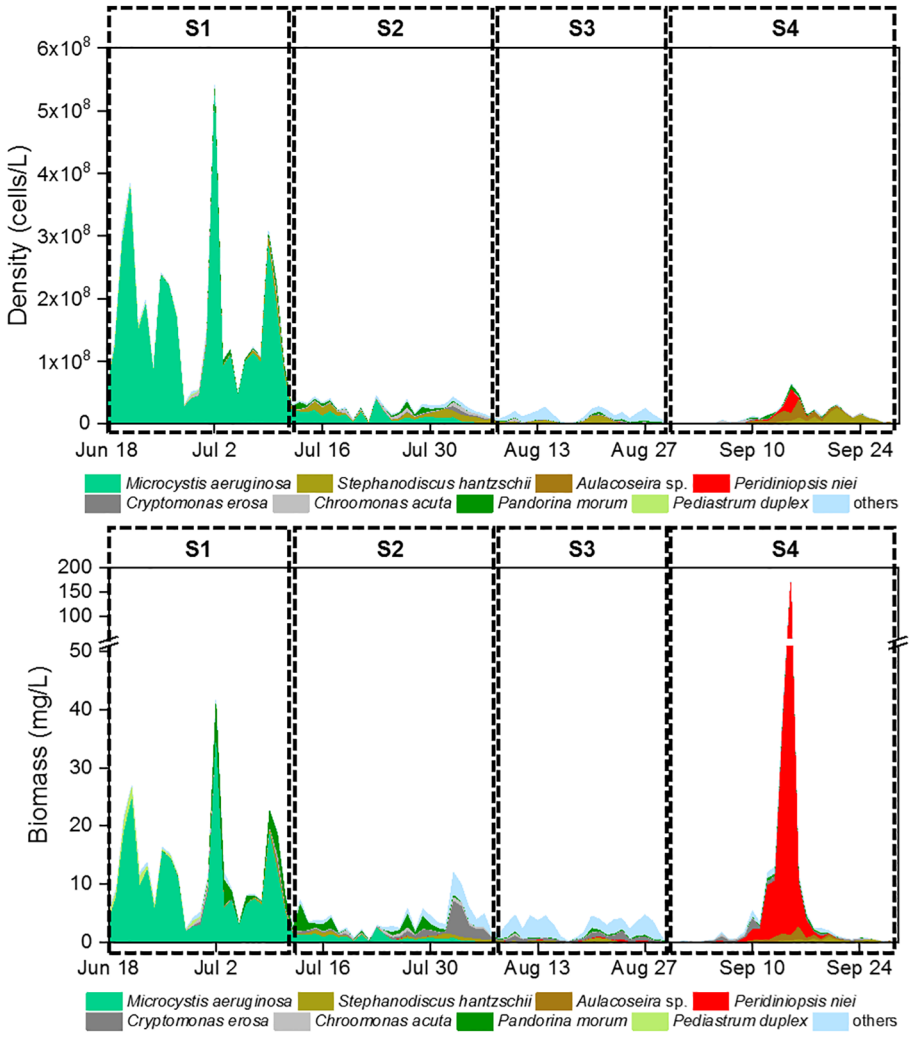


FIGURE 2
Daily changes of phytoplankton density and phytoplankton biomass.

10.3389/fpls.2024.1390019

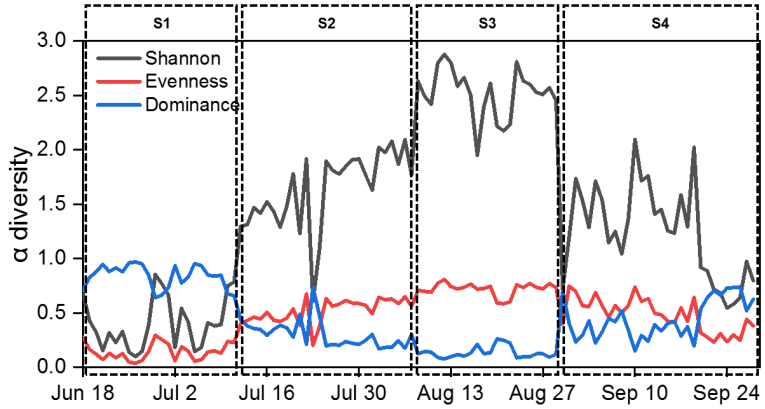


FIGURE 3
Daily changes of α diversity indices during the study period.

TABLE 1 Statistical summary of environmental conditions, phytoplankton density, biomass and diversity.

| | S1 (Jun 18~Jul 11) | S2 (Jul 12~Aug 7) | S3 (Aug 8~29) | S4 (Aug 30~Sep 28) | Differences |
|---|---|---|---|---|---|
| Prep (mm/day) | 5.50 (0.00~37.00) | 4.86 (0.00~36.20) | 10.72 (0.00~77.60) | 1.83 (0.00~36.10) | 0.851 |
| Wind (m/s) | 1.51 (0.40~3.40) | 1.54 (0.50~3.70) | 1.55 (0.30~4.20) | 1.25 (0.10~3.90) | 0.315 |
| PAR (mol/$m^2$/day) | 34.29 (9.89~59.39) | 36.80 (8.06~52.39) | 31.43 (3.78~50.98) | 23.93 (5.86~44.23) | 0.148 |
| WL (m) | 145.50 (145.02~145.88) | 145.57 (145.21~145.88) | 145.75 (145.31~145.90) | 145.73 (145.21~145.87) | <0.001 |
| DFWL (m/day) | 0.23 (0.09~0.70) | 0.24 (0.09~0.44) | 0.19 (0.08~0.51) | 0.17 (0.06~0.51) | 0.002 |
| RWCS | 64.75 (37.76~108.52) | 94.71 (41.55~166.82) | 89.88 (52.05~174.22) | 57.59 (18.32~122.28) | <0.001 |
| Zeu (m) | 2.88 (1.76~4.67) | 3.96 (2.63~5.03) | 3.22 (2.05~3.87) | 3.21 (0.57~4.34) | <0.001 |
| SD (m) | 0.97 (0.20~1.80) | 1.18 (0.80~2.00) | 0.92 (0.40~1.20) | 0.87 (0.10~1.50) | 0.001 |
| WT (°C) | 26.02 (24.87~27.45) | 27.73 (26.04~28.70) | 27.06 (24.92~29.02) | 24.46 (19.83~26.51) | <0.001 |
| Cond (μs/cm) | 321.46 (293.00~343.00) | 302.89 (277.00~319.00) | 273.73 (165.00~328.00) | 217.70 (102.00~307.00) | <0.001 |
| DO (mg/L) | 13.51 (9.65~17.50) | 10.80 (6.94~13.46) | 10.90 (7.04~15.96) | 9.78 (7.01~14.22) | 0.001 |
| pH | 8.95 (8.60~9.20) | 8.57 (8.10~9.00) | 8.60 (8.10~9.00) | 8.56 (8.00~9.20) | <0.001 |
| TN (mg/L) | 1.53 (1.14~2.30) | 1.41 (1.08~2.09) | 1.26 (1.07~1.69) | 1.19 (0.79~2.45) | <0.001 |
| $NH_4$-N (mg/L) | 0.28 (0.02~0.74) | 0.12 (0.02~0.29) | 0.08 (0.01~0.21) | 0.06 (0.01~0.29) | <0.001 |
| $NO_3$-N (mg/L) | 1.09 (0.69~1.43) | 1.16 (0.87~1.46) | 1.06 (0.88~1.43) | 1.02 (0.68~2.32) | 0.002 |
| TP (mg/L) | 0.06 (0.02~0.13) | 0.04 (0.01~0.09) | 0.03 (0.01~0.06) | 0.09 (0.01~0.30) | <0.001 |
| $PO_4$-P (mg/L) | 0.04 (0.01~0.09) | 0.02 (0.01~0.05) | 0.02 (0.01~0.06) | 0.04 (0.01~0.20) | <0.001 |
| DSi (mg/L) | 2.94 (2.43~3.53) | 3.07 (2.30~3.79) | 3.37 (2.47~4.37) | 6.36 (4.93~8.48) | <0.001 |
| TN/TP | 30.16 (11.62~61.00) | 45.57 (16.67~145.00) | 48.88 (19.50~113.00) | 19.77 (4.30~49.00) | <0.001 |
| Density (cells/L) | 1.68E8 (3.00E7~5.41E8) | 2.75E7 (2.72E6~4.50E7) | 1.51E7 (7.80E5~2.79E7) | 1.35E7 (1.58E5~6.42E7) | <0.001 |
| Biomass (mg/L) | 12.59 (2.15~41.60) | 3.97 (0.45~12.01) | 3.03 (0.22~4.75) | 9.29 (0.03~171.10) | <0.001 |
| Maer density (cells/L) | 1.56E8 (2.76E7~5.23E8) | 1.14E7 (1.03E6~3.83E7) | 2.87E5 (0~2.24E6) | 2.11E3 (0~6.32E4) | <0.001 |
| Pnie density (cells/L) | 0 | 1.17E3 (0~1.05E4) | 2.16E4 (0~1.37E5) | 1.83E6 (0~3.79E7) | <0.001 |
| Shannon | 0.41 (0.10~0.86) | 1.64 (0.61~2.09) | 2.52 (1.95~2.88) | 1.24 (0.55~2.10) | <0.001 |
| Evenness | 0.15 (0.04~0.30) | 0.52 (0.20~0.68) | 0.72 (0.59~0.81) | 0.48 (0.23~0.75) | <0.001 |
| Dominance | 0.84 (0.64~0.97) | 0.31 (0.17~0.73) | 0.14 (0.08~0.26) | 0.45 (0.15~0.74) | <0.001 |

stage was characterized by a bloom of *Microcystis aeruginosa* which dominated the community. This stage had the lowest Shannon and evenness and the highest dominance. S2, occurring from July 12$^{nd}$ to August 7$^{th}$, represented a stage in which the dominance of *Microcystis aeruginosa* decreased, and other species including *Peridiniopsis niei* began to appear. S3, from August 8$^{th}$ to 29$^{th}$, was characterized by a continued decrease in total density and a reduction of total biomass to the minimal levels. *Peridiniopsis niei* continued to increase, and the highest Shannon and evenness and the lowest dominance was recorded. S4, from August 30$^{th}$ to September 28$^{th}$, represented the stage of *Peridiniopsis niei* bloom. During this stage, the total density decreased to the minimum level, while the total biomass showed drastic variations. A statistical analysis was performed on all environmental factors and the aforementioned biotic factors to evaluate their average values, ranges of variation among these four stages, and the significance of the differences using Friedman's two-way analysis of variance by ranks in Table 1. The results showed significant differences between the stages for all factors except the meteorological factors.

## 3.2 Response of phytoplankton community to environmental factors

Pairwise comparisons of different environmental variables in Figure 4 revealed stronger correlations between physical and chemical factors, as well as between internal chemical factors. Significantly strong positive correlations (Spearman's r > 0.6) were observed between SD and Zeu, WT and RWCS, pH and DO, $NH_4$-N and DO, TN/TP and WT, and pairwise between TN, $NO_3$-N and Cond. Significantly strong negative correlations (Spearman's r< -0.6) were found only between DSi and WT, DSi and Cond, and TN/TP and TP. Phytoplankton total density and *Microcystis aeruginosa* density showed a stronger correlation with $NH_4$-N. Total phytoplankton biomass and the density of *Peridiniopsis niei* showed a stronger correlation with TP and $PO_4$-P. Evenness showed a relatively higher correlation with pH and $NH_4$-N, while dominance showed a relatively higher correlation with $NH_4$-N.

Many explanatory variables closely associated with the phytoplankton community were collected in this study, but their collective effect on changes within the phytoplankton community remains elusive. In addition, there are individual effects and interactions among these explanatory variables that pique our interest. Variation partitioning analyses (VPA) decompose total variability into the effects of pure explanatory variables, interaction effects between explanatory variables, and unexplained residuals, and help to address the aforementioned questions. In this study, phytoplankton variation was explained by 19 environmental factors, categorized into three groups: six meteorological and hydrological factors, four physical factors, and nine chemical factors. Together, they accounted for 0.51 of the total variation (Figure 5). Individually, their explanatory power was 0.05, 0.06, and 0.11, respectively. The interaction effect between the three groups was 0.05. Notably, the interaction between physical and chemical factors emerged as the most significant explanation for the observed variation in phytoplankton community composition, contributing 0.19 to the total variation.

The db-RDA technique was used to investigate the dissimilarity (Bray-Curtis distance) between phytoplankton communities among different sampling days and their relationships with environmental factors (Figure 6). Forward selection was used to identify significant

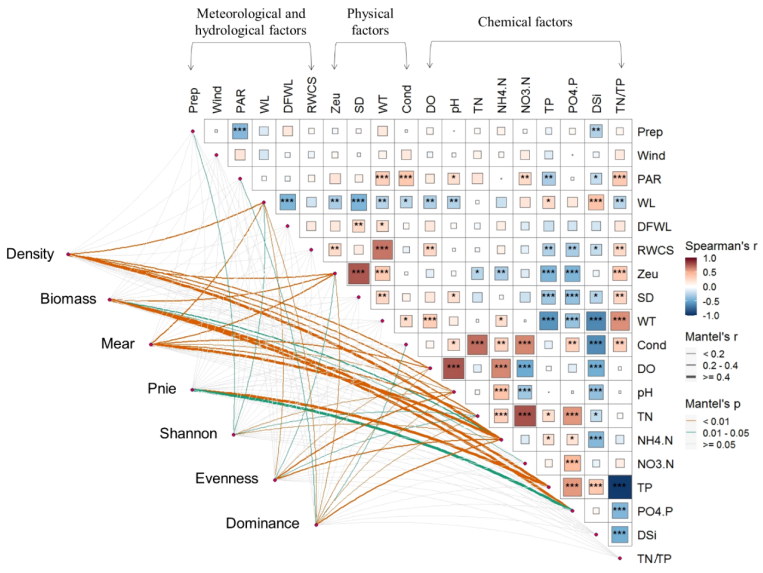


FIGURE 4
Relationship between environmental variables and phytoplankton total density (density), total biomass (biomass), density of Maer (Maer) and Pnie (Pnie), α diversity indices (Shannon, Evenness, and Dominance) through Mantel tests. Pairwise comparisons of different environmental variables are presented in the top-right section.*0.01≤p<0.05, **0.001≤p<0.01, *** denotes p<0.001

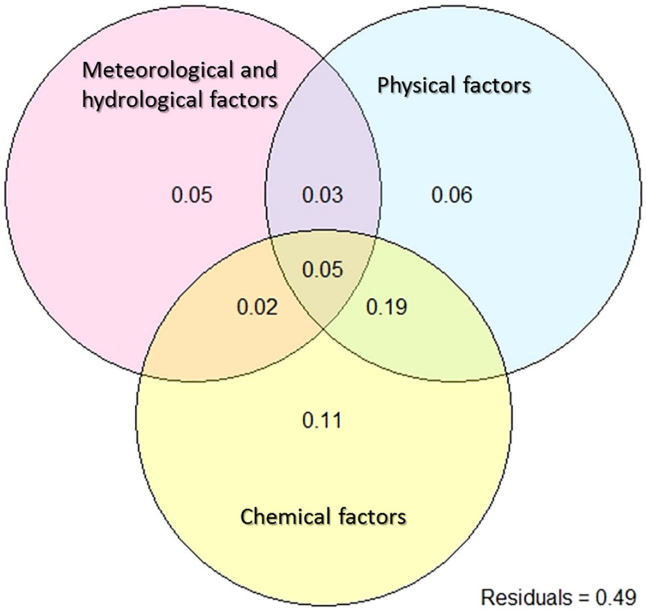


FIGURE 5
Variation partitioning analysis to show the percentages of explained variations for the phytoplankton composition. Variation was partitioned by meteorological and hydrological factors (Prep, Wind, PAR, WL, DFWL, and RWCS), physical factors (Zeu, SD, WT, and Cond) and chemical factors (DO, pH, TN, $NH_4$-N, $NO_3$-N, TP, $PO_4$-P, DSi, TN/TP).

environmental factors, including DSi, $NO_3$-N, $NH_4$-N, pH, WT, RWCS, and Zeu in this study. Variance Inflation Factor (VIF) testing indicated no significant collinearity among the environmental factors (VIF< 4.5). Collectively, all db-RDA axes explained 18.82% of the total variability in phytoplankton data, with the first three axes contributing 8.08%, 4.12%, and 2.88%, respectively. Key environmental factors associated with the first axis were DSi (0.18), $NH_4$-N (-0.26), and pH (-0.17); with WT (-0.21), Zeu (-0.15), and RWCS (-0.14) for the second axis; and with $NO_3$-N (-0.15) for the third axis. Global tests showed significance for all db-RDA axes under the reduced model (F = 4.3781, p = 0.001, 999 permutations). Individual tests showed significance for each of the first three axes (F = 13.1637, p = 0.007; F = 6.7134, p = 0.007; F = 4.6818, p = 0.007). There was a clear separation of phytoplankton communities among the four stages. Stage S1 sites had higher $NH_4$-N and pH with *Microcystis aeruginosa* as the dominant species. Stage S2 sites had higher WT, Zeu, and RWCS, with *Stephanodiscus hantzschii* and *Chroomonas*

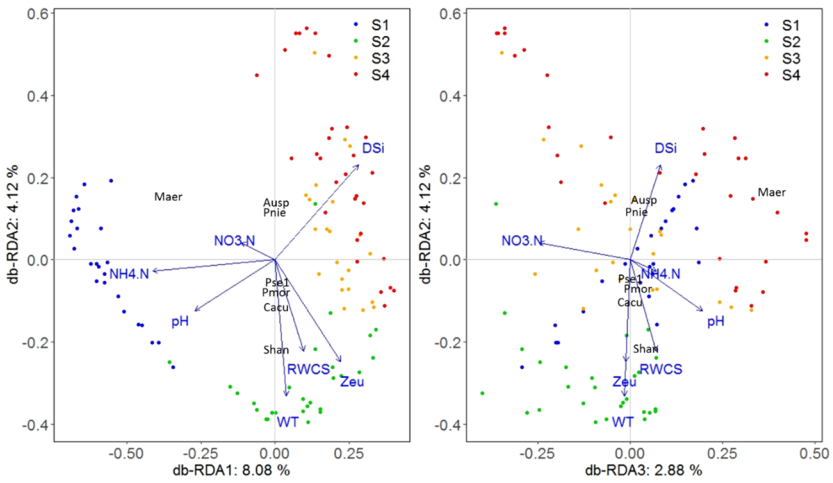


FIGURE 6
Phytoplankton community ordination based on db-RDA technique.

*acuta* as dominant species. Stage S4 sites had higher DSi, with *Peridiniopsis niei* and *Aulacoseira* sp. as dominant species.

## 3.3 Structure characteristics of phytoplankton community

The β diversity of the phytoplankton community was assessed and further partitioned into richness difference (RichDiff) and replacement (Repl) in Figure 7. Lower similarity in Figure 7 indicated higher β diversity, and vice versa. The β diversities based on abundance data were higher than those based on presence/absence data. Pairwise comparison of phytoplankton communities in stage 4 showed the lowest average similarity and the highest β diversity. In all stages, Repl contributed more to the variation than RichDiff with presence/absence data, while RichDiff contributed more to the variation than Repl with abundance data. Pairwise comparisons revealed an increase in average β diversity with stage progression, i.e., β diversity in stage 1< stages 1-2< 1-3< 1-4, 2< 2-3< 2-4, and 3< 3-4. For presence/absence data, RichDiff contributed more between stages 1 and 3, and stages 3 and 4, while Repl contributed more between the other pairs of stages. For abundance data, Repl contributed more between stages 2 and 3, while RichDiff contributed more between the other pairs of stages.

The co-occurrence network was used to elucidate the dynamic interactions and structure within the phytoplankton communities over time for each stage (Figure 8). In each stage, the proportion of species forming the network was relatively low, with most species changing independently. Among the species forming the network, there were some shared species across stages 2, 3, and 4, for example, *Stephanodiscus minutulus* and *Cyclotella stelligera*. However, in stage 1, the only shared species was *Pandorina morum*. The Topological characteristics of the co-occurrence networks for each stage are presented in Table 2. All nodes (i.e., all species) were shown to facilitate comparison of differences between the stages, but only those edges with connections were shown. Stages 1 and 3 showed almost opposite topological characteristics. Stage 1 had the highest average degree, graph density, and average clustering coefficient, and the lowest connected components and average path length. However, stage 3 had the lowest average degree, average weighted degree, graph density, and the highest modularity, connected component, and average path length. In addition, S2 had the lowest modularity, and S4 had the lowest average clustering coefficient.

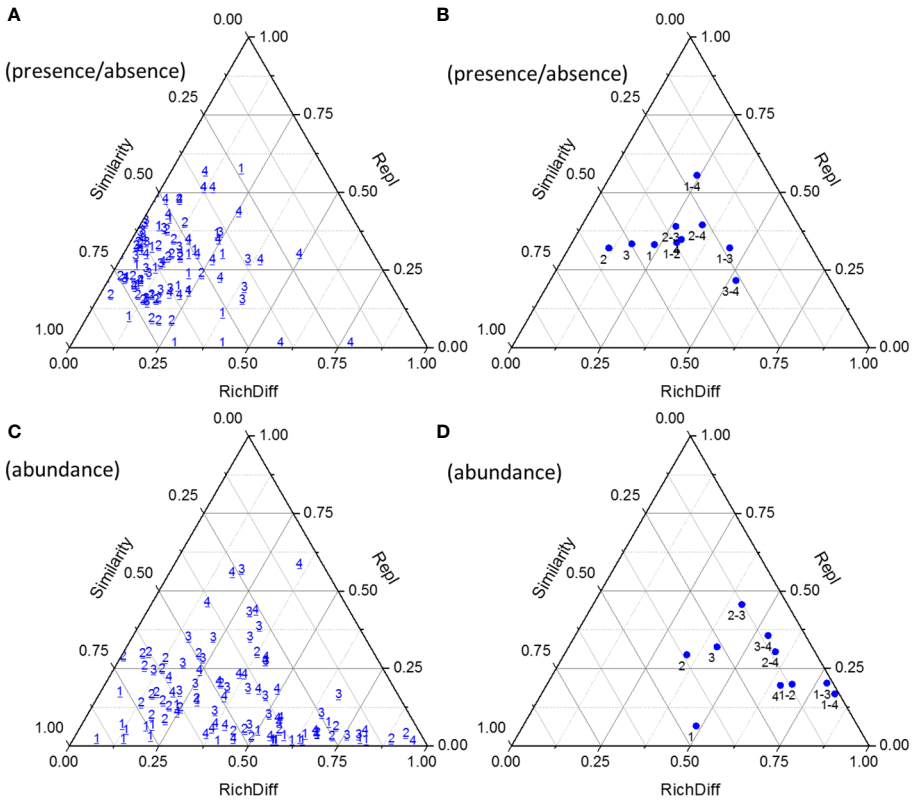


FIGURE 7
Triangular plots of β diversity comparisons for phytoplankton communities between successive days (with presence/absence data, **(A)** with abundance data, **(C)** and between days within and between stages (with presence/absence data, **(B)** with abundance data, **(D)**. The position of each point is determined by a triplet of values from the Similarity, RichDiff (richness difference), and Repl (replacement) matrices; each triplet sums to 1. The numbers 1~4 indicated the stage 1~4.

10.3389/fpls.2024.1390019

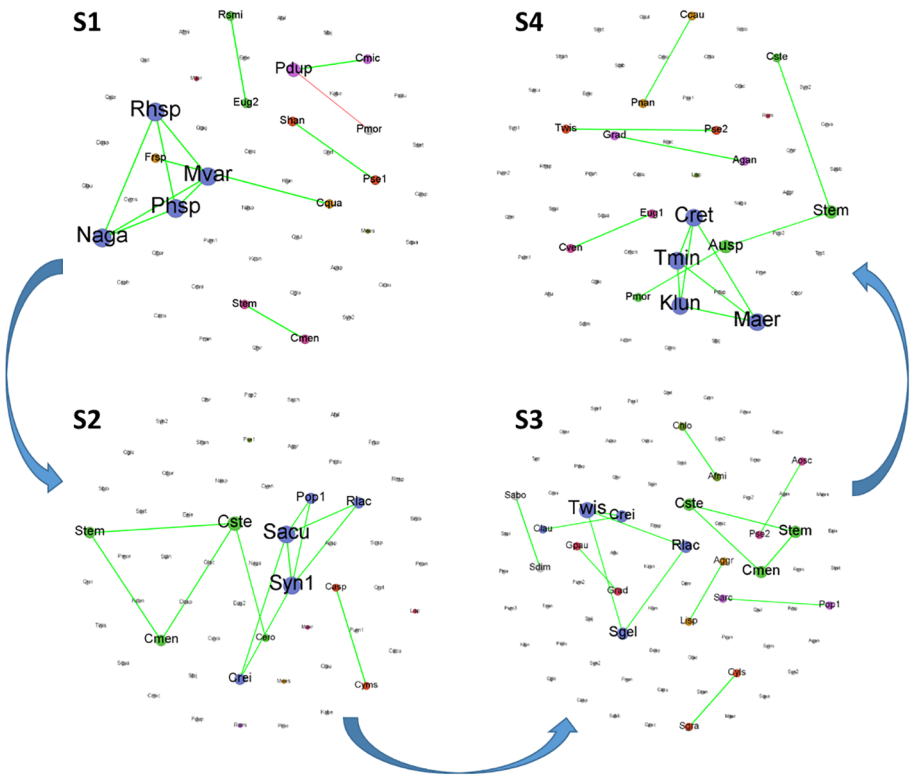


FIGURE 8
Co-occurrence networks of phytoplankton community at species level based on Spearman correlation analysis for each stage. (Green and red curves between nodes represent positive and negative correlations, respectively).

## 4 Discussion

Algal blooms have emerged as a significant environmental problem in inland waters (Hou et al., 2022) and pose a significant threat to public health and aquatic ecosystems worldwide (Brooks et al., 2016). Daily sampling provides a more detailed view of the phytoplankton bloom process compared to the broader dynamics captured by weekly sampling. Our previous weekly study (Wang et al., 2011) missed the peaks of both *Microcystis aeruginosa* on July 2nd and *Peridiniopsis niei* on September 15th, despite overlapping study periods. Inaccurate time scales can lead to misinterpretation of key factors influencing algal community composition and confound studies of growth dynamics (Gupta et al., 2023). There is an urgent need for fine-scale and structured information on phytoplankton communities to fully understand the conceptual mechanisms driving bloom development, which will provide technical support for watershed management. Different studies use different definitions of the biomass threshold for identifying

TABLE 2 Topological characteristics of co-occurrence networks for each stage.

| | S1 | S2 | S3 | S4 |
|---|---|---|---|---|
| Nodes | 49 | 57 | 77 | 57 |
| Edges | 12 | 12 | 15 | 13 |
| Average Degree | 0.49 | 0.421 | 0.39 | 0.456 |
| Average Weighted Degree | 0.401 | 0.38 | 0.347 | 0.436 |
| Graph Density | 0.01 | 0.008 | 0.005 | 0.008 |
| Modularity | 0.668 | 0.557 | 0.824 | 0.699 |
| Connected Components | 40 | 49 | 64 | 47 |
| Average Clustering Coefficient | 0.8 | 0.792 | 0.762 | 0.667 |
| Average Path Length | 1.077 | 1.294 | 1.35 | 1.25 |

bloom occurrence. For example, Tett (1987) defines exceptional blooms as those that exceed a chlorophyll threshold of 100 μg/L. In practice, a chlorophyll *a* level of 15 μg/L is often used as a standard for algaecide application (Hudnell et al., 2010). In our study, the peak chlorophyll *a* levels in stages 1 and 4 reached 70.80 μg/L and 706.44 μg/L, respectively (unpublished data). However, it is not appropriate to compare two types of phytoplankton blooms, *Microcystis* and *Peridiniopsis* blooms, based on chlorophyll *a* concentrations alone. The *Microcystis* bloom had higher density but lower biomass and chlorophyll *a* concentration and lasted longer. In contrast, the *Peridiniopsis* bloom had lower density but higher biomass and chlorophyll *a* concentration, with its clear advantage lasting one to two days. Consideration of phytoplankton community structure provides a more insightful framework for studying bloom dynamics.

Species dominance in the environment is typically not attributed to the influence of a single environmental factor, but is often determined by complex nonlinear relationships involving many environmental variables. Wind- driven hydrodynamic conditions are often an important factor in determining the extent of phytoplankton blooms (Wu et al., 2015). Light and the hydrodynamic conditions also play a critical role in the development and maintenance of blooms (Wang et al., 2020; Summers and Ryder, 2023). However, in this study, the influence of meteorological and hydrological factors was less than that of physiochemical factors (Figure 5). Excessive nutrient enrichment in water bodies undoubtedly promotes the growth of harmful cyanobacteria (Nowicka-Krawczyk et al., 2022). Throughout the study period, the density of *Microcystis aeruginosa* showed a stronger correlation with $NH_4$-N (Figure 4). The *Microcystis* bloom created conditions that could further increase its dominance, such as higher pH and lower Zeu (Table 1). These conditions favor the development of cyanobacterial blooms (Amorim and Moura, 2021). In addition to being photoautotrophic, cyanobacteria are known to use several ecophysiological strategies to outcompete eukaryotic algae and ensure their mass dominance in the phytoplankton. These strategies include the presence of gas vesicle aggregates, rapid cell division, and the use of specific metabolic pathways, among others (Li et al., 2016). Summers and Ryder (2023) concluded that prolonged stratification reduces competition, decreases diversity, and leads to cyanobacteria-dominated blooms. In our study, stages 1 and 2 had relatively higher RWCS, but there was a drastic decrease in the abundance of *Microcystis*, due in part to reductions in TN and $NH_4$-N. This suggests that nutrient availability may contribute more significantly than stratification to the transformation of the phytoplankton community towards a reduction of *Microcystis* blooms. Furthermore, the influence of rainfall could not be excluded, as rainfall occurred on July 1$^{st}$ (11.6 mm/day) and 2$^{nd}$ (0.3 mm/day).

Freshwater dinoflagellates, including *Peridiniopsis*, are found in many aquatic ecosystems worldwide and can sometimes lead to harmful blooms that adversely affect water quality (Viner-Mozzini et al., 2003; Yatigammana et al., 2011). Dinoflagellates possess several abilities, such as tolerance to high irradiance, vertical migration within the water column to optimize photosynthesis and growth, and the secretion of toxins, which allow them to compete, thrive, and dominate within the phytoplankton community (Viner-Mozzini et al., 2003; Regel et al., 2004). In our study, *Peridiniopsis niei* density showed a stronger correlation with TP and $PO_4$-P, highlighting the importance of phosphorus in maintaining their dominance. Wu et al. (2017) also showed that high phosphorus increased the photosynthetic efficiency of *Peridiniopsis* and stimulated its growth. However, certain environmental factors, such as lower RWCS in stage 4, did not provide suitable conditions to maintain their competitive advantage. The dominance of *Peridiniopsis niei* persisted for one to two days, possibly due to the rainfall events that occurred on September 15$^{th}$ (0.1 mm/day). A similar phenomenon was reported by Zhou et al. (2011), who attributed the decrease in phytoplankton biomass and the disappearance of blooms to heavy rainfall.

Despite the morphological and physiological differences between cyanobacteria and dinoflagellates, reservoirs provide ecological conditions conducive to their success. The possession of aerotopes or flagella allows individuals to dominate in newly created regimes with less turbulence (Bordet et al., 2017). Although TP reduction is widely used as a primary strategy to mitigate the severity of harmful algal blooms (Pick, 2016), cases have shown that TP decreases can be accompanied by increases in chlorophyll *a* concentrations, suggesting that other abiotic factors may also influence the observed trends (Huang et al., 2020). The study by Nowicka-Krawczyk et al. (2022) showed that the composition of cyanobacterial blooms is strongly influenced by the nitrogen/phosphorus (N/P) ratio, with N/P explaining 13.3% of the variation and $PO_4$-P explaining 10.5%. In hypereutrophic waters (TP > 0.1 mg/L), phytoplankton biomass was found to increase with additions of both phosphorus and nitrogen (Filstrup and Downing, 2017). Therefore, it is critical to consider the TN : TP ratio for these systems (Summers and Ryder, 2023). Some studies have considered N/P as a factor influencing phytoplankton structure, rather than just absolute N and P concentrations (Liu et al., 2024; Yang et al., 2020). In this study, the maximum concentrations of TP reached 0.13 and 0.30 mg/L in stages 1 and 4, respectively. Therefore, the ratio of TN : TP should be considered. We correlated TN, TP, and TN : TP with the biomass proportion of *Microcystis aeruginosa* and *Peridiniopsis niei* for the sampling days when either *Microcystis aeruginosa* or *Peridiniopsis niei* was present (see Figure 9). The results showed that a high TN concentration, low TP concentration, and high TN : TP ratio corresponded to a high biomass proportion of *Microcystis aeruginosa*. Conversely, a low TN concentration, high TP concentration, and low TN : TP ratio corresponded to a high biomass proportion of *Peridiniopsis niei*. This contrasting response of *Microcystis aeruginosa* and *Peridiniopsis niei* suggests that TN : TP plays an important role in maintaining the competitive advantages of different dominant bloom species.

The bloom-forming taxa significantly influenced the composition and structure of the phytoplankton. *Microcystis aeruginosa* blooms significantly reduced phytoplankton species richness, Shannon diversity, and evenness, reaching the lowest levels observed (refer to Figure 3 and Table 2), consistent with the findings of Escalas et al. (2019). Similarly, blooms of

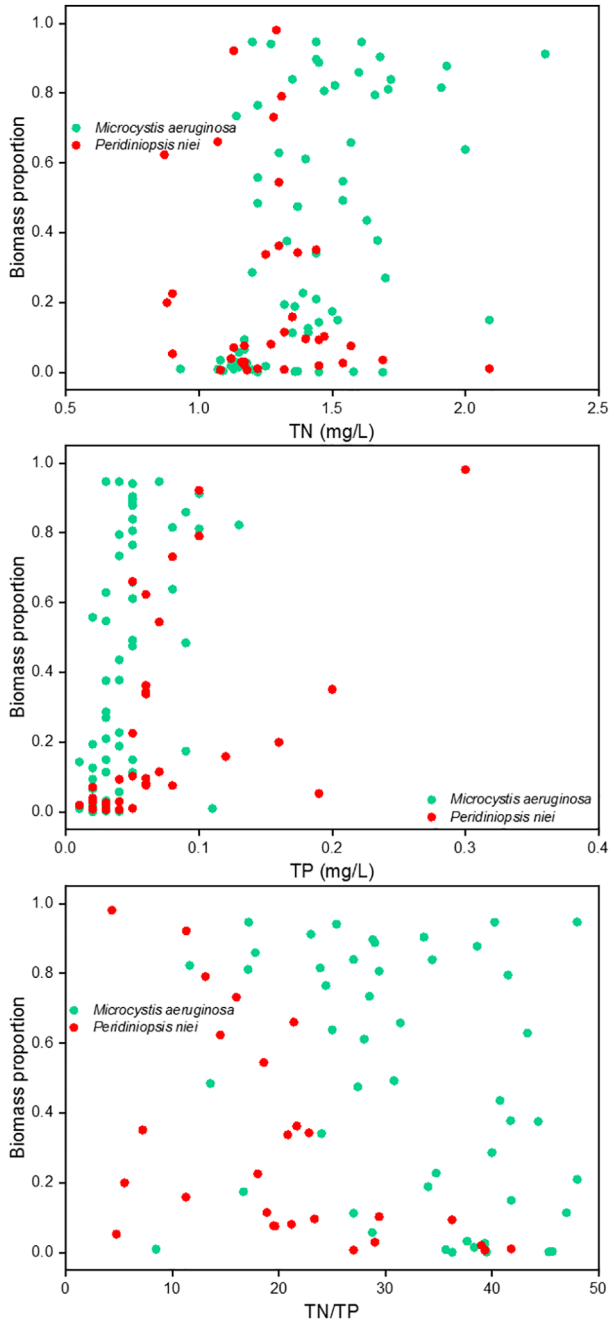


FIGURE 9
Correlation relationships between TN, TP, as well as TN : TP and biomass proportion of *Microcystis aeruginosa* and *Peridiniopsis niei*.

*Peridiniopsis niei* also resulted in reduced phytoplankton species richness, Shannon diversity, and evenness, consistent with recent findings by Amorim and Moura (2021). In addition, intense blooms of cyanobacteria and dinophyta are known to cause fish kills by depleting oxygen concentrations during biomass decomposition (Meichtry de Zaburlín et al., 2016), leading to significant disruptions in aquatic food webs, ecosystem functioning, and ecosystem service provision (Sukenik et al., 2015). However, throughout the entire study period, stage 3 exhibited low total density and total biomass, with the highest species richness (as indicated by the highest nodes in Table 2), Shannon diversity, and evenness, as well as the lowest dominance index. The successful growth of *Peridiniopsis niei* after stage 3, despite the initial low phytoplankton density, indicates its resilience under reduced competition from other phytoplankton.

The β diversity of phytoplankton can serve as an excellent model for elucidating the mechanisms that shape aquatic communities in reservoirs (de Moura et al., 2022). Studies examining replacement rates and variations in phytoplankton richness or abundance can be interpreted as indicators of ecosystem function, given the significant dependence of reservoir trophic webs on phytoplankton dynamics (Znachor et al., 2020). In this study, β diversities based on abundance data were higher than those based on presence/absence data. Repl had a greater effect on β diversity differences based on presence/absence data. This may indicate that during blooms dominated by different species and at different stages of bloom development, certain species had replaced others, resulting in variations in β diversity. Conversely, RichDiff had a greater effect on β diversity differences based on species abundance data. This suggests the presence of species with significant differences in abundance between samples, particularly dominant phytoplankton bloom species, and that these differences in abundance were one of the main drivers of β diversity differences. These results indicate that β diversity differences throughout the phytoplankton bloom process included significant species turnover and abundance gradients, both of which jointly influenced the differences in phytoplankton species composition on different sampling days. Szabo et al. (2019) suggested that both abundance and binary data sets should be considered when assessing ecological uniqueness, as they can shed light on different ecological interpretation patterns, and de Moura et al. (2022) also identified some differences between data types.

Increasing evidence suggests that the ability of microbial systems to support ecological functions and resist environmental pressures is an emergent property resulting from interactions among many taxa (Escalas et al., 2019). Network-based approaches provide an integrated representation of interactions among different taxa within microbial communities (Deng et al., 2012). However, studies on the structure of phytoplankton networks are still limited (Carey et al., 2017; Tarafdar et al., 2023). Each phytoplankton network constructed in this study represents the covariation in phytoplankton density over time for each stage, with similar responses to environmental changes or interactions among phytoplankton species (Rottjers and Faust, 2018). The co-occurrence networks of stages 1 and 4 had relatively high average degree and graph density, low connected components and average path length. This combination of features may reflect a relatively dense and evenly connected network, where connections between nodes are tight and the entire network is a relatively cohesive unit. Such a network structure may indicate efficient information propagation, shorter path lengths, and higher network accessibility under certain circumstances. Although composed of fewer nodes and links for stage 1 in Table 2, the *Microcystis*-dominated networks could be considered as more complex than the others, as they have a higher graph density and a higher average number of links (degree) per node. Similar results were reported in the study of Escalas et al.

(2019). Furthermore, the co-occurrence networks in stage 3 were relatively special, with the lowest average degree and graph density, but the highest number of nodes, edges, modularity, connected components, and average path length. This indicated that there were some sparsely connected small-world structures within the community, resulting in a lower clustering coefficient for nodes within the community; however, the overall community division remained compact. It has been reported that networks with small-world structures tend to be more robust to perturbations and random loss of species (Peura et al., 2015). A slightly more positive correlation at stage 3 also suggests that high cooperative interactions among species may result in a more stable community structure and thus more resilient to environmental changes (Tarafdar et al., 2023).

## 5 Conclusion

The study analyzed the dynamics of the phytoplankton community during a low-water level period (June to September) when blooms of *Microcystis aeruginosa* and *Peridiniopsis niei* occurred sequentially in a large subtropical reservoir bay. The entire bloom process was clearly delineated into four stages based on daily changes in total and relative phytoplankton abundance and biomass, and α diversity including Shannon, evenness and dominance. *Microcystis aeruginosa* maintained significant dominance for almost a month in stage 1, with low Shannon and evenness but a high dominance index. This was followed by stage 2, where total density and biomass decreased dramatically, but *Microcystis aeruginosa* still accounted for some proportion. Phytoplankton total density and biomass continued to decrease in stage 3, which was characterized by the highest Shannon and evenness but the lowest dominance index. *Peridiniopsis niei* bloomed in stage 4, but its dominant advantages lasted only one to two days. Total phytoplankton density and *Microcystis aeruginosa* density showed a stronger correlation with $NH_4$-N, while total phytoplankton biomass and *Peridiniopsis niei* density showed a stronger correlation with TP and $PO_4$-P. The TN : TP ratio could be considered as an important indicator to determine whether *Microcystis aeruginosa* or *Peridiniopsis niei* dominated the phytoplankton community. Precipitation partially contributed to their significant decrease or disappearance. Variation partitioning analyses (VPA) indicated that physical and chemical factors and their interactions explained more variation in phytoplankton data than meteorological and hydrological factors. DSi, $NH_4$-N, pH, WT, Zeu, and RWCS were identified as key environmental factors associated with phytoplankton community variation using the db-RDA technique. The β diversity of the phytoplankton community was assessed and further partitioned into richness difference (RichDiff) and replacement (Repl). The results showed an increase in average β diversity with stage progression, i.e., β diversity in stage 1< stages 1-2< 1-3< 1-4, 2< 2-3< 2-4, and 3< 3-4. In all stages, Repl contributed more to the variation than RichDiff with presence/absence data, while RichDiff contributed more to the variation than Repl with abundance data. Co-occurrence network analysis revealed that stage 1 had the highest average degree, graph density, and average clustering coefficient, along with the lowest connected components and average path length, indicating the most complex structure. However, stage 3 had the lowest average degree, average weighted degree, graph density, along with the highest modularity, connected component, and average path length, suggesting that the network for stage 3 was relatively sparse, despite maintaining a compact overall community division.

## Data availability statement

The raw data supporting the conclusions of this article will be made available by the authors, without undue reservation.

## Author contributions

LT: Data curation, Investigation, Writing – original draft. LW: Formal analysis, Methodology, Visualization, Writing – review & editing. QC: Conceptualization, Project administration, Writing – review & editing.

## Funding

The author(s) declare financial support was received for the research, authorship, and/or publication of this article. This study was supported by Hubei Key Laboratory of Wetland Evolution & Ecological Restoration, the Strategic Priority Research Program of CAS (XDA23040500), National S&T Basic Work of China (2014FY120200), and the National Natural Science Foundation of China (30330140).

## Conflict of interest

The authors declare that the research was conducted in the absence of any commercial or financial relationships that could be construed as a potential conflict of interest.

## Publisher's note

# References


Amorim, C. A., and Moura, A. N. (2021). Ecological impacts of freshwater algal blooms on water quality, plankton biodiversity, structure, and ecosystem functioning. *Sci. Total Environ.* 758, 143605. doi: 10.1016/j.scitotenv.2020.143605

Basset, A., Carrada, G. C., Fedele, M., and Sabetta, L. (2008). Equilibrium concept in phytoplankton communities. *Encyclopedia Ecology Acad. Press* 2, 1394–1402. doi: 10.1016/B978-008045405-4.00711-4

Bordet, F., Fontanarrosa, M. S., and O'Farrell, I. (2017). Influence of light and mixing regime on bloom - forming phytoplankton in a subtropical reservoir. *River Res. Appl.* 33, 1315–1326. doi: 10.1002/rra.3189

Brooks, B. W., Lazorchak, J. M., Howard, M. D., Johnson, M. V. V., Morton, S. L., Perkins, D. A., et al. (2016). Are harmful algal blooms becoming the greatest inland water quality threat to public health and aquatic ecosystems? *Environ. Toxicol. Chem.* 35, 6–13. doi: 10.1002/etc.3220

Cai, Q. (2007). *Protocols for standard observation and measurement in aquatic ecosystems* (Beijing, China: Chinese Environmental Science Press).

Cai, Q., and Hu, Z. (2006). Studies on eutrophication problem and control strategy in the Three Gorges Reservoir. *Acta Hydrobiologica Sin.* 30, 7–11. doi: 10.3321/j.issn:1000-3207.2006.01.002

Cai, Q., Liu, M., He, Y., Zeng, X., and Jiang, T. (2010). *Climate change impact assessment report for the three gorges reservoir area of the yangtze river* (Beijing, China: China Meteorological Press).

Carey, C. C., Brown, B. L., and Cottingham, K. L. (2017). The cyanobacterium *Gloeotrichia echinulata* increases the stability and network complexity of phytoplankton communities. *Ecosphere* 8, e01830. doi: 10.1002/ecs2.1830

Carstensen, J., Henriksen, P., and Heiskanen, A. S. (2007). Summer algal blooms in shallow estuaries: Definition, mechanisms, and link to eutrophication. *Limnology Oceanography* 52, 370–384. doi: 10.4319/lo.2007.52.1.0370

de Moura, W. B., da Silva, P. R. L., Baumgartner, G., Bueno, N. C., and Bortolini, J. C. (2022). Site contributions to phytoplankton beta diversity along two subtropical reservoirs. *Aquat. Sci.* 84, 59. doi: 10.1007/s00027-022-00890-3

Deng, Y., Jiang, Y., Yang, Y., He, Z., Luo, F., and Zhou, J. (2012). Molecular ecological network analyses. *BMC Bioinf.* 13, 1–20. doi: 10.1186/1471-2105-13-113

Ding, D., Arif, M., Liu, M., Li, J., Hu, X., Geng, Q., et al. (2022). Plant-soil interactions and C: N: P stoichiometric homeostasis of plant organs in riparian plantation. *Front. Plant Sci.* 13. doi: 10.3389/fpls.2022.979023

Escalas, A., Catherine, A., Maloufi, S., Cellamare, M., Hamlaoui, S., Yéprémian, C., et al. (2019). Drivers and ecological consequences of dominance in periurban phytoplankton communities using networks approaches. *Water Res.* 163, 114893. doi: 10.1016/j.watres.2019.114893

Filstrup, C., and Downing, J. (2017). Relationship of chlorophyll to phosphorus and nitrogen in nutrient-rich lakes. *Inland Waters* 7, 385–400. doi: 10.1080/20442041.2017.1375176

Griffith, A. W., and Gobler, C. J. (2020). Harmful algal blooms: a climate change co-stressor in marine and freshwater ecosystems. *Harmful Algae* 91, 101590. doi: 10.1016/j.hal.2019.03.008

Gupta, A., Hantush, M. M., and Govindaraju, R. S. (2023). Sub-monthly time scale forecasting of harmful algal blooms intensity in Lake Erie using remote sensing and machine learning. *Sci. Total Environ.* 900, 165781. doi: 10.1016/j.scitotenv.2023.165781

Ho, J. C., Michalak, A. M., and Pahlevan, N. (2019). Widespread global increase in intense lake phytoplankton blooms since the 1980s. *Nature* 574, 667–670. doi: 10.1038/s41586-019-1648-7

Hou, X., Feng, L., Dai, Y., Hu, C., Gibson, L., Tang, J., et al. (2022). Global mapping reveals increase in lacustrine algal blooms over the past decade. *Nat. Geosci.* 15, 130–134. doi: 10.1038/s41561-021-00887-x

Hu, H., and Wei, Y. (2006). *The freshwater algae of China—Systematics, taxonomy and ecology* (Beijing, China: Science Press).

Huang, Z., Li, Y., Chen, Y., Li, J., Xing, Z., Ye, M., et al. (2006). *Water quality prediction and water environmental carrying capacity calculation for Three Gorges Reservoir* (Beijing, China: China WaterPower Press).

Huang, J., Zhang, Y., Arhonditsis, G. B., Gao, J., Chen, Q., and Peng, J. (2020). The magnitude and drivers of harmful algal blooms in China's lakes and reservoirs: A national-scale characterization. *Water Res.* 181, 115902. doi: 10.1016/j.watres.2020.115902

Hudnell, H. K., Jones, C., Labisi, B., Lucero, V., Hill, D. R., and Eilers, J. (2010). Freshwater harmful algal bloom (FHAB) suppression with solar powered circulation (SPC). *Harmful Algae* 9, 208–217. doi: 10.1016/j.hal.2009.10.003

Huisman, J., Codd, G. A., Paerl, H. W., Ibelings, B. W., Verspagen, J. M. H., and Visser, P. M. (2018). Cyanobacterial blooms. *Nat. Rev. Microbiol.* 16, 471–483. doi: 10.1038/s41579-018-0040-1

Leitão, M., Morata, S. M., Rodriguez, S., and Vergon, J. P. (2003). The Effect of perturbations on phytoplankton assemblages in a deep reservoir (Vouglans, France). *Hydrobiologia* 502, 73–83. doi: 10.1023/B:HYDR.0000004271.08002.73

Li, X., Dreher, T., and Li, R. (2016). An overview of diversity, occurrence, genetics and toxin production of bloom-forming *Dolichospermum* (Anabaena) species. *Harmful Algae* 54, 54–68. doi: 10.1016/j.hal.2015.10.015

Liu, D., Huang, Y., and Ji, D. (2013). *Algal blooms and ecological regulation in tributaries of Three Gorges Reservoir China* (Beijing, China: Water Resources and Hydropower Press).

Liu, Q., Wang, Y., Li, Y., Li, Y., Wang, Y., Zhou, B., et al. (2021). Nutrient alteration drives the impacts of seawater acidification on the bloom-forming dinoflagellate *karenia mikimotoi*. *Front. Plant Sci.* 12. doi: 10.3389/fpls.2021.739159

Liu, F., Zhang, H., Wang, Y., Yu, J., He, Y., and Wang, D. (2024). Hysteresis analysis reveals how phytoplankton assemblage shifts with the nutrient dynamics during and between precipitation patterns. *Water Res.* 251, 121099. doi: 10.1016/j.watres.2023.121099

Mcardle, B. H., and Anderson, M. J. (2001). Fitting multivariate models to community data: A comment on distance-based redundancy analysis. *Ecology* 82, 290–297. doi: 10.1890/0012-9658(2001)082[0290:FMMTCD]2.0.CO;2

Meichtry de Zaburlín, N., Vogler, R. E., Molina, M. J., and Llano, V. M. (2016). Potential distribution of the invasive freshwater dinoflagellate *Ceratium furcoides* (Levander) Langhans (Dinophyta) in South America. *J. Phycology* 52, 200–208. doi: 10.1111/jpy.12382

Ministry of Environmental Protection of China (2014). *Bulletin on the ecological and environmental monitoring results of the TGP*, (2003-2013). Available online at: https://www.cnemc.cn/zzjj/jgsz/sts/gzdt_sts/

Naselli-Flores, L. (2000). Phytoplankton assemblages in twenty-one Sicilian reservoirs: relationships between species composition and environmental factors. In Reynolds, C.S., Dokulil, M., and Padisák, J. (eds) The Trophic Spectrum Revisited. Developments in Hydrobiology, 150 (Dordrecht, Netherlands: Springer).

Nowicka-Krawczyk, P., Żelazna-Wieczorek, J., Skrobek, I., Ziułkiewicz, M., Adamski, M., Kaminski, A., et al. (2022). Persistent cyanobacteria blooms in artificial water bodies—an effect of environmental conditions or the result of anthropogenic change. *Int. J. Environ. Res. Public Health* 19, 6990. doi: 10.3390/ijerph19126990

Oksanen, J., Simpson, G. L., Blanchet, F. G., Kindt, R., Legendre, P., Minchin, P. R., et al. (2022). *Package 'vegan': Community Ecology Package. R package version 2.6-4*. Available online at: https://rdrr.io/cran/vegan/

Olokotum, M., Mitroi, V., Troussellier, M., Semyalo, R., Bernard, C., Montuelle, B., et al. (2020). A review of the socioecological causes and consequences of cyanobacterial blooms in Lake Victoria. *Harmful Algae* 96, 101829. doi: 10.1016/j.hal.2020.101829

Ou, T., Zhang, M., Huang, Y., Wang, L., Wang, F., Wang, R., et al. (2022). Role of rhizospheric Bacillus megaterium HGS7 in maintaining mulberry growth under extremely abiotic stress in hydro-fluctuation belt of three gorges reservoir. *Front. Plant Sci.* 13. doi: 10.3389/fpls.2022.880125

Padisák, J., Barbosa, F., Koschel, R., and Krienitz, L. (2003). Deep layer cyanoprokaryota maxima in temperate and tropical lakes. *Archiv Für Hydrobiologie (Special Issues Advanced Limnology)* 58, 175–199.

Peura, S., Bertilsson, S., Jones, R. I., and Eiler, A. (2015). Resistant microbial cooccurrence patterns inferred by network topology. *Appl. Environ. Microbiol.* 81, 2090–2097. doi: 10.1128/AEM.03660-14

Pick, F. R. (2016). Blooming algae: a Canadian perspective on the rise of toxic cyanobacteria. *Can. J. Fisheries Aquat. Sci.* 73, 1149–1158. doi: 10.1139/cjfas-2015-0470

Regel, R. H., Brookes, J. D., and Ganf, G. G. (2004). Vertical migration, entrainment and photosynthesis of the freshwater dinoflagellate *Peridinium cinctum* in a shallow urban lake. *J. Plankton Res.* 26, 143–157. doi: 10.1093/plankt/fbh008

Reid, A. J., Carlson, A. K., Creed, I. F., Eliason, E. J., Gell, P. A., Johnson, P. T. J., et al. (2019). Emerging threats and persistent conservation challenges for freshwater biodiversity. *Biol. Rev.* 94, 849–873. doi: 10.1111/brv.12480

Reynolds, C. S. (2006). *Ecology of phytoplankton* (Cambridge, England: Cambridge University Press).

Rottjers, L., and Faust, K. (2018). From hairballs to hypotheses-biological insights from microbial networks. *FEMS Microbiol. Rev.* 42, 761–780. doi: 10.1093/femsre/fuy030

Sukenik, A., Quesada, A., and Salmaso, N. (2015). Global expansion of toxic and non-toxic cyanobacteria: effect on ecosystem functioning. *Biodiversity Conserv.* 24, 889–908. doi: 10.1007/s10531-015-0905-9

Summers, E. J., and Ryder, J. L. (2023). A critical review of operational strategies for the management of harmful algal blooms (HABs) in inland reservoirs. *J. Environ. Manage.* 330, 117141. doi: 10.1016/j.jenvman.2022.117141

Szabo, B., Lengyel, E., Padisak, J., and Kovacs, C. S. (2019). Benthic diatom metacommunity across small freshwater lakes: driving mechanisms, β-diversity and ecological uniqueness. *Hydrobiologia* 828, 183–198. doi: 10.1007/s10750-018-3811-9

Tarafdar, L., Mohapatra, M., Muduli, P. R., Kumar, A., Mishra, D. R., and Rastogi, G. (2023). Co-occurrence patterns and environmental factors associated with rapid onset of *Microcystis aeruginosa* bloom in a tropical coastal lagoon. *J. Environ. Manage.* 325, 116580. doi: 10.1016/j.jenvman.2022.116580

Tett, P. (1987). The ecophysiology of exceptional blooms. *Rapport Proces-verbaux Des. Reunions. Conseil Int. pour l'Exploration la Mer* 187, 47–60.

Viner-Mozzini, Y., Zohary, T., and Gasith, A. (2003). Dinoflagellate bloom development and collapse in Lake Kinneret: A sediment trap study. *J. Plankton Res.* 25, 591–602. doi: 10.1093/plankt/25.6.591

Wang, L., Cai, Q., Xu, Y., Kong, L., Tan, L., and Zhang, M. (2011). Weekly dynamics of phytoplankton functional groups under high water level fluctuations in a subtropical reservoir-bay. *Aquat. Ecol.* 45, 197–212. doi: 10.1007/s10452-010-9346-4

Wang, J., Wang, B., and Luo, Z. (1997). *Glossary of the yangtze river* (Wuhan, China: Wuhan Press).

Wang, H., Zhao, D., Chen, L., Giesy, J. P., Zhang, W., Yuan, C., et al. (2020). Light, but not nutrients, drives seasonal congruence of taxonomic and functional diversity of phytoplankton in a eutrophic highland lake in China. *Front. Plant Sci.* 11. doi: 10.3389/fpls.2020.00179

Wetzel, R., and Likens, G. (2000). *Limnological analyses* Vol. 3 (Springer: New York, America). doi: 10.1007/978-1-4757-3250-4

Wu, X., Li, C., Chen, L., Zhao, Y., and Wang, H. (2017). Response mechanism of *Peridiniopsis* bloom to phosphorus in Xiangxi River Bay of Three Gorges Reservoir. *J. Lake Sci.* 29, 1054–1060. doi: 10.18307/2017.0503

Wu, T., Qin, B., Brookes, J., Shi, K., Zhu, G., Zhu, M., et al. (2015). The influence of changes in wind patterns on the areal extension of surface cyanobacterial blooms in a large shallow lake in China. *Sci. Total Environ.* 518, 24–30. doi: 10.1016/j.scitotenv.2015.02.090

Yang, Y., Pan, J. Y., Han, B. P., and Naselli-Flores, L. (2020). The effects of absolute and relative nutrient concentrations (N/P) on phytoplankton in a subtropical reservoir. *Ecol. Indic.* 115, 106466. doi: 10.1016/j.ecolind.2020.106466

Yatigammana, S. K., Ileperuma, O. A., and Perera, M. B. U. (2011). Water pollution due to a harmful algal bloom: A preliminary study from two drinking water reservoirs in Kandy, Sri Lanka. *J. Natl. Sci. of* 39, 91–94. doi: 10.4038/jnsfsr.v39i1.2930

Zeng, C., Xing, R., and Huang, B. (2023). Phytoplankton in headwater streams: spatiotemporal patterns and underlying mechanisms. *Front. Plant Sci.* 14. doi: 10.3389/fpls.2023.1276289

Zhao, W., Li, Y., Jiao, Y., Zhou, B., Vogt, R. D., Liu, H., et al. (2017). Spatial and temporal variations in environmental variables in relation to phytoplankton community structure in a eutrophic river-type reservoir. *Water* 9, 754. doi: 10.3390/w9100754

Zhou, B., Shi, K., Wang, W., Zhang, D., Qin, B., Zhang, Y., et al. (2022). Phytoplankton succession phenology trends in the backwaters of the three gorges reservoir in China and their drivers: Results from satellite observations. *Ecol. Indic.* 143, 109435. doi: 10.1016/j.ecolind.2022.109435

Zhou, G., Zhao, X., Bi, Y., Liang, Y., Hu, J., Yang, M., et al. (2011). Phytoplankton variation and its relationship with the environment in Xiangxi Bay in spring after damming of the Three-Gorges, China. *Environ. Monit. Assess.* 176, 125–141. doi: 10.1007/s10661-010-1571-8

Znachor, P., Nedoma, J., Hejzlar, J., Seda, J., Komarkova, J., Kolař, V., et al. (2020). Changing environmental conditions underpin long-term patterns of phytoplankton in a freshwater reservoir. *Sci. Total Environ.* 710, 135626. doi: 10.1016/j.scitotenv.2019.135626

frontiers | Frontiers in Plant Science

TYPE Original Research
PUBLISHED 17 May 2024
DOI 10.3389/fpls.2024.1375898



OPEN ACCESS

EDITED BY
Qiang Yang,
German Centre for Integrative Biodiversity Research (iDiv), Germany

REVIEWED BY
Min Zhang,
Huazhong Agricultural University, China
Yongjiu Cai,
Chinese Academy of Sciences (CAS), China
Ying Liu,
Nanchang University, China

*CORRESPONDENCE
Qingchuan Chou
chouqc@ihb.ac.cn

RECEIVED 24 January 2024
ACCEPTED 22 April 2024
PUBLISHED 17 May 2024

CITATION
Ren W, Yao Y, Gao X, Wang H, Wen Z, Ni L, Zhang X, Cao T and Chou Q (2024) Water depth affects submersed macrophyte more than herbivorous snail in mesotrophic lakes. *Front. Plant Sci.* 15:1375898. doi: 10.3389/fpls.2024.1375898



# Water depth affects submersed macrophyte more than herbivorous snail in mesotrophic lakes

Wenjing Ren[1], Yiqian Yao[2,3], Xiaoyu Gao[2,3], Hao Wang[2,3], Zihao Wen[2,3], Leyi Ni[2], Xiaolin Zhang[2], Te Cao[2] and Qingchuan Chou[2*]

[1]State Key Laboratory of Marine Resource Utilization in South China Sea, Hainan University, Haikou, China, [2]State Key Laboratory of Freshwater Ecology and Biotechnology, Institute of Hydrobiology, Chinese Academy of Sciences, Wuhan, China, [3]University of Chinese Academy of Sciences, Beijing, China

**Introduction:** Water depth (WD) and snail abundance (SA) are two key factors affecting the growth of submersed aquatic plants in freshwater lake ecosystems. Changes in WD and SA drive changes in nutrients and other primary producers that may have direct or indirect effects on submersed plant growth, but which factor dominates the impact of both on aquatic plants has not been fully studied.

**Methods:** To investigate the dominant factors that influence aquatic plant growth in plateau lakes, a one-year field study was conducted to study the growth of three dominant submersed macrophyte (i.e., *Vallisneria natans*, *Potamogeton maackianus*, and *Potamogeton lucens*) in Erhai Lake.

**Results:** The results show that, the biomass of the three dominant plants, *P.maackianus*, is the highest, followed by *P.lucens*, and *V.natans* is the lowest. Meanwhile, periphyton and snails attached to *P.maackianus* are also the highest. Furthermore, WD had a positive effect on the biomass of two submersed macrophyte species of canopy-type *P.maackianus* and *P.lucens*, while it had a negative effect on rosette-type *V.natans*. Snail directly inhibited periphyton attached on *V.natans* and thereby increasing the biomass of aquatic plants, but the effect of snails on the biomass of the other two aquatic plants is not through inhibition of periphyton attached to their plants.

**Discussion:** The dominant factors affecting the biomass of submersed macrophyte in Erhai Lake were determined, as well as the direct and indirect mechanisms of WD and snails on the biomass of dominant submersed macrophyte. Understanding the mechanisms that dominate aquatic plant change will have implications for lake management and restoration.

KEYWORDS

**submersed macrophytes, water depth, herbivory, periphyton, snail abundance**

## Introduction

Submerged macrophytes serve as major primary producers in freshwater lakes and provide a range of ecological services and functions (Moss, 1990; Scheffer, 1998). For example, submerged macrophytes can provide extensive substrate, habitat, shelter and food resources for periphyton, invertebrates and fish, remove nutrients from the water column and sediment, inhibit sediment resuspension and improve water transparency, thereby influencing a series of ecological processes (Moss, 1990; Scheffer et al., 1993; Jeppesen et al., 1998). However, as with other components of freshwater ecosystems, submersed macrophyte growth limitation and biomass reduction can be influenced by a combination of biotic and abiotic factors, including WD, light, nutrients and macroinvertebrates (Zhang et al., 2020a; Yuan et al., 2021; Ren et al., 2022; Wen et al., 2022).

The distribution and growth of submersed macrophytes are closely linked to WD. WD affects submerged macrophytes both directly and indirectly by altering a number of other environmental variables, such as the intensity of underwater light and nutrients (Wang et al., 2019; Wang et al., 2021b; Zhang et al., 2022). Many studies have shown that deep water can attenuate underwater light intensity and inhibit the growth and spread of submersed macrophytes (Yuan et al., 2021; Chen et al., 2023). In addition, shallow areas of lakes are susceptible to wind and wave disturbance, which can cause changes such as sediment resuspension, reduced water transparency, and increased concentrations of nitrogen, phosphorus (Van Zuidam and Peeters, 2015; Xu et al., 2022; Zhou et al., 2022). Thus, differences in WD can affect the composition and biomass of submersed macrophytes in freshwater lakes by altering a variety of factors in the water column. Furthermore, the response and adaptability of submersed macrophytes with different growth forms to WD differ in freshwater ecosystems (He et al., 2019; Meng et al., 2023). *Vallisneria natans*, *Potamogeton maackianus* and *Potamogeton lucens* are three common and dominant submersed macrophytes in Erhai lake, Yunnan Province, China, and their growth forms are different: *V.natans* is a rosette-forming species, and *P.maackianus*, *P.lucens* shows canopy growth (Wang et al., 2021a; Yu et al., 2022; Wen et al., 2022). Therefore, there may be differences in the pathways affected by submersed macrophytes of different growth forms.

In addition to WD effects, variation in SA may also contribute to changes in aquatic macrophyte biomass (Sheldon, 1987; Zhi et al., 2020). In general, as common benthic invertebrates in freshwater lakes, snails are generally regarded as generalist herbivores with diverse food sources including organic detritus, periphyton, decaying and living aquatic macrophytes (Brönmark, 1990; Yang et al., 2020; Ren et al., 2022). A complex relationship among snails, periphyton and macrophytes has been shown in many previous studies (Li H. et al., 2020; Yang et al., 2020; Zhi et al., 2020; Ren et al., 2022). For example, snails can indirectly promote the growth of submersed macrophytes by directly scraping periphyton attached to the surface of aquatic plants (Yang et al., 2020; Ren et al., 2022). In addition, snails can also directly graze macrophytes thereby inhibiting aquatic plant growth, especially at high snail densities (Zhi et al., 2020). Furthermore, snails can increase nutrient levels in the water column through excretion, which is likely to affect the relationship between periphyton and macrophytes. However, early studies were relatively short, or only conducted only under controlled experimental conditions in mesocosms (Yang et al., 2020; Ren et al., 2022), and these studies do not necessarily reflect the interactions between snails, periphyton and macrophytes observed in filed lakes. Furthermore, different plants typically have different leaf complexity (Dibble and Thomaz, 2009), with increased periphyton biomass associated with higher leaf complexity in macrophytes (Ferreiro et al., 2013; Hao et al., 2017; Zhi et al., 2020). Thus, heterogeneity of macrophytes with different structures may influence the relationship among snail, periphyton, and macrophyte.

A large number of studies have been conducted on the effects of environmental factors such as water depth, light availability, snail abundance and water column nutrient content on the biomass, community structure and distribution of submersed aquatic plants (Olsen et al., 2015; Li et al., 2020a; Qin et al., 2020; Zhang et al., 2020b), and they have primarily focused on a single factor or in the mesocosm experiment (Yu et al., 2015; Zhi et al., 2020; Zhang et al., 2020b; Ren et al., 2022; Chen et al., 2023). However, the comprehensive effects of WD, SA and other environmental factors on submersed aquatic plants are still unknown in plateau lakes with complex ecological processes and require investigation in field lakes.

Erhai is a large plateau lake with important ecological significance in Yunnan Province, China (Li et al., 2020b). The declines of submersed macrophytes due to anthropogenic activities and eutrophication has been repeatedly reported (Fu et al., 2018). In our field survey, *P.maackianus*, *P.lucens*, and *V.natans* were found to be the top three dominant submersed macrophytes in Erhai lake. Therefore, we conducted a one-year quarterly survey and measured the biomass of the three aquatic plants species in different WD, as well as periphyton, snail and the other environmental factors. In the present study, we identify the dominant environmental factors that influence the respective biomass of different growth forms in freshwater lakes. we hypothesized that 1) The effects of WD on submersed macrophyte biomass vary among species; 2) Snails promote submersed macrophyte growth by grazing on periphyton, but different species of aquatic plant species may be affected differently; 3) WD may have a dominant effect on the biomass of submersed plants with different growth forms rather than SA, because the distribution of snails may be affected by water depth (according to our field observations).

## Materials and methods

### Study area

The study was conducted out at Erhai Lake, Yunnan Province, China (25°55′N,100°78′E). Erhai Lake is a large subtropical freshwater lake in China. It covers a water surface area of 252 $km^2$ and has an average depth of 10 m (with a maximum depth of 20 m). In recent decades, external nutrient inputs to the lake have also increased as a result of increased anthropogenic activities, and the water quality of

Erhai Lake has changed from oligotrophic to mesotrophic (Lin et al., 2020), which caused the submersed macrophyte community to shift from being dominated by *Potamogeton maackianus* to being jointly dominated by *V.natans* and *P.maackianus* (He et al., 2015; Wang et al., 2021a). From September 2019 to August 2020, we conducted quarterly surveys and sampling in eight bays around Erhai Lake for one year to investigate the effects of water depth and snail abundance on the three dominant plants in Erhai Lake. The location of Erhai Lake, the distribution of sampling bays and sampling points are shown in Figure 1.

## Measurement of water physiochemical parameters and phytoplankton biomass

We designed three parallel transects in each bay, and the sampling points on each transect were set at intervals of 1m WD. The sampling WD are 1 m, 2 m, 3 m, 4 m, 5 m, and 6 m respectively. Prior to water sampling, WD was measured at each site and 2 L of mixed water samples were collected at 50 cm below the water surface, at the intermediate depth and at 50 cm above the sediment surface. The collected water samples were acidified and stored at 4° C, and transported to the laboratory as soon as possible, and the water column concentrations of total nitrogen (TN), total phosphorus (TP), orthophosphate ($PO_4$-P), nitrate ($NO_3$-N) and ammonium nitrogen ($NH_4$-N) were determined in accordance with standard methods. After filtering the water samples through Whatman GF/C glass fiber filters, chlorophyll-a (Chl a) was determined by the ethanol-thermal method (Liu et al., 2020).

Use a water quality analyzer (YSI, USA) to measure physical and chemical indicators of the water column including pH, dissolved oxygen (DO), conductivity (C), total dissolved solids (TDS) and oxidation-reduction potential (ORP) at each sampling point in the field. Photosynthetically active radiation (PAR) was determined at 0.5 m WD intervals (0, 0.5, 1, 1.5, 2, 2.5 … m) on the basis of the actual WD of the sampling point with the Li-1400 data logger (Li-1400; Li-Cor Company, Lincoln, NE, USA). The calculation equation for the light extinction coefficient (K) of the water column is as follows: $K = -(1/d) \ln (I_d/I_s)$. In the equation, d is the water depth, $I_d$ is the PAR value at the water depth d, and Is is the PAR value at the water surface (Krause-Jensen et al., 1998).

## Measurements of macrophytes, periphyton and snails

Submersed macrophytes were collected with a rotating harvester hook (sampling area: 0.2 $m^2$) at each sampling site after water sampling was completed. The plants obtained were cleaned and identified according to species, and then the three dominant species (*V.natans, P.maackianuss* and *P.lucens*) were selected and weighed separately, and then placed in sealed bags and brought to the laboratory for subsequent processing. Furthermore, prior to bagging, one plant per variety was chosen at random, individually placed in a sealed plastic bag and brought to the laboratory, and then tap water was added to the sealed bag several times to remove periphyton attached to the plant by shaking thoroughly. The periphyton solution obtained after several shakes was fixed with Lugol's reagent, precipitated for 48 hours and concentrated to a final volume of 40-50 ml for storage. The mass and abundance of the periphyton was then calculated by counting the concentrated periphyton solution using a counting chamber (0.1 ml) under a microscope at 400 times magnification. Periphyton biomass was calculated as the mass of periphyton attached to the plants divided by the weight of the host plant and expressed in mg $g^{-1}$. Finally,

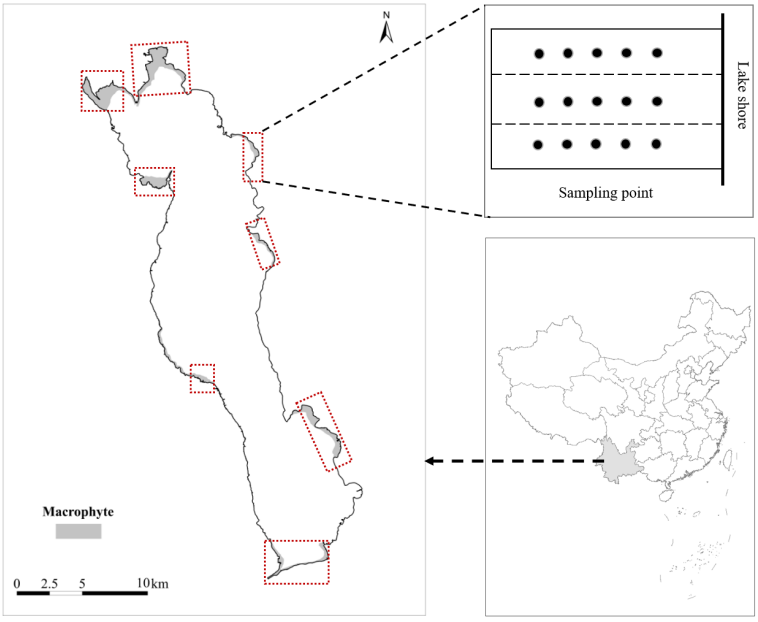


FIGURE 1
The location of Erhai Lake and sampling bays.

three species of the plants, which were packed separately and returned to the laboratory, were further processed to collect the snails. Each species of submersed macrophytes brought back to the laboratory in sealed bags were rinsed several times, and the rinsed solution was filtered through a sieve with a pore size of 1 mm. At the end, the snails collected in the sieve were counted and weighed.

## Data analysis

Homogeneity of variance and normal distribution tests were conducted on all data before analysis. Before conducting variance analysis and constructing structural equations, the data of three aquatic plants, snail abundance, periphyton biomass, and water nutrients were all log (x+1) transformed to meet the data analysis requirements. Differences in the biomass of the three submersed macrophytes *V.natans, P.maackianuss* and *P.lucens*, as well as periphyton and snail attachment to the three plants and environmental variables (TN, TP, Chl a, and K), were analyzed using one-way ANOVA and non-parametric tests. A Kruskal-Wallis test was performed using the "ggpubr" package to determine differences in in biomass and their periphyton and snail among the three species and environmental variables.

The R package "lmerTest" was used for the following analysis. A multivariate linear mixed model was constructed to detect the effects of WD, snail, nutrients (TN and TP), and light (K) on the biomass of three macrophyte specie and their periphyton biomass, using as a random variable. The standardized regression coefficient for each explanatory variable implies the change in the average response per unit increase in the associated predictor variable, holding all other predictor variables constant. In addition, we quantified the inclusive R2 for WD, snail, nutrients (TN and TP) and light (K) based on linear mixed effects model fitting using the "partR2" package in R. The inclusive R2 here is the variance explained by the predictor without taking into account covariance with other predictors. Higher values of inclusive R2 indicate that a predictor is more important in explaining the variance of macrophyte biomass (*V.natans, P. maackianuss* and *P.lucens*).

Structural equation modeling (SEM) was used to analyze the effects of WD, nutrients and snails on the biomass of three submersed aquatic plants in subtropical lakes. We used the R package "piecewiseSEM" to construct the SEM, adding a random effect of season in each path. An overall test of fit of the SEM was performed using Fisher's c, degrees of freedom, and p-values.

# Results

## Difference in biomass of *V.natans*, *P.maackianuss*, and *P.lucens*

The biomass of the three submersed macrophyte species showed different variation trends in the four seasons (Figure 2). The biomass of *V.natans* has no significant difference among four seasons, with an average biomass of 1.64kg $m^{-2}$. Meanwhile, there were significant differences in the biomass of *P.maackianuss* and *P.lucens* among the four seasons. Among them, the biomass of *P.maackianuss* was highest in spring and winter, and lowest in summer and autumn, with values of 4.89-5.86 kg $m^{-2}$ and 3.49-3.91kg $m^{-2}$ respectively, whereas the biomass of *P.lucens* was opposite, with biomass of 1.2-1.59 kg $m^{-2}$ in spring and winter and 2.30-2.50 kg $m^{-2}$ in summer and autumn. Over the four seasons, the average of *V.natans*, *P.maackianuss* and *P.lucens* biomass was 1.64 ± 1.58 kg $m^{-2}$, 4.62 ± 3.91 kg $m^{-2}$ and 2.32 ± 1.83 kg $m^{-2}$, respectively.

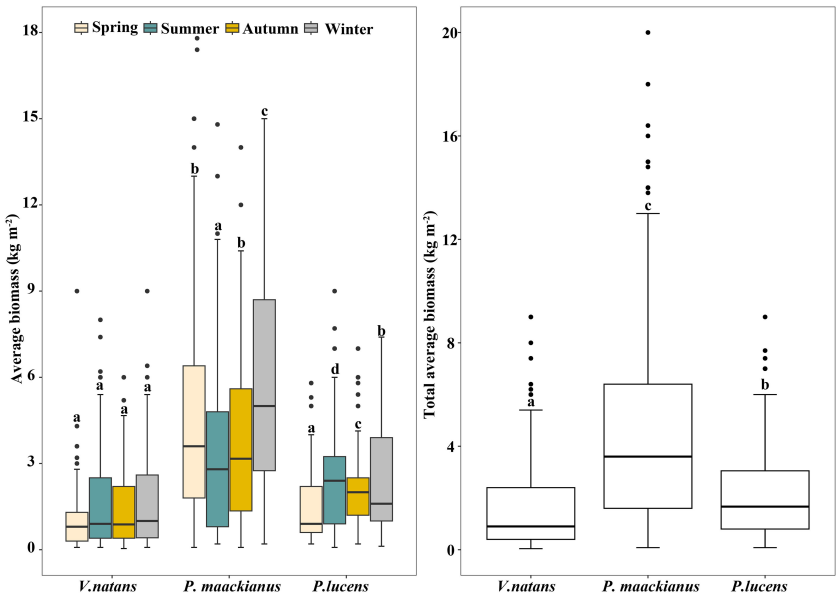


FIGURE 2
Biomass of three dominant submersed macrophytes in Erhai Lake across four seasons. Mean and standard deviation are shown in each bar. The different letters on the bars indicate significant differences at $p < 0.05$.

## Difference in snail and periphyton attached on *V.natans*, *P.maackianuss*, and *P.lucens*

There were significant differences in SA and periphyton biomass on the three species among the four seasons (Figure 3) . Snail abundance and periphyton biomass on three submerged macrophyte species (with similar trends) were higher in autumn and winter than in spring and summer, and no major differences were found between spring summer and autumn winter, except for *P.lucens*. The abundance of snails on *P.lucens* was significantly lower in winter than in autumn, while the opposite was true for periphyton biomass. In general, there were significant differences in the average SA and periphyton biomass on the three submersed macrophyte species. The average SA and periphyton biomass on *V.natans* was the lowest, 7.04 mg $g^{-1}$, followed by *P.lucens*, and the highest was *P.maackianus*.

## Changes in environmental factors

Overall, TN, TP, Chl a and light extinction coefficient (K) differed significantly among the four seasons, and showed similar trends of variation, with the highest values in summer and autumn and lowest values in spring and winter. For TN, 0.76 mg $L^{-1}$ and 0.63 mg $L^{-1}$ were the highest and lowest values, respectively. The highest and lowest values for TP were 0.043 mg $L^{-1}$ and 0.035 mg $L^{-1}$, respectively (Figure 4). The highest values of Chl a and K were 20.3 mg $L^{-1}$ and 2.15, respectively, and the lowest values were 12.7 mg $L^{-1}$ and 0.95 (Figure 4).

## Effects of multiple driving factors on macrophytes biomass

The multivariate linear mixed model showed that WD had a significant negative effect on *V.natans* biomass (β= -0.22, p<0.01), while it had a significant positive effect on *P.maackianus* (β= 0.124, p<0.001) and *P.lucens* biomass (β= 0.182, p<0.05) (Table 1). Meanwhile, WD had a significant negative effect on all periphyton (β= -0.21, p<0.001; β= -0.135, p<0.001), except for periphyton attached on *P.lucens* (β= -0.067, p>0.05). SA had a significant positive effect on the biomass of three plants (*V.natans*: β= 0.28, p<0.01; *P.maackianus*: β= 0.329, p<0.001; *P.lucens*: β= 0.368, p<0.001) and periphyton attaches to *P.maackianus* (β= 0.143, p<0.001). For nutrients, TP has a positive effect on periphyton attached to the three plant species (β = 0.116, p < 0.05; β = 0.09, p < 0.05; β = 0.124, p < 0.05) and phytoplankton (Chl a: β = 0.236, p < 0.001) (Table 1). Among the five variables, we found that WD and SA were the most important drivers affecting three plant species, accounting for 14.8-27.2%, 14.7-24.4% of the variance respectively (Figure 5).

## Effect of snail, nutrients and water depth on macrophytes biomass

Piecewise SEM results showed that WD and SA could have direct or indirect effects on macrophyte biomass (Figure 6). Overall, the model explained 34%, 57%, and 38% of the variation in biomass of the three aquatic species, respectively. Specifically, WD had a

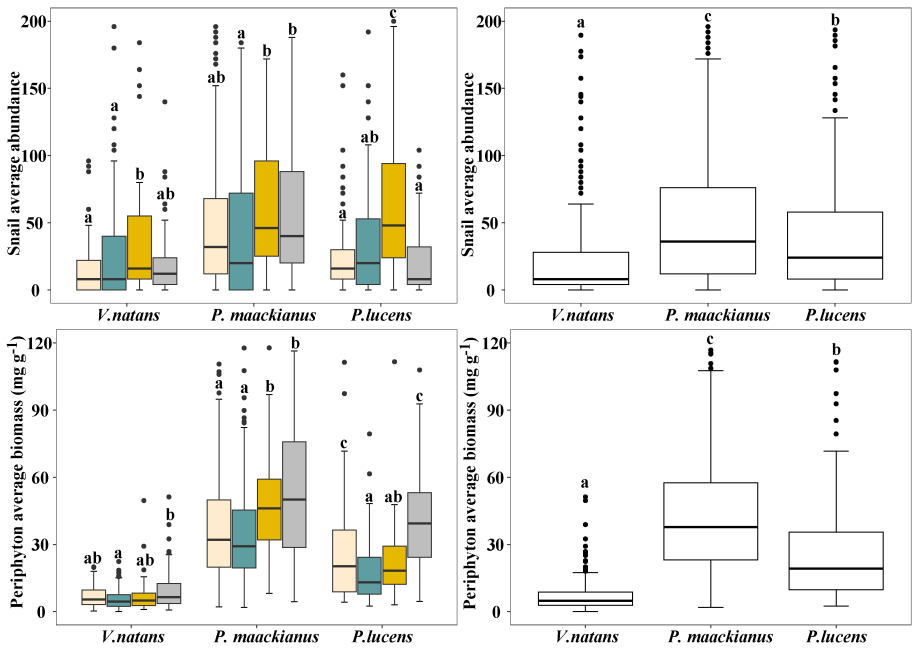


FIGURE 3
Changes in SA and periphyton biomass attached to three submerged macrophytes. Mean and standard deviation are shown in each bar. The different letters on the bars indicate significant differences at p < 0.05.

TABLE 1 Effect of water depth (WD), snail abundance (SA), nutrients (TN and TP), and light extinction coefficient (K) on three species macrophytes biomass and their periphyton biomass in a multivariate linear mixed model.

| | n | R2 of fixed effects | Intercept | WD | K | SA | TN | TP |
|---|---|---|---|---|---|---|---|---|
| *V.natans* biomass | 328 | 0.358 | -0.015 | -0.22** | 0.076 | 0.28** | 0.2* | 0.2* |
| Periphyton on *V.natans* | 328 | 0.256 | 1.25*** | -0.21*** | 0.011 | 0.052 | 0.069 | 0.116* |
| *P.maackianus* biomass | 576 | 0.52 | -0.007 | 0.124* | 0.042 | 0.329*** | -0.11 | -0.072 |
| Periphyton on *P.maackianus* | 576 | 0.144 | 1.78*** | -0.135** | -0.058 | 0.143*** | -0.028 | 0.09* |
| *P.lucens* biomass | 184 | 0.517 | -0.169 | 0.182* | 0.096 | 0.368*** | 0.077 | -0.011 |
| Periphyton on *P.lucens* | 184 | 0.654 | 1.544*** | -0.067 | -0.255** | -0.028 | 0.423* | 0.124* |
| Chl a | 312 | 0.457 | 0.949*** | 0.34*** | -0.151* | -0.04 | 0.056 | 0.236*** |

Data were standardized before analysis. Significance level: *** = $p < 0.001$; ** = $p < 0.01$; * = $p < 0.05$.

direct negative effect on *V.natans*, but a significant positive effect on *P.maackianus* and *P.lucens*. SA directly inhibits periphyton attached to *V.natans* and thereby increasing the biomass of aquatic plants, but the effect of snails on the biomass of the other two aquatic plants is not through inhibition of periphyton attached to their plants.

## Discussion

Our results showed that WD inhibited the growth of *V.natans*, but significantly increased the biomass of *P.maackianus* and *P.lucens*. SA significantly inhibited periphyton attached to *V.natans*, thereby enhancing its host plant biomass, but it was difficult to offset the negative effect of WD on *V.natans*. Meanwhile, snails did not have a positive impact on their hosts by significantly inhibiting the periphyton attached to the *P.maackianus* and *P.lucens*. Overall, the three dominant species are mainly affected by WD, which means that WD has a greater impact on submersed plants than snail grazing in Erhai Lake, a mesotrophic lake.

WD is one of the most important factors influencing the growth and distribution of submersed macrophytes (Olsen et al., 2015; Su et al., 2018; Li et al., 2020a; Qin et al., 2020), and many studies has shown that variation of WD can have both an effect on underwater light availability and play an important role in the nutrient status of lakes (Li et al., 2020a; Qin et al., 2020; Yang et al., 2022; Chen et al., 2023). Generally, with the increase of water depth, the intensity of underwater light decreases, which is not conducive to the growth of submersed macrophytes (Yuan et al., 2021; Chen et al., 2023). In our results, WD significantly inhibited the biomass of *V.natans* biomass while at the same time significantly improving the biomass of *P.maackianus* and *P.lucens*. The reason for the inconsistent

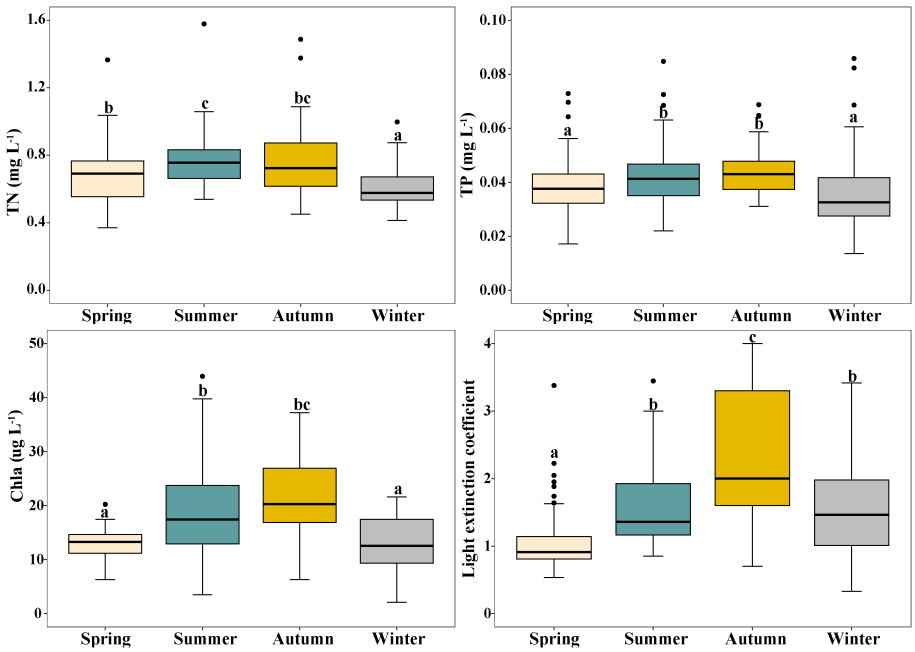


FIGURE 4
Changes in total nitrogen (TN), total phosphorus (TP), phytoplankton chlorophyll- a (Chl a) and light extinction coefficient (K) in Erhai Lake across four seasons. Mean and standard deviation are shown in each bar. The different letters on the bars indicate significant differences at $p < 0.05$.

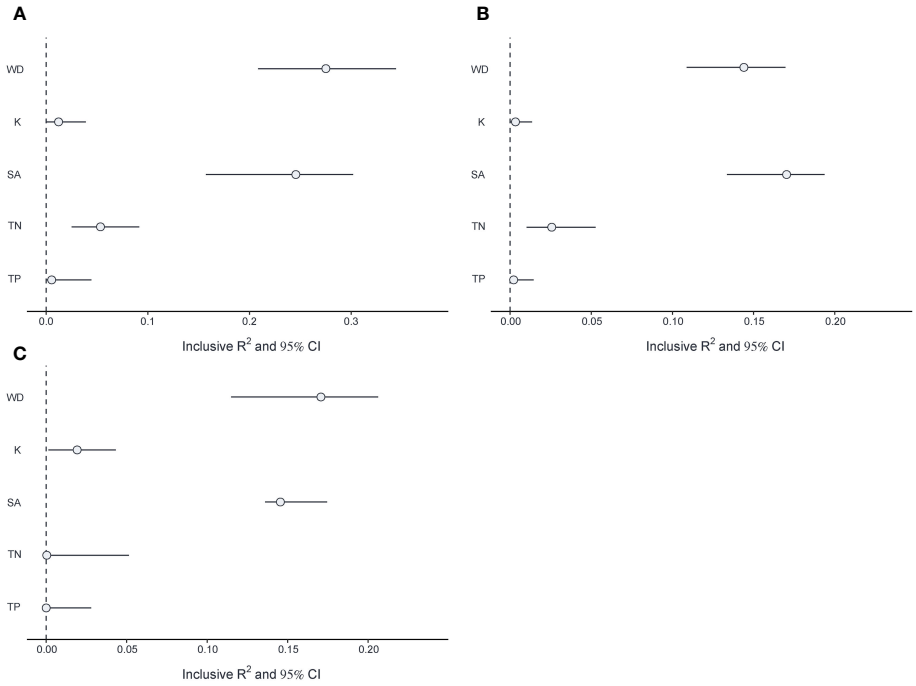


FIGURE 5
Inclusive R2 and 95% CI for each driver on **(A)** *V.natans* biomass and **(B)** *P.maackianuss* biomass and **(C)** *P.lucens* biomass.

results on the effect of water depth on different plant biomass may be that the different growth types of the dominant macrophytes respond differently to underwater light caused by WD. *V.natans*, as a rosette-type submersed macrophyte with its stems and leaves under water, responds to changes in water depth by regulating leaves chlorophyll a concentration and photosynthetic efficiency, whereas *P.maackianus* and *P.lucens*, as canopy-type submersed plants, respond to changes in water depth by extending their

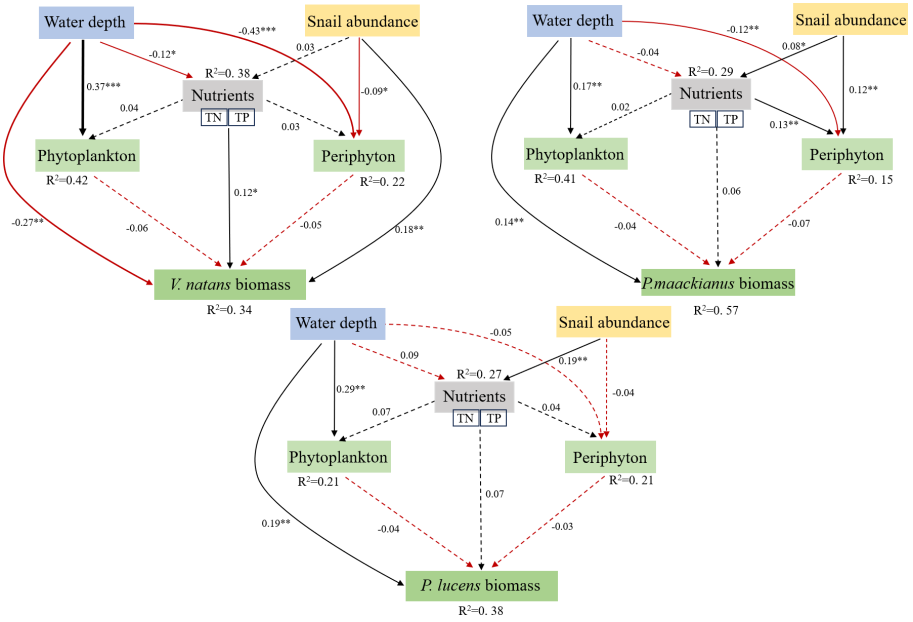


FIGURE 6
Piecewise structural equation model (SEM) showing the effects of WD, SA and nutrients on macrophyte biomass directly and indirectly. Solid black line shows a significant positive correlation and the solid red line shows a significant negative correlation, with the dotted line indicates no significance. Standardized path coefficients (similar to relative regression weights) are shown as numbers next to the path lines. Next to each response variable in the model is the proportion of variance explained (R2). Model fit: *V.natans*: Fisher's C = 2.139, P=0.508; *P. maackianus*: Fisher's C = 0.469, P=0.791; *P.lucens*: Fisher's C = 0.214, P=0.899. *p < 0.0 5, **p < 0.01, ***p < 0.001.

shoot length to the water surface (Chen et al., 2016; He et al., 2019). In addition, *V.natans* biomass was the lowest among the three dominant macrophytes, followed by *P.lucens*, and *P.maackianus* biomass was the highest. This indicates that within the range of 0-6m water depth, the attenuation of underwater light intensity caused by deeper WD has a greater inhibitory effect on rosette-type plants than on canopy-type plants. In other words, rosette-type *V.natans* is more susceptible to deeper WD and light suppression. For example, Li et al. (2021) found strong suppression of both *V.natans* and *H.verticillata* biomass in deeper water (250cm), whereas only *V.natans* was suppressed in intermediate water depth (150cm). Moreover, we also found nutrient significantly enhanced the growth of *V.natans* and had no significant effect on the other two plants, suggesting that *V.natans* may have a broad nutrient-absorption capacity. The adaptation of these species to their environment may explain the differences in biomass.

The impact of snails on aquatic plants depends on the snail abundance (Jones and Sayer, 2003; Zhi et al., 2020). While macrophytes can also be used as a food source by snails, it is generally accepted that periphyton constitutes a larger proportion of the snail diet than macrophytes. For example, Zhi et al. (2020) reported an effective removal of periphyton from four macrophyte species (*Myriophyllum spicatum, Potamogeton wrightii, P. crispus*, and *P. oxyphyllus*) by herbivorous snails, resulting in a significant increase in host plant biomass. Nevertheless, high densities of snails can consume both plants and periphyton, resulting in no positive effect on submerged macrophytes (Zhi et al., 2020). In this study, we observed that when the abundance of snails attached to *V.natans* is approximately 13 ind $m^{-2}$, they exerted significant feeding pressure on the periphyton, and contributed to an increase in host plant biomass. This is also in line with the results of previous studies. For example, Ren et al. (2022) found when the initial density of herbivorous snail was 16 ind $m^{-2}$, *V.natans* biomass could be promoted by removing periphyton attached to host plant leaves. However, despite the higher abundance of snails on *P.maackianus* (45 ind $m^{-2}$) and *P.lucens* (32 ind $m^{-2}$), there was no obvious effect on the periphyton and their host plants. This may also be due to the fact that snail have other abundant food sources besides periphyton and their host plants, which may require further verification.

Changes in WD are often accompanied by changes in the physical and chemical parameters of the water column, which will inevitably affect the growth of submersed macrophyte, either directly or indirectly (Meng et al., 2023). For example, external disturbances such as wind and waves tend to resuspend sediments and release nutrients (TN and TP) from the sediments into the water column, reducing clarity in shallow areas (Tammeorg et al., 2015; Baastrup Spohr et al., 2016; Tong et al., 2017). Our results found that the concentration of TN, TP and Chla showed similar trends of variation, with the highest values in summer and autumn and lowest values in spring and winter. In addition, the average concentrations of TN and TP (0.76 mg $L^{-1}$ and 0.036 mg $L^{-1}$, respectively) were highest in the depth range 0-2m, which were higher than those in the depth range 2-4m and 4-6m. Meanwhile, *V.natans* biomass was the highest in 0-2m water depth (consistent with the change of TN and TP), while the biomass of *P.maackianus* and *P.lucens* were the highest in 2-4m and 4-6m, respectively. Although the concentration of TN and TP in the water column strongly influence the biomass of *V.natans*, and snails also promote *V.natans* growth by inhibiting periphyton, but it is difficult to offset the direct negative effects of WD on *V.natans*. In addition, we found that WD significantly increased the biomass of *P.maackianus* and *P.lucens*, while SA significantly affected the nutrient contents in the water column but did not significantly affect *P.maackianus* and *P.lucens*, indicating that aquatic plants are directly controlled by WD and less affected by nutrient contents and SA.

In conclusion, the three dominant aquatic plants in a meso-eutrophic lake Erhai were mainly and directly affected by WD, and snail only had a positive and direct promotion effect on the rosette-type *V.natans* by grazing the periphyton attached to its host plant, but had no significant effect on the other two canopy-type submersed plants (*P.maackianus* and *P.lucens*). WD can directly inhibit the increase of *V.natans* biomass, but significantly increased the biomass of *P.maackianus* and *P.lucens*. SA significantly inhibited periphyton attached to *V.natans*, thereby increasing aquatic plant biomass, but it was difficult to offset the negative effect of WD on *V.natans*. For *P.maackianus* and *P.lucens*, although SA significantly affected the nutrient content of the water column, it did not significantly affect the biomass of *P.maackianus* and *P.lucens*. Overall, aquatic plants are directly controlled by WD and less affected by nutrient contents and SA in the mesotrophic lake.

## Data availability statement

The raw data supporting the conclusions of this article will be made available by the authors, without undue reservation.

## Author contributions

WR: Investigation, Methodology, Writing – original draft, Writing – review & editing, Conceptualization, Data curation, Formal analysis, Funding acquisition, Project administration, Resources, Software, Supervision, Validation, Visualization. YY: Investigation, Methodology, Writing – original draft, Writing – review & editing. XG: Methodology, Investigation, Writing – original draft, Writing – review & editing. HW: Formal analysis, Methodology, Writing – original draft, Writing – review & editing. ZW: Formal analysis, Methodology, Writing – original draft, Writing – review & editing. LN: Supervision, Writing – original draft, Writing – review & editing. XZ: Supervision, Writing – original draft, Writing – review & editing. TC: Supervision, Writing – original draft, Writing – review & editing. QC: Supervision, Writing – original draft, Writing – review & editing.

## Funding

The author(s) declare financial support was received for the research, authorship, and/or publication of this article. This study

was supported by the National Natural Science Foundation of China (Grant No.32201340, Grant No. 32101319).

## Conflict of interest

The authors declare that the research was conducted in the absence of any commercial or financial relationships that could be construed as a potential conflict of interest.

## Publisher's note



## References

Baastrup Spohr, L., Moller, C. L., and Sand Jensen, K. (2016). Water-level fluctuations affect sediment properties, carbon flux and growth of the isoetid Littorella uniflora in oligotrophic lakes. *Freshw. Biol.* 61, 301–315. doi: 10.1111/fwb.12704

Brönmark, C. (1990). How do herbivorous freshwater snails affect macrophytes?–A comment. *Ecology* 71, 1212–1215. doi: 10.1111/fwb.12704

Chen, J., Cao, T., Zhang, X., Xi, Y., Ni, L., and Jeppesen, E. (2016). Differential photosynthetic and morphological adaptations to low light affect depth distribution of two submersed macrophytes in lakes. *Sci. Rep.* 6, 34028. doi: 10.1038/srep34028

Chen, S., Jiang, L., Ma, S., Wu, Y., Ye, Q., Chang, Y., et al. (2023). Response of a submersed macrophyte (Vallisneria natans) to water depth gradients and sediment nutrient concentrations. *Sci. Total Environ.* 912, 169154–169154. doi: 10.1016/j.scitotenv.2023.169154

Dibble, E. D., and Thomaz, S. M. (2009). Use of fractal dimension to assess habitat complexity and its influence on dominant invertebrates inhabiting tropical and temperate macrophytes. *J. Freshw. Ecol.* 24, 93–102. doi: 10.1080/02705060.2009.9664269

Ferreiro, N., Giorgi, A., and Feijoo, C. (2013). Effects of macrophyte architecture and leaf shape complexity on structural parameters of the epiphytic algal community in a Pampean stream. *Aquat. Ecol.* 47, 389–401. doi: 10.1007/s10452-013-9452-1

Fu, H., Yuan, G., Lou, Q., Dai, T., Xu, J., Cao, T., et al. (2018). Functional traits mediated cascading effects of water depth and light availability on temporal stability of a macrophyte species. *Ecol. Indic.* 89, 168–174. doi: 10.1016/j.ecolind.2018.02.010

Hao, B., Wu, H., Cao, Y., Xing, W., Jeppesen, E., and Li, W. (2017). Comparison of periphyton communities on natural and artificial macrophytes with contrasting morphological structures. *Freshw. Biol.* 62, 1783–1793. doi: 10.1111/fwb.12991

He, L., Zhu, T., Cao, T., Li, W., Zhang, M., Zhang, X., et al. (2015). Characteristics of early eutrophication encoded in submersed vegetation beyond water quality: a case study in Lake Erhai, China. *Environ. Earth Sci.* 74, 3701–3708. doi: 10.1007/s12665-015-4202-4

He, L., Zhu, T., Wu, Y., Li, W., Zhang, H., Zhang, X., et al. (2019). Littoral slope, water depth and alternative response strategies to light attenuation shape the distribution of submersed macrophytes in a mesotrophic lake. *Front. Plant Sci.* 10. doi: 10.3389/fpls.2019.00169

Jeppesen, E., Jensen, J. P., Sndergaard, M., Lauridsen, T., and Sandby, K. (1998). Changes in nitrogen retention in shallow eutrophic lakes following a decline in density of cyprinids. *Archiv fur Hydrobiol.* 142, 129–151. doi: 10.1127/archiv-hydrobiol/142/1998/129

Jones, J. I., and Sayer, C. D. (2003). Does the fish–invertebrate–periphyton cascade precipitate plant loss in shallow lakes? *Ecology* 84, 2155–2167. doi: 10.1890/02-0422

Krause-Jensen, D., Sand-Jensen, K. J. L.Oceanography (1998). Light attenuation and photosynthesis of aquatic plant communities. *Limnol. Oceanogr.* 43, 396–407. doi: 10.4319/lo.1998.43.3.0396

Li, H., Li, Q., Luo, X., Fu, J., and Zhang, J. (2020a). Responses of the submersed macrophyte Vallisneria natans to a water depth gradient. *Sci. Total Environ.* 701, 134944. doi: 10.1016/j.scitotenv.2019.134944

Li, J., Bai, Y., and Alatalo, J. M. (2020b). Impacts of rural tourism-driven land use change on ecosystems services provision in Erhai Lake Basin, China. *Ecosyst. Serv.* 42, 101081. doi: 10.1016/j.ecoser.2020.101081

Li, Q., Han, Y., Chen, K., Huang, X., Li, K., and He, H. (2021). Effects of water depth on the growth of the submerged macrophytes vallisneria natans and hydrilla verticillata: implications for water level management. *Water* 13 (18), 2590. doi: 10.3390/w13182590

Lin, S., Shen, S., Zhou, A., and Lyu, H. (2020). Sustainable development and environmental restoration in Lake Erhai, China. *J. Clean. Prod.* 258, 120758. doi: 10.1016/j.jclepro.2020.120758

Liu, H., Zhou, W., Li, X., Chu, Q., Tang, N., Shu, B., et al. (2020). How many submersed macrophyte species are needed to improve water clarity and quality in Yangtze floodplain lakes? *Sci. Total Environ.* 724, 138267.

Meng, Z., Yu, X., Xia, S., Zhang, Q., Ma, X., and Yu, D. (2023). Effects of water depth on the biomass of two dominant submersed macrophyte species in floodplain lakes during flood and dry seasons. *Sci. Total Environ.* 877, 162690–162690. doi: 10.1016/j.scitotenv.2023.162690

Moss, B. (1990). Engineering and biological approaches to the restoration from eutrophication of shallow lakes in which aquatic plant communities are important components Biomanipulation Tool for Water Management. *Hydrobiology* 200, 367–377. doi: 10.1007/BF02530354

Olsen, S., Chan, F., Li, W., Zhao, S., Sondergaard, M., and Jeppesen, E. (2015). Strong impact of nitrogen loading on submersed macrophytes and algae: a long-term mesocosm experiment in a shallow Chinese lake. *Freshw. Biol.* 60, 1525–1536. doi: 10.1111/fwb.12585

Qin, B., Zhou, J., Elser, J. J., Gardner, W. S., Deng, J., and Brookes, J. D. (2020). Water depth underpins the relative roles and fates of nitrogen and phosphorus in lakes. *Environ. Sci. Technol.* 54, 3191–3198. doi: 10.1021/acs.est.9b05858

Ren, W., Wen, Z., Cao, Y., Wang, H., Yuan, C., Zhang, X., et al. (2022). Cascading effects of benthic fish impede reinstatement of clear water conditions in lakes: A mesocosm study. *J. Environ. Manage.* 301, 113898. doi: 10.1016/j.jenvman.2021.113898

Scheffer, M. (1998). *Ecology of Shallow Lakes* (Dordrecht: Kluwer Academic Publishers).

Scheffer, M., Hosper, S. H., Meijer, M. L., Moss, B., and Jeppesen, E. (1993). Alternative equilibria in shallow lakes. *Trends Ecol. Evol.* 8, 275–279. doi: 10.1016/0169-5347(93)90254-M

Sheldon, S. P. (1987). The effects of herbivorous snails on submersed macrophyte communities in Minnesota Lakes. *Ecology* 68, 1920–1931. doi: 10.2307/1939883

Su, H., Zhu, T., Bai, X., Ni, L., Xie, P., and Zhang, X. (2018). Seed germination indicates adaptive transgenerational plasticity in a submersed macrophyte. *Front. Plant Sci.* 9, 1592. doi: 10.3389/fpls.2018.01592

Tammeorg, O., Horppila, J., Laugaste, R., Haldna, M., and Niemisto, J. (2015). Importance of diffusion and resuspension for phosphorus cycling during the growing season in large, shallow Lake Peipsi. *Hydrobiologia* 760, 133–144. doi: 10.1007/s10750-015-2319-9

Tong, Y., Liang, T., Wang, L., and Li, K. (2017). Simulation on phosphorus release characteristics of Poyang Lake sediments under variable water levels and velocities. *J. Geogr. Sci.* 27, 697–710. doi: 10.1007/s11442-017-1401-9

Van Zuidam, B. G., and Peeters, E. T. H. M. (2015). Wave forces limit the establishment of submersed macrophytes in large shallow lakes. *Limnol. Oceanogr.* 60, 1536–1549. doi: 10.1002/lno.10115

Wang, H., Fu, H., Wen, Z. H., Yuan, C. B., Zhang, X. L., Ni, L. Y., et al. (2021a). Seasonal patterns of taxonomic and functional beta diversity in submerged macrophytes at a fine scale. *Ecol. Evol.* 11 (14), 9827–9836. doi: 10.1002/ece3.7811

Wang, L., Han, Y., Yu, H., Fan, S., and Liu, C. (2019). Submersed vegetation and water quality degeneration from serious flooding in Liangzi Lake, China. *Front. Plant Sci.* 10, 1504. doi: 10.3389/fpls.2019.01504

Wang, S., Gao, Y., Jia, J., Kun, S., Lyu, S., Li, Z., et al. (2021b). Water level as the key controlling regulator associated with nutrient and gross primary productivity changes in a large floodplain-lake system (Lake Poyang), China. *J. Hydrol.* 599, 126414. doi: 10.1016/j.jhydrol.2021.126414

Wen, Z., Wang, H., Zhang, Z., Cao, Y., Yao, Y., Gao, X., et al. (2022). Depth distribution of three submersed macrophytes under water level fluctuations in a large plateau lake. *Aquat. Bot.* 176, 103451. doi: 10.1016/j.aquabot.2021.103451

Xu, L., Hu, Q., Liao, L., Duan, Z., Liu, S., Chen, L., et al. (2022). Hydrological isolation affected the chemo-diversity of dissolved organic matter in a large river-connected lake (Poyang Lake, China). *Sci. Total Environ.* 851, 158047. doi: 10.1016/j.scitotenv.2022.158047

Yang, L., He, H., Guan, B., Yu, J., Yao, Z., Zhen, W., et al. (2020). Mesocosm experiment reveals a strong positive effect of snail presence on macrophyte growth, resulting from control of epiphyton and nuisance filamentous algae: Implications for

shallow lake management. *Sci. Total Environ.* 705, 135958. doi: 10.1016/j.scitotenv.2019.135958

Yang, C., Shi, X., Nan, J., Huang, Q., Shen, X., and Li, J. (2022). Morphological responses of the submersed macrophyte Vallisneria natans along an underwater light gradient: A mesocosm experiment reveals the importance of the Secchi depth to water depth ratio. *Sci. Total Environ.* 808, 152199. doi: 10.1016/j.scitotenv.2021.152199

Yu, Q., Wang, H., Li, Y., Shao, J., Liang, X., Jeppesen, E., et al. (2015). Effects of high nitrogen concentrations on the growth of submersed macrophytes at moderate phosphorus concentrations. *Water Res.* 83, 385–395. doi: 10.1016/j.watres.2015.06.053

Yu, Q., Wang, H., Wang, H., Xu, C., Liu, M., Ma, Y., et al. (2022). Effects of high ammonium loading on two submersed macrophytes of different growth form based on an 18-month pond experiment. *Front. Plant Sci.* 13. doi: 10.3389/fpls.2022.939589

Yuan, H., Wang, H., Zhou, Y., Jia, B., Yu, J., Cai, Y., et al. (2021). Water-level fluctuations regulate the availability and diffusion kinetics process of phosphorus at lake water-sediment interface. *Water Res.* 200, 117258. doi: 10.1016/j.watres.2021.117258

Zhang, X., Guo, K., Lu, C., Awais, R. M., Jia, Y., Zhong, L., et al. (2020a). Effects of origin and water depth on morphology and reproductive modes of the submersed plant Vallisneria natans. *Global Ecol. Conserv.* 24, e01330. doi: 10.1016/j.gecco.2020.e01330

Zhang, P., Kuramae, A., van Leeuwen, C. H. A., Velthuis, M., van Donk, E., Xu, J., et al. (2020b). Interactive effects of rising temperature and nutrient enrichment on aquatic plant growth, stoichiometry, and palatability. *Front. Plant Sci.* 11. doi: 10.3389/fpls.2020.00058

Zhang, M., Wen, S., Wu, T., Wang, S., Li, X., Gong, W., et al. (2022). Patterns of internal nitrogen and phosphorus loadings in a cascade reservoir with a large water level gradient: Effects of reservoir operation and water depth. *J. Environ. Manage.* 320, 115884. doi: 10.1016/j.jenvman.2022.115884

Zhi, Y., Liu, Y., Li, W., and Cao, Y. (2020). Responses of four submersed macrophytes to freshwater snail density (Radix swinhoei) under clear-water conditions: a mesocosm study. *Ecol. Evol.* 10, 7644–7653. doi: 10.1002/ece3.6489

Zhou, J., Leavitt, P. R., Zhang, Y., and Qin, B. (2022). Anthropogenic eutrophication of shallow lakes: is it occasional? *Water Res.* 221, 118728. doi: 10.1016/j.watres.2022.118728

frontiers | Frontiers in Plant Science

TYPE Original Research
PUBLISHED 09 July 2024
DOI 10.3389/fpls.2024.1424300



OPEN ACCESS

EDITED BY
Jun Xu,
Chinese Academy of Sciences (CAS), China

REVIEWED BY
Xin-Sheng Chen,
Anhui University, China
Hanxi Wang,
Harbin Normal University, China
Xiaolin Zhang,
Chinese Academy of Sciences (CAS), China
Feng Li,
Chinese Academy of Sciences (CAS), China

*CORRESPONDENCE
Yongjiu Cai
caiyj@niglas.ac.cn

RECEIVED 27 April 2024
ACCEPTED 06 June 2024
PUBLISHED 09 July 2024

CITATION
Yang K, Yin Y, Xu Y, Wang S, Gao M, Peng K, Luo J, Gao J and Cai Y (2024) Hydrometeorological conditions drive long-term changes in the spatial distribution of *Potamogeton crispus* in a subtropical lake. *Front. Plant Sci.* 15:1424300. doi: 10.3389/fpls.2024.1424300



# Hydrometeorological conditions drive long-term changes in the spatial distribution of *Potamogeton crispus* in a subtropical lake

Ke Yang[1,2], Yi Yin[1,2], Ying Xu[1,2], Shaobo Wang[3], Mingyuan Gao[4], Kai Peng[1], Juhua Luo[1,2], Junfeng Gao[1,2] and Yongjiu Cai[1,2]*

[1]Key Laboratory of Lake and Watershed Science for Water Security, Nanjing Institute of Geography and Limnology, Chinese Academy of Sciences, Nanjing, China, [2]University of Chinese Academy of Sciences, Beijing, China, [3]Jiangsu Surveying and Design Institute of Water Resources Co., Ltd., Yangzhou, China, [4]Jiangsu Province Hydrology and Water Resources Investigation Bureau, Nanjing, China

Globally, anthropogenic disturbance and climate change caused a rapid decline of submerged macrophytes in lake ecosystems. *Potamogeton crispus* (*P. crispus*), a species that germinates in winter, explosively expanded throughout many Chinese lakes, yet the underlying mechanism remained unclear. Here, this study examined the long-term changes in the distribution patterns of *P. crispus* in Lake Gaoyou by combining remote sensing images and hydrometeorological data from 1984 to 2022 and water quality data from 2009 to 2022. It aims to unravel the relationships between the distribution patterns of *P. crispus* and hydrometeorological and water quality factors. The results showed that the area of *P. crispus* in Lake Gaoyou showed a slight increase from 1984 to 2009, a marked increase from 2010 to 2019, followed by a decline after 2020. Spatially, *P. crispus* was primarily distributed in the western and northern parts of Lake Gaoyou, with less distribution in the central and southeastern parts of the lake. Wind speed (WS), temperature (Temp), water level (WL), ammonia nitrogen ($NH_3$-N), and Secchi depth (SD) were identified as the key factors regulating the variation in the *P. crispus* area in Lake Gaoyou. We found that the *P. crispus* area showed an increasing trend with increasing Temp, WL, and SD and decreasing WS and $NH_3$-N. The influence of environmental factors on the area of *P. crispus* in Lake Gaoyou varied among seasons. The results indicated that hydrometeorology (WS, Temp, and WL) may override water quality ($NH_3$-N and SD) in driving the succession of *P. crispus* distribution. The findings of this study offer valuable insights into the recent widespread expansion of *P. crispus* in shallow lakes across Eastern China.

KEYWORDS

***Potamogeton crispus*, spatiotemporal pattern, climate change, hydrometeorology, water quality, shallow lakes**

# 1 Introduction

As a crucial producer in aquatic ecosystems, macrophytes not only prevent sediment resuspension, reduce nutrient release, and inhibit the growth of phytoplankton, but also provide habitats for various aquatic organisms (Søndergaard et al., 2010). As one of the important types of macrophyte, submerged macrophytes play an important role in ecological restoration; the water body in which they are present typically has low nutrient levels and phytoplankton biomass (Sayer et al., 2010). Generally, submerged macrophytes absorb nutrients from the water body during their growth period, significantly improving water quality and increasing transparency (Wu and Hua, 2014). However, extensive submerged macrophyte decomposition following excessive growth can have negative impacts on aquatic ecosystems by depleting dissolved oxygen (DO) in the water, which is an important cause of water quality degradation in macrophyte-dominated eutrophic lakes (Roman et al., 2001; Wang et al., 2018). Therefore, maintaining an appropriate level of submerged macrophyte coverage is essential for maintaining water quality and aquatic ecosystem stability, as well as for ecological restoration (Temmink et al., 2021).

Over the past few decades, many lake ecosystems in China have undergone rapid degradation, characterized mainly by reduction in macrophyte coverage, dominance of single species, and overgrowth of specific species (Cao et al., 2015; Dong et al., 2022). These phenomena were influenced by various factors, including global climate change and anthropogenic activities. Previous studies have indicated that an increase in temperature promotes the germination of macrophytes, affecting their reproductive strategies, interactions, and species richness (Zhang YL et al., 2016; Li et al., 2017; Fares et al., 2020; Kim and Nishihiro, 2020). Changes in hydrological conditions such as water level and flow velocity are important factors contributing to the significant decrease in submerged macrophyte coverage and diversity (Breugnot et al., 2008; Luo et al., 2015). Anthropogenic activities may cause eutrophication in lakes and trigger a shift from macrophyte-dominated to phytoplankton-dominated states; a regime shift theory had been developed to describe the abrupt changes (Scheffer et al., 1993; Akasaka et al., 2010; Zhang PY et al., 2016). Previous studies have explored the impact of environmental factors on submerged macrophyte decline, investigating the spatiotemporal variability of the distribution of submerged macrophyte in eastern lakes such as Lake Taihu in China through field investigation, controlled experiment, remote sensing, and ecological modeling (Zhang YL et al., 2016; Dong et al., 2022). These studies mainly focused on the decline of macrophyte coverage. However, studies on the explosive growth of single species are also necessary; in recent years, *Potamogeton crispus* (*P. crispus*) has expanded explosively in many shallow lakes in China and disrupted water quality and the stability of aquatic ecosystems (Cao et al., 2015; Huang et al., 2022).

*P. crispus* is a submerged macrophyte that requires lower temperatures during its growth period; it usually germinates in the winter, grows in the spring, and then degrade in late spring and early summer (Jian et al., 2003; Woolf and Madsen, 2003). Because of this unique phenological character, *P. crispus* has emerged as a predominant submerged macrophyte species in most shallow lakes in Eastern China in spring (Cao et al., 2015; Chen et al., 2017). Among these, there were few submerged macrophyte species in Lake Gaoyou, and *P. crispus* has emerged as a dominant species in recent years; it spread across the entire lake during spring (Tian et al., 2019; Xia et al., 2022). Following its bloom period, *P. crispus* decomposes quickly, releasing nutrients that have a substantial negative influence on water quality and the stability of aquatic ecosystems, potentially endangering the safety of the local water supply security (Wang et al., 2018; Huang et al., 2022). Therefore, elucidating the factors influencing the growth of *P. crispus* appears to be quite important. Since the 1990s, there have been field investigations on macrophyte communities in some lakes, such as Lake Nansi and Lake Dongping (Yu et al., 2017; Xia et al., 2022). In recent years, some studies used remote sensing technologies to interpret and identify wetlands and macrophyte distribution (Wang et al., 2019; Huang et al., 2021). However, there have been few studies on the long-term spatiotemporal variability of the distribution and driving factors of *P. crispus*.

Here, this study combined remote sensing images and hydrometeorological factors of Lake Gaoyou from 1984 to 2022 and water quality factors from 2009 to 2022 to achieve the following research objectives: (1) clarify the long-term changes in distribution characteristics of *P. crispus* in Lake Gaoyou, and (2) disentangle the relative importance of hydrometeorology and water quality factors in regulating the area of *P. crispus* in Lake Gaoyou. We hypothesized that long-term changes in distribution patterns of *P. crispus* were strongly related to hydrometeorological conditions compared to water quality because of climate change in the past decades (Wu et al., 2021; Xia et al., 2022). This study could provide insights into understanding the mechanisms behind the recent large-scale blooms of *P. crispus* in shallow lakes of Eastern China.

# 2 Materials and methods

## 2.1 Study area

Lake Gaoyou (32°30′–33°05′N, 119°06′–119°25′E) is located in the central part of Jiangsu Province, China, in the downstream area of the Huai River; it mainly receives water from the Huai River (Figure 1). The total area of the water body is 728 km$^2$. Lake Gaoyou is situated in the subtropical monsoon climate zone, with an average annual precipitation of 1,029 mm and an average annual evaporation of 890 mm (Chen et al., 2017). The prevailing wind direction is southeast. The main rivers along the lake include Linong River, Baita River, and Qinlan River. Lake Gaoyou is a typical overflow lake, primarily playing a crucial role in flood control and water supply. More importantly, it serves as a water source for the Eastern Route of the South-to-North Water Diversion Project (ER-SNWDP), thus contributing to water diversion benefits and drinking water safety (Qu et al., 2020). However, Lake Gaoyou is undergoing drastic changes in hydrological regime and is strongly impacted by anthropogenic activities such as reclamation and enclosed aquaculture, leading to eutrophication (Guo et al., 2023).

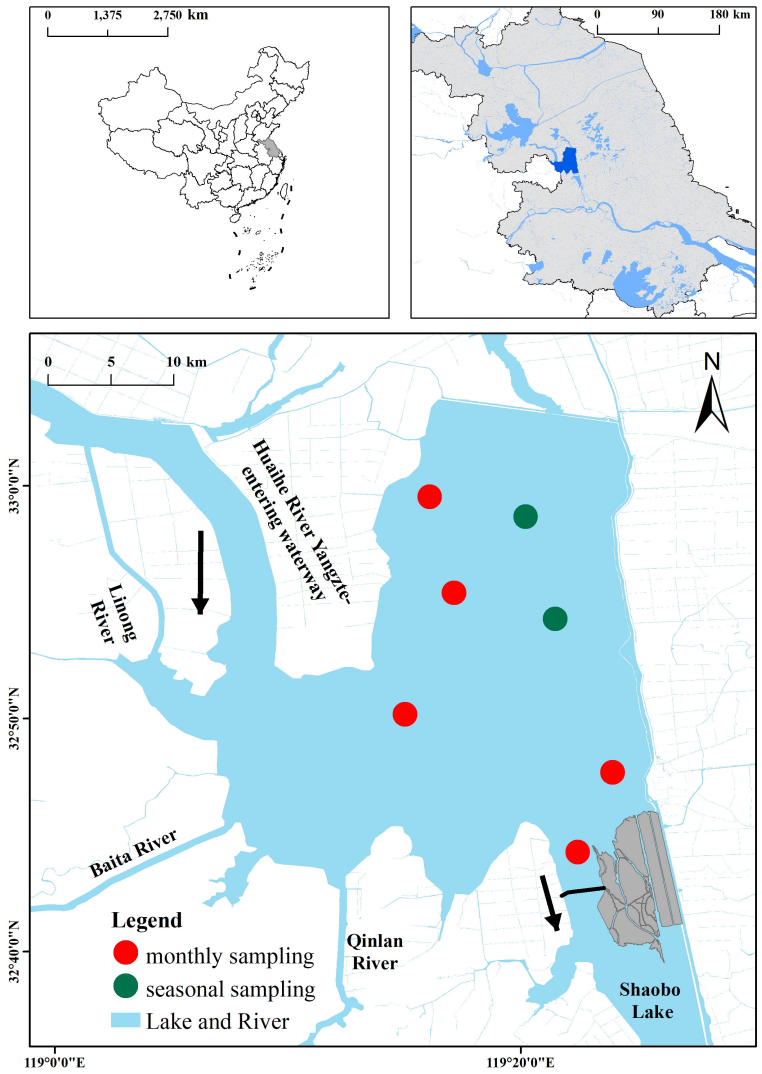


FIGURE 1
Map showing Lake Gaoyou and the distribution of sampling sites. Red circles indicate the monthly sampling sites and green circles indicate the seasonal sampling sites.

## 2.2 Remote sensing data collection and analysis

The remote sensing data for this study are Landsat 5 and Landsat 8 satellite data, with a spatial resolution of 30 m. The Landsat series images of Lake Gaoyou obtained are atmospheric-corrected surface reflectance data. The obtained image data are near-cloudless images (cloud cover <20%) during the submerged macrophyte (especially *P. crispus*) growth period in April and May.

This study employed a remote sensing-based automatic classification algorithm for the extraction of macrophytes, which is able to distinguish algal blooms, emergent/floating-leaved macrophytes, and submerged macrophytes in eutrophic lakes. The decision tree is composed of two vegetation indices and their respective thresholds (Supplementary Figure 1): the Aquatic Vegetation Index (AVI) (Luo et al., 2023) and the Normalized Difference Vegetation Index (NDVI). Here, AVI was calculated based on the humidity coefficient and reflectance of various bands after the Landsat tasseled cap transformation and was used to extract the macrophyte area (Equation 1). NDVI was used to extract the floating-leaved vegetation and emergent macrophyte (FEM) area (Equations 1, 2). The specific process is as follows: (1) By a threshold value $a$, the study area was divided into macrophyte areas and non-macrophyte areas: the pixel with AVI > $a$ was identified as macrophyte and the remaining pixels were non-macrophyte. (2) In the macrophyte area, further classification was carried out by a threshold value $b$. The pixel with NDVI > $b$ was classified as FEM and the remaining pixels were submerged macrophytes. Among them, the threshold $a$ for AVI was a dynamic threshold, which varies for images acquired on different dates. It was obtained through a mixed linear model (Equation 3). The NDVI threshold was derived from extensive empirical data training, aimed at extracting FEM in Lake Gaoyou. The universal threshold $b$ = 0.2 for NDVI was acquired through the threshold statistical graph obtained by the maximum gradient method. The AVI, NDVI, $S_{m,i}(\lambda)$ formula was expressed as Equations 1-3:

$$AVI = -\sum_{i=1}^{6} k(\lambda_i) R(\lambda_i) \quad (1)$$

$$NDVI = (R_{NIR} - R_{Red})/(R_{NIR} + R_{Red}) \quad (2)$$

$$S_{m,i}(\lambda) = p \times S_{W,i}(\lambda) + (1 - p) \times S_V(\lambda) \quad (3)$$

where $k(\lambda_i)$ represents the wetness coefficient of the tasseled cap transformation for band $i$ in different satellite images. $R(\lambda_i)$ represents the surface reflectance of the corresponding spectral band $i$; $R_{NIR}$, $R_{Red}$, and $R_{SWIR1}$ are the reflectances of the near-infrared, red, and short-wave infrared bands, respectively; $\lambda_{NIR}$, $\lambda_{Red}$, and $\lambda_{SWIR1}$ correspond to the central wavelengths of the near-infrared, red, and short-wave infrared bands, respectively; $S_{m,i}(\lambda)$, $S_{W,i}(\lambda)$, and $S_V(\lambda)$ represent the spectra of mixed materials, pure water, and pure vegetation, respectively; $p$ represents the proportion of the pure water spectrum in the spectral mixture. Accuracy evaluation results of the classification confusion matrix are displayed in Supplementary Table 1.

Owing to the typical spectral characteristics of vegetation exhibited by FEM growing in the lakeshore zone, which has stronger spectral signals compared to submerged macrophytes, they are easily distinguishable from each other. *P. crispus* dominates the submerged macrophyte population in Lake Gaoyou, with the distribution of other species being quite limited (Tian et al., 2019; Xia et al., 2022). Additionally, considering that other submerged macrophytes are in their germination phase in April and May, while *P. crispus* is in its rapid growth phase with its stems closest to the water surface, exhibiting relatively strong spectral signals at this time. Therefore, we selected satellite images from April and May to identified the area of *P. crispus* in Gaoyou Lake. The remote sensing images from 2011 to 2013 and 2015 have high cloud content or contain stripes. By downloading Landsat 7 ETM and Landsat 8 OLI satellite data, visual interpretation was conducted to extract the area of *P. crispus* for these years.

## 2.3 Meteorological, hydrological, and water quality data

The meteorological factors, air temperature (Temp), wind speed (WS), and precipitation (PP) from 1984 to 2022, were obtained from the National Weather Science Data Center (https://data.cma.cn/). The hydrological factor [water level (WL)] data from 1984 to 2022 were obtained from the Jiangsu Provincial Hydrology and Water Resources Investigation Bureau. The water quality data from 2009 to 2022 were obtained from field surveys and sampling analysis.

The water quality survey conducted between 2009 and 2022 involved seven sampling sites (Figure 1), namely, two seasonal sampling sites across the lake (February, May, August, and November/December) and five monthly sampling sites. After the initial processing, the collected water samples were further detected and analyzed in the laboratory, ultimately yielding data on seven water quality parameters. Secchi depth (SD) was measured with the Secchi disk, and DO was measured with a portable multi-parameter water quality meter (YSI Professional Plus, USA). Surface, middle, and bottom water samples taken with a Plexiglas sampler were pooled and kept cool in a 1-L refrigerated container (at 4°C) and transported to the laboratory within 24 h. Total nitrogen (TN) was determined by potassium persulfate oxidation and UV spectrophotometry, and total phosphorus (TP) was determined by ammonium molybdate spectrophotometry. Ammonia nitrogen ($NH_3$-N) was determined using the nano reagent photometric method, and the permanganate index ($COD_{Mn}$) was determined using the dichromate method. Chlorophyll a (Chl-*a*) was determined using a spectrophotometer (UV-2450, Shimadzu Co., Ltd., Japan) after filtering known amounts of water through a GF/F (Whatman International Ltd., Maidstone, England) filter.

The flowchart of the grouping of environmental factors to analyze the area of *P. crispus* is shown in Supplementary Figure 2.

## 2.4 Data analysis

To understand the variation trend of *P. crispus* area, the "lm" function was used to analyze the long-term temporal changes of environmental factors in Lake Gaoyou. Subsequently, the "segmented" package was employed to fit segmented models to the time series of *P. crispus* area over the years. As *P. crispus* germinates in winter and blooms in spring, we examined the effects of environmental factors on the *P. crispus* area based on data of winter (from December of the previous year to March), spring (from April to May), and the entire year (from January to December). To identify the key environmental factors explaining the area of *P. crispus*, the "cor.test" function was employed to analyze the correlation between the area of *P. crispus* and meteorological factors, hydrological factors, and water quality factors. To perform stepwise regression analysis and select the main driving factors explaining the area of *P. crispus*, the "step" function was used. Subsequently, the "lm" function was employed to fit the area of *P. crispus* with the selected factors.

The "vegan" package was used for variation partitioning analysis to analyze the importance of two types of factors (hydrometeorological factors and water quality factors) in influencing the area of *P. crispus*.

The "ggplot2" package was used to visualize the above analysis results. In addition, $p < 0.05$ is considered to have a statistically significant difference in all analyses. Data analysis was performed using relevant packages in R version 4.3.2, and the plots were generated on both Origin and R platforms.

# 3 Results

## 3.1 Temporal changes in the environment factors

The hydrometeorological factors during the bloom period of *P. crispus* showed significant changes from 1984 to 2022 (Figure 2, Supplementary Figures 3, 4). For example, in spring, the Temp (18.22 ± 1.08°C) increased markedly over time and reached its

maximum of 20.53°C in 2017, followed by a decreasing trend between 2017 and 2020. Conversely, WS (2.65 ± 0.35 m/s) declined significantly from 2013 to 2019 and reached its minimum of 1.92 m/s, with a noticeable rebound from 2019 to 2020, followed by a subsequent decline. The annual average WL (5.79 ± 0.25 m) increased significantly over time and reached its maximum of 6.21 m in 2018. From 2009 to 2022, the main water quality factors of Lake Gaoyou also showed significant temporal variations. For example, in spring, Chl-*a* (0.012 ± 0.004 mg/L) increased markedly and reached its maximum of 0.019 mg/L in 2018. DO (8.25 ± 0.39 mg/L) and SD (0.34 ± 0.04 m) showed a fluctuating trend. TP (0.06 ± 0.01 mg/L) increased from 2009 to 2013 and peaked at 0.08 mg/L in 2013, followed by fluctuating changes. TN (1.06 ± 0.31 mg/L) showed considerable fluctuation, mostly remaining at approximately 1.0 mg/L. $COD_{Mn}$ (4.17 ± 0.30 mg/L) showed an overall slight increasing trend and reached its maximum of 4.79 mg/L in 2020, followed by a declining trend.

In addition, some water quality factors showed a significantly seasonal difference (Figure 3). The investigated lake in spring had a median TP concentration of 0.059 (0.036–0.076) mg/L and a median $COD_{Mn}$ concentration of 4.17 (3.68–4.79) mg/L. However, TP and $COD_{Mn}$ concentration for the entire year were 0.070 (0.054–0.080) mg/L and 4.41 (3.95–4.88) mg/L, respectively. TP and $COD_{Mn}$ in spring were significantly lower than the concentration for the entire year ($p < 0.001$ for TP and $p < 0.05$ for $COD_{Mn}$). DO also showed pronounced differences among three periods and had a significantly higher median concentration of 10.92 (10.27–11.63) mg/L in winter than the other two ($p < 0.001$).

## 3.2 Long-term trends and the spatial distribution of *P. crispus*

The segmented linear fitting results indicated that the variation in the area of *P. crispus* between 1984 and 2022 can be divided into three time periods (Figure 4). From 1984 to 2009, the area of *P. crispus* in Lake Gaoyou slightly increased from approximately 37.86 km² to approximately 100 km², with a relatively low distribution

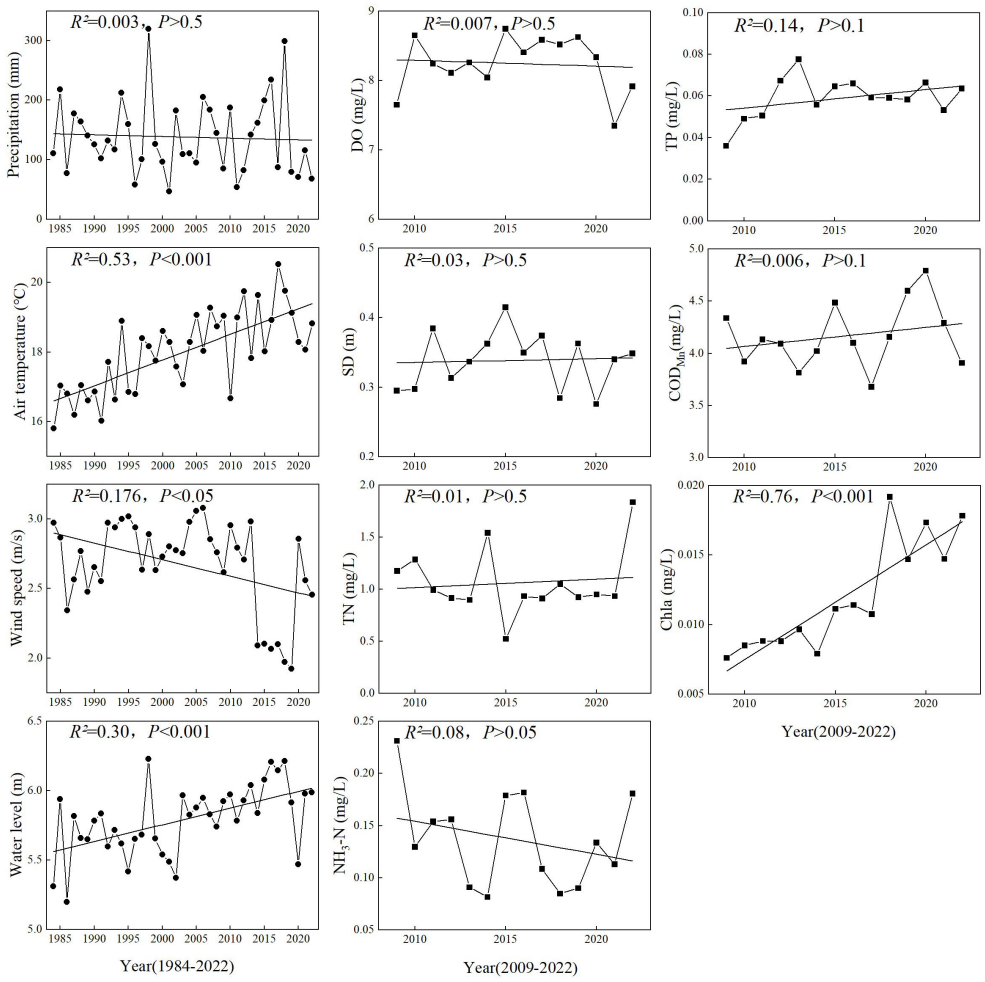


FIGURE 2
Temporal changes in hydrometeorological and water quality variables in spring. See the main text for abbreviations.

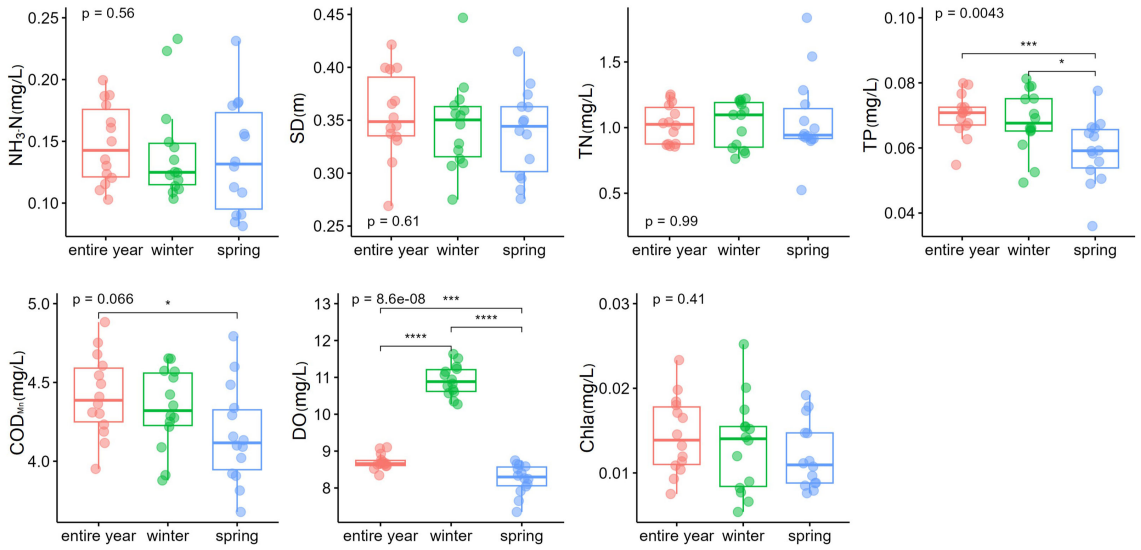


FIGURE 3
Comparisons of water quality in different seasons. *$p < 0.05$; ***$p < 0.001$. ****$p < 0.0001$..

area. From 2010 to 2019, the area of *P. crispus* began to markedly increase ($p < 0.001$), exhibiting a large-scale bloom trend with an average area of 291.31 km², and reached its maximum of 395.51 km². After 2019, the area of *P. crispus* showed a rapid decrease ($p < 0.05$) and reached 136.78 km² in 2022.

From a spatial perspective, *P. crispus* was primarily distributed in the western and northern parts of Lake Gaoyou, with less distribution in the central and southeastern parts of the lake (Figure 5; Supplementary Figure 5). From 1984 to 2010, *P. crispus* in Lake Gaoyou transitioned from a scattered distribution in the northern part of the lake to extending towards the western part, gradually increasing in area. From 2010 to 2019, *P. crispus* continued to extend towards the southeastern part of the lake and spread from the surrounding areas towards the central part of the lake, rapidly expanding in area. From 2019 to 2022, the area covered by *P. crispus* decreased rapidly as it receded from the central part of the lake towards the surrounding areas.

## 3.3 Factors driving the distribution pattern succession of *P. crispus*

### 3.3.1 Correlation analysis

The results of the Pearson correlation analysis showed that the area of *P. crispus* in Lake Gaoyou showed a significantly positive correlation with Temp and WL ($p < 0.001$) and a significantly negative correlation with WS ($p < 0.001$). The correlations between water quality factors for different periods and the area of *P. crispus* varied (Figure 6A): In the analysis of environmental factors in winter, the area of *P. crispus* was positively correlated with SD ($p < 0.05$). In the analysis of environmental factors in spring, the area of *P. crispus* was negatively correlated with $NH_3$-N ($p < 0.05$).

### 3.3.2 Stepwise regression analysis

The stepwise regression analysis showed that the five most important factors influencing the change in *P. crispus* area in Lake

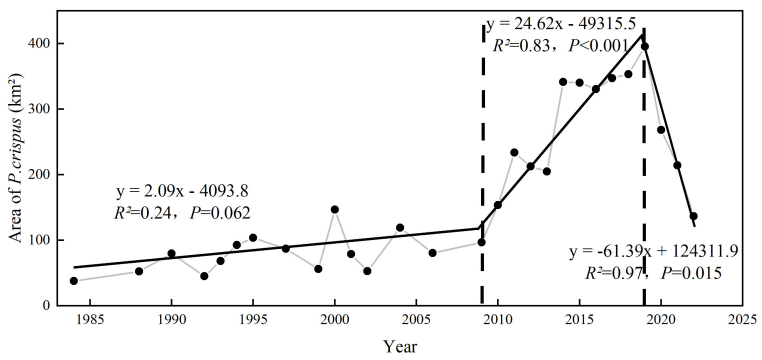


FIGURE 4
The variation in the area of *P. crispus* in Lake Gaoyou from 1984 to 2022.

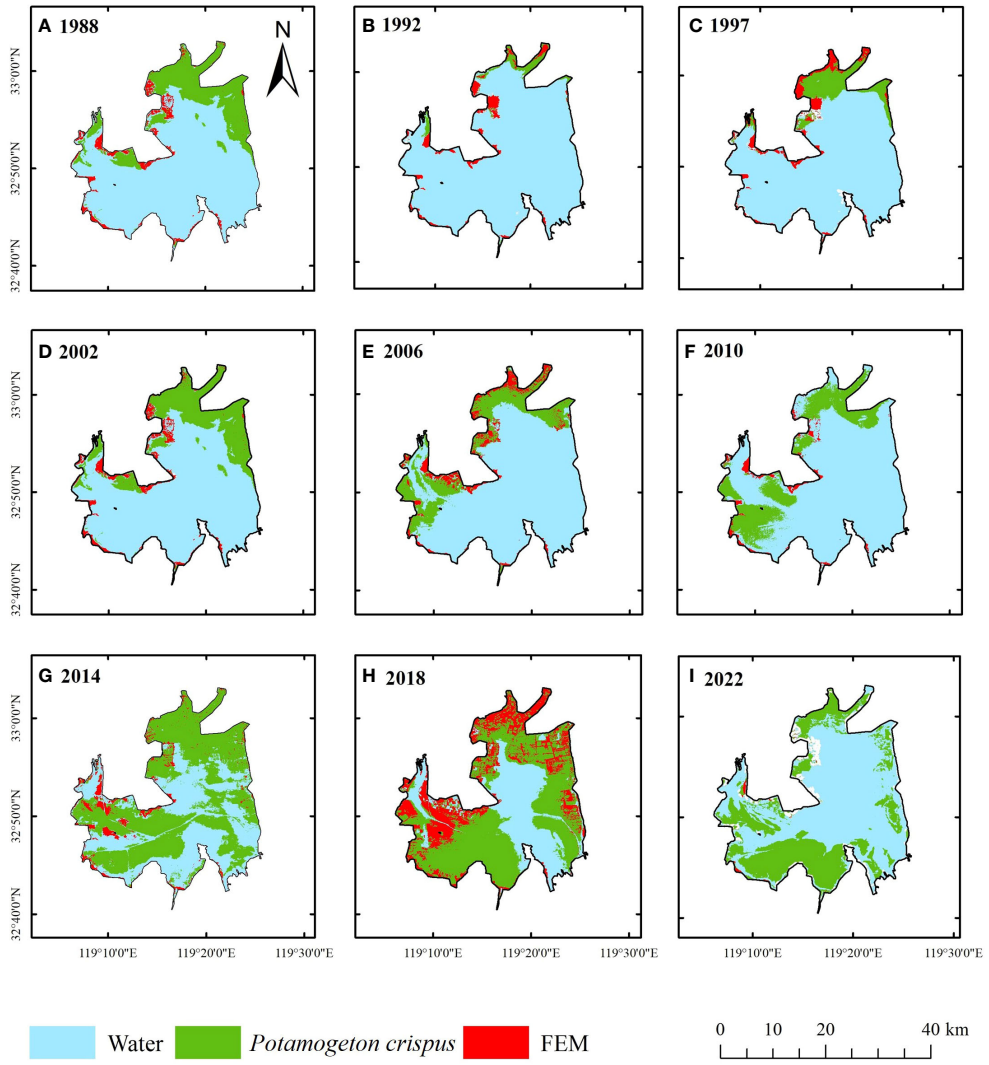


FIGURE 5
Changes in the spatial distribution of the *P. crispus* area in Lake Gaoyou from 1984 to 2022. **(A)** 1988 **(B)** 1992 **(C)** 1997 **(D)** 2002 **(E)** 2006 **(F)** 2010 **(G)** 2014 **(H)** 2018 **(I)** 2022. FEM, floating-leaved and emergent macrophyte.

Gaoyou were WS, Temp, WL, $NH_3$-N, and SD (Table 1). In particular, the area of *P. crispus* was found to correlate closely with hydrometeorology, and the contribution of WS was particularly significant ($p < 0.001$). The area of *P. crispus* consistently showed a negative association with WS and a positive relationship with SD in the analysis of three periods ($p < 0.05$). In the analysis of entire-year and winter environmental factors, Temp and WL ($p < 0.05$) were two important factors, both of which were positively correlated with the area of *P. crispus* (Supplementary Figures 7, 8). In the analysis of entire-year and spring environmental factors, the area of *P. crispus* showed a significantly negative correlation with $NH_3$-N ($p < 0.05$) (Figure 6B), and the relative contributions of the variables to explain the total variation were $NH_3$-N > SD. The regression models selected with significance ($p < 0.001$) between hydrometeorology and the area of *P. crispus* for different periods had a total explanation of 72.6%, 75.2%, and 64.0%, respectively. The regression models selected with significance between water quality and the area of *P. crispus* for different periods had a total explanation of 36.4%, 34.0% ($p < 0.05$), and 44.9% ($p < 0.05$), respectively.

### 3.3.3 Variation partitioning analysis

The results of the variation partitioning analysis showed that the *P. crispus* presented significant differences among the different periods. In the analysis of entire environmental factors, WS and Temp accounted for 60.2% of the variation in the *P. crispus* area, with their interaction with $NH_3$-N and SD explained 15.0% (Figure 7A). For winter environmental factors, WS and WL explained 39.7% of the variation in the *P. crispus* area, with the shared fraction with SD explained 30.5% (Figure 7B). For spring environmental factors, WS explained 35.4% of the variation in the *P. crispus* area, with their interaction with $NH_3$-N and SD explained 21.0% (Figure 7C).

The variation partitioning analysis for all three periods indicated that hydrometeorological factors (Temp, WS, and WL)

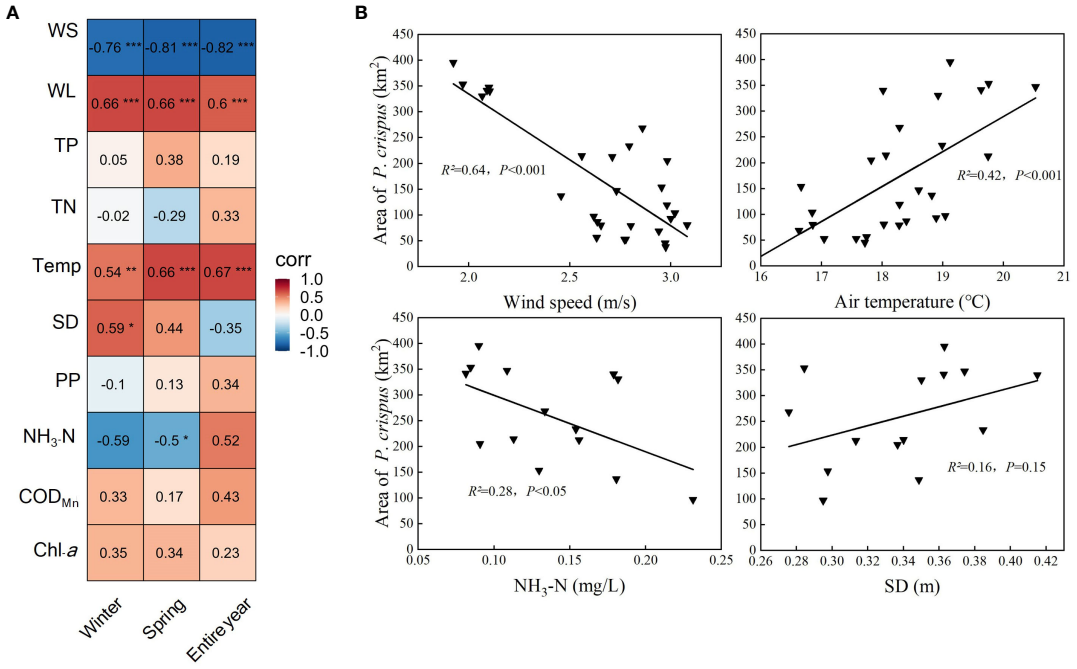


FIGURE 6
Correlation analysis between the area of *P. crispus* and environmental factors. **(A)** Relationships between the area of *P. crispus* and environmental factors. The numbers in each grid represent the correlation coefficients between the area of *P. crispus* and environmental factors. **(B)** Linear fitting of the area of *P. crispus* and environmental factors in spring. * $p < 0.05$; ** $p < 0.01$; *** $p < 0.001$.

accounted for the high amount of variation in the *P. crispus* area in Lake Gaoyou compared to water quality ($NH_3$-N, and SD), playing a dominant role in driving the changes in the area of *P. crispus*. Additionally, the interaction between hydrometeorology and water quality explained a higher proportion of variation in the area of *P. crispus* in winter, whereas its amount of explanation was lower for the entire year.

# 4 Discussion

## 4.1 Main driving factors affecting the distribution of *P. crispus*

The five most important factors influencing the change in the *P. crispus* area in Lake Gaoyou were WS, Temp, WL, $NH_3$-N, and SD. Among them, WS played a crucial role in the variation of the *P. crispus* area (Table 1). On one hand, WS can affect the growth of *P. crispus* by influencing the hydrodynamic conditions of the lake. Macrophytes in lakes are often affected by water flow resistance, which is frequently over 25 times more resistant compared to terrestrial vegetation under similar wind speeds (Denny and Gaylord, 2002). Submerged macrophytes will also show different biomechanical characteristics subject to the wind and wave conditions (Zhu et al., 2015). Consequently, most submerged macrophytes float to the water's surface when strong winds and waves cause stems to break or entire plants to be uprooted. This causes a significant decrease in submerged macrophytes in shallow lakes, or even their disappearance, which reduces the macrophytes' biomass and coverage (Riis and Biggs, 2003; Yang et al., 2004; Breugnot et al., 2008; Angradi et al., 2013). Consistent with previous findings, in this study, WS was an important variable that negatively contributed to the *P. crispus* area (Table 1); the *P. crispus* area showed an increasing trend with declining WS from 2010 to 2019. On the other hand, wind speed is often significantly negatively correlated with transparency in shallow lakes (Soria et al., 2021), which is similar to the results of this study (Supplementary Figure 9). Increased wind speeds can intensify hydrodynamic disturbances in lakes, causing lake sediments to appear in resuspension and reducing transparency (Soria et al., 2021). A decline in transparency inhibits plant photosynthesis, which was unfavorable for the growth of *P. crispus* in Lake Gaoyou. According to the spatial distribution of *P. crispus* in Lake Gaoyou, the area of *P. crispus* in the southeastern part of the lake was perennially small. This may be due to the fact that this area serves as a flood channel where the southeast monsoon prevails, which was prone to stronger hydrodynamic disturbances leading to lower water transparency, thus inhibiting the growth of *P. crispus*.

Generally, water depth has been considered a significant factor influencing the growth of submerged macrophytes. Typically, there is a negative correlation between water depth and the biomass of submerged macrophytes (Li et al., 2021). However, in shallow lakes, increasing the water depth probably creates a favorable growing habitat for submerged macrophytes by changing the temperature, DO content, and underwater light intensity and by expanding the growth space for these plants (Fu et al., 2014, 2018; Su et al., 2018). On the other hand, changes in water depth or level often interact with factors such as wind speed to influence submerged

TABLE 1 The multiple regression model results for the area of *P. crispus* and environmental factors.

| Area | Factor | $R^2$ (%) | *F* | *p* | Variables | Standardized coefficients |
|---|---|---|---|---|---|---|
| Entire year | Hydrometeorology | 72.6 | 36.75 | <0.001 | WS | −0.674 *** |
| | | | | | Temp | 0.290 * |
| | Water quality | 36.4 | 3.146 | 0.083 | $NH_3$-N | −0.452 |
| | | | | | SD | 0.404 |
| Winter | Hydrometeorology | 75.2 | 37.86 | <0.001 | WS | −0.837*** |
| | | | | | WL | 0.288* |
| | Water quality | 34.0 | 6.167 | <0.05 | SD | 0.583* |
| Spring | Hydrometeorology | 64.0 | 46.12 | <0.001 | WS | −0.800 *** |
| | Water quality | 45.0 | 4.489 | <0.05 | $NH_3$-N | −0.537* |
| | | | | | SD | 0.407 |

*$p < 0.05$; ***$p < 0.001$.

macrophytes (Van Zuidam and Peeters, 2015). An increase in water depth often leads to a decrease in the intensity of wind–wave disturbances (Søndergaard et al., 2003). This, to some extent, mitigated the negative effects of wave disturbance on SD, thereby promoting the expansion of the *P. crispus* area.

The stepwise linear regression model conducted in our study indicated that $NH_3$-N concentration and SD were the two important water quality variables that contributed to the area of *P. crispus* (Table 1). The improvement in water transparency helps to increase the underwater light intensity, thereby improving photosynthesis efficiency in plants and consequently promoting the growth of *P. crispus* (Wang et al., 2017). Previous studies also concluded that macrophytes showed a decreasing trend due to a deteriorating underwater light environment. In our study, $NH_3$-N negatively contributed to the area of *P. crispus*. High concentrations of ammonium ions can interfere with the nitrogen metabolism of *P. crispus* (Zhang YL et al., 2016; Dong et al., 2022), and physiological stress caused by high concentrations of ammonia nitrogen in the water can also lead to a decrease in the biomass of *P. crispus* (Cao et al., 2015). Several laboratory and field studies have demonstrated that macrophytes in lakes can experience damage and even disappear when there is a high concentration of nitrogen,

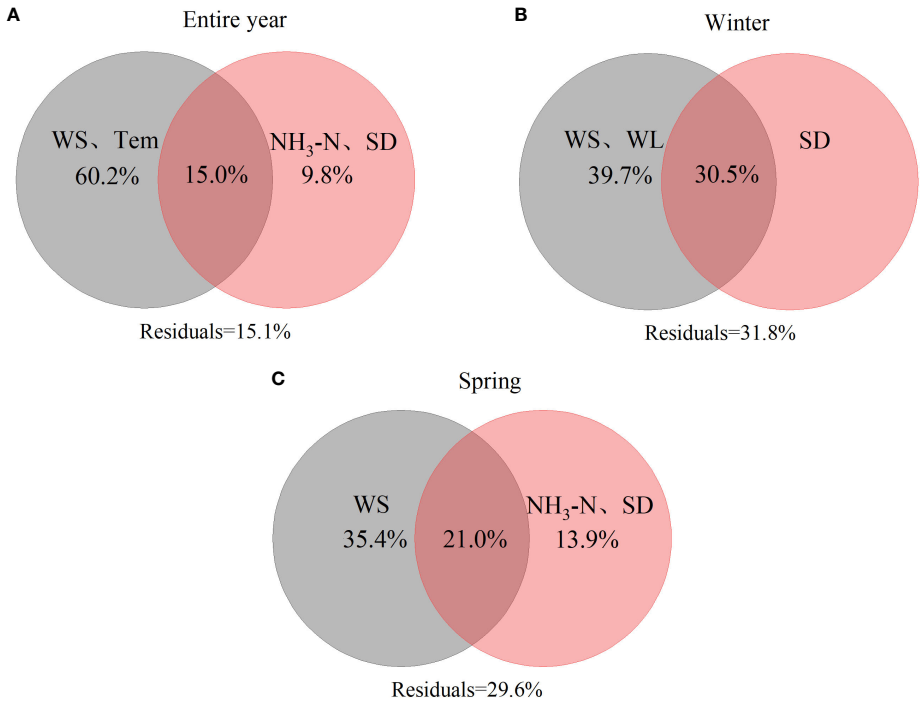


FIGURE 7
The differences in the relative contributions of hydrometeorology and water quality to the area of *P. crispus*. **(A)** entire year, **(B)** winter, **(C)** spring. Values < 0 are not shown.

particularly ammonia nitrogen (Moss et al., 2012; Olsen et al., 2015; Yu et al., 2015; Zhang YL et al., 2016). The conclusion has also been confirmed by site-specific observation and remote sensing mapping (Zhang YL et al., 2016). These findings imply that the increasing SD and decreasing $NH_3$-N concentration in Lake Gaoyou may enhance the area of *P. crispus* from 2010 to 2019.

Additionally, *P. crispus* has an interactive relationship with water quality. Submerged macrophytes improve local water transparency by reducing sediment resuspension and absorbing nutrients from the water; thus, there is a positive feedback relationship between submerged macrophyte and local water transparency in shallow lake ecosystems (Su et al., 2019). Similarly, *P. crispus* needs to absorb nutrients such as ammonia nitrogen from sediment and water through its roots and stems to support growth (Li et al., 2015).

## 4.2 Seasonal characteristics of driving factors

The influence of environmental factors in different seasons on the area of *P. crispus* in Lake Gaoyou varied (Table 1). In this study, $NH_3$-N significantly contributed to the fluctuation of *P. crispus* area in spring, while no statistical difference was observed for $NH_3$-N in winter. Conversely, WL in winter significantly contributed to the variation in the *P. crispus* area, while no statistical difference was observed for water level in spring.

Water level itself generally does not directly affect macrophytes but often influences plant growth by altering other environmental factors (Van Zuidam and Peeters, 2015). Increasing fluctuation frequency increases disturbance to plants, leading to increased nutrient loss and tissue damage (Bornette et al., 2008). High-frequency fluctuations in the water level can also lead to the resuspension of sediments, increasing water turbidity, thereby inhibiting the growth of macrophytes (Coops and Hosper, 2002; Luo et al., 2015). In May, Lake Gaoyou experiences a period of rising water levels, with significant fluctuations in water levels (Jiang et al., 2023). The flow velocity may rise simultaneously with water level during this period (Zhang et al., 2017). The rising flow velocity intensifies water disturbance, which is unfavorable for the growth of *P. crispus*. Compared to spring, water level fluctuations were smaller in winter, which may be the reason why the positive effect of WL changes on the expansion of the *P. crispus* area was more significant in winter.

The interactions between $NH_3$-N and *P. crispus* showed a seasonal difference. On one hand, in a shallow eutrophic water body, macrophytes can assimilate a large amount of nitrogen from sediments via their roots during the growing season (Xie et al., 2013). The efficiency of assimilating and utilizing nitrogen increases when *P. crispus* blooms in spring. On the other hand, toxic effects cause the various growth indices of *P. crispus*, such as leaf length, leaf mass, and root length, to decline with increasing nitrogen and ammonia concentrations (Yu et al., 2015). Therefore, in Lake Gaoyou, the relatively higher concentration of $NH_3$-N in spring compared to winter may explain a more noticeable inhibitory effect of $NH_3$-N on the growth of *P. crispus* during spring.

The temperature was only screened as a significant influencing factor in the factor analysis at the annual scale. This was primarily because the multivariate stepwise regression algorithm aimed to balance model stability and simplicity. Because of the significant correlation between factors (such as Temp and WS, $p < 0.05$), where WS coincided with Temp covariation, there was some redundancy in information (Supplementary Figure 6). Once WS entered the model, Temp could not enter to the same extent. However, from the correlation coefficients, it could be observed that Temp was significantly correlated with the area of *P. crispus*. Research related to the influence of temperature on *P. crispus* indicated that warming treatments significantly increased plant height and total biomass (Yan et al., 2021). As a submerged macrophyte that grows in winter and spring, *P. crispus* will enter the growing season earlier and occupy more spatial ecological niches as the winter gets warmer (Li et al., 2018). Consistent with previous studies, the results of this study demonstrate that an increase in Temp had a positive effect on the growth of *P. crispus* in Lake Gaoyou (Table 1; Figures 2, 4).

## 4.3 Relative importance of hydrometeorology and water quality

The primary influencing factors for the growth of *P. crispus* in Lake Gaoyou were hydrometeorological factors (Temp, WS, and WL), which fits with our hypothesis. Moreover, the relative importance of the interaction between hydrometeorology and water quality varied across different periods. The interaction between hydrometeorology and water quality showed a higher explanation in winter, whereas it was lower over the entire year (Figure 7).

Against the backdrop of global climate change, increasing water temperatures, storm events, and associated long-term flooding have had a significant impact on the health of aquatic ecosystems dominated by macrophytes worldwide, thereby affecting the growth of macrophytes in lakes (Zhang et al., 2017). Research on large-scale vegetation in global lakes indicated that climate variables have a greater impact on species selection at a large spatial scale (García-Girón et al., 2020). Similar to previous studies, at the large spatial scale of Lake Gaoyou, climate had a more significant impact on the growth of *P. crispus* compared to anthropogenic activities. Furthermore, temperature changes have a significant impact on the growth of submerged macrophytes. For example, *Elodea canadensis* biomass increases directly with warmer temperatures as opposed to nutrient enrichment (Wu et al., 2021). Similarly, the drastic fluctuations in Temp in the Lake Gaoyou area also have significantly influenced the changes in the area covered by *P. crispus*.

Climate change is not a uniform warming process; its impact on winter is particularly noticeable (Franssen and Scherrer, 2008). Macrophytes can overwinter in an aboveground form under warmer winter (Havens et al., 2015). Warmer winters increase the number of branch and total biomass of macrophytes, thereby enhancing overwinter survival rates (Liu et al., 2016). Additionally, this study revealed that the interaction between winter WS and SD was more significant. It was possible that winter WS affected the growth of *P. crispus* via influencing SD, making the impact of winter WS on the expansion of *P. crispus* more significant. Additionally, this study revealed that the interaction between winter WS and SD was more

significant ($p < 0.05$) (Supplementary Figure 9). It was possible that winter WS affected the growth of *P. crispus* by influencing SD, making the impact of winter WS on the expansion of *P. crispus* more significant.

## 5 Conclusion

Ensuring adequate appropriate coverage of submerged macrophyte growth is vital for maintaining water quality and ecosystem stability. The area of *P. crispus* in Lake Gaoyou showed a slight increase from 1984 to 2009, followed by a marked increase from 2010 to 2019, and then a decline after 2020. We found that the variation in the *P. crispus* area was highly influenced by WS, Temp, WL, $NH_3$-N, and SD in Lake Gaoyou and showed seasonality in response to hydrometeorology and water quality parameters. Hydrometeorology factors appeared to exert a more substantial influence on the area covered by *P. crispus* than water quality parameters. The significantly decreasing WS and the increasing Temp and WL resulted in explosive trends in the area of *P. crispus*. Overall, our study revealed the long-term distribution pattern of *P. crispus* in Lake Gaoyou and identified key factors regulating the distribution of *P. crispus*. The proliferation of specific species would disrupt water quality and aquatic ecosystem stability. Therefore, effective lake management should include enhanced macrophyte monitoring and timely intervention measures to counteract the excessive growth of specific species, thereby safeguarding water resources for the China ER-SNWDP.

## Data availability statement

The raw data supporting the conclusions of this article will be made available by the authors, without undue reservation.

## Author contributions

KY: Writing – original draft, Writing – review & editing, Formal analysis, Visualization, Methodology. YY: Writing – original draft, Writing – review & editing, Data curation. YX: Writing – review & editing, Data curation. SW: Writing – review & editing, Data curation. MG: Writing – original draft, Data curation, Investigation. KP: Writing – review & editing, Data curation, Methodology. JL: Writing – review & editing, Methodology, Visualization. JG: Writing – review & editing. YC: Conceptualization, Formal analysis, Funding acquisition, Methodology, Writing – original draft, Writing – review & editing.

## Funding

The author(s) declare financial support was received for the research, authorship, and/or publication of this article. This study was supported by the National Natural Science Foundation of China (32071572), the Key Laboratory of Lake and Watershed Science for Water Security (NKL2023-ZD02), and the Youth Innovation Promotion Association CAS (2020316).

## Conflict of interest

Author SW was employed by the company Jiangsu Surveying and Design Institute of Water Resources Co., Ltd.

The remaining authors declare that the research was conducted in the absence of any commercial or financial relationships that could be construed as a potential conflict of interest.

## Publisher's note



## Supplementary material

The Supplementary Material for this article can be found online at: https://www.frontiersin.org/articles/10.3389/fpls.2024.1424300/full#supplementary-material

## References

Akasaka, M., Takamura, N., Mitsuhashi, H., and Kadono, Y. (2010). Effects of land use on aquatic macrophyte diversity and water quality of ponds. *Freshw. Biol.* 55, 909–922. doi: 10.1111/j.1365-2427.2009.02334.x

Angradi, T. R., Pearson, M. S., Bolgrien, D. W., Bellinger, B. J., Starry, M. A., and Reschke, C. (2013). Predicting submerged aquatic vegetation cover and occurrence in a Lake Superior estuary. *J. Great Lakes Res.* 39, 536–546. doi: 10.1016/j.jglr.2013.09.013

Bornette, G., Tabacchi, E., Hupp, C., Puijalon, S., and Rostan, J. C. (2008). A model of plant strategies in fluvial hydrosystems. *Freshw. Biol.* 53, 1692–1705. doi: 10.1111/j.1365-2427.2008.01994.x

Breugnot, E., Dutartre, A., Laplace-Treyture, C., and Haury, J. (2008). Local distribution of macrophytes and consequences for sampling methods in large rivers. *Hydrobiologia.* 610, 13–23. doi: 10.1007/s10750-008-9418-9

Cao, J., Mu, X. W., Gao, J., Jiang, W., Zhu, J. H., Gu, J. W., et al. (2015). Analysis of the hazards and countermeasures of Potamogeton crispus outbreak in Lake Luoma. *J. Aquaculture.* 35, 42–44. doi: 10.3969/j.issn.1004-2091.2015.09.015

Chen, Z. G., Lin, Z. J., Zhou, X. H., Wang, M. Y., Feng, D. Y., Han, X., et al. (2017). Pollutants dynamic release of Potamogeton crispus during decomposition process. *J. Arid Land.* 31, 153–159. doi: 10.13448/j.cnki.jalre.2017.262

Coops, H., and Hosper, S. H. (2002). Water-level Management as a Tool for the Restoration of Shallow Lakes in the Netherlands. *Lake Reservoir Manage.* 18, 293–298. doi: 10.1080/07438140209353935

Denny, M., and Gaylord, B. (2002). The mechanics of wave-swept algae. *J. Exp. Biol.* 1355–1362. doi: 10.1242/jeb.205.10.1355

Dong, B. L., Zhou, Y. Q., Jeppesen, E., Qin, B. Q., and Shi, K. (2022). Six decades of field observations reveal how anthropogenic pressure changes the coverage and community of submerged aquatic vegetation in a eutrophic lake. *Sci. Total Environ.* 842, 156878. doi: 10.1016/j.scitotenv.2022.156878

Fares, A. L. B., Calvão, L. B., Torres, N. R., Gurgel, E. S. C., and Michelan, T. S. (2020). Environmental factors affect macrophyte diversity on Amazonian aquatic ecosystems inserted in an anthropogenic landscape. *Ecol. Indic.* 113, 106231. doi: 10.1016/j.ecolind.2020.106231

Franssen, H. J. H., and Scherrer, S. C. (2008). Freezing of lakes on the Swiss plateau in the period 1901–2006. *Int. J. Climatol.* 28, 421–433. doi: 10.1002/joc.1553

Fu, H., Yuan, G. X., Lou, Q., Dai, T. T., Xu, J., Cao, T., et al. (2018). Functional traits mediated cascading effects of water depth and light availability on temporal stability of a macrophyte species. *Ecol. Indic.* 89, 168–174. doi: 10.1016/j.ecolind.2018.02.010

Fu, H., Zhong, J. Y., Yuan, G. X., Xie, P., Guo, L. G., Zhang, X. L., et al. (2014). Trait-based community assembly of aquatic macrophytes along a water depth gradient in a freshwater lake. *Freshw. Biol.* 59, 2462–2471. doi: 10.1111/fwb.12443

García-Girón, J., Heino, J., Baastrup-Spohr, L., Bove, C. P., Clayton, J., De Winton, M., et al. (2020). Global patterns and determinants of lake macrophyte taxonomic, functional and phylogenetic beta diversity. *Sci. Total Environ.* 723, 138021. doi: 10.1016/j.scitotenv.2020.138021

Guo, L. C., Mo, L. W., Su, Y. Y., Hu, X. D., and Xu, D. D. (2023). Studying the metazoan zooplankton community characteristics and evaluating the water quality based on the ecological and functional zones in gaoyou lake. *Water.* 15, 3357. doi: 10.3390/w15193357

Havens, K. E., Pinto-Coelho, R. M., Beklioğlu, M., Christoffersen, K. S., Jeppesen, E., Lauridsen, T. L., et al. (2015). Temperature effects on body size of freshwater crustacean zooplankton from Greenland to the tropics. *Hydrobiologia.* 743, 27–35. doi: 10.1007/s10750-014-2000-8

Huang, F. F., Zhang, K., Huang, S. X., and Lin, Q. (2021). Patterns and trajectories of macrophyte change in East China's shallow lakes over the past one century. *Sci. China Earth Sci.* 64, 1735–1745. doi: 10.1007/s11430-020-9806-9

Huang, S. X., Zhang, K., Lin, Q., Liu, J. B., and Shen, J. (2022). Abrupt ecological shifts of lakes during the Anthropocene. *Earth Sci. Rev.* 227, 103981. doi: 10.1016/j.earscirev.2022.103981

Jian, Y. X., Li, B., Wang, J. B., and Chen, J. K. (2003). Control of turion germination in Potamogeton crispus. *Aquat. Bot.* 75, 59–69. doi: 10.1016/S0304-3770(02)00165-1

Jiang, Y. S., Lu, X. M., Zhao, L. L., Xiao, F., Xue, K., and Lu, X. P. (2023). Analysis of hydrological regime changes characteristics in Gaoyou Lake from 1990 to 2020. *JiangSu Water Resourses.* 12, 14–19. doi: 10.16310/j.cnki.jssl.2023.12.009

Kim, J. Y., and Nishihiro, J. (2020). Responses of lake macrophyte species and functional traits to climate and land use changes. *Sci. Total Environ.* 736, 139628. doi: 10.1016/j.scitotenv.2020.139628

Li, C., Wang, T., Zhang, M., and Xu, J. (2018). Maternal environment effect of warming and eutrophication on the emergence of curled pondweed, potamogeton crispus L. *Water.* 10, 1285. doi: 10.3390/w10091285

Li, J. H., Yang, X. Y., Wang, Z. F., Shan, Y., and Zheng, Z. (2015). Comparison of four aquatic plant treatment systems for nutrient removal from eutrophied water. *Bioresour. Technol.* 179, 1–7. doi: 10.1016/j.biortech.2014.11.053

Li, Q. S., Han, Y. Q., Chen, K. Q., Huang, X. L., Li, K. Y., and He, H. (2021). Effects of Water Depth on the Growth of the Submerged Macrophytes Vallisneria natans and Hydrilla verticillata: Implications for Water Level Management. *Water.* 13, 2590. doi: 10.3390/w13182590

Li, Z., He, L., Zhang, H., Urrutia-Cordero, P., Ekvall, M. K., Hollander, J., et al. (2017). Climate warming and heat waves affect reproductive strategies and interactions between submerged macrophytes. *Glob Chang Biol.* 23, 108–116. doi: 10.1111/gcb.13405

Liu, J. C., Chen, X. W., Wang, Y. L., Li, X., Yu, D., and Liu, C. H. (2016). Response differences of Eichhornia crassipes to shallow submergence and drawdown with an experimental warming in winter. *Aquat. Ecol.* 50, 307–314. doi: 10.1007/s10452-016-9579-y

Luo, F. L., Jiang, X. X., Li, H. L., and Yu, F. H. (2015). Does hydrological fluctuation alter impacts of species richness on biomass in wetland plant communities? *J. Plant Ecol.* 9, 434–441. doi: 10.1093/jpe/rtv065

Luo, J. H., Ni, G. G., Zhang, Y. L., Wang, K., Shen, M., Cao, Z. G., et al. (2023). A new technique for quantifying algal bloom, floating/emergent and submerged vegetation in eutrophic shallow lakes using Landsat imagery. *Remote Sens. Environ.* 287, 113480. doi: 10.1016/j.rse.2023.113480

Moss, B., Jeppesen, E., Søndergaard, M., Lauridsen, T. L., and Liu, Z. (2012). Nitrogen, macrophytes, shallow lakes and nutrient limitation: resolution of a current controversy? *Hydrobiologia.* 710, 3–21. doi: 10.1007/s10750-012-1033-0

Olsen, S., Chan, F., Li, W., Zhao, S., Søndergaard, M., and Jeppesen, E. (2015). Strong impact of nitrogen loading on submerged macrophytes and algae: a long-term mesocosm experiment in a shallow Chinese lake. *Freshw. Biol.* 60, 1525–1536. doi: 10.1111/fwb.12585

Qu, X., Chen, Y., Liu, H., Xia, W., Lu, Y., Gang, D. D., et al. (2020). A holistic assessment of water quality condition and spatiotemporal patterns in impounded lakes along the eastern route of China's South-to-North water diversion project. *Water Res.* 185, 116275. doi: 10.1016/j.watres.2020.116275

Riis, T., and Biggs, B. J. F. (2003). Hydrologic and hydraulic control of macrophyte establishment and performance in streams. *Limnol. Oceanogr.* 48, 1488–1497. doi: 10.4319/lo.2003.48.4.1488

Roman, C. T., Barrett, N. E., and Portnoy, J. W. (2001). Aquatic vegetation and trophic condition of Cape Cod (Massachusetts, U.S.A.) kettle ponds. *Hydrobiologia.* 443, 31–42. doi: 10.1023/A:1017540002675

Sayer, C. D., Burgess, A. M. Y., Kari, K., Davidson, T. A., Peglar, S., Yang, H., et al. (2010). Long-term dynamics of submerged macrophytes and algae in a small and shallow, eutrophic lake: implications for the stability of macrophyte-dominance. *Freshw. Biol.* 55, 565–583. doi: 10.1111/j.1365-2427.2009.02353.x

Scheffer, M., Hosper, S. H., Meijer, M.-L., Moss, B., and Jeppesen, E. (1993). Alternative equilibria in shallow lakes. *Trends Ecol. Evol.* 8, 275–279. doi: 10.1016/0169-5347(93)90254-M

Søndergaard, M., Johansson, L. S., Lauridsen, T. L., JØrgensen, T. B., Liboriussen, L., and Jeppesen, E. (2010). Submerged macrophytes as indicators of the ecological quality of lakes. *Freshw. Biol.* 55, 893–908. doi: 10.1111/j.1365-2427.2009.02331.x

Søndergaard, M., Peder, J. J., and Jeppesen, E. (2003). Role of sediment and internal loading of phosphorus in shallow lakes. *Hydrobiologia.* 343, 506–509. doi: 10.1023/B:HYDR.0000008611.12704.dd

Soria, J., Jover, M., and Domínguez-Gómez, J. A. (2021). Influence of wind on suspended matter in the water of the albufera of valencia (Spain). *J. Mar. Sci. Eng.* 9, 343. doi: 10.3390/jmse9030343

Su, H., Zhu, T. S., Bai, X. H., Ni, L., Xie, P., and Zhang, X. L. (2018). Seed germination indicates adaptive transgenerational plasticity in a submerged macrophyte. *Front. Plant Sci.* 9. doi: 10.3389/fpls.2018.01592

Su, H. J., Chen, J., Wu, Y., Chen, J. F., Guo, X. C., Yan, Z. B., et al. (2019). Morphological traits of submerged macrophytes reveal specific positive feedbacks to water clarity in freshwater ecosystems. *Sci. Total Environ.* 684, 578–586. doi: 10.1016/j.scitotenv.2019.05.267

Temmink, R. J. M., Dorenbosch, M., Lamers, L. P. M., Smolders, A. J. P., Rip, W., Lengkeek, W., et al. (2021). Growth forms and life-history strategies predict the occurrence of aquatic macrophytes in relation to environmental factors in a shallow peat lake complex. *Hydrobiologia.* 848, 3987–3999. doi: 10.1007/s10750-021-04618-6

Tian, C. C., Guo, C. B., and Wu, X. Q. (2019). Distribution of submerged plants and its relationship with environmental factors in Gaoyou Lake. *Acta Hdrobiologica sinica.* 43, 423–430. doi: 10.7541/2019.052

Van Zuidam, B. G., and Peeters, E. T. H. M. (2015). Wave forces limit the establishment of submerged macrophytes in large shallow lakes. *Limnol. Oceanogr.* 60, 1536–1549. doi: 10.1002/lno.10115

Wang, S. S., Gao, Y. N., Li, Q., Gao, J. F., Zhai, S. H., Zhou, Y., et al. (2019). Long-term and inter-monthly dynamics of aquatic vegetation and its relation with environmental factors in Taihu Lake, China. *Sci. Total Environ.* 651, 367–380. doi: 10.1016/j.scitotenv.2018.09.216

Wang, L. Z., Liu, Q. J., Hu, C. W., Liang, R. J., Qiu, J. C., and Wang, Y. (2018). Phosphorus release during decomposition of the submerged macrophyte Potamogeton crispus. *Limnology.* 19, 355–366. doi: 10.1007/s10201-018-0538-2

Wang, J. Q., Song, Y. Z., and Wang, G. X. (2017). Causes of large Potamogeton crispus L. population increase in Xuanwu Lake. *Environ. Sci. pollut. Res.* 24, 5144–5151. doi: 10.1007/s11356-016-6514-7

Woolf, T. E., and Madsen, J. D. (2003). Seasonal biomass and carbohydrate allocation patterns in southern minnesota curlyleaf pondweed populations. *J. Aquat. Plant Manage.* 41, 113–118.

Wu, H. P., Hao, B. B., Jo, H., and Cai, Y. P. (2021). Seasonality and species specificity of submerged macrophyte biomass in shallow lakes under the influence of climate warming and eutrophication. *Front. Plant Sci.* 12. doi: 10.3389/fpls.2021.678259

Wu, D., and Hua, Z. L. (2014). The effect of vegetation on sediment resuspension and phosphorus release under hydrodynamic disturbance in shallow lakes. *Ecol. Eng.* 69, 55–62. doi: 10.1016/j.ecoleng.2014.03.059

Xia, W., Zhu, B., Zhang, S., Liu, H., Qu, X., Liu, Y., et al. (2022). Climate, hydrology, and human disturbance drive long-term, (1988-2018) macrophyte patterns in water diversion lakes. *J. Environ. Manage.* 319, 115726. doi: 10.1016/j.jenvman.2022.115726

Xie, D., Yu, D., You, W. H., and Wang, L. G. (2013). Algae mediate submerged macrophyte response to nutrient and dissolved inorganic carbon loading: a mesocosm study on different species. *Chemosphere.* 93, 1301–1308. doi: 10.1016/j.chemosphere.2013.07.008

Yan, Z. W., Wang, Q. Y., Li, Y., Wu, L., Wang, J. N., Xing, B., et al. (2021). Combined effects of warming and nutrient enrichment on water properties, growth, reproductive strategies and nutrient stoichiometry of Potamogeton crispus. *Environ. Exp. Bot.* 190, 104572. doi: 10.1016/j.envexpbot.2021.104572

Yang, Y. Q., Yu, D., Li, Y. K., Xie, Y. H., and Geng, X. H. (2004). Phenotypic plasticity of two submersed plants in response to flooding. *J. Freshw. Ecol.* 19, 69–76. doi: 10.1080/02705060.2004.9664514

Yu, Q. Z., Dong, J., Liu, E. F., Zhou, L., Liang, C. L., Zhang, H. Z., et al. (2017). Analysis on vegetation spatio-temporal variation of Nansi Lake based on MODIS. *For. Resour. Management.*, 144–152. doi: 10.13466/j.cnki.lyzygl.2017.01.023

Yu, Q., Wang, H. Z., Li, Y., Shao, J. C., Liang, X. M., Jeppesen, E., et al. (2015). Effects of high nitrogen concentrations on the growth of submersed macrophytes at moderate phosphorus concentrations. *Water Res.* 83, 385–395. doi: 10.1016/j.watres.2015.06.053

Zhang, P. Y., Bakker, E. S., Zhang, M., and Xu, J. (2016). Effects of warming on Potamogeton crispus growth and tissue stoichiometry in the growing season. *Aquat. Bot.* 128, 13–17. doi: 10.1016/j.aquabot.2015.08.004

Zhang, Y. L., Jeppesen, E., Liu, X. H., Qin, B. Q., Shi, K., Zhou, Y. Q., et al. (2017). Global loss of aquatic vegetation in lakes. *Earth Sci. Rev.* 173, 259–265. doi: 10.1016/j.earscirev.2017.08.013

Zhang, Y. L., Liu, X. H., Qin, B. Q., Shi, K., Deng, J. M., and Zhou, Y. Q. (2016). Aquatic vegetation in response to increased eutrophication and degraded light climate in Eastern Lake Taihu: Implications for lake ecological restoration. *Sci. Rep.* 6, 23867. doi: 10.1038/srep23867

Zhu, G. R., Zhang, M., Cao, T., and Ni, L. Y. (2015). Associations between the morphology and biomechanical properties of submerged macrophytes: implications for its survival and distribution in Lake Erhai. *Environ. Earth Sci.* 74, 3907–3916. doi: 10.1007/s12665-015-4267-0

frontiers | Frontiers in Plant Science

TYPE Original Research
PUBLISHED 25 July 2024
DOI 10.3389/fpls.2024.1404718



OPEN ACCESS

EDITED BY
Jun Xu,
Chinese Academy of Sciences (CAS), China

REVIEWED BY
Hong Chang,
Beijing Forestry University, China
Lan Wang,
Chinese Academy of Sciences (CAS), China
Bo-Tao Zhang,
Beijing Normal University, China

*CORRESPONDENCE
Hailei Su
suhailei666@163.com
Yuan Wei
weiyuanshiwo@126.com

RECEIVED 21 March 2024
ACCEPTED 03 July 2024
PUBLISHED 25 July 2024

CITATION
Fang H, Zhen Z, Yang F, Su H and Wei Y (2024) Epiphytic bacterial community composition on four submerged macrophytes in different regions of Taihu Lake.
*Front. Plant Sci.* 15:1404718.
doi: 10.3389/fpls.2024.1404718



# Epiphytic bacterial community composition on four submerged macrophytes in different regions of Taihu Lake

Hongda Fang[1], Zhuo Zhen[2], Fan Yang[2], Hailei Su[3]* and Yuan Wei[3]*

[1]College of Harbour and Coastal Engineering, Jimei University, Xiamen, China, [2]Key Laboratory of Urban Environment and Health, Institute of Urban Environment, Chinese Academy of Sciences, Xiamen, China, [3]State Key Laboratory of Environmental Criteria and Risk Assessment, Chinese Research Academy of Environmental Sciences, Beijing, China

The epiphytic bacteria in aquatic ecosystems, inhabiting a unique ecological niche with significant ecological function, have long been the subject of attention. Habitat characteristics and plant species are believed to be important in controlling the assembly of epiphytic bacteria. However, the underlying principle governing the assembly of the epiphytic bacterial community on macrophytes is far from clear. In this study, we systematically compared the diversity and community composition of epiphytic bacteria both in different habitats and on different species of macrophytes where they were attached. Results suggested that neither the plant species nor the habitat had a significant effect on the diversity and community of epiphytic bacteria independently, indicating that the epiphytic bacterial community composition was correlated to both geographical distance and individual species of macrophytes. Furthermore, almost all of the abundant taxa were shared between different lake regions or macrophyte species, and the most abundant bacteria belonged to Proteobacteria and Firmicutes. Our results demonstrated that the competitive lottery model may explain the pattern of epiphytic bacterial colonization of submerged macrophyte surfaces. This research could provide a new perspective for exploring plant–microbe interaction in aquatic systems and new evidence for the lottery model as the mechanism best explaining the assembly of epiphytic bacteria.

KEYWORDS

**epiphytic bacteria, submerged macrophyte, host-specificity, habitat heterogeneity, lottery model**

# 1 Introduction

Submerged macrophytes, providing a linkage between sediment and overlying water, play an important role in the biological productivity and stability of the structure and function of aquatic ecosystems (Horppila and Nurminen, 2003). They are also used as indicators of the ecological quality of lakes because they have a clear response to eutrophication (Søndergaard et al., 2010). Furthermore, submerged macrophytes with a large surface area enhanced the density of surface-associated organisms, such as algae, invertebrates, and bacteria (Jeppesen, 1998). In aquatic systems, a large number of bacteria, which were described as epiphytic bacteria in previous studies (Andrews and Harris, 2000; Pollard, 2010), inhabit surfaces of submerged macrophytes. According to previous studies, epiphytic bacteria exhibited a higher diversity and a distinct community composition compared to the surrounding bacterioplankton (He et al., 2014; Levi et al., 2017) and play important ecological roles in aquatic ecosystems (Ma et al., 2021). Moreover, epiphytic bacteria may also have complex interactions with their host plants. These interactions are manifested as competitive, mutualistic, and commensalistic (Wijewardene et al., 2022). Despite these findings, epiphytic biofilms are understudied compared to other periphytic biofilms in freshwater ecosystems (Wijewardene et al., 2022). Ignoring the understanding of the role macrophytes play as a substrate for epiphytic bacteria may underestimate the importance of macrophytes in freshwater ecosystems.

For decades, the relationship between epibiotic bacterial community and environmental factors (including host plants, spatial and geographical heterogeneity) and hypotheses regarding bacterial community assembly has been studied extensively (Knief et al., 2010; He et al., 2012; Liao et al., 2016; Levi et al., 2017). However, due to differences in research emphasis and technical matters, there were some inconsistencies and even contradictory conclusions in different scientific reports. Therefore, the relationship between bacterial composition and host plants/habitats, and the mechanisms of community assembly are still poorly understood. There are two theories explaining the mechanism of bacterial community assembly. One is the traditional niche-based theory, which emphasizes abiotic and biotic factors, such as environmental physicochemical properties, habitat heterogeneity, and species interactions (Ramette and Tiedje, 2007; Dumbrell et al., 2010; Gilbert et al., 2012). The other is the neutral theory that only considers random processes, such as birth, death, colonization, immigration, and speciation or dispersal limitations (Vanwonterghem et al., 2014). Recent investigations have suggested that both neutral and niche processes play a critical role in the assembly of entire bacterial communities (Liao et al., 2016). In the case of epiphytic bacteria, some studies demonstrated that the composition of the epiphytic bacterial community may be influenced by the host plant and habitat heterogeneity (Hempel et al., 2008), while other studies suggested that plant-specific effects could shape the composition of epiphytic bacteria on aquatic plants (He et al., 2012; Yu et al., 2022). These references provided valuable information about the complex interaction between epiphytic bacteria and their host plants. However, few studies have systematically investigated the influence of habitat heterogeneity and plant–host specificity on the community composition of epiphytic bacteria. Given that situation, we questioned whether different host plants or their respective habitat determined the epiphytic bacterial community composition.

In the study, we collected four species of submerged macrophytes (*Ceratophyllum demersum*, *Vallisneria natans*, *Myriophyllum verticillatum*, and *Potamogeton crispus*) from three regions of Taihu Lake with different trophic status. This work aimed to 1) ascertain whether macrophyte species or their habitats determine epiphytic bacterial community composition, 2) investigate the mechanisms of assembly for epiphytic bacteria, and 3) give directions to further research.

# 2 Materials and methods

## 2.1 Study sites and sample collection

Taihu Lake, the third largest shallow freshwater lake (2,338 km$^2$, average depth 1.9 m) in China, is located in the Yangtze River Delta (Qin et al., 2007). There are strong environmental gradients and habitat patterns in Taihu Lake (Dong et al., 2017). In this study, samples were collected from three regions of Taihu Lake: Wuli Lake (W), Southern Taihu (ST), and Eastern Taihu Lake (ET) (Figure 1). Wuli Lake, an arm of Meiliang Bay in the north of Taihu Lake, is a hyper-eutrophic bay located in Wuxi City. The Southern Taihu Lake features less embayment, little macrophyte coverage, and relatively good water quality and is classified as mesotrophic water. Eastern Taihu Lake, a shallow macrophyte-dominated bay and the area where the dilution water flows out of the lake (Hu et al.,

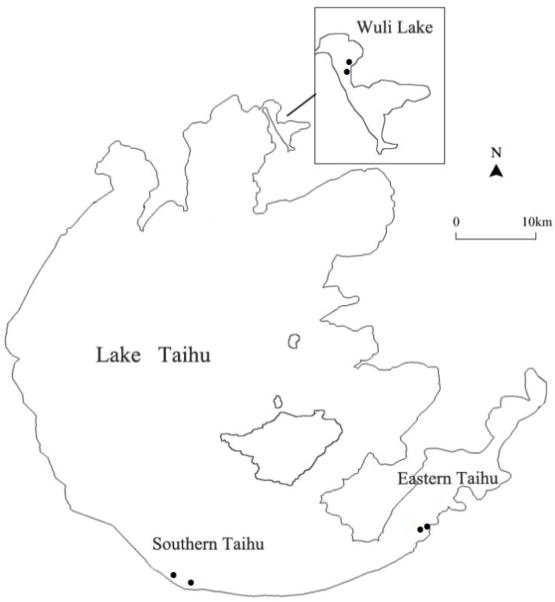


FIGURE 1
Map of Lake Taihu showing the sampling locations in Southern Taihu Lake, Eastern Taihu Lake, and Wuli Lake.

2010), is generally considered the least nutrient-impacted region of Taihu Lake.

Four macrophytes were collected by hand or hook on July 24–26, 2016. For each plant species, three to five individual plants at a similar growth stage were collected randomly in three selected regions of Taihu Lake and Wuli Lake (Table 1). Plants were stored individually in sterile plastic bags on ice and transported to the laboratory. Water parameters such as pH, temperature, chlorophyll-*a*, and conductivity were measured using a multi-parameter water quality analyzer (YSI 6600v2) prior to sample collection (Supplementary Table S1).

## 2.2 Detachment of epiphytic biofilm

Epiphytic bacteria attached to submerged macrophytes were collected following the method previously described in published literature (Hempel et al., 2009; He et al., 2012). Briefly, 2 g of each macrophyte with similar growth vigor was selected and rinsed with sterile deionized water three times to remove large particles adhering to the plant surface. Then, the macrophytes were transferred to a sterile 50-mL polyethylene tube containing 40 mL of sodium pyrophosphate (0.1 mol/L $Na_4P_2O_7{\cdot}10H_2O$, NaPPi). The epiphytic bacteria were detached by ultra-sonication for 3 min, followed by 30 min of shaking (225 r/min) and subsequent 3 min of ultra-sonication. The suspensions were filtered onto a 0.22-μm polycarbonate membrane (Millipore, Billerica, MA, USA) to collect the detached epiphytic bacteria and stored at −20°C for DNA extraction.

## 2.3 DNA extraction and PCR amplification

DNA was extracted using the Fast DNA® SPIN Kit for Soil (MP Biomedicals, Irvine, CA, USA) according to the manufacturer's protocol. The extracted DNA samples were stored at −20°C for further molecular analyses.

TABLE 1 Plant species and sampling locations.

| Site description | Plant species | Sample code |
|---|---|---|
| Eastern Taihu Lake | *Myriophyllum verticillatum* | ET-M |
| | *Vallisneria natans* | ET-V |
| | *Potamogeton crispus* | ET-P |
| Southern Taihu Lake | *Myriophyllum verticillatum* | ST-M |
| | *Vallisneria natans* | ST-V |
| | *Potamogeton crispus* | ST-P |
| | *Ceratophyllum demersum* | ST-C |
| Wuli Lake | *Myriophyllum verticillatum* | W-M |
| | *Vallisneria natans* | W-V |
| | *Ceratophyllum demersum* | W-C |

PCR was performed to amplify the variable regions of the bacterial 16S rRNA gene (V3–V4) with the primers 341 F (5′-CCTAYGGGRBGCASCAG-3′) and 806R (5′-GGACTACNN GGGTATCTAAT-3′) with sample-identifying barcodes. The PCR mixture with a total volume of 50 μL that included 5 μL of 10× Buffer KOD, 1.5 mM $MgSO_4$, 0.2 mM dNTPs, 0.3 μM each of the forward and reverse primers, 1.0 U of KOD DNA Polymerase, 100–300 ng of DNA template, and double-distilled water ($ddH_2O$). The reaction was performed as follows: initial incubation step at 94°C for 2 min; followed by 30 cycles of denaturation at 98°C for 10 sec, annealing at 65°C for 30 sec, and extension at 68°C for 30 sec; and final extension at 68°C for 5 min. PCR products were further purified with Agencourt AMPure XP Beads (Beckman Coulter, Brea, CA, USA), and the concentrations were quantified using the ABI StepOnePlus Real-Time PCR System (Life Technologies, Carlsbad, CA, USA). The purified PCR products were combined at equimolar ratios and submitted to Gene Denovo Biotechnology Company (Guangzhou, China) for sequencing on the Illumina HiSeq 2500 PE250 platform.

## 2.4 Sequence analysis

The raw data were filtered and assembled. Raw data obtained after sequencing included dirty reads containing adapters or low-quality bases. Reads with N bases accounting for more than 10% or low quality (containing less than 80% of bases with Q-value > 20) were filtered from the raw data. The filtered reads were then assembled into tags according to the overlap between paired-end reads. The redundant tags were removed from raw tags to obtain unique tags using Mothur (v.1.34.0). The obtained unique tags were then used to calculate the abundance. Operational taxonomic units (OTUs) (97% identity) were clustered using unique tags by Mothur (v.1.34.0) (Schloss et al., 2009). Sequences were taxonomically classified using a 0.5 confidence threshold against the RDP Database (DeSantis et al., 2006). Sequence data have been deposited in the National Center for Biotechnology Information (NCBI) Sequence Read Archive (SRA) database under BioProject PRJNA513113 (sample accession numbers SAMN10696321–SAMN10696330).

## 2.5 Definition of abundant, rare, and conditionally rare taxa

Microbial communities are normally composed of a few abundant and many rare species, and these two subcommunities may have fundamentally different characteristics and ecological roles (Logares et al., 2014). In this study, we defined and classified all OTUs into six categories in accordance with previous studies (Dai et al., 2016; Xue et al., 2018). Briefly, the OTUs with an abundance ≥ 1% in all samples were defined as abundant taxa (ATs); the OTUs with an abundance<0.01% in all samples were defined as rare taxa (RTs); the OTUs with an abundance between 0.01 and 1% in all samples were defined as moderate taxa (MTs); the OTUs with an abundance below 1% in all samples and<0.01% in

some samples were defined as conditionally rare taxa (CRTs); the OTUs with abundance ≥0.01% in all samples and ≥1% in some samples but never rare (<0.01%) were defined as conditionally abundant taxa (CATs); OTUs with abundance varying from rare (<0.01%) to abundant (≥1%) were defined as conditionally rare and abundant taxa (CRATs). In this study, we combined ATs, CATs, CRATs, and MTs as ATs to perform further analyses.

## 2.6 Analysis of community diversity

To investigate the diversity of epiphytic bacteria, the α-diversity (including Chao1, ACE, Simpson, and Shannon indices) was calculated for each sample (Kemp and Aller, 2004). To assess sample adequacy, rarefaction curves (3% distance cutoff) were also constructed. Rarefaction curves and α-diversity were performed using Mothur (v.1.34.0). One-way analysis of variance (ANOVA) was performed using SPSS 20.0 (IBM Corp., Armonk, NY, USA) to test the habitat and host plant effects on epiphytic bacterial community composition. The Venn diagram was used to depict the similarities and differences between communities. The Venn diagram was constructed based on the epiphytic bacteria of different submerged macrophytes and different habitats.

First, the Bray–Curtis similarity matrix was calculated to determine the similarity of the epiphytic bacterial community composition between the samples at the OTU level. The cluster analysis based on the Bray–Curtis coefficient was used to investigate the phylogenetic composition differences of microbial communities among 10 samples. Then, the Bray–Curtis similarity matrix was calculated based on samples within the same habitat or the same host plant. The non-metric multidimensional scaling (NMDS) analysis was employed for detecting possible differences in epiphytic bacterial community composition among different habitats and host plants. Analysis of similarities (ANOSIM) was performed to evaluate the significant difference ($p < 0.01$) between groups. Complete separation is indicated by $R = 1$, whereas $R = 0$ indicates no separation (Chen et al., 2017). The NMDS analysis and ANOSIM were performed using the PRIMER v.6.0 package. For this analysis, the data sets ATs, CRTs, and RTs were used.

## 2.7 Niche breadth

Studies have shown that the microbial communities of habitat specialists are more vulnerable to disturbance than those of habitat generalists (Logares et al., 2013; Liu et al., 2017). In this study, to measure habitat specialization, the niche breadth was calculated according to the following formula (Levins, 1968):

$$B_j = \frac{1}{\sum_{i=1}^{N} P_{ij}^2}$$

where *Bj* is the niche breadth and *Pij* is the percentage of the individuals of species *j* present in habitat *i*. The OTUs with mean relative abundances $\leqq 2 \times 10^{-5}$ were excluded from the analysis, as these taxa may appear to be specialized even if they are not. In this study, there are three types of lake regions with each type representing a habitat.

Species with higher and lower values of niche breadth can be considered generalists and specialists, respectively (Pandit et al., 2009). Compared with habitat specialists, habitat generalists exhibited a more even distribution along a broader range of habitats. Therefore, we classified OTUs as habitat generalists and specialists according to outlier detection.

## 2.8 Predicted functional profiles

Given the need to predict the Kyoto Encyclopedia of Genes and Genomes (KEGG) Orthology (KO) functional profiles of microbial communities, Phylogenetic Investigation of Communities by Reconstruction of Unobserved States (PICRUSt) was developed (Kemp and Aller, 2004). KEGG pathway variability between different habitats or host plants was compared using NMDS or ANOSIM, respectively.

# 3 Result

## 3.1 Taxonomic composition of epiphytic bacterial communities

A total of 515,407 high-quality sequence reads were obtained from all 10 samples and were clustered into 30,435 OTUs based on a 97% similarity level. The sequences that could be annotated to the family level in all 10 samples ranged from 58.51% to 92.00%; therefore, "family" was chosen as the best classification level for the 10 samples (Supplementary Figure S1).

Significant differences in bacterial abundance among the 10 samples were found in accordance with the bacterial distribution at different taxonomic levels (Figure 2). At the phylum level, Proteobacteria were the most dominant group in all 10 samples, which occupied 40.12% (epiphytic bacteria of *C. demersum* in Southern Taihu Lake) to 82.35% (epiphytic bacteria of *V. natans* in Eastern Taihu Lake). The major phyla were Firmicutes (1.56% to 49.05% in each sample), Bacteroidetes (2.42% to 12.84%), Actinobacteria (0.23% to 5.62%), Planctomycetes (0.25% to 4.09%), and Cyanobacteria (0.16% to 23.45%) (Figure 2A). Although the abundances of phyla were significantly different between samples, the composition was similar. Furthermore, Alphaproteobacteria, Betaproteobacteria, and Gammaproteobacteria were the dominant classes of Proteobacteria occupying more than 97.9% of Proteobacteria (Figure 2B). At the family level, Bacillaceae and Aeromonadaceae belonging to Firmicutes and Proteobacteria, respectively, were dominant in epiphytic bacteria (Figure 2D).

## 3.2 Epiphytic bacterial diversity

The coverage of the 10 samples ranged from 88.60% to 98.45%, suggesting that there still may be some microbes remaining undetermined (Supplementary Table S2). Rarefaction curves of

10.3389/fpls.2024.1404718

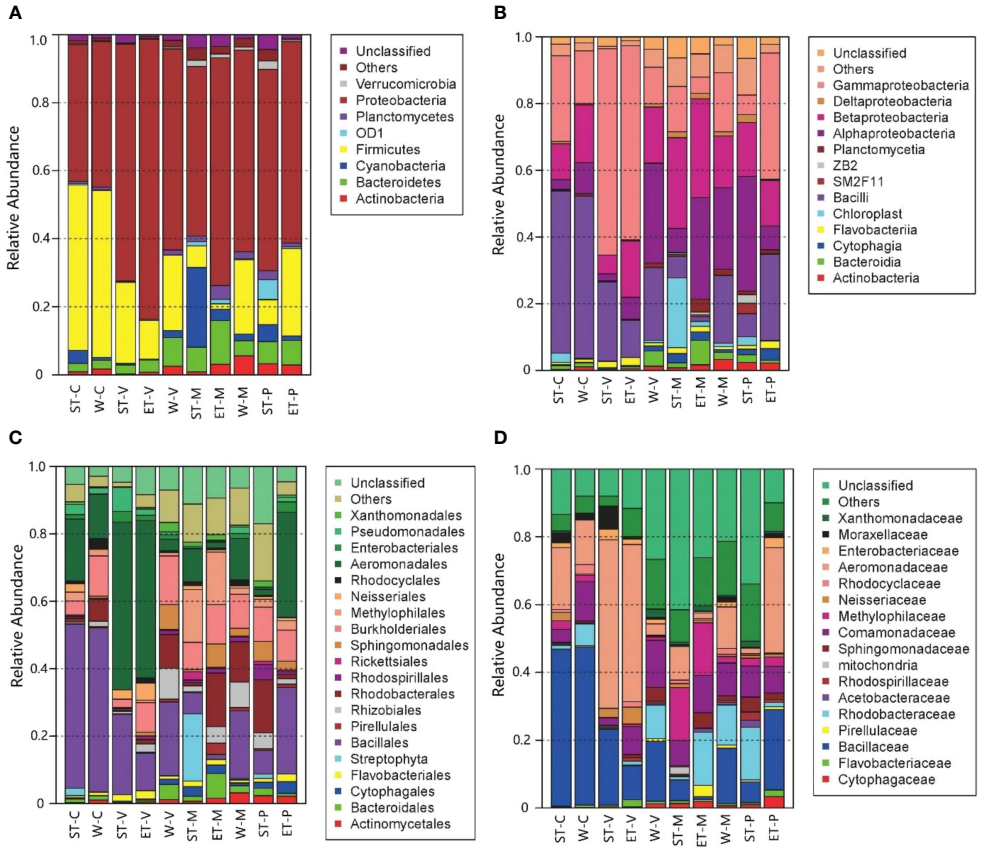


FIGURE 2
Distribution of epiphytic bacteria in different samples at different taxonomic levels. **(A)** Phylum level, **(B)** class level, **(C)** order level, and **(D)** family level. "Others" refers to the taxa with maximum abundance<2% in any sample. Sequences that could not be classified into any known group were assigned as "Unclassified".

the 10 samples did not approach saturation at the 0.03 cutoff level, indicating that the amount of sequencing data was not enough to cover all of the sampled species and that a greater bacterial diversity existed in the samples (Supplementary Figure S2).

The diversity and community richness of epiphytic bacteria were reflected by the Chao1, ACE, Shannon–Wiener, and Simpson indices. The average community richness indices (number of OTUs, ACE, and Chao 1) in Wuli Lake were higher than in Eastern Taihu Lake and Southern Taihu Lake (Figure 3). The Shannon–Wiener index ranged from 4.27 to 6.00 (average 4.92) for Eastern Taihu Lake, 2.85 to 6.42 (average 4.36) for Southern Taihu Lake, and 3.37 to 6.22 (average 5.21) for Wuli Lake (Figure 3). The average Simpson index in Southern Taihu Lake (0.14) was higher than that in Wuli Lake (0.10) and Eastern Taihu Lake samples (0.08) (Figure 3). However, no statistically significant difference ($p > 0.05$) was observed in diversity indices, suggesting similar species richness and equitability between different lake regions. The one-way ANOVA indicated that neither habitat nor host plant had a significant effect on the alpha-diversity indices (including OTU number, Chao 1, ACE, Shannon–Wiener diversity index, and Simpson diversity index) (Supplementary Table S3).

For the bacterial taxa, the distribution characteristics of the three categories identified were as follows: i) 50 (0.16%) OTUs with 290,715 (56.40%) sequences were recognized as ATs, ii) 2,932 (9.63%) OTUs with 175,681 (34.09%) sequences were defined as CRTs, and iii) as many as 27,453 (90.20%) OTUs with 49,011 (9.51%) sequences were classified as RTs (Supplementary Table S4).

## 3.3 Variations of epiphytic bacterial community composition

To estimate the patterns of bacterial compositional dissimilarity between samples, the cluster analysis based on the Bray–Curtis coefficient was employed (Supplementary Figure S3). Interestingly, among component communities, epiphytic bacterial communities did not group according to host plant or habitat.

In terms of relative abundance, our results revealed that all three subcommunities (abundance, conditionally rare, and rare taxa) did not cluster strongly by host plant or habitat, especially the rare subcommunity (Figure 4A), which was confirmed by the ANOSIM comparison between epiphytic bacterial subcommunities (Table 2). In abundant taxa, Wuli Lake showed a striking separation compared to the other two lake regions, especially Southern Taihu, which suggested that the abundant bacterial subcommunities were vulnerable to environmental variations (Figure 4A).

Venn analyses were employed to evaluate the similarity of diversity and community composition between the epiphytic

10.3389/fpls.2024.1404718

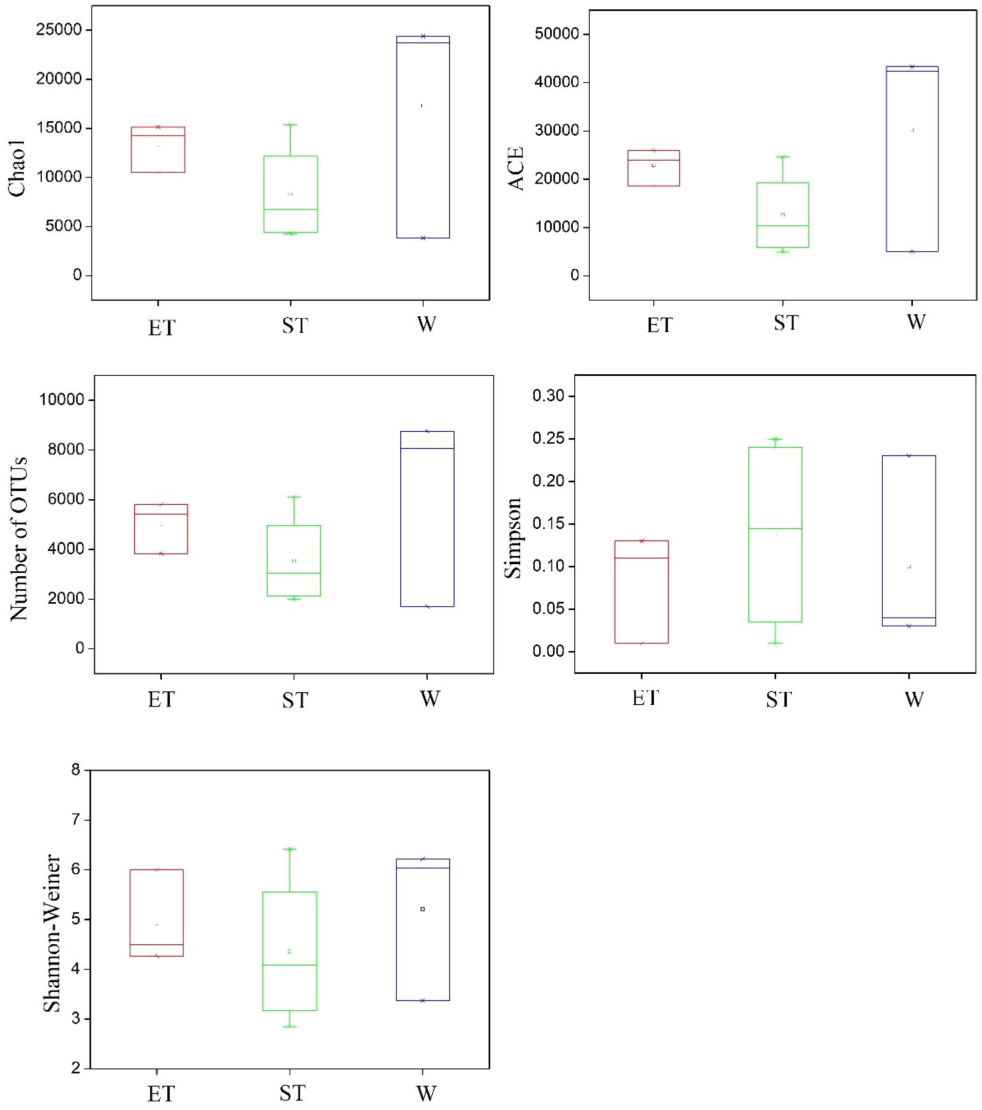


FIGURE 3
Comparison of alpha-diversity of the epiphytic bacterial communities among three different lake regions. The operational taxonomic units (OTUs) were defined at 97% sequence similarity threshold. The ends of the box represent the 25th and 75th percentiles, the whiskers represent minimum and maximum range, and the center lines represent the median.

bacterial communities according to lake regions or macrophyte species (Figures 4B, C). In the case of the three lake regions, almost all abundant taxa (48 OTUs out of 50 OTUs) were shared among habitats, and most of the unique OTUs belonged to either conditionally rare taxa or rare taxa (Figure 4B). A similar pattern was displayed for the epiphytic bacterial community composition according to macrophyte species (Figure 4C).

Microhabitat niche breadth ranged from 1.00 to 2.98 (Figure 5A). The niche breadth of epiphytic bacteria displayed variability at different host plants (Figure 5A). Mean niche breadth values of epiphytic bacteria were the highest in the host plant *M. verticillatum* (B = 1.45) and *V. natans* (B = 1.44), followed by *C. demersum* (B = 1.25) and *P. crispus* (B = 1.18). For all of the host plants, it could be observed that there were more OTUs identified as habitat specialists than habitat generalists (Figure 5B).

## 3.4 Functional annotation and categorization

In order to compare functional differences among different samples, biological functions were predicted and annotated with KEGG pathways. In total, all the OTUs to 139 KEGG pathways were assigned. The most highly represented category was "metabolism pathways", occupying 66% to 69%, suggesting that the epibiotic bacteria have strong metabolic activity (Supplementary Table S6 and Figure 6A). The "Environmental Information Processing" pathways were also well presented, accounting for 17% to 20% (Supplementary Table S6 and Figure 6A). The predicted functional distribution was not grouped based on either the lake regions or the type of macrophytes (Figure 6B), indicating that neither the habitats nor the host plants could significantly influence bacterial functional groups, which is confirmed by the

10.3389/fpls.2024.1404718

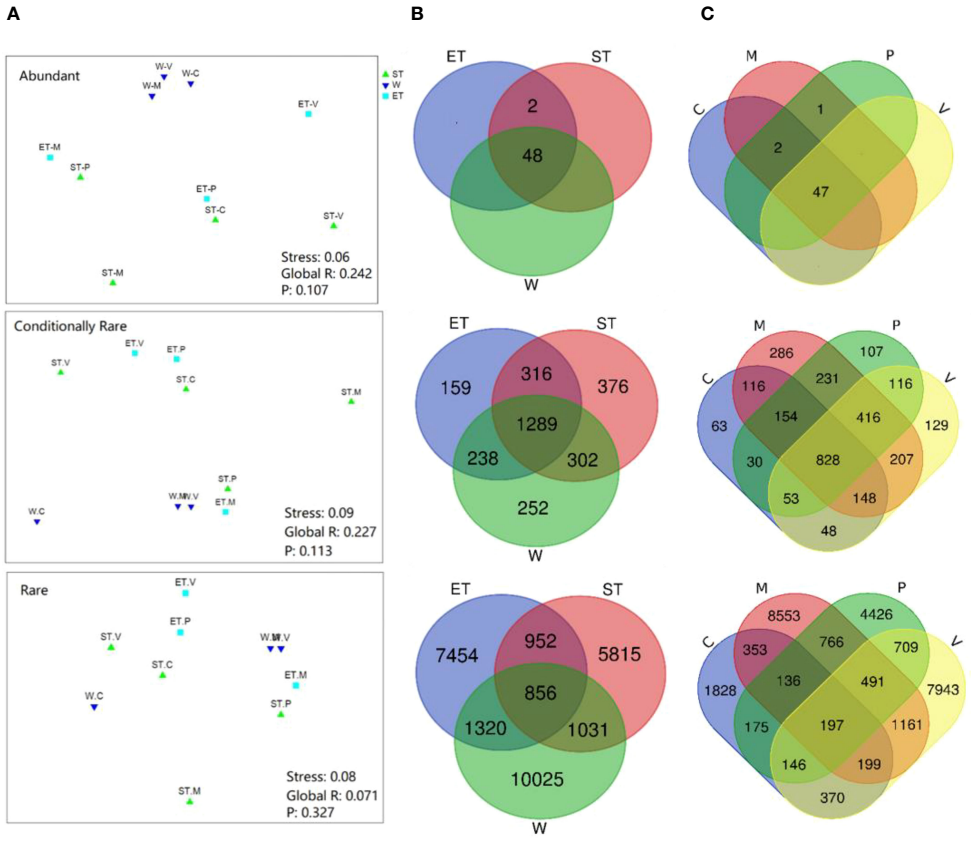


FIGURE 4
Comparison of beta-diversity of the epiphytic bacterial community among different habitats or host plants. **(A)** Non-metric multidimensional scaling (NMDS) ordination of epiphytic bacterial communities based on the Bray–Curtis dissimilarity. **(B)** Venn diagram showing the shared bacterial operational taxonomic units (OTUs) between three habitats (48 abundant OTUs, 1,289 conditionally rare OTUs, and 856 rare OTUs). **(C)** Venn diagram showing the shared bacterial OTUs between four different types of submerged macrophytes (47 abundant OTUs, 828 conditionally rare OTUs, and 197 rare OTUs).

**TABLE 2** Results of the ANOSIM and the pairwise analyses comparing epiphytic bacterial communities among different host plants and habitats.

| Groups | Abundant taxa | Conditionally rare taxa | Rare taxa |
|---|---|---|---|
| C vs. V | 0 | 0.167 | −0.167 |
| C vs. M | 0.25 | 0 | 0.167 |
| C vs. P | 0.5 | 0 | 0.25 |
| V vs. M | 0.593 | 0.333 | 0.111 |
| V vs. P | 0 | −0.083 | −0.25 |
| M vs. P | −0.083 | −0.333 | −0.417 |
| ST vs. W | 0.407* | 0.259 | 0.13 |
| ST vs. ET | −0.019 | 0.093 | 0.093 |
| W vs. ET | 0.296 | 0.296 | 0 |

The operational taxonomic units (OTUs) were defined at 97% sequence similarity threshold. Values show the R-value, and asterisks denote significant differences at the $p < 0.05$ level. ANOSIM, analysis of similarities.

ANOSIM comparisons between differentially abundant KEGG pathways (Supplementary Table S5).

# 4 Discussion

Many reports have described the diversity and community composition of epiphytic bacteria on submerged macrophytes. Most studies focused on comparing the composition of the epiphytic bacterial community from either different macrophytes (Ma et al., 2008; He et al., 2012; Gordon-Bradley et al., 2014) or different habitats (Hempel et al., 2008; Levi et al., 2017). However, the current understanding of epiphytic biofilm–macrophyte-specific relationships is far from sufficient. In this study, we aimed to systematically investigate whether different macrophytes or their habitats determine epiphytic bacteria assembly, which will provide clues for understanding the epiphytic biofilm–macrophyte interactions and their roles in freshwater ecosystems.

## 4.1 Effects of different habitats on epiphytic bacterial community

Previous studies have demonstrated that variations in habitats strongly influenced the composition of bacterial communities

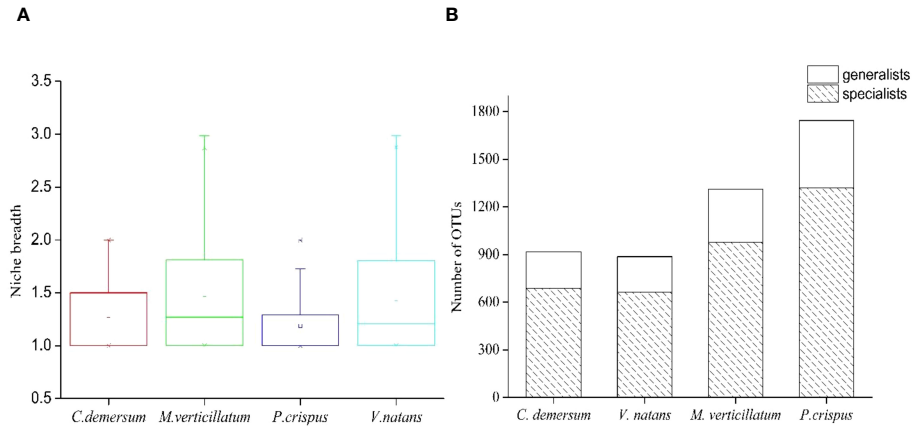


FIGURE 5
Habitat specialization of different operational taxonomic units (OTUs) based on niche breadth. **(A)** Distribution of niche breadth values of epiphytic bacteria that attached to different host plants. **(B)** The OTU number of generalists and specialists belonged to different host plants.

(Hempel et al., 2008; Levi et al., 2017). Physical habitat characteristics can affect the composition and abundance of epiphytic bacteria by creating microhabitats (Levi et al., 2017). In contrast, our results showed that the composition of the epiphytic bacterial community was not significantly different between different habitats, and the ANOSIM found no significant intra-lake heterogeneity in microbial community structure at different relative abundances (abundant, conditionally rare, and rare taxa) except for the Wuli Lake region and Southern Taihu lake region in abundance taxa (Table 2). Cai et al. (2013) obtained similar results when investigating the epiphytic bacterial community structure of *Potamogeton malaianus* Miq. at two lake regions in Taihu Lake. In our study, all the taxa with different relative abundances did not display a separation pattern between groups, whereas the taxa exhibited different responses to the habitats (Figure 4A). Typically, the abundant taxa occupy a broad niche and are capable of competitively utilizing a series of limited resources, thus providing driving mechanisms for specific ecological processes (Qin et al., 2022; Zhu et al., 2023). Moreover, the abundant taxa could be more sensitive in response to environmental filtering during colonization (Zhu et al., 2023). In this study, Wuli Lake had a higher degree of eutrophication than the other two lake regions, and the physicochemical properties of lake water differ significantly; therefore, the abundant taxa of Wuli Lake showed a striking separation compared to the other two lake regions. Xian et al. (2018) reported that epiphytic bacteria exhibited a higher diversity in a lower-nutrient environment, which was due to the plant status at different nutrient states. In our experiment, the epibiotic bacteria of macrophytes, which were collected from the least nutrient-impacted region (Eastern Taihu Lake), did not always exhibit higher diversity (Supplementary Table S2 and Figure 3). In brief, the habitats did not have a decisive influence on epiphytic bacterial community composition.

Furthermore, more habitat specialists than generalists were found in the epiphytic bacterial community (Figure 5B). Habitat specialists are predicted to be more vulnerable to disturbance than habitat generalists and exhibit specific environmental fitness (Swihart et al., 2003; Michael et al., 2015). Due to the weak ecological tolerance capacity, the specialists were easily affected by environmental disturbance. A recent study showed that habitat specialists showed stronger distance-decay patterns and weaker environmental adaptation than habitat generalists and exhibited higher network complexity and modularity when suffering from environmental stress (Sun et al., 2024). Therefore, when habitats change, the resulting microbial community of epiphytic bacteria is likely to be filled by a series of habitat specialists, which would change the community composition and function.

The reasons for the highly similar epiphytic bacterial community composition between different habitats may be due to the following: i) the epiphytic bacteria not only can absorb nutrients from water but also can use the organic compounds and nutrients secreted by the macrophytes, which may reduce the effects of different habitats on epiphytic bacteria (Cai et al., 2013). ii) The epiphytic bacterial communities may have relatively strong resistance to environmental pressure, thus weakening the environmental fluctuation of the surrounding water (Dong et al., 2014). iii) The epiphytic bacterial communities are also related to the growth state and morphology of the host plant (Crump and Koch, 2008; Lachnit et al., 2011; He et al., 2012).

## 4.2 Effects of plant species on epiphytic bacterial community

Several studies indicated that the different physical or biochemical characteristics of leaves could result in host-specific communities on different plant species (Lachnit et al., 2011; He et al., 2014). In our study, we saw a more complex picture. The ANOSIM suggested that there were no significant differences in community structure at three relative abundances (abundant, conditionally rare, and rare taxa) between different host plants (Table 2). However, epiphytic bacterial communities on *C. demersum* from two lake regions (Southern Taihu Lake and Wuli Lake) showed a similar community composition and appeared to be

10.3389/fpls.2024.1404718

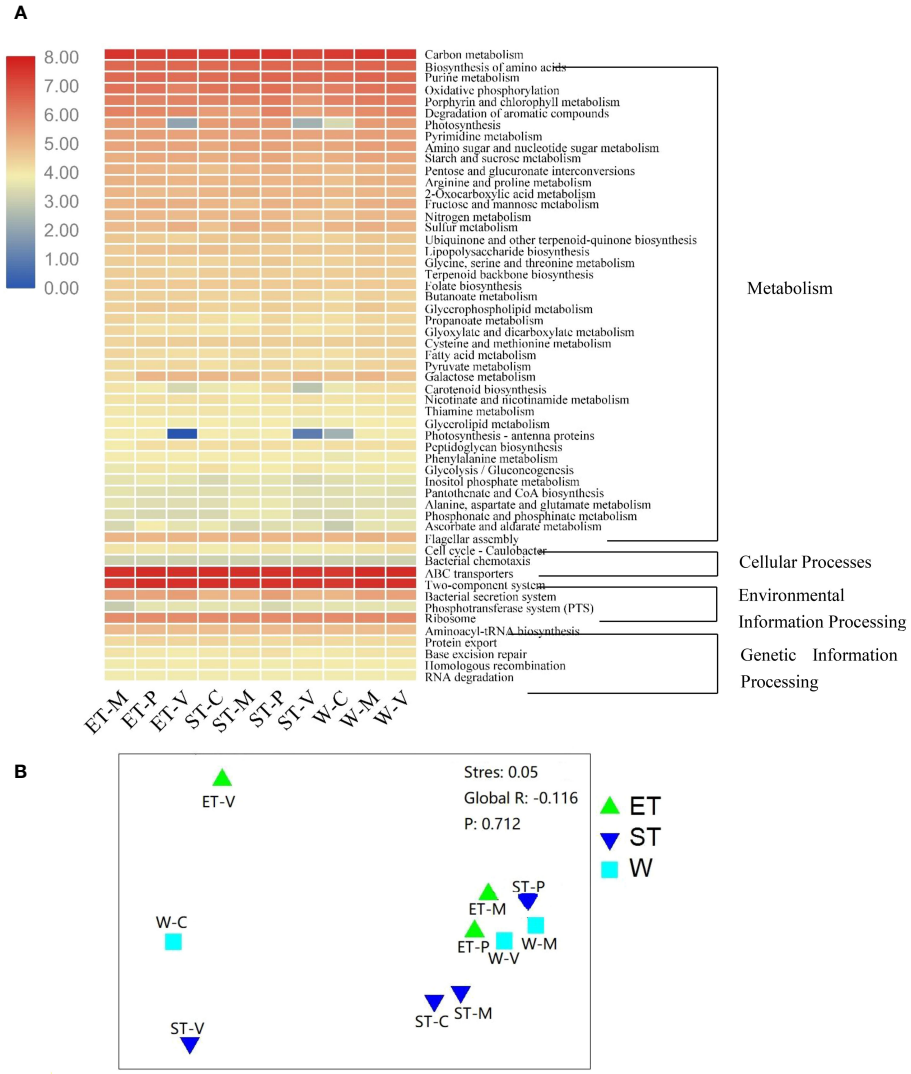


FIGURE 6
**(A)** Heatmap of differentially abundant Kyoto Encyclopedia of Genes and Genomes (KEGG) pathways among different samples. KEGG pathways with obvious increasing or decreasing trends are displayed in red or blue colors, respectively. **(B)** Non-metric multidimensional scaling (NMDS) analysis based on the calculated Bray–Curtis dissimilarities between the functional gene family abundances of samples.

host-specific (Figure 2 and Supplementary Figure S3). Furthermore, the bacterial diversity and bacterial community structure of the four submerged macrophytes were not typical and stable as expected (Supplementary Table S2). For instance, the Shannon diversity index showed that *V. natans* had the greatest diversity in Wuli Lake and the lowest diversity in Southern Taihu Lake.

The epiphytic bacteria *M. verticillatum* and *V. natans* displayed a wider niche range than the epiphytic bacteria *C. demersum* and *P. crispus*, suggesting that the epiphytic bacteria *M. verticillatum* and *V. natans* were able to occupy a greater range of habitat types (Figure 5A). Hence, species with broader niche breadth had a higher probability of dispersal, thereby resulting in widespread or ubiquitous distribution.

These results indicated that there were sophisticated relationships between epibiotic bacteria and their host plants. To be specific, the epiphytic bacteria on *C. demersum* appear to be host-specific, while epiphytic bacteria on the other three submerged macrophytes were not significantly related to the host plant (Figure 2 and Supplementary Figure S3). The reason may be that the epiphytic bacteria occupy a special ecological niche where they can acquire nutrients from both water body and plant tissues. Hence, the variations in epiphytic bacterial communities may be related to macrophyte species, habitat conditions, or a combination of these factors depending on which factor is overwhelming.

## 4.3 Variation in functional potential of epibiotic bacteria

The predicted functional communities were not separated, as expected, based on habitats or macrophyte species when examining the functions of the epiphytic bacteria (Figure 6B). These pathways have been adapted to respond to a wide variety of stimuli. Theoretically, the physicochemical properties of the water body

seem to be an essential factor in the functional variation. However, when contrasting the predicted functional variability of epiphytic bacteria, a stable functional distribution was found across different lake regions and macrophyte species (Figure 6A, Supplementary Tables S5; S6). This is congruent with previous research on a marine system, where functional categories were found to be evenly distributed across different zones, while taxonomic compositions varied markedly between subjects (Sunagawa et al., 2015).

In this study, the community composition of all the samples exhibited high variability (Figure 3), while the functional categories displayed a stable distribution (Figure 6). This suggested that although microbial communities within the same ecosystem may not be identical, their functions may exhibit a high degree of similarity, which is known as "functional redundancy" (Louca et al., 2018; Zhu et al., 2024). These findings were consistent with the redundancy hypothesis, which assumes that there are more than one species sharing common biogeochemical attributes within an ecosystem, thereby conferring ecosystem functions a degree of resilience to disturbance (Naeem, 1998). Moreover, we also observed striking differences among the samples even in the same habitat (Figures 2 and 4A), which could not be explained by the neutral model. Therefore, we suggested that the "lottery hypothesis" may be an appropriate model to be able to explain the assembly of epiphytic bacteria. This hypothesis asserts that species with similar ecologies will occupy a niche within an ecosystem based on stochastic recruitment (Brum and Esteves, 2001). Neutral models of community assembly also work on the assumption of ecological equivalence. The difference is that the neutral model assumes the ecological equivalence broadly, while the lottery model makes this assumption for defined groups of species sharing a particular niche (Brum and Esteves, 2001). More specifically, in the lottery model, there is functional redundancy in an ecosystem, and those bacteria that happen to encounter and occupy the surface of macrophytes first are those that will subsequently colonize it.

## 5 Conclusion

Results indicated that the composition of epiphytic bacterial communities was related to macrophyte species, habitat conditions, or a combination of these factors depending on which factor is overwhelming. There are restrictions and limitations with previous studies that emphasized host specificity or environmental heterogeneity in epiphytic bacterial community composition. The assembly strategies of epiphytic bacteria are much more complex than we expected. We believe that there are three main reasons for these inconsistencies: limitations of technology, finite set of samples, and the diversity and complexity of the environment. Our work provided a new perspective for exploring plant–microbe interaction in aquatic systems. This research also provided new evidence for the lottery model as the mechanism that best explains the assembly of epiphytic bacteria.

## Data availability statement

The original contributions presented in the study are included in the article/Supplementary Material. Further inquiries can be directed to the corresponding authors.

## Author contributions

HF: Data curation, Investigation, Methodology, Validation, Writing – original draft. ZZ: Software, Writing – review & editing. FY: Investigation, Writing – review & editing. HS: Resources, Writing – review & editing. YW: Writing – review & editing.

## Funding

The author(s) declare financial support was received for the research, authorship, and/or publication of this article. This study was financially supported by the National Key Research and Development Program of China (Nos. 2022YFF1301304 and 2021YFC3200104) and the Opening fund of the State Key Laboratory of Environmental Criteria and Risk Assessment (sklecra2016ofp05).

## Conflict of interest

The authors declare that the research was conducted in the absence of any commercial or financial relationships that could be construed as a potential conflict of interest.

## Publisher's note



## Supplementary material

The Supplementary Material for this article can be found online at: https://www.frontiersin.org/articles/10.3389/fpls.2024.1404718/full#supplementary-material

# References


Andrews, J. H., and Harris, R. F. (2000). The ecology and biogeography of microorganisms on plant surfaces. *Annu. Rev. Phytopathol.* 38, 145–180. doi: 10.1146/annurev.phyto.38.1.145

Brum, P. R., and Esteves, F. A. (2001). Changes in abundance and biomass of the attached bacterial community throughout the decomposition of three species of aquatic macrophytes. *Oecol. Bras.* 9, 7. doi: 10.4257/oeco

Cai, X., Gao, G., Tang, X., Dong, B., and Song, Y. (2013). The response of epiphytic microbes to habitat and growth status of Potamogeton malaianus Miq. in Lake Taihu. *J. Basic Microbiol.* 53, 828–837. doi: 10.1002/jobm.201200220

Chen, W. D., Pan, Y. B., Yu, L. Y., Yang, J., and Zhang, W. J. (2017). Patterns and processes in marine microeukaryotic community biogeography from Xiamen coastal waters and intertidal sediments, Southeast China. *Front. Microbiol.* 8. doi: 10.3389/fmicb.2017.01912

Crump, B. C., and Koch, E. W. (2008). Attached bacterial populations shared by four species of aquatic angiosperms. *Appl. Environ. Microbiol.* 74, 5948–5957. doi: 10.1128/AEM.00952-08

Dai, T. J., Zhang, Y., Tang, Y. S., Bai, Y. H., Tao, Y. L., Huang, B., et al. (2016). Identifying the key taxonomic categories that characterize microbial community diversity using full-scale classification: a case study of microbial communities in the sediments of Hangzhou Bay. *FEMS Microbiol. Ecol.* 92 (10), fiw.150. doi: 10.1093/femsec/fiw150

DeSantis, T. Z., Hugenholtz, P., Larsen, N., Rojas, M., Brodie, E. L., Keller, K., et al. (2006). Greengenes, a chimera-checked 16S rRNA gene database and workbench compatible with ARB. *Appl. Environ. Microbiol.* 72, 5069–5072. doi: 10.1128/AEM.03006-05

Dong, B. L., Qin, B. Q., Li, W., and Gao, G. (2017). Growth and community composition of submerged macrophytes in Lake Taihu (China): assessment of changes in response to sediment characteristics. *Wetlands* 37, 233–243. doi: 10.1007/s13157-016-0861-5

Dong, B., Han, R., Wang, G., and Gao, X. (2014). O2, pH, and redox potential microprofiles around Potamogeton malaianus measured using microsensors. *PloS One.* 9 (7), e101825. doi: 10.1371/journal.pone.0101825

Dumbrell, A., Nelson, M., Helgason, T., Dytham, C., and Fitter, A. H. (2010). Relative roles of niche and neutral processes in structuring a soil microbial community. *ISME J.* 4, 337–345. doi: 10.1038/ismej.2009.122

Gilbert, J. A., Steele, J. A., Caporaso, J. G., Steinbrück, L., Reeder, J., Temperton, B., et al. (2012). Defining seasonal marine microbial community dynamics. *ISME J.* 6, 298–308. doi: 10.1038/ismej.2011.107

Gordon-Bradley, N., Lymperopoulou, D. S., and Williams., H. N. (2014). Differences in Bacterial Community Structure on Hydrilla verticillata and Vallisneria americana in a Freshwater Spring. *Microbes Environ.* 29, 67–73. doi: 10.1264/jsme2.ME13064

He, D., Ren, L. J., and Wu, Q. L. (2012). Epiphytic bacterial communities on two common submerged macrophytes in Taihu Lake: diversity and host-specificity. *Chin. J. Oceanol. Limnol.* 30, 237–247. doi: 10.1007/s00343-012-1084-0

He, D., Ren, L. J., and Wu, Q. L. (2014). Contrasting diversity of epibiotic bacteria and surrounding bacterioplankton of a common submerged macrophyte, Potamogeton crispus, in freshwater lakes. *FEMS Microbiol. Ecol.* 90, 551–562. doi: 10.1111/fem.2014.90.issue-3

Hempel, M., Blume, M., Blindow, I., and Gross, E. M. (2008). Epiphytic bacterial community composition on two common submerged macrophytes in brackish water and freshwater. *BMC Microbiol.* 8, 58. doi: 10.1186/1471-2180-8-58

Hempel, M., Grossart, H. P., and Gross, E. M. (2009). Community composition of bacterial biofilms on two submerged macrophytes and an artificial substrate in a pre-alpine lake. *Aquat. Microb. Ecol.* 58, 79–94. doi: 10.3354/ame01353

Horppila, J., and Nurminen, L. (2003). Effects of submerged macrophytes on sediment resuspension and internal phosphorus loading in Lake Hiidenvesi (southern Finland). *Water Res.* 37, 4468–4474. doi: 10.1016/S0043-1354(03)00405-6

Hu, L. M., Hu, W. P., Zhai, S. H., and Wu, H. Y. (2010). Effects on water quality following water transfer in Lake Taihu, China. *Ecol. Eng.* 36, 471–481. doi: 10.1016/j.ecoleng.2009.11.016

Jeppesen, E. (1998). *The structuring role of submerged macrophytes in lakes* (Springer: New York).

Kemp, P. F., and Aller, J. Y. (2004). Bacterial diversity in aquatic and other environments: what 16S rDNA libraries can tell us. *FEMS Microbiol. Ecol.* 47, 161–177. doi: 10.1016/S0168-6496(03)00257-5

Knief, C., Ramette, A., Frances, L., Alonso-Blanco, C., and Vorholt, J. A. (2010). Site and plant species are important determinants of the Methylobacterium community composition in the plant phyllosphere. *ISME J.* 4, 719–728. doi: 10.1038/ismej.2010.9

Lachnit, T., Meske, D., Wahl, M., Harder, T., and Schmitz, R. (2011). Epibacterial community patterns on marine macroalgae are host-specific but temporally variable. *Environ. Microbiol.* 13, 655–665. doi: 10.1111/j.1462-2920.2010.02371.x

Levi, P. S., Starnawski, P., Poulsen, B., Baattrup-Pedersen, A., Schramm, A., and Riis, T. (2017). Microbial community diversity and composition varies with habitat characteristics and biofilm function in macrophyte-rich streams. *Oikos* 126, 398–409. doi: 10.1111/oik.03400

Levins, R. (1968). *Evolution in changing environments: some theoretical explorations* (New Jersey: Princeton University Press). doi: 10.1515/9780691209418

Liao, J. Q., Cao, X. F., Zhao, L., Wang, J., Gao, Z., Wang, M. C., et al. (2016). The importance of neutral and niche processes for bacterial community assembly differs between habitat generalists and specialists. *FEMS Microbiol. Ecol.* 92 (11), fiw174. doi: 10.1093/femsec/fiw174

Liu, M., Yu, Z., Yu, X. Q., Xue, Y. Y., Huang, B. Q., and Yang, J. (2017). Invasion by cordgrass increases microbial diversity and alters community composition in a mangrove nature reserve. *Front. Microbiol.* 8, 2503. doi: 10.3389/fmicb.2017.02503

Logares, R., Audic, S., Bass, D., Bittner, L., Boutte, C., Christen, R., et al. (2014). Patterns of rare and abundant marine microbial eukaryotes. *Curr. Biol.* 24, 813–821. doi: 10.1016/j.cub.2014.02.050

Logares, R., Lindström, E. S., Langenheder, S., Logue, J. B., Paterson, H., Laybourn-Parry, J., et al. (2013). Biogeography of bacterial communities exposed to progressive long-term environmental change. *ISME J.* 7, 937–948. doi: 10.1038/ismej.2012.168

Louca, S., Polz, M. F., Mazel, F., Albright, M. B., Huber, J. A., O'Connor, M. I., et al. (2018). Function and functional redundancy in microbial systems. *Nat. Ecol. Evol.* 2, 936–943. doi: 10.1038/s41559-018-0519-1

Ma, J., Shi, R. J., Han, R. M., Ji, M., Xu, X. G., and Wang, G. X. (2021). Community structure of epiphytic bacteria on and the surrounding bacterioplankton in Hongze Lake. *Mar. Freshw. Res.* 72, 997–1003. doi: 10.1071/MF20212

Ma, J. F., Yamaji, N., Mitani, N., Xu, X. Y., Su, Y. H., McGrath, S. P., et al. (2008). Transporters of arsenite in rice and their role in arsenic accumulation in rice grain. *Proc. Natl. Acad. Sci. U. S. A.* 105, 9931–9935. doi: 10.1073/pnas.0802361105

Michael, D. R., Kay, G. M., Crane, M., Florance, D., MacGregor, C., Okada, S., et al. (2015). Ecological niche breadth and microhabitat guild structure in temperate Australian reptiles: Implications for natural resource management in endangered grassy woodland ecosystems. *Austral Ecol.* 40, 651–660. doi: 10.1111/aec.12232

Naeem, S. (1998). Species redundancy and ecosystem reliability. *Conserv. Biol.* 12, 39–45. doi: 10.1111/j.1523-1739.1998.96379.x

Pandit, S. N., Kolasa, J., and Cottenie, K. (2009). Contrasts between habitat generalists and specialists: an empirical extension to the basic metacommunity framework. *Ecology* 90, 2253–2262. doi: 10.1890/08-0851.1

Pollard, P. C. (2010). Bacterial activity in plant (Schoenoplectus validus) biofilms of constructed wetlands. *Water Res.* 44, 5939–5948. doi: 10.1016/j.watres.2010.07.047

Qin, B., Xu, P., Wu, Q., Luo, L., and Zhang, Y. (2007). Environmental issues of Lake Taihu, China. *Hydrobiologia* 581, 3–14. doi: 10.1007/s10750-006-0521-5

Qin, Z. R., Zhao, Z. H., Xia, L. L., Wang, S. Y., Yu, G. W., and Miao, A. H. (2022). Responses of abundant and rare prokaryotic taxa in a controlled organic contaminated site subjected to vertical pollution-induced disturbances. *Sci. Total Environ.* 853, 158625. doi: 10.1016/j.scitotenv.2022.158625

Ramette, A., and Tiedje, J. M. (2007). Multiscale responses of microbial life to spatial distance and environmental heterogeneity in a patchy ecosystem. *Proc. Natl. Acad. Sci. U. S. A.* 104, 2761–2766. doi: 10.1073/pnas.0610671104

Schloss, P. D., Westcott, S. L., Ryabin, T., Hall, J. R., Hartmann, M., Hollister, E. B., et al. (2009). Introducing mothur: open-source, platform-independent, community-supported software for describing and comparing microbial communities. *Appl. Environ. Microbiol.* 75, 7537–7541. doi: 10.1128/AEM.01541-09

Søndergaard, M., Johansson, L. S., Lauridsen, T. L., Jørgensen, T. B., Liboriussen, L., and Jeppesen, E. (2010). Submerged macrophytes as indicators of the ecological quality of lakes. *Freshw. Biol.* 55, 893–908. doi: 10.1111/j.1365-2427.2009.02331.x

Sun, J. X., Zhou, H. B., Cheng, H. N., Chen, Z., and Wang, Y. G. (2024). Distinct strategies of the habitat generalists and specialists in the Arctic sediments: Assembly processes, co-occurrence patterns, and environmental implications. *Mar. pollut. Bull.* 205, 116603. doi: 10.1016/j.marpolbul.2024.116603

Sunagawa, S., Coelho, L. P., Chaffron, S., Kultima, J. R., Labadie, K., Salazar, G., et al. (2015). Structure and function of the global ocean microbiome. *Science* 348 (6237), 1261359. doi: 10.1126/science.1261359

Swihart, R. K., Gehring, T. M., Kolozsvary, M. B., and Nupp, T. E. (2003). Responses of 'resistant'vertebrates to habitat loss and fragmentation: the importance of niche breadth and range boundaries. *Divers. Distrib.* 9, 1–18. doi: 10.1046/j.1472-4642.2003.00158.x

Vanwonterghem, I., Jensen, P., Dennis, P., Hugenholtz, P., Rabaey, K., and Tyson, G. (2014). Deterministic processes guide long-term synchronised population dynamics in replicate anaerobic digesters. *ISME J.* 8, 2015–2028. doi: 10.1038/ismej.2014.50

Wijewardene, L., Wu, N., Fohrer, N., and Riis, T. (2022). Epiphytic biofilms in freshwater and interactions with macrophytes: Current understanding and future directions. *Aquat. Bot.* 176, 103467. doi: 10.1016/j.aquabot.2021.103467

Xian, L., Wan, T., Cao, Y., Sun, J., Wu, T., Zhao, S., et al. (2018). Structural variability and functional association in the epiphytic bacteria assemblies of freshwater macrophytes (Myriophyllum spicatum). *bioRxiv* 316893. doi: 10.1101/316893

Xue, Y. Y., Chen, H. H., Yang, J. R., Liu, M., Huang, B. Q., and Yang, J. (2018). Distinct patterns and processes of abundant and rare eukaryotic plankton communities following a reservoir cyanobacterial bloom. *ISME J.* 12, 2263–2277. doi: 10.1038/s41396-018-0159-0

Yu, W. C., Li, J. H., Ma, X. W., Lv, T., Wang, L. G., Li, J. R., et al. (2022). Community structure and function of epiphytic bacteria attached to three submerged macrophytes. *Sci. Total Environ.* 835, 155546. doi: 10.1016/j.scitotenv.2022.155546

Zhu, L., Li, W., Huang, C. H., Tian, Y., and Xi, B. D. (2024). Functional redundancy is the key mechanism used by microorganisms for nitrogen and sulfur metabolism during manure composting. *Sci. Total Environ.* 912, 169389. doi: 10.1016/j.scitotenv.2023.169389

Zhu, M. H., Qi, X., Yuan, Y. B., Zhou, H. Y., Rong, X. F., Dang, Z., et al. (2023). Deciphering the distinct successional patterns and potential roles of abundant and rare microbial taxa of urban riverine plastisphere. *J. Hazard Mater.* 450, 131080. doi: 10.1016/j.jhazmat.2023.131080

frontiers | Frontiers in Plant Science

TYPE Original Research
PUBLISHED 15 January 2025
DOI 10.3389/fpls.2024.1500947



OPEN ACCESS

EDITED BY
Jun Xu,
Chinese Academy of Sciences (CAS), China

REVIEWED BY
Milan Szabo,
HUN-REN Biological Research Centre, Hungary
Kazuhiro Kogame,
Hokkaido University, Japan

*CORRESPONDENCE
Shinya Yoshikawa
syoshika@fpu.ac.jp

RECEIVED 24 September 2024
ACCEPTED 17 December 2024
PUBLISHED 15 January 2025

CITATION
Maegawa Y, Takahashi F, Hiyama T and Yoshikawa S (2025) Night-break treatment with blue and green lights regulates erect thallus formation in the brown alga *Petalonia fascia* (KU-1293). *Front. Plant Sci.* 15:1500947. doi: 10.3389/fpls.2024.1500947



# Night-break treatment with blue and green lights regulates erect thallus formation in the brown alga *Petalonia fascia* (KU-1293)

Yuya Maegawa[1], Fumio Takahashi[2], Tsunami Hiyama[1] and Shinya Yoshikawa[1*]

[1]Faculty of Marine Science and Technology, Fukui Prefectural University, Obama, Fukui, Japan, [2]Faculty of Pharmaceutical Sciences, Toho University, Funabashi, Chiba, Japan

In this study, we investigated the photoperiodic responses regulating erect thallus formation in *Petalonia fascia* (KU-1293). We found that, through critical day length analysis and night break treatment culture experiments, *P. fascia* formed erect thalli under short-day conditions, indicating a genuine photoperiodic response. The critical day length for this morphological change was 10–11 h. Notably, night-break treatment with blue light (BL) and green light (GL) inhibited, whereas that with red light (RL) enhanced erect thallus formation. *P. fascia* was more sensitive to BL than to GL, requiring approximately 100-times less light to exhibit similar effects. Furthermore, promotion of erect thallus formation by RL was not negated by far-red light, suggesting the presence of a novel RL receptor distinct from the classical phytochrome system in terrestrial plants. These findings highlight the complexity of light wavelength interactions in regulating photoperiodic responses and suggest the presence of unique photoreceptors for day-length perception and erect thallus formation in *P. fascia*.

KEYWORDS

**photomorphogenesis, blue light receptor, green light receptor, phaeophyceae, photoperiodism**

## Introduction

Brown algae are among the major primary producers in coastal ecosystems. Similar to land plants, alternating generation and morphology in response to physical conditions, such as light, temperature, and dehydration, are important for the environmental adaptation of immobile brown algae. Seasonal changes are among the most influential environmental factors for brown algae. They sense the seasonal transitions based on day length, regulate physiological activities, and alternate generations. Many studies have investigated photoperiodism in land plants, with most focusing on morphological formation, such as flower bud formation and fruit ripening (Thomas and Vince-Prue,

1997). The response of an organism to day length is known as photoperiodism. Many studies have reported photoperiodism in animals, fungi and terrestrial plants (Nelson et al., 2010). In angiosperms, night-break (NB) treatment, which involves a short period of light irradiation in the middle of the dark period, is among the most useful methods for photoperiodism analysis (Thomas and Vince-Prue, 1997). As the day length affects the total amount of photosynthetic products involved in growth and physiological functions, NB treatment helps in determining whether certain morphogenesis is induced by a photoperiodic response (photoperiodism) (Parker et al., 1950). Moreover, NB treatment with monochromatic light helps to identify the photoreceptors controlling photoperiodic responses (Parker et al., 1945). In land plants, photoperiodically controlled responses are dependent on photoreceptors rather than photosynthesis. Analysis of the NB action spectrum revealed that photoperiodicity in short-day (SD) plants is regulated by the perception of phytochromes to red light (RL) and far-red light (FR) (Thomas and Vince-Prue, 1997).

To date, only physiological experiments have been conducted on brown algae, with only a few studies investigating photoreceptors using molecular biology techniques. Photomorphogenesis controlled by the photoperiod has been reported in several genera of brown algae, including erect thallus formation in *Scytosiphon lomentaria* (Dring and Lüning, 1975a), gamete formation in *Sphacelaria rigidula* (Ten Hoopen et al., 1983), sorus formation in *Saccharina* and *Undaria* (Lüning, 1986, Lüning, 1988; Pang and Lüning, 2004), stem elongation in *Sargassum muticum* (Hwang and Dring, 2002), and receptacle initiation in *Ascophyllum nodosum* and *Sargassum horneri* (Terry and Moss, 1980; Yoshikawa et al., 2014). These reports suggest that the photoperiod is an essential environmental factor affecting the seasonality of brown algae and that brown algae possess photoreceptors to perceive day length. However, the specific receptor molecules involved in photoperiodism in brown algae remain elusive. This is due to the scarcity of studies analyzing the wavelengths controlling photoperiodism in brown algae (Dring and Lüning, 1975a; Terry and Moss, 1980; Yoshikawa et al., 2014) despite the important effect of light quality on photoperiodic responses and photoreceptor molecules.

Analysis of the effect of NB treatment on erect thallus formation in *S. lomentaria* revealed that the photoperiodic responses are regulated only by blue light (BL) (Dring and Lüning, 1975a). In contrast, NB treatment with RL and BL induces receptacle formation in *A. nodosum* (Terry and Moss, 1980). We previously showed that NB treatment with green light (GL) and BL effectively initiates receptacle formation in *Sargassum horneri* (Yoshikawa et al., 2014). However, whether brown algae have common photoreceptors associated with photoperiodism remains unclear. Moreover, differences in light quality related to photoperiodism hinder the comprehensive understanding of photoperiodism in brown algae. To determine the photoreceptors controlling photoperiodism in brown algae, we focused on the photoperiodic responses affecting erect thallus formation in *Petalonia fascia* in this study. A previous study reported that *P. fascia* forms an erect thallus from a discoid thallus under SD conditions (Roeleveld et al., 1974), suggesting that the erect thallus formation is a photoperiodic response in *P. fascia*. However, detailed physiological analysis of the photoperiodism of *P. fascia* has not yet been performed. Here, we analyzed the effects of various light intensities and qualities on erect thallus formation and photoperiodic responses in *P. fascia*.

# Materials and methods

## Materials

A strain of *P. fascia* (KU-1293) was obtained from the Kobe University Macro-Algal Collection.

## Culture conditions

For subculture, *P. fascia* was cultured in the ESI medium (Tatewaki, 1966) without Tris at 15°C under 30 μmol photons $m^{-2}$ $s^{-1}$ fluorescent lamp light (FL20SSEX-D; Toshiba, Tokyo, Japan) and long-day (LD) conditions (16 h light and 8 h dark). The same temperature conditions and medium were used in all experiments. Thalli were pinched off from the subculture and incubated in a flask with 100 mL medium for two weeks as a pre-culture.

## Light–dark cycle and NB treatment

To determine whether erect thallus formation depends on photoperiodism, we investigated erect thallus formation using critical day length and NB treatment. The pre-cultured discoid thalli of *P. fascia* were statically cultured in a 24-well plate (14530; Thermo Fisher Scientific, MA, USA) under 30 μmol photons $m^{-2}$ $s^{-1}$ fluorescent lamp light and various light: dark regimes from 9:15 h to 16:8 h. After 24 d, erect thallus formation rate was calculated by dividing the number of erect thalli formed in a well by the amount of chlorophyll a (μg) in the same well. The number of erect thalli within the well was counted using a stereomicroscope (SZX-10; Olympus, Tokyo, Japan) equipped with a digital camera (DP12; Olympus). Chlorophyll a content of the well was calculated from the absorbance values using 90% acetone (Jeffrey and Humphrey, 1975). In NB treatment, 1-h light was provided 7 h after the start of the dark period under short-day conditions (SD, 10 h light and 14 h dark). The following light sources were used for NB: white light (WL), BL (LED illuminators ISL-150×150-BB LED illuminators; peak wavelength: 472 nm; full width at half maximum: 24 nm; CCS Inc., Kyoto, Japan), GL (QFC45-100PG; peak wavelength: 531 nm; full width at half maximum: 21 nm; ACETEC, Tokyo, Japan) with a sharp cut-off filter (SC52; Fujifilm, Tokyo, Japan), RL (ISL-150×150-RR; peak wavelength: 654 nm; full width at half maximum: 18 nm; CCS), and FR (ISL-150×150-FR; peak wavelength: 738 nm; full width at half maximum: 27 nm; CCS).

10.3389/fpls.2024.1500947

Intensity of each light source was adjusted by changing the distance between the light source and plate or using an ND filter (ND-0.1; Fujifilm). Light intensity in NB treatment with BL, GL, and RL was 10 μmol photons $m^{-2}$ $s^{-1}$. Light intensity in NB treatment with FR was 50 μmol photons $m^{-2}$ $s^{-1}$. Emission spectra (Supplementary Figure 1) and photon fluence rates of the light sources used for NB treatment were measured using the Light Analyser LA-105 (Nippon Medical & Chemical Instruments Co., Ltd., Osaka, Japan). To assess the difference in sensitivity to BL and GL, effects of different durations (60–3600 s) of NB treatment with various intensities (0.1–10 μmol photons $m^{-2}$ $s^{-1}$) of BL and GL on erect thallus formation were examined (Supplementary Table 1).

Significant differences among groups were analyzed using one-way analysis of variance, followed by the Bonferroni test.

## *In vivo* absorption spectrum

The *in vivo* absorption spectrum of discoid thallus was acquired with Spectrophotometer U-3300 (Hitachi, Ltd., Tokyo, Japan). Thalli were suspended in the culture medium and placed in a 10-mm path-length cuvette. Absorbance was recorded at 1-nm intervals across 400 to 700 nm wavelengths. To obtain the relative absorption spectrum, the absorbance at 437 nm, which showed the highest value, was normalized to 1, and the absorbance at 700 nm, which showed the lowest value, was normalized to 0.

# Results

## Erect thallus formation under SD conditions

Consistent with previous reports (Roeleveld et al., 1974), almost all thalli of *P. fascia* were discoid (disc thalli) under LD (Figure 1A), and erect thalli were formed only under SD conditions (Figure 1B). Erect thalli grew directly from the discoid thalli. Erect thallus formation was low under LD conditions and high under SD conditions.

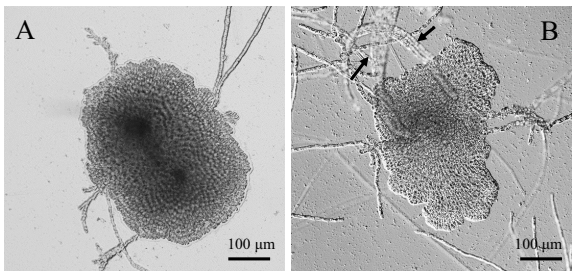


FIGURE 1
Photoperiod-dependent changes in the morphology of *Petalonia fascia*. **(A)**. Discoid thalli under long-day (LD) conditions. **(B)**. Erect thalli (arrows) produced on the discoid thalli under short-day (SD) conditions.

## Critical day length for erect thallus formation

Discoid thalli were cultured for various day lengths to determine the critical day length for erect thallus formation (Figure 2). When the discoid thalli were cultured with a day length over 11 h, only a few erect thalli were formed. Erect thallus formation rate with the 11-h day length was 1.8 Cha $(\mu g)^{-1}$. No significant differences in erect thallus formation rates were observed from the 11- to 16-h day lengths. In contrast, erect thallus formation rates with 9- and 10-h day lengths were 9.0 and 9.1 Cha $(\mu g)^{-1}$, respectively, which were significantly higher than that with 11-h day length ($P < 0.01$; Figure 2). Erect thallus formation rate with the 10-h day length was approximately four-times higher than that with the 11-h day length. These results suggest that the critical day length for erect thallus formation is between 10 and 11 h in *P. fascia*.

## NB treatment for erect thallus formation

Next, NB experiments were performed to confirm that erect thallus formation is influenced by photoperiodism and identify the effective wavelength to control photoperiodism. Erect thallus formation rate was 0.2 Cha $(\mu g)^{-1}$ after 1-h NB treatment with WL, which was almost the same as that under LD conditions (0.1) but significantly lower than that under SD conditions (6.4 Cha $(\mu g)^{-1}$; $P < 0.01$; Figure 3). These results indicate that erect thallus formation in *P. fascia* is regulated by photoperiodism. Next, we investigated the effects of various wavelengths of NB treatment on the erect thallus formation rate. As shown in Figure 3, NB treatment with BL and GL inhibited erect thallus formation, leading to erect thallus formation rates of 0.3 and 0.4 Cha $(\mu g)^{-1}$, respectively (Figure 3). Erect thallus formation rate under these conditions was significantly lower than that under normal SD conditions ($P < 0.01$). Notably, erect thallus formation rate was higher after NB treatment with RL (21.8 Cha $(\mu g)^{-1}$) than under SD conditions ($P < 0.05$; $n = 24$; Figure 3), being more than twice the value under SD conditions. However, no significant difference was

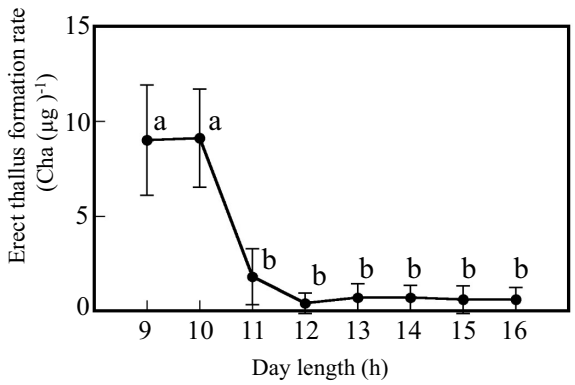


FIGURE 2
Critical day length for erect thallus formation in *P. fascia*. After 24 d of culture, erect thallus formation rates were evaluated. Bars indicate the standard deviations. Letters indicate the significant means determined using the Bonferroni test ($P < 0.01$; $n = 24$).

10.3389/fpls.2024.1500947

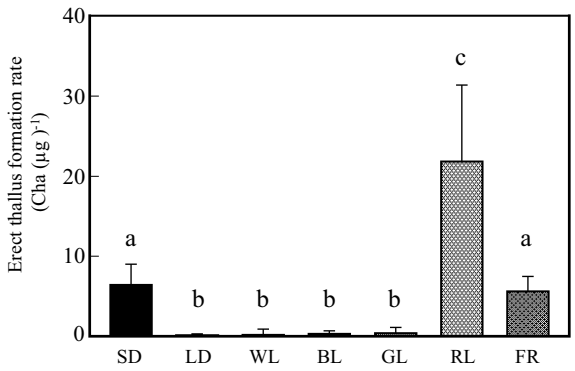


FIGURE 3
Effects of night-break treatment with different wavelengths of light on erect thallus formation in *P. fascia*. Thallus of *P. fascia* underwent night-break treatment for 1 h with white light (WL), blue light (BL), green light (GL), red right (RL), and far-red light (FR) 7 h after the start of the dark period. Erect thallus formation rates under LD and SD conditions are shown. After 24 d of culture, erect thallus formation rates were evaluated. Bars indicate the standard deviations. Letters indicate the significant means determined using the Bonferroni test ($P < 0.05$; $n = 24$).

observed in the erect thallus formation rate after NB treatment with FR (5.6 Cha $(\mu g)^{-1}$) and under SD conditions ($P > 0.05$; $n = 24$).

To investigate the sensitivity of day-length perception to BL and GL in *P. fascia*, we analyzed the relationship between total quantum irradiation (Supplementary Table 1) and erect thallus formation. Erect thallus formation rate decreased with increasing photon quantities in NB treatment with BL and GL. However, erect thallus formation in *P. fascia* showed very high sensitivity to BL rather than to GL (Figure 4; Supplementary Figure 2). More than 30 μmol photons $m^{-2}$ (1.5 μmol photons $m^{-2}$ $s^{-1}$, 20 s) irradiation in NB treatment with BL significantly decreased the erect thallus formation rate compared to that under SD conditions (Supplementary Figure 2). At photon quantities < 600 μmol photons $m^{-2}$, effect of GL on erect thallus formation was significantly weaker than that of BL ($P < 0.01$; Figure 4; Supplementary Figure 2). More than 3600 μmol photons $m^{-2}$ (1 μmol photons $m^{-2}$ $s^{-1}$, 3600 s) irradiation was needed to achieve the same effect with BL. These results revealed that the sensitivity to BL was almost 100-times higher than that to GL for erect thallus formation in *P. fascia*.

To estimate the photosynthetically utilized radiation (PUR) absorbed primarily by photosynthetic pigments, we obtained *in vivo* absorption spectra of *P. fascia* from 400–700 nm (Supplementary Figure 3). The relative absorbance values for BL (472 nm)and GL (532 nm) were 0.84 and 0.55, respectively, indicating that blue light is absorbed approximately 1.5 times more than green light, primarily by photosynthetic pigments. Considering the PUR absorption (Supplementary Figure 3) and the light intensities that inhibit erect thallus formation (Figure 4; Supplementary Figure 2), it is estimated that the sensitivity to BL in erect thallus formation is about 150 times higher than to GL.

## Verification of photoreversibility

In some angiosperms, phytochrome-mediated RL responses, such as seed germination and flowering, are cancelled by FR (Thomas and Vince-Prue, 1997). Therefore, in this study, we examined whether increased erect thallus formation by photoreceptors, such as phytochromes, in *P. fascia* was cancelled by NB treatment with FR. Notably, 1-h FR irradiation following NB treatment with RL did not cancel the effect of RL, and erect thallus formation rate was significantly higher than that under SD conditions (Figure 5; $P < 0.01$; $n = 24$).

Recent studies have focused on the biochemical analyses of diatom phytochromes. Phytochromes of diatoms and brown algae are reversible under GL and RL exposure (Rockwell et al., 2014). To assess the relationship between RL-induced erect thallus formation and photoperiodic response, effects of 1-h GL irradiation following NB with RL (G/R) and 1-h RL irradiation following NB with GL (R/G) were analyzed (Figure 6). Regardless of whether RL

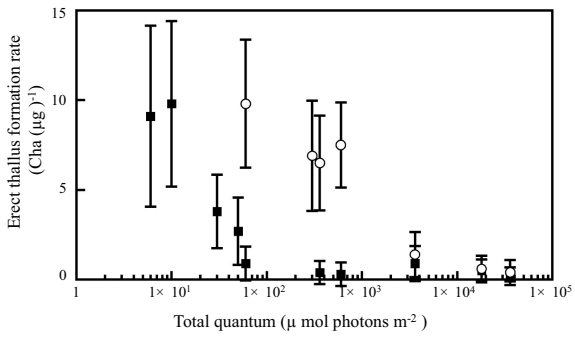


FIGURE 4
Effects of the total quantum of night-break treatment with BL and GL on erect thallus formation in *P. fascia*. Open circles and closed squares indicate the effects of GL and BL, respectively. After 24 d of culture, erect thallus formation rates were evaluated. Bars indicate the standard deviations.

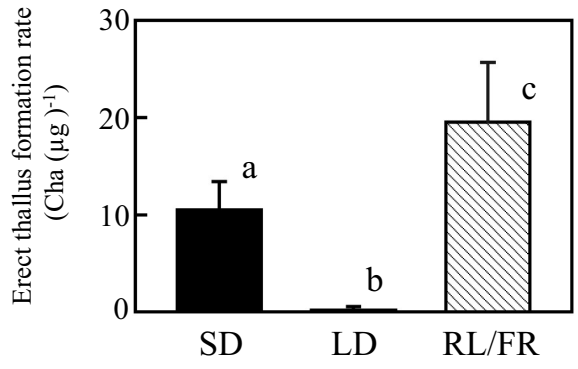


FIGURE 5
Effect of FR irradiation immediately after RL irradiation on erect thallus formation in *P. fascia*. Effect of 1-h night-break treatment with RL, followed by 1-h FR irradiation on erect thallus formation was examined. Erect thallus formation rates under LD and SD conditions are shown. After 24 d of culture, erect thallus formation rates were evaluated. Bars indicate the standard deviations. Letters indicate the significant means determined using the Bonferroni test ($P < 0.01$; $n = 24$).

10.3389/fpls.2024.1500947

irradiation was performed before or after GL irradiation, only the effect of GL was observed. Erect thallus formation rates under LD, G/R, and R/G conditions were 0.6, 0.2, and 0.5 Cha $(\mu g)^{-1}$, respectively, which were significantly lower than that under SD conditions (8.5 Cha $(\mu g)^{-1}$; $P < 0.01$; $n = 24$). These results suggest that the effect of RL on erect thallus formation is limited to SD conditions. Collectively, all NB experiments revealed that *P. fascia* uses BL and GL to perceive day length.

## Discussion

Previous studies on the life cycle of *P. fascia* have reported erect thallus formation under SD conditions (Roeleveld et al., 1974). However, to date, no study has conducted physiological analysis to determine whether this phenomenon is controlled by a genuine photoperiodic response or the total light period. In this study, we demonstrated that erect thallus formation in *P. fascia* is regulated by photoperiodism.

Previous studies reported that the light quality affects photoperiodism in three brown algal species: *Scytosiphon lomentaria*, *Ascophyllum nodosum*, and *Sargassum horneri* (Dring and Lüning, 1975a; Terry and Moss, 1980; Yoshikawa et al., 2014). These reports are consistent with our findings on BL-controlled photoperiodism. Therefore, BL is possibly a common mechanism for day-length perception in brown algae. Here, 10 s of dim light NB treatment with BL (total quantum: 30 µmol photons $m^{-2}$) inhibited erect thallus formation, indicating the high sensitivity of *P. fascia* to BL. This effect is comparable to that observed in *S. lomentaria* after NB treatment with BL (total quantum 20 µmol photons $m^{-2}$) (Dring and Lüning, 1975a).

Notably, effects of NB treatment with GL on *P. fascia* in this study were clearly different from those in previous studies on *S. lomentaria*. Dring and Lüning reported that the action spectrum for erect thallus formation in *S. lomentaria* had no effect in the wavelength range of 501–724 nm (Dring and Lüning, 1975a cf.; Figure 5). Differences between our results and previous findings on the effects of GL may be due to differences in the total quantum rather than differences in the experimental organisms. Here, NB treatment with 1 µmol photons $m^{-2}$ $s^{-1}$ (60 min; total quantum 3600 µmol photons $m^{-2}$) GL inhibited erect thallus formation in *P. fascia*. In contrast, Dring and Lüning reported that NB treatment with 1 µmol photons $m^{-2}$ $s^{-1}$ (1 min; total quantum 60 µmol photons $m^{-2}$) GL has no effect on erect thallus formation. As the total quantum of GL irradiation in this study was 60-times higher than that in the study by Dring and Lüning, GL effectively suppressed erect thallus formation in *P. fascia*.

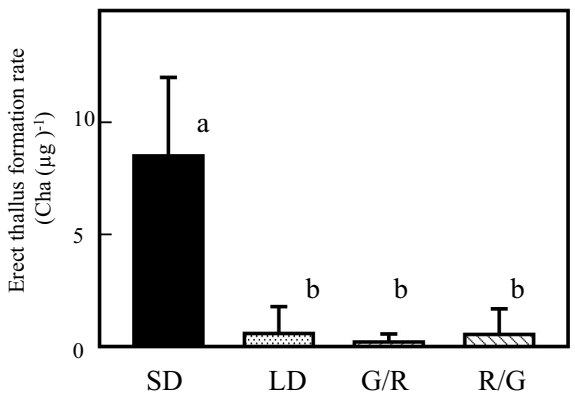


FIGURE 6
GL effects on *Petalonia fascia* are cancelled by RL and vice versa. Effect of 1-h night-break treatment with GL, followed by 1-h RL irradiation on erect thallus formation was examined (G/R). Effect of 1-h night-break with RL, followed by 1-h GL irradiation on erect thallus formation was examined (R/G). Erect thallus formation rates under LD and SD conditions are shown. After 24 d of culture, erect thallus formation rates were evaluated. Bars indicate the standard deviations. Letters indicate the significant means determined using the Bonferroni test ($P < 0.01$; $n = 24$).

The light intensity and duration of GL exposure used in this study were comparable to those observed in the natural growth environment of *P. fascia*. GL intensity of 1 µmol photons $m^{-2}$ $s^{-1}$ may cause disc thallus formation in *P. fascia*. As GL is more prominent than BL in phytoplankton-rich environments (Jaubert et al., 2017), the mechanism to measure day length using GL is helpful for the environmental adaptation of *P. fascia*. BL-and GL mediating photoperiodic responses have been reported in *S. horneri* (Yoshikawa et al., 2014). However, only a few studies have investigated the spectral quality related to photoperiodism in brown algae. Moreover, whether most brown algae use GL in the same manner as BL to measure day length remains unclear. Future studies should investigate the photoperiodicity and light quality in other brown algal groups to determine whether photoperiodicity control via GL is a shared characteristic among brown algae.

The BL photoreceptors, aureochromes and cryptochromes, are possible photoreceptors controlling photoperiodism in *P. fascia* based on the identified photoreceptor genes in the brown alga *Ectocarpus siliculosus* (Cock et al., 2010).

Aureochromes are BL receptors unique to stramenopiles. Although their functions in brown algae remain unknown, they are involved in branch formation in the xanthophyte *Vaucheria frigida* (Takahashi et al., 2007) and cell division in diatoms (Huysman et al., 2013). Recent studies in diatoms have reported that aureochromes are involved in light-dependent responses, including photoprotection (Zhang et al., 2024) and the regulation of the circadian clock (Madhuri et al., 2024). As aureochromes are composed of a BL-sensing LOV domain and b-zip domain that binds to DNA, they perform dual functions: photoreception and regulation of gene expression (Takahashi et al., 2007; Takahashi, 2016). Therefore, aureochromes may be the key photoreceptors involved in photoperiodism and gene expression control in brown algae. However, as aureochromes exhibit an absorption spectrum similar to that of typical flavin proteins and the absorption does not include the GL region (> 500 nm) (Hisatomi et al., 2013), involvement of aureochromes in the regulation of photoperiodism in *P. fascia* suggesting the existence of another GL photoreceptor for photoperiodism in *P. fascia*. Cryptochromes are BL receptors that function as day-length sensors in *Arabidopsis* (Mockler et al., 2003). Although cryptochrome is a receptor that primarily absorbs BL, reduced cryptochrome has an absorbance spectrum that extends into the GL range (Lin et al., 1995a, b), suggesting that cryptochromes may perceive both BL and GL in *P. fascia*. Although homologous cryptochrome genes have been identified in brown algae, their physiological functions remain unknown.

In this study, we demonstrated that NB treatment with RL enhanced erect thallus formation. Similarly, Lüning also reported that continuous irradiation with RL enhances erect thallus formation in *P. fascia* (1973). Some studies have reported BL-induced photomorphogenesis in brown algae (Dring and Lüning, 1975a, b, Lüning, 1981; Lüning and Dring, 1975; Wang et al., 2010; Yoshikawa et al., 2014); however, studies on RL-induced photomorphogenesis are rare (Duncan and Foreman, 1980; Lüning, 1973; Müller and Clauss, 1976). RL photoreceptor phytochrome-mediated photoresponse, which is also observed in terrestrial plants, is cancelled by FR irradiation shortly after RL irradiation (Thomas and Vince-Prue, 1997). In brown algae, only one response, potentially involving phytochromes, has been reported. FR induces stipe elongation in *Nereocystis luetkeana*, which is cancelled by RL irradiation (Duncan and Foreman, 1980). In this study, FR did not counteract the RL response in *P. fascia* (Figure 5). The response of *P. fascia* to RL may be a different type of photoreceptor-mediated response from that of *N. luetkeana*.

The phytochrome gene has been identified in *E. siliculosus* genome (Cock et al., 2010; Rockwell et al., 2014). As the spectrum of the recombinant protein of *E. siliculosus* phytochrome shows RL and GL photoconversion (Rockwell et al., 2014), we investigated whether the effects of GL are counteracted by RL irradiation immediately after GL irradiation and vice versa in this study. Notably, only the effects of GL were observed in experiments with GL irradiation, regardless of whether it was performed before or after RL irradiation. This result suggests that photoreceptors undergoing photoconversion with RL and GL are not involved in erect thallus formation in *P. fascia*. When GL irradiation preceded RL irradiation, RL did not promote erect thallus formation. This suggests that RL-induced erect thallus formation is not involved in day length perception but rather acts as a promoter under SD. Therefore, RL photoreceptors may function downstream of BL and GL receptors for day-length perception.

In conclusion, this study revealed that *P. fascia* uses both BL and GL for photoperiodic regulation, showing higher sensitivity to BL for erect thallus formation under SD conditions. RL further promotes erect thallus formation in NB treatment under SD conditions. Overall, this study provides insights into the photoperiodic strategies of brown algae from a physiological perspective and establishes a basis for future molecular biological studies on photoreceptor mechanisms.

## Data availability statement

The original contributions presented in the study are included in the article/Supplementary Material. Further inquiries can be directed to the corresponding author.

## Author contributions

YM: Investigation, Writing – original draft. FT: Supervision, Writing – review & editing. TH: Investigation, Writing – review & editing. SY: Conceptualization, Writing – original draft, Writing – review & editing.

## Funding

The author(s) declare financial support was received for the research, authorship, and/or publication of this article. This work was supported in part by Grants-in-Aid for Scientific Research (No. 26440156) and the Fukui Prefectural University for Strategic Issue Research Promotion.

## Acknowledgments

This manuscript was proofread and partially revised using OpenAI's ChatGPT (GPT-4). The AI tool was utilized to check for grammatical errors, improve clarity, and ensure consistency in the English text. Final decisions on content were made by the authors.

## Conflict of interest

The authors declare that the research was conducted in the absence of any commercial or financial relationships that could be construed as a potential conflict of interest.

## Publisher's note



## Supplementary material

The Supplementary Material for this article can be found online at: https://www.frontiersin.org/articles/10.3389/fpls.2024.1500947/full#supplementary-material

# References


Cock, J. M., Sterck, L., Rouzé, P., Scornet, D., Allen, A. E., Amoutzias, G., et al. (2010). The Ectocarpus genome and the independent evolution of multicellularity in brown algae. *Nature.* 465, 617–621. doi: 10.1038/nature09016

Dring, M. J., and Lüning, K. (1975a). A photoperiodic response mediated by blue light in the brown alga *Scytosiphon lomentaria*. *Planta.* 125, 25–32. doi: 10.1007/BF00388870

Dring, M. J., and Lüning, K. (1975b). Induction of two-dimensional growth and hair formation by blue light in the brown alga *Scytosiphon lomentaria*. *Z. für Pflanzenphysiologie.* 75, 107–117. doi: 10.1016/S0044-328X(75)80107-3

Duncan, M. J., and Foreman, R. E. (1980). Phytochrome-mediated stipe elongation in the kelp nereocystis (Phaeophyceae). *J. Phycol.* 16, 138–142. doi: 10.1111/j.1529-8817.1980.tb03008.x

Hisatomi, O., Takeuchi, K., Zikihara, K., Ookubo, Y., Nakatani, Y., Takahashi, F., et al. (2013). Blue light-induced conformational changes in a light-regulated transcription factor, aureochrome-1. *Plant Cell Physiol.* 54 (1), 93–106. doi: 10.1093/pcp/pcs160

Huysman, M. J., Fortunato, A. E., Matthijs, M., Costa, B. S., Vanderhaeghen, R., Van den Daele, H., et al. (2013). AUREOCHROME1a-mediated induction of the diatom-specific cyclin dsCYC2 controls the onset of cell division in diatoms (*Phaeodactylum tricornutum*). *Plant Cell.* 25, 215–228. doi: 10.1105/tpc.112.106377

Hwang, E. K., and Dring, M. J. (2002). Quantitative photoperiodic control of erect thallus production in *Sargassum muticum*. *Bot. Mar.* 45, 471–475. doi: 10.1515/BOT.2002.049

Jaubert, M., Bouly, J. P., d'Alcalà, M. R., and Falciatore, A. (2017). Light sensing and responses in marine microalgae. *Curr. Opin. Plant Biol.* 37, 70–77. doi: 10.1016/j.pbi.2017.03.005

Jeffrey, S. T., and Humphrey, G. F. (1975). New spectrophotometric equations for determining chlorophylls a, b, c1 and c2 in higher plants, algae and natural phytoplankton. *Biochemie und physiologie der pflanzen.* 167 (2), 191–194. doi: 10.1016/S0015-3796(17)30778-3

Lin, C., Ahmad, M., Gordon, D., and Cashmore, A. R. (1995b). Expression of an Arabidopsis cryptochrome gene in transgenic tobacco results in hypersensitivity to blue, UV-A, and green light. *PNAS.* 92, 8423–8427. doi: 10.1073/pnas.92.18.8423

Lin, C., Robertson, D. E., Ahmad, M., Raibekas, A. A., Jorns, M. S., Dutton, P. L., et al. (1995a). Association of flavin adenine dinucleotide with the Arabidopsis blue light receptor CRY1. *Science.* 269, 968–970. doi: 10.1126/science.7638620

Lüning, K. (1973). The influence of light quality on the development of the brown algae *Petalonia* and *Scytosiphon*. *Br. Phycol J.* 8, 333–338. doi: 10.1080/00071617300650361

Lüning, K. (1981). Egg release in gametophytes of *Laminaria saccharina*: induction by darkness and inhibition by blue light and UV. *Br. Phycol J.* 16, 379–393. doi: 10.1080/00071618100650441

Lüning, K. (1986). New frond formation in *Laminaria hyperborea* (Phaeophyta): a photoperiodic response. *Br. Phycol J.* 21, 269–273. doi: 10.1080/00071618600650311

Lüning, K. (1988). Photoperiodic control of sorus formation in the brown alga *Laminaria saccharina*. *Mar. Ecol. Prog. Ser.* 45, 137–144. doi: 10.3354/meps045137

Lüning, K., and Dring, M. J. (1975). Reproduction, growth and photosynthesis of gametophytes of *Laminaria saccharina* grown in blue and red light. *Mar. Biol.* 29, 195–200. doi: 10.1007/BF00391846

Madhuri, S., Lepetit, B., Fürst, A. H., and Kroth, P. G. (2024). A knockout of the photoreceptor ptAureo1a results in altered diel expression of diatom clock components. *Plants.* 13, 1465. doi: 10.3390/plants13111465

Mockler, T., Yang, H., Yu, X., Parikh, D., Cheng, Y. C., Dolan, S., et al. (2003). Regulation of photoperiodic flowering by Arabidopsis photoreceptors. *PNAS.* 100, 2140–2145. doi: 10.1073/pnas.0437826100

Müller, S., and Clauss, H. (1976). spects of photomorphogenesis in the brown alga dictyota dichotoma. *Z. für Pflanzenphysiologie* 78, 461–465. doi: 10.1016/S0044-328X(76)80095-5

Nelson, R. J., David, L. D., and David, E. S. (2010). *Photoperiodism: the biological calendar* (New York: Oxford University Press).

Pang, S., and Lüning, K. (2004). Photoperiodic long-day control of sporophyll and hair formation in the brown alga *Undaria pinnatifida*. *J. Appl. Phycol.* 16, 83–92. doi: 10.1023/B:JAPH.0000044773.52572.8b

Parker, M. W., Hendricks, S. B., and Borthwick, H. A. (1950). Action spectrum for the photoperiodic control of floral initiation of the long-day plant *Hyoscyamus Niger*. *Bot. Gazette.* 111, 242–252. doi: 10.1086/335592

Parker, M. W., Hendricks, S. B., Borthwick, H. A., and Scully, N. J. (1945). Action spectrum for the photoperiodic control of floral initiation in Biloxi soybean. *Science.* 102, 152–155. doi: 10.1126/science.102.2641.152

Rockwell, N. C., Duanmu, D., Martin, S. S., Bachy, C., Price, D. C., Bhattacharya, D., et al. (2014). Eukaryotic algal phytochromes span the visible spectrum. *PNAS.* 111, 3871–3876. doi: 10.1073/pnas.1401871111

Roeleveld, J. G., Duisterhof, M., and Vroman, M. (1974). On the year cycle of *Petalonia fascia* in the Netherlands. *J. Sea Res.* 8, 410–426. doi: 10.1016/0077-7579(74)90009-X

Takahashi, F. (2016). Blue-light-regulated transcription factor, Aureochrome, in photosynthetic stramenopiles. *J. Plant Res.* 129, 189–197. doi: 10.1007/s10265-016-0784-5

Takahashi, F., Yamagata, D., Ishikawa, M., Fukamatsu, Y., Ogura, Y., Kasahara, M., et al. (2007). AUREOCHROME, a photoreceptor required for photomorphogenesis in stramenopiles. *PNAS.* 104, 19625–19630. doi: 10.1073/pnas.0707692104

Tatewaki, M. (1966). Formation of a crustaceous sporophyte with unilocularsporangia in *Scytosiphon lomentaria*. *Phycologia* 6, 62–66. doi: 10.2216/i0031-8884-6-1-62.1

Ten Hoopen, A., Bos, S., and Breeman, A. M. (1983). Photoperiodic response in the formation of gametangia of the long-day plant *Sphacelaria rigidula* (Phaeophyceae). *Mar. Ecol. Prog. Ser.* 13, 285–289. doi: 10.3354/meps013285

Terry, L. A., and Moss, B. L. (1980). The effect of photoperiod on receptacle initiation in *Ascophyllum nodosum* (L.) Le Jol. *Br. Phycol J.* 15, 291–301. doi: 10.1080/00071618000650301

Thomas, B., and Vince-Prue, D. (1997). *Photoperiodism in plants. 2nd ed* (London: Academic Press).

Wang, W. J., Sun, X. T., Wang, G. C., Xu, P., Wang, X. Y., Lin, Z. L., et al. (2010). Effect of blue light on indoor seedling culture of *Saccharina japonica* (Phaeophyta). *J. Appl. Phycol.* 22, 737–744. doi: 10.1007/s10811-010-9514-x

Yoshikawa, S., Kamiya, M., and Ohki, K. (2014). Photoperiodic regulation of receptacle induction in *Sargassum horneri* (Phaeophyceae) using clonal thalli. *Phycol Res.* 62, 206–213. doi: 10.1111/pre.12052

Zhang, H., Xiong, X., Guo, K., Zheng, M., Cao, T., Yang, Y., et al. (2024). A rapid aureochrome opto-switch enables diatom acclimation to dynamic light. *Nat. Commun.* 15, 5578. doi: 10.1038/s41467-024-49991-7

frontiers | Frontiers in Plant Science

TYPE Original Research
PUBLISHED 06 February 2025
DOI 10.3389/fpls.2025.1497064



OPEN ACCESS

EDITED BY
Yi Zhou,
Chinese Academy of Sciences (CAS), China

REVIEWED BY
Vesselin Baev,
Plovdiv University "Paisii Hilendarski", Bulgaria
Sumaira Rasul,
Bahauddin Zakariya University, Pakistan

*CORRESPONDENCE
Chang Liu
liuchang_bio@foxmail.com

†These authors have contributed equally to this work and share first authorship

RECEIVED 16 September 2024
ACCEPTED 17 January 2025
PUBLISHED 06 February 2025

CITATION
Zhao H, Dong X, Yang D, Ge Q, Lu P and Liu C (2025) New insights into the salt-responsive regulation in eelgrass at transcriptional and post-transcriptional levels. *Front. Plant Sci.* 16:1497064. doi: 10.3389/fpls.2025.1497064



# New insights into the salt-responsive regulation in eelgrass at transcriptional and post-transcriptional levels

Huan Zhao[1,2†], Xu Dong[1,2†], Dazuo Yang[1,2], Qingchao Ge[1,2], Peng Lu[1,2] and Chang Liu[2,3*]

[1]College of Fisheries and Life Science, Dalian Ocean University, Dalian, China, [2]Key Laboratory of Marine Bio-resources Restoration and Habitat Reparation in Liaoning Province, Dalian Ocean University, Dalian, China, [3]Department of Nursing, Zibo Vocational Institute, Zibo, China

**Introduction:** The adaptation mechanisms of marine plants to the environments have garnered significant attention in recent years. Eelgrass (*Zostera marina*), a representative marine angiosperm, serves as an ideal model for investigating the mechanisms underlying salt tolerance.

**Methods:** This study integrated mRNA, sRNA, and degradome sequencing data to identify key genes associated with salt tolerance in eelgrass.

**Results:** The results indicate that a series of genes involved in biological processes such as "in response to water deprivation" and "biosynthesis of secondary metabolites" respond to salt stress. Analysis of cis-regulatory elements and expression similarities suggests that the ABA synthase 9-cis-epoxycarotenoid dioxygenase (NCED) may be regulated by ERF members, while phenylalanine ammonia-lyase (PAL) may be regulated by MYB members. At the post-transcriptional regulation level, miRNA156 and miRNA166 might be involved in the response by regulating potential target genes, such as members of the WRKY and HD-ZIP families. Additionally, eelgrass exhibits unique responses to salt, such as the up-regulation of genes involved in the "fucose biosynthetic process". These findings enhance our understanding of how eelgrass adapts to the marine environment.

**Discussion:** As a marine monocotyledon, eelgrass is helpful to find conserved salt tolerance mechanisms by cross-species comparison. By examining the transcriptional responses of homologous genes in eelgrass, rice, and maize, we identified several groups of genes that are conserved in their response to salt stress. These conserved gene resources may provide targets for genetic engineering to improve the salt tolerance of crops.

KEYWORDS

***Zostera marina*, salt stress response, miRNA, transcription factor, comparative transcriptome, degradome sequencing, gene regulation**

# 1 Introduction

Seagrass, a widely distributed coastal angiosperm, plays a crucial role in marine ecosystem functioning and global carbon sequestration (Ma X. et al., 2021). In order to adapt to the marine environment, seagrass has evolved different morphological (e.g. osmotic capacities), ultrastructural (e.g. absence of the real cuticle) and physiological characteristics (e.g. polyanionic, low-methylated pectins and sulfated galactans in cell walls) to tolerate salinity (Olsen et al., 2016; Wissler et al., 2011; Sandoval-Gil et al., 2023). Hence, salinity is considered as one of the major factors that condition the distribution, ecology and biology of seagrasses. Changes in salinity have the potential to impact on growth and biomass production of seagrass (Sandoval-Gil et al., 2023). In recent years, salinity levels in some seagrass beds are frequently influenced by extreme climate events such as continuous evaporation under high temperature or water exchange by rainfall (Koch et al., 2007; Tomasello et al., 2009), as well as human activities including the discharge from desalination factories (Cambridge et al., 2019), which are seriously threatened the maintenance of seagrass beds.

Eelgrass (*Zostera marina*), a member of the Angiosperms within the Monocotyledon group, is widely distributed in the coastal areas of the Northern Hemisphere (Zhang Y. et al., 2023). It is considered as one of the marine ecological model species for revealing adaptation to marine life. The activities of Na+/H+ exchangers in the plasma membrane of eelgrass have been involved in salinity tolerance (Rubio et al., 2011). Nitric oxide (NO) is also reported to play a crucial role in regulating the salinity tolerance of eelgrass by enhancing antioxidant defense mechanisms, as well as by modulating osmotic balance and energy metabolism (Wang X. et al., 2024). The analysis of the genome has revealed eelgrass exhibits some cell wall characteristics similar to those of macroalgae, which facilitate the retention of water and ions (Olsen et al., 2016). Genome-wide analysis in eelgrass revealed a reduced number of aquaporins and higher expression of plasma membrane intrinsic proteins (PIPs) compared to terrestrial plants (Shivaraj et al., 2017). These studies have revealed many genomic changes responsible for marine physiological adaptations, particularly regarding salinity tolerance.

Transcription factors (TFs) could activate or inhibit the transcription of target genes by binding specific DNA sequence (Yoon et al., 2020). Stress-responsive TFs such as the members of AP2/ERF and ARF, control the gene transcription in abscisic acid (ABA) and jasmonic acid (JA) signaling which are the key stress hormones in plant response to abiotic stress. Numerous studies have highlighted the regulatory functions of those two stress-responsive TFs in mediating terrestrial plants' responses to salinity. For instance, *ERF106MZ* in rice or *EREB57* in maize are reported to mediate ABA signaling under salinity stress (Chen et al., 2023; Zhu et al., 2023). The salt tolerance role of *ARF5* in sweet potato has been functionally verified in transgenic *Arabidopsis thaliana* and is associated with ABA signaling (Kang et al., 2018). However, in many species, ARFs are down-regulated at high salinity, suggesting that members of this family may play a negative role (Ye et al., 2020; Wang C. et al., 2024). Besides, other TFs including MYB, NAC, bHLH and WRKY, are also predicted to be differentially expressed under salinity stress. For example, the *AtMYB20* in *A. thaliana* is up-regulated by salt stress, and transgenic plants overexpressing *AtMYB20* showed improved tolerance to salt stress (Cui et al., 2013). The heterologous overexpression of strawberry *FaMYB63* in *A. thaliana* increased salt tolerance by reactive oxygen species (ROS) clearance (Wang S. et al., 2024). *SlNAC4* in *Suaeda liaotungensis* was also verified to enhance tolerance to salt by regulating ABA metabolism through heterologous overexpressed (Liu et al., 2023). *ThNAC13* in *Tamarix hispida* was proved to improve salt tolerance by binding to *ThPP2* gene to enhance antioxidant enzyme activity (Liu R. et al., 2024). *MYC2*, a bHLH family member in *A. thaliana* and *BpWRKY32* in *Betula platyphylla* were verified to increase salt tolerance (Verma et al., 2020; Liu Z. et al., 2024). In summary, these TFs primarily influence salt stress response and tolerance by modulating the expression of downstream genes, which participate in enhancing the antioxidant system, maintaining ion balance, regulating proline synthesis and ABA response. However, there is a notable scarcity of studies investigating these regulatory factors in seagrass species.

Plant microRNAs (miRNAs), typically consisting of 20-24 nucleotides, are also important post-transcriptional regulatory molecules (Begum, 2022). miRNAs could influence the expression of target genes. The function of stress-responsive miRNAs and their target under salt stress have been studied in model plants and some economic terrestrial crops. The expression of Tch-miR167 was negatively correlated to the expression of *TcARF6*, which indicated that *TcARF6* increases salt tolerance in *Tamarix chinensis* by post-transcriptional regulation (Ye et al., 2020). The miR393 in *A. thaliana* regulated the salt-responsive pathway by scaffold protein RACK1A mediated ABA signaling pathways (Denver and Ullah, 2019). Overexpression of Osa-miR319a in transgenic creeping bentgrass *Agrostis stolonifera* inhibited the expression of *AsPCF6*, *AsPCF8*, *AsTCP14*, and *AsNAC60*, and modified the salt tolerance of transgenic plant (Zhou et al., 2013). The ABA receptor genes *NtPYL2* and *NtSAPK3* showed up-regulated expression in TaemiR408 tobacco lines, which indicated that TaemiR408 is associated with the miRNA modulation for ABA signaling to improve salt tolerance (Bai et al., 2018). miR172a and miR172b in cereal crops, miR398 in tomato and miR528-AO in rice were also proved to play a regulatory role in maintaining ROS homeostasis during salt stress (Cheng et al., 2021; He et al., 2021; Wang et al., 2021). In contrast, research on the role of miRNAs in aquatic plants under environmental stress conditions remains limited. Studies addressing the response of microRNAs to salt stress have been reported in species such as *Dunaliella salina* (Gao et al., 2019) and *Spirulina platensis* (Zhao et al., 2016). Some miRNAs in eelgrass have been identified by genomic analysis by Olsen et al. (2016) and Ma et al. (2021), which provide information for further research on the regulation mechanism of miRNA under abiotic stress.

The function of TFs and microRNAs in terrestrial plants have been identified as important regulatory elements that enable plants to withstand salt stress. Compared to terrestrial plants, the transcriptional and post-transcriptional response of those regulator in seagrass under stress remain elusive. Previous studies on eelgrass exhibited that high salinity not only inhibits seed

germination but also effect the growth rate and survival of eelgrass (Zhang Y.-H. et al., 2023; Zhang Y. et al., 2023). In order to investigate the molecular mechanism and identify the potential regulatory factors, we performed a comprehensive analysis on the transcriptional response of eelgrass to salt stress using mRNA sequencing and small RNA sequencing data. Based on differential expression characteristics and similarity in expression trends, we identified various TFs, miRNAs, and functional target genes that may be associated with salt tolerance in eelgrass. The relationship between target genes and miRNAs was predicted and proved by degradome sequencing. This discovery provides more information about the molecular mechanisms underlying the adaptation of eelgrass to hypersalinity. Furthermore, we chose two terrestrial economic crops, rice and maize which also belong to Monocotyledon, to compare the homologous differential expression genes (DEGs) in response to salt stress. The comparative analysis not only sheds light on the conserved and specific mechanism in eelgrass adaption to hypersalinity but also provides gene resources for functional verification in terrestrial model species.

# 2 Materials and methods

## 2.1 Plant and sampling

The eelgrass used in this study was sourced from a seedling factory in Qingdao, Shandong Province of China. Initially, the plants underwent a cleaning process and were then methodically arranged within a temporary tank. The base of the temporary storage tank comprised sand and stone that had undergone high-temperature sterilization, with the filtered seawater. The seawater was maintained with temperature of 17.5°C and salinity of 30, while the light intensity was approximately 120 μmol/($m^2$·s). Following three days of cultivation, the plants exhibiting robust growth were selected and transferred to experimental boxes No. 1 and No. 2, with seawater salinities of 30 and 50 (Xu et al., 2015), respectively. After 12 hours of treatment, the plants were removed from the boxes and promptly placed in liquid nitrogen for rapid freezing. A total of 6 plants were sampled in each treatment to build three biological replicates (with 2 plants being mixed to form a sample) for small RNA and mRNA sequencing. Different tissues were separated with sterile scissor. As the individual root samples did not provide enough material for sequencing, we mixed the stem and root together as one tissue (SR tissue). Besides, another 3 plants under high salt conditions were collected as a mixed sample for degradome sequencing.

## 2.2 RNA-seq library construction and sequencing

The total RNA was extracted using the RNAprep Pure Plant Kit DP441 (Tiangen, Beijing, China) according to the kit instructions. Then, mRNA was purified from total RNA using poly-T oligo-attached magnetic beads. Fragmentation was carried out using divalent cations under elevated temperature in First Strand Synthesis Reaction Buffer. First strand cDNA was synthesized using random hexamer primer and M-MuLV Reverse Transcriptase (RNase H-). Second strand cDNA synthesis was subsequently performed using DNA Polymerase I and RNase H. Remaining overhangs were converted into blunt ends via exonuclease/polymerase activities. After adenylation of 3' ends of DNA fragments, Adaptor with hairpin loop structure were ligated to prepare for hybridization. In order to select cDNA fragments of preferentially 370-420 bp in length, the library fragments were purified with AMPure XP system. Then PCR was performed with Phusion High-Fidelity DNA polymerase, Universal PCR primers and Index (X) Primer. At last, PCR products were purified. After the library construction is completed, preliminary quantification is carried out using Qubit, and the library is diluted to 1.5ng/ul. Subsequently, the inserted fragments of the library are detected. Once the inserted fragments meet expectations, the effective concentration of the library is accurately quantified using realtime PCR to ensure the quality of the library. The qualified libraries were pooled and sequenced on Illumina sequencing platforms, according to effective library concentration and data amount required.

## 2.3 Small RNA library construction and sequencing

The total RNA extracted was also used for small RNA sequencing (Zhang M. et al., 2023; Hu et al., 2021). We used NEB Next® Multiplex Small RNA Library Prep Set (NEB E7300L) for small RNA library construction. The 5 'end of small RNA has a complete phosphate group and the 3' end of small RNA has a hydroxyl group. So special 3' and 5' adaptors were ligated to the 3' and 5' ends of small RNA based on the special structure of the 3' and 5' end of small RNA, respectively. Following this step, the first strand cDNA was synthesized subsequent to hybridizing with the reverse transcription primer. Subsequently, the double-stranded cDNA library was created via PCR enrichment. The libraries containing insertions ranging from 18 to 40 bp were then readied for sequencing after purification and size selection. Upon completion of the library construction process, the inserted fragments were quantified and the effective concentration (9~14.41 nmol/L) was assessed to ensure the quality of the libraries. The qualified libraries were pooled and sequenced on Illumina sequencing platforms, according to effective library concentration and data amount required. To gather more data for analysis, additional sequencing runs were conducted on four small RNA samples (L30-2, L30-3, L50-2, L50-3), which were collectively labeled as "batch2".

## 2.4 RNA-seq data analysis

The RNA-seq data was subjected to quality assessment using Fastqc and then preprocessed using trim-galore v0.6.10. Basic data information, such as sequence number and sequence length, was obtained using the seqkit v2.1.0. The preprocessed data was then aligned to the reference genome Zostera marina v3.1 from

Phytozome13 using hisat2 v2.2.1. The results were sorted using samtools, and the quantification of gene loci was performed with featureCounts v2.0.6. Additionally, stringtie v2.2.2 was utilized to compute Fragments Per Kilobase of transcript per Million mapped reads (FPKM). Additionally, the sample R50-1 was excluded from further analysis due to its low mapping rate. Besides, we analyzed the PRJNA342750 data from NCBI related to the NaCl response.

The DESeq2 R package was used to analyze gene expression differences based on read count data, with the criteria for DEGs screening set as false discovery rate (FDR) ≤ 0.05 and fold change (FC) ≥ 2. The identified DEGs were classified according to their differential expression in different tissues, and the R package ComplexHeatmap was utilized to draw heat maps. The gene annotation was downloaded from Phytozome13, and complemented by eggNOG and KASS for GO and KEGG annotation. Mercator4 was utilized for mapman annotation of genes. Functional enrichment analysis was performed using the R package clusterProfiler (FDR ≤ 0.05).

## 2.5 Construction of gene co-expression network in eelgrass

To reveal the transcriptional regulatory network of eelgrass in response to high salt stress, we first conducted co-expression network analysis using the Weighted Gene Co-expression Network Analysis (WGCNA) package. Our dataset was combined with 58 additional samples obtained from the NCBI database (refer to Supplementary Data S2). In the initial stages of data preprocessing, we utilized Sratoolkit for data format conversion and Trim-galore for the identification and removal of adaptors and low-quality reads. Subsequently, the preprocessed data were aligned to a reference genome using hisat2. RSeQC was employed to ascertain the strand specificity of the mapped data. Following this, Stringtie was employed to compute the gene expression levels in fragments per kilobase of transcript per million mapped reads (FPKM), with genes exhibiting a Coefficient of Variation (CV) ≥ 1 retained for further analysis. Then, the gene expression values were log2-transformed (log2[FPKM+1]) for normalization. To construct an appropriate correlation weighting value (soft threshold) for co-expression network prediction, we utilized the pickSoftThreshold function in the R package WGCNA, with a criterion of SFT.R.sq ≥ 0.85 to ensure a scale-free network structure. Subsequently, we determined the soft threshold value of 8 for network construction. The one-step method (blockwiseModule function, parameters: networkType="signed hybrid"; minModuleSize=30; mergeCutHeight=0.25) was then employed to build the network, and eigengene analysis was applied to illustrate the gene expression trends within each module. Finally, we used the R package Complex Heatmap to generate heat maps to visualize the distribution of DEGs in co-expression modules.

## 2.6 Identification of microRNAs and DEmiRNAs

Small RNA data were aligned to the reference genome Zostera marina v3.1. The mapping files were merged to identify microRNAs using ShortStack v3.8.5 and miRDeep-P2 v1.1.4. Subsequently, bedtools v2.30.0 was employed to distinguish the same and unique MIRNA loci predicted by the two tools. The non-coding RNAs such as rRNA, tRNA, snRNA, and snoRNA were excluded from this analysis. For the identification of these non-coding RNAs, distinct prediction tools including barrnap, tRNAscan-SE, and Infernal-Rfam were utilized.

The pre-miRNA sequences were extracted based on the predicted MIRNA loci. Then, RNAfold (https://www.tbi.univie.ac.at/RNA/tutorial/) was used to examine the secondary structure of pre-miRNAs. Simultaneously, the predicted mature miRNA sequences were compared with those documented in miRbase (http://www.mirbase.org/) to determine miRNA families based on similarity. Meanwhile, we compared the MIRNA and gene location to classify the MIRNA into two types: the intragenic ones and the intergenic ones.

The read counts for miRNA and other sRNA loci were calculated using the ShortStack. According to the correlation analysis on the expression of small RNAs, we removed four samples in subsequent analysis, including L30.1, L50.1, SR30.3, and SR50.2. The R package EdgeR was used for counts per million (CPM) quantification. Differentially expressed miRNAs (DEmiRNAs) were identified using both EdgeR and DESeq2, with a threshold of p-value ≤ 0.05. The online tool psRNATarget (2017 release) was employed to predict miRNA target genes.

## 2.7 qRT-PCR detection of DEGs and DEmiRNAs

We utilized the SteadyPure Plant RNA Extraction Kit (Accurate Biotechnology, Changsha, Hunan, China) for mRNA extraction and the Evo M-MLV Reverse Transcription Kit (Accurate Biotechnology, Changsha, Hunan, China) for reverse transcription of RNA. For small RNA extraction, we utilized the SteadyPure Tissue and Cell Small RNA Extraction Kit (Accurate Biotechnology, Changsha, Hunan, China) followed by reverse transcription using the miRcute Enhanced miRNA cDNA First Strand Synthesis Kit (Tiangen, Beijing, China). The procedures were conducted according to the instructions. Quantitative real-time PCR (qRT-PCR) experiments were carried out using 7500 Fast Real-Time PCR equipment, with the following thermal cycling conditions: 95°C for 30s, followed by 40 cycles at 95°C for 5s and 60°C for 30s. In total, 9 DEGs and 4 DEmiRNAs were verified. The primers for these genes and miRNAs are listed in Supplementary Data S12. For normalization, *18S rRNA* and *U6* served as the reference gene, and relative expression changes were calculated using the $2^{-\Delta\Delta Ct}$ method. The statistical analysis was performed using the function t.test in R software.

## 2.8 Degradome sequencing and analysis

Total RNA was isolated and purified using TRIzol reagent (Invitrogen, Carlsbad, CA, USA) following the manufacturer's procedure. The RNA amount and purity of each sample were

quantified using NanoDrop ND-1000 (NanoDrop, Wilmington, DE, USA). The RNA integrity was assessed by Agilent 2100 with RIN number >7.0.

Poly(A) RNA is purified from plant total RNA (20μg) using poly-T oligo-attached magnetic beads using two rounds of purification. Because of the 3′ cleavage product of the mRNA contains a 5′-monophosphate, the 5' adapters were ligated to the 5' end of the 3′ cleavage product of the mRNA by the RNA ligase. The next step is reverse transcription to make the first strand of cDNA with a 3′-adapter random primer and size selection was performed with AMPureXP beads. Then the cDNA was amplified with PCR by the following conditions: initial denaturation at 95°C for 3 min; 15cycles of denaturation at 98°C for 15 s, annealing at 60°C for 15 s, and extension at 72°C for 30 s; and then final extension at 72°C for 5 min. The average insert size for the final cDNA library was 200-400 bp. At last, we performed the 50bp single-end sequencing on an Illumina Hiseq 2500 (LC Bio, China) following the vendor's recommended protocol.

Degradome sequencing data were analyzed using ACGT101-DEG (LC Sciences, Houston, Texas, USA), which incorporates CleaveLand4. The analysis began with the preprocessing of sequences and followed by the creation of degradome density file. The miRNA sequences were aligned with the reference transcript sequence to identify potential clipping sites. Finally, the integration of sequencing data and comparison results allowed for the identification of targets and cutting sites which are supported by evidence of degradation fragments, and obtain the P-values.

## 2.9 Prediction of cis-regulatory elements and corresponding TFs

The 1000 bp upstream sequence of DEGs and the 2000 bp upstream sequence of MIRNA loci were extracted, followed with cis-regulatory element prediction carried out using FIMO v4.11.2 (parameter: default) with the JASPAR2024_CORE_non-redundant database. The classification of cis-regulatory elements was based on the prediction results obtained from plantTFDB for the corresponding proteins documented in the JASPAR database. At the same time, we used the plantCARE online tool to make additional predictions.

The TFs of eelgrass were predicted using the Plant Transcription Factor Database (plantTFDB) available at http://planttfdb.cbi.pku.edu.cn/. The expression patterns of these TFs were compared with those predicted target genes. TFs with a Pearson correlation coefficient (PCC) of 0.8 or higher were selected as candidate regulators. Cytoscape v3.10.2 (https://cytoscape.org/) was employed for visualization of the transcriptional regulatory network.

## 2.10 Gene family analysis

Based on the results of functional enrichment analysis in eelgrass and references to genes involved in salt tolerance in terrestrial plants, we selected a set of genes for gene family analysis.

Aquaporins in eelgrass containing PF00230 domains were identified by hmmscan 3.4 (parameter:-E $10^{-5}$). Four classes of ion channel proteins, the NHX, KEA, and CHX family genes were gathered from the research of Olsen et al. (2016). Blast comparison was performed based on the protein sequences to find the corresponding gene IDs in Zostera marina v3.1. Additionally, genes possessing the PF01699 domain were classified as members of the $Ca^{2+}/H^{+}$exchanger antiporter (CAX) family using the hmmscan tool with a parameter setting of -E $10^{-5}$. Antioxidant enzyme genes, including superoxide dismutase (SOD), catalase (CAT), and glutathione peroxidase (GPX) collected based on the research of Olsen et al. (2016). Blast comparisons were carried out using the protein sequences to determine the corresponding gene IDs in Zostera marina v3.1. Moreover, a list of ascorbate peroxidase (APX) family genes from *A. thaliana* was retrieved from NCBI, and the homologous genes in eelgrass were identified using OrthoFinder. Moreover, OrthoFinder was utilized to identify homologous genes in eelgrass based on hormone-related genes in *A. thaliana* summarized by Altmann et al. (2020). Genes involved in the salt overly sensitive (SOS) pathway were identified by first compiling a list of *A. thaliana* genes associated with this pathway (Sandoval-Gil et al., 2023). Subsequently, using the *A. thaliana* gene IDs, the ortherFinder identification results were utilized to locate the corresponding genes in eelgrass.

Using protein sequences, we employed blastp v2.12.0 (parameters: -evalue $10^{-10}$, -max_target_seqs 5) to identify the top five homologous genes in *A. thaliana*, rice, and maize to construct phylogenetic tree. Besides, to compare the response to salinity across species, 100 rice sra data and 57 maize sra data (Supplementary Data S9) were downloaded from the NCBI. The reference genome was obtained from Ensembl Plants. Data preprocessing, sequence alignment, gene expression quantification, and identification of DEGs were performed following the same procedures as those for the samples of eelgrass. The GO annotation of genes in rice and maize was performed by eggNOG. To identify the set of genes that are widely up-regulated in rice and maize, we counted sample comparisons for up-regulated DEGs. Then, we selected the genes based on the top 10% percentile of comparison counts and performed functional enrichment analysis.

# 3 Results

## 3.1 The transcriptional response of genes under salt stress

The raw data of RNA-seq includes 41.8-53.4 million reads, and the mapping rate of most samples is greater than 80%. We identified a total of 409 DEGs between the samples under salinity 50 and 30 treatment using DESeq2 (Supplementary Data S1; Supplementary Figure S1A), including 188 genes from leaf tissue and 236 genes from SR tissue (the mixed tissue of stem and root). Additionally, an analysis of the PRJNA342750 dataset revealed 334 DEGs in leaf tissues in response to NaCl. There was minimal overlap among the DEGs identified across the three groups (Supplementary Figure S1B), indicating distinct responses to salt stress in different tissues and under varying experimental conditions.

We performed functional enrichment analysis on the DEGs identified in our data, which revealed several enriched GO terms and KEGG pathways such as "response to water deprivation (GO:0009414)", "MAPK signaling pathway-plant (map04016)", "Biosynthesis of secondary metabolites (map01110)", "Phenylpropanoid biosynthesis (map00940)" (Figure 1; Supplementary Figures S1C, D). DEGs in GO:0009414 were predominantly up-regulated in leaf, including members of the PP2C family (*Zosma01g16060*), ERF family members (*Zosma05g33490* and *Zosma03g37150*), Late embryogenesis abundant protein (*Zosma05g03710*), and the UPF0057 family gene (*Zosma03g14850*). Conversely, DEGs in map04016 were primarily down-regulated in leaf, including family members of MAPKKK (*Zosma03g00830*, *Zosma03g00810*), ERF (*Zosma06g29270*), WRKY (*Zosma06g26970*), and CALM (*Zosma06g17200*). What's more, DEGs in map01110 were mainly up-regulated in SR tissue, including Cinnamate 4-coumarate: CoA ligase (*Zosma01g00600*), trans-cinnamate 4-monooxygenase (*Zosma02g22230*), cinnamoyl-CoA reductase (*Zosma03g12930*), phenylalanine ammonia-lyase (*Zosma03g22300*), cinnamyl-alcohol dehydrogenase (*Zosma06g25800*), chalcone synthase (*Zosma01g25890*), and chalcone isomerase (*Zosma06g21110*). MapMan annotation and enrichment results indicated that salt stress may induce programmed cell death (Supplementary Figure S1C). *Zosma03g26890* is a proline dehydrogenase and down-regulated under salt stress, indicating the proline accumulation might be enhanced in eelgrass. (Supplementary Figure S1D). Additionally, plant hormones such as ABA and gibberellin may play a role in the response to salt stress (Supplementary Figure S1D).

By examining the overlapping DEGs, we identified four genes (*Zosma02g20240*, *Zosma04g22590*, *Zosma05g04820*, *Zosma05g31200*) that were up-regulated in all three comparisons (Supplementary Figure S1B). *Zosma05g04820* is a member of the AP2/ERF family, and its homologous genes participate in abiotic stress such dehydration (Sakuma et al., 2002). *Zosma04g22590* encodes NCED is a crucial enzyme in the biosynthesis of ABA (Qin and Zeevaart, 1999), of which homologous genes function in drought tolerance (Iuchi et al., 2001). *Zosma02g20240* belongs to the CAX family of cation antiporters, of which the homologous gene is involved in calcium transport (Emery et al., 2012). *Zosma05g31200* is a senescence-associated protein, of which homologous genes are involved in various abiotic stress including salt stress (Barajas-Lopez et al., 2021). The transcriptional response of these four DEGs was further verified through qRT-PCR assays (Figure 2).

We observed that the tissue-specific responsive genes account for a large proportion of the DEGs identified by our data (Supplementary Figure S1B). Consistently, the results of functional enrichment analysis on these gene sets (Supplementary Figure S1E) were similar to those described above (Figure 1), which indicate enhanced and impaired biological processes in different tissues. Especially, we found that an enriched GO term "fucose biosynthetic process" was identified from up-regulated genes in leaf. In a previous study, fucose was found as the main component of extracted polysaccharides in *Lessonia* (Zou et al., 2019). This raises the question of whether fucose is involved in the adaptation of marine plants to high-salt environments. What's more, we examined the specific DEGs in response to NaCl (identified by PRJNA342750 data): 118 genes were up-regulated, which were involved in biological processes such as "response to stimulus (GO: 0050896)", "cobalamin biosynthetic process (GO: 0009236)" and "heme biosynthetic process (GO: 0006783)"; 167 genes were down-regulated, which were involved in the process such as "carbohydrate metabolic process (GO: 0005975)" and "mucilage metabolic process (GO: 0010191)". These results help us to gain a deeper understanding of the response of eelgrass to salinity changes at the organ level.

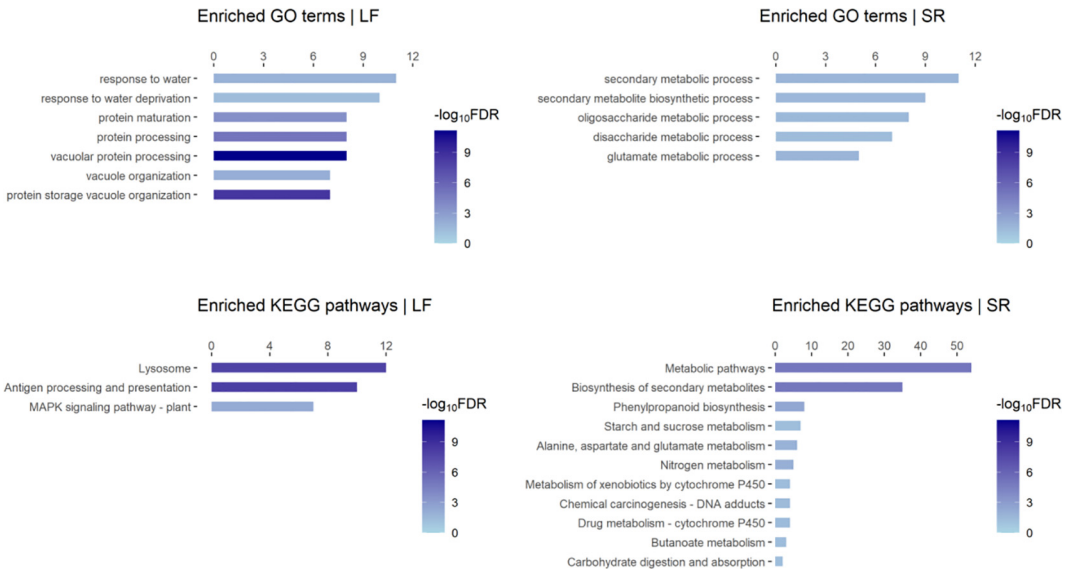


FIGURE 1
Enriched GO terms and KEGG pathways of responsive DEGs to high salt in eelgrass. "LF" refers to the leaf; "SR" refers to the mixed tissue of stem and root. The length of the bar refers to the count of DEGs in a Go-term or KEGG pathway.

10.3389/fpls.2025.1497064

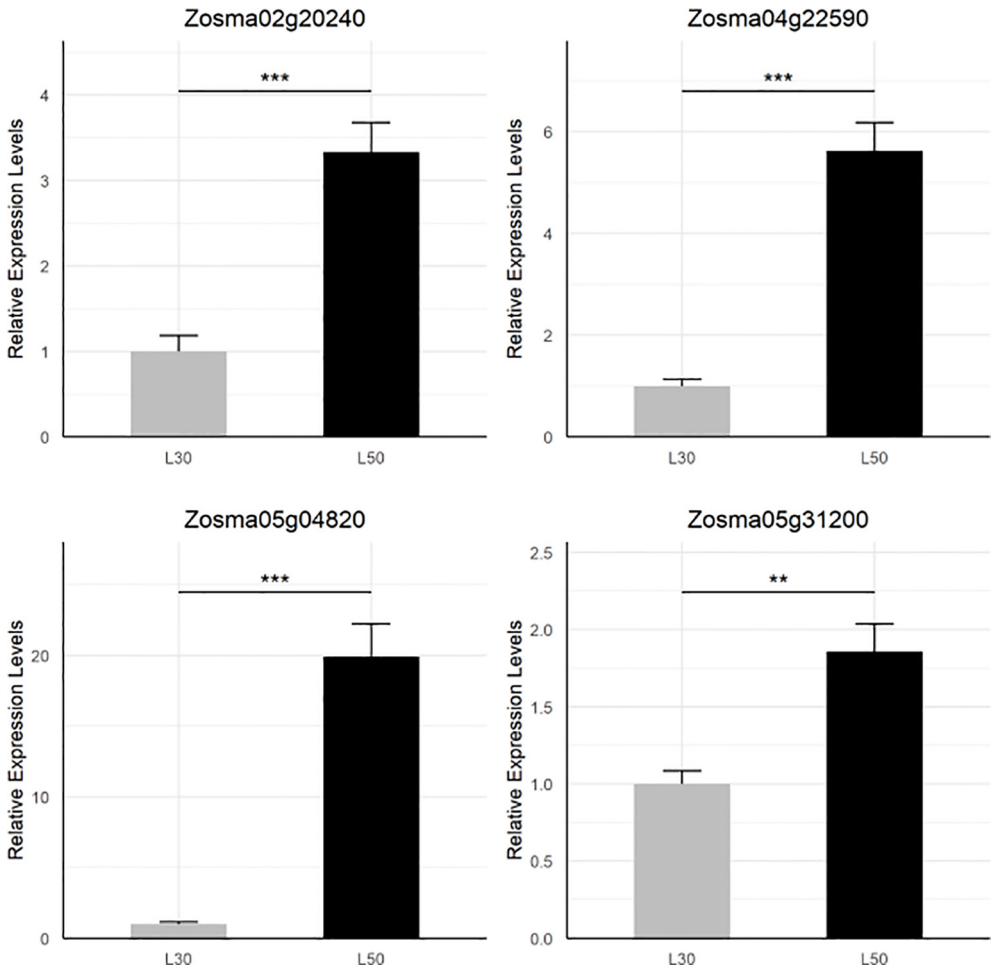


FIGURE 2
qRT-PCR validation of four DEGs that are up-regulated in all comparisons. The star marks on statistical charts represent the statistical significance: "*" stands for P < 0.05, "**" stands for P < 0.01, "***" stands for P < 0.001.

## 3.2 Salt-responsive DEGs in co-expression modules

Utilizing our data and transcriptome data from 58 samples of eelgrass obtained from NCBI (Supplementary Data S2), we constructed a gene co-expression network that revealed a total of 36 gene modules, each containing at least 30 genes (Supplementary Data S3; Supplementary Figures S2A, B). The analysis (Supplementary Figure S2C) indicated that the up-regulated genes under salt stress in leaf were predominantly distributed in the M3, M4, M6, and M7 modules, while the down-regulated genes in leaf were primarily found in the M1, M2, M4, and M6 modules. In SR tissue, most of the up-regulated genes were distributed in the M4 and M6 modules, while the down-regulated genes were mainly distributed in the M2, M4, M6, and M7 modules.

We focused on the salt-responsive DEGs in modules M4, M6, and M9 due to their expression patterns (Figure 3A; Supplementary Figure S2B): M4 exhibited a high expression primarily in leaf. M6 was notably expressed in leaf, stems, and roots. M9 showed predominant expression in stem and root. M4 harbored a number of metal transporters that were up-regulated (Supplementary Figure S2D), such as the mitochondrial iron transporter (*Zosma03g13600*) and several heavy metal-associated domain-containing proteins (*Zosma04g04780*, *Zosma02g05210*, *Zosma02g16380*). Conversely, many DEGs related to photosynthesis in M4 were significantly down-regulated (Supplementary Figure S2D), including the light-harvesting complex I chlorophyll a/b binding proteins (*Zosma02g19650*, *Zosma03g33730*, *Zosma03g35370*, *Zosma05g20560*) and the photosystem II reaction center *PSB28* protein (*Zosma03g24460*). Furthermore, several nutrition-related DEGs in leaf were up-regulated (Supplementary Figure S2D), including nitrite reductase (*Zosma02g18160*, *Zosma03g25160*) in M4, nitrate transmembrane transporters (*Zosma05g08330*), proton/phosphate symporters (*Zosma05g32160*) and ferritin (*Zosma02g21810*) in M6. These findings suggest a shift in the nutritional status of eelgrass under salt stress. Additionally, M6 contains a few up-regulated DEGs associated with calcium-dependent signaling (Supplementary Figure S2D), such as calmodulin-related calcium sensor proteins (*Zosma01g15140*, *Zosma01g36630*, *Zosma04g24750*), indicating heightened calcium signaling activity in response to high salinity. A set of up-regulated DEGs in M9 were involved in secondary metabolism (Supplementary Figure S2D), such as phenylalanine

10.3389/fpls.2025.1497064

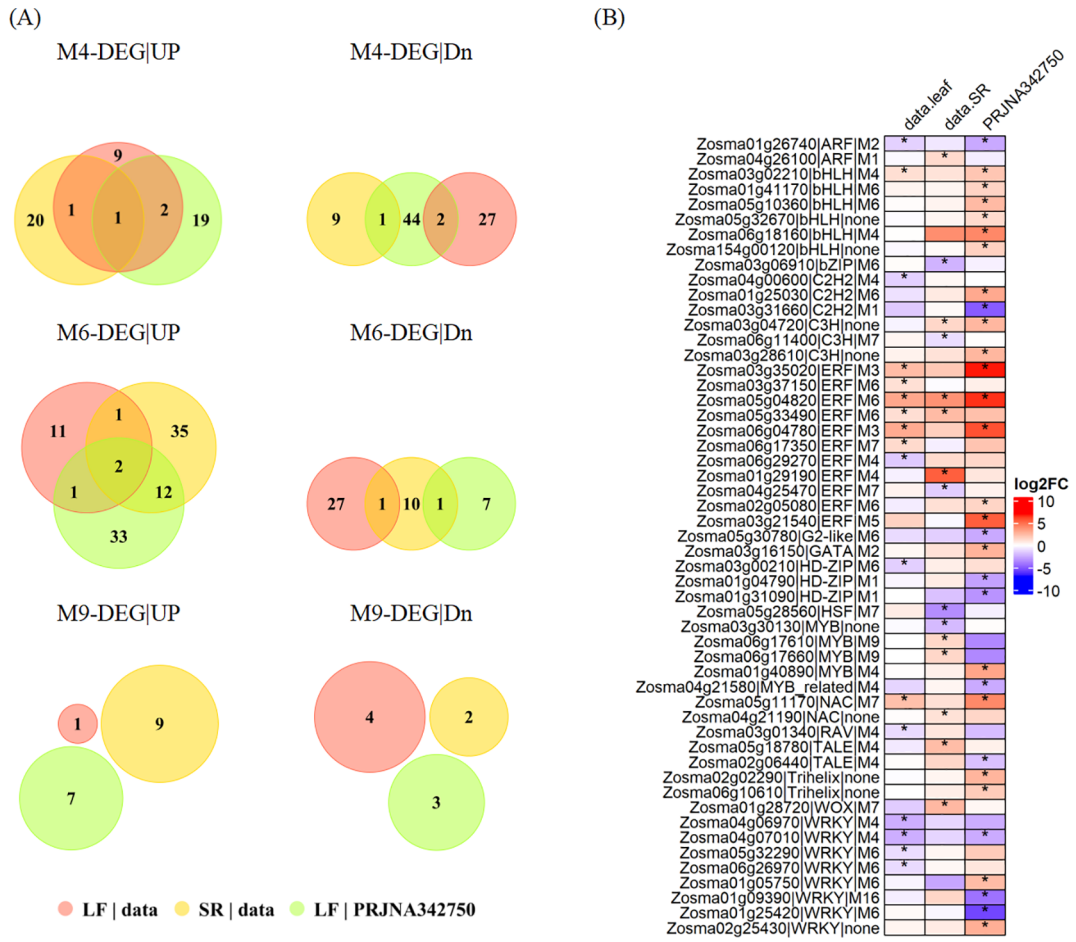


FIGURE 3
Salt-responsive DEGs in WGCNA modules. **(A)** Up-regulated or down-regulated genes in response to high salinity assigned to M4, M6 and M9. **(B)** The transcriptional response of TFs to high salinity. The asterisk stands for a significant difference in the expression comparison.

ammonia-lyase (*Zosma03g22300*), cinnamoyl-CoA reductase (*Zosma03g12930*) and glutamate decarboxylase (*Zosma02g19830*), indicating that the plants might undergo secondary metabolic changes in stem and root.

TFs are potential regulators for genes in co-expression modules. The M4 module contains 12 salt-responsive TFs. Three of these TFs were up-regulated in leaf, including two bHLH family members (*Zosma03g02210*, *Zosma06g18160*) and one MYB family member (*Zosma01g40890*). Two of these TFs were up-regulated in SR tissue, including one ERF family member (*Zosma01g29190*) and one TALE family member (*Zosma05g18780*). The M6 module includes 14 salt-responsive TFs. Eight of these TFs were up-regulated in leaf, including four ERF family members (*Zosma03g37150*, *Zosma05g04820*, *Zosma05g33490*, *Zosma02g05080*), two bHLH family members (*Zosma01g41170*, *Zosma05g10360*), one *C2H2* family member (*Zosma01g25030*), and one WRKY family member (*Zosma01g05750*). Two ERF family members (*Zosma05g04820* and *Zosma05g33490*) were up-regulated in SR tissue. M9 module contains 2 salt-responsive TFs, which belong to MYB family members (*Zosma06g17610* and *Zosma06g17660*) and show up-regulated expression in SR tissue. How these TFs regulate the response of eelgrass to salt stress is an issue that remains to be resolved. (Figure 3B; Supplementary Figure S2E; Supplementary Data S4). We analyzed the cis-regulatory elements located within the 1000 bp region upstream of DEGs. Our findings revealed that the motifs potentially binding TFs such as bHLH, ERF and MYB family members (Supplementary Figure S2F) are universally distributed in the promoter of DEGs. Moreover, predictions from the PlantCARE indicate that plant hormone signals, such as ABA and JA, may also contribute to the regulatory mechanisms in eelgrass (Supplementary Figure S2G).

## 3.3 Identification and classification of microRNAs

In this study, a total of 172 MIRNA loci were identified through the analysis of small RNA sequencing data (Figure 4A). miRDeep-P2 exhibited a higher sensitivity compared to Shortstack, being able to identify 157 miRNAs independently. Additionally, ShortStack detected 6 miRNAs that were not identified by miRDeep-P2. Of these sites, 9 were found to be identified by both the Shortstack and miRDeep-P2 tools, which are considered the most reliable sites for MIRNA. The majority of these miRNAs were found to be located on

10.3389/fpls.2025.1497064

chromosomes (Supplementary Figure S3A), with a few being situated on the scaffold. The length distribution of the identified mature sequences was predominantly 20-22 nt, aligning with the typical length characteristics of miRNAs in plants (Figure 4C).

Subsequently, a comparison was conducted between the mature sequences obtained from the predicted sites and those documented in miRbase (Figure 4B). This comparison led to the annotation of a total of 38 miRNAs belonging to known MIRNA families, while an additional 134 miRNAs were identified as *de novo* loci (Supplementary Data S5). Among the known families, *MIR156* was identified to have the highest number of loci in eelgrass, specifically containing six members. Moreover, several other families, including *MIR166*, *MIR172*, *MIR164*, *MIR396*, *MIR319*, and *MIR390*, were found to have more than two members each.

Simultaneously, the relative positions of MIRNAs to neighboring genes were assessed. A total of 41 MIRNAs were categorized as intragenic, while 131 were categorized as intergenic (Supplementary Figure S3B). Among the intragenic MIRNAs, 31 were located within intron regions, 3 were found in exon regions, and 7 spanned both introns and exons (Supplementary Figure S3C). For 78.3% of the intergenic MIRNAs were located within 20,000 bp of an upstream gene (Supplementary Figure S3D).

## 3.4 Salt-responsive miRNAs in eelgrass

We identified a total of 14 DEmiRNAs in response to salt stress using edgeR and DESeq2. There were 8 overlapped DEmiRNAs identified by both tools, including *MIR166a*, *MIR166d*, *MIR172d* and a series of *de novo* loci (Figure 5A; Supplementary Figure S3E; Supplementary Data S6). The transcriptional responses of miRNAs from these loci such as miR156, miR166 and NOVEL008 were further validated through qRT-PCR assays (Figure 5C; Supplementary Figure S3F). To uncover the potential mechanisms regulating miRNA expression, we analyzed the cis-regulatory elements within the 2000 bp upstream region of MIRNAs. The results showed that there were many potential TF binding sites upstream of the MIRNA. The binding sites for TFs such as bZIP, C2H2, and Dof are widely present (Supplementary Figures S4A, B). Additionally, predictions from plantCARE indicated that the upstream regions of DEmiRNAs were enriched in cis-regulatory elements associated with abiotic stress and hormone responses. It suggests that diverse signaling pathways, such as those related to osmotic stress (STRE) and JA (CGTCA-motif and TGACG-motif), play a role in regulating microRNA expression in eelgrass (Supplementary Figure S4C).

## 3.5 miRNA-target module in eelgrass

We employed psRNATarget to predict microRNA target genes, of which 35 were DEGs in response to salt stress and potentially targeted by DEmiRNA (Supplementary Data S7). There are a number of target genes whose expression changes are negatively correlated with their corresponding miRNAs, such as miR156 and miR166. Among them, *Zosma06g26970*, is a member of WRKY family and identified as a target gene for miR156; *Zosma03g00210*, is a member of the HD-ZIP family and identified as a target gene for miR166 (Figure 5B). Both of them exhibit down-regulated expression at high salinity, of which homologous genes has been reported to be involved in salt stress (Jiang and Deyholos, 2009; Yadav et al., 2021). The responses of these miRNAs and their target genes were further validated through qRT-PCR assays (Figure 5C).

We also employed degradome sequencing to investigate the target sites of microRNAs (miRNAs), resulting in identification of 91 reliable miRNA-target pairs (Supplementary Data S8). 86.8% of these miRNA-target pairs were consistent with the predicted pairs identified by psRNATarget. Among the predicted targets, we found two genes were DEGs in response to salt stress. *Zosma04g26100*, a potential target of miRNA160 (Figure 6), exhibited up-regulation in SR tissue. The homolog of *Zosma04g26100*, *athARF16* (*AT4G30080*) plays roles in root cap cell differentiation and is regulated by both miRNA160 and plant hormones (Wang et al., 2005; Bascom, 2023). The relatively insignificant response of miRNA160 might facilitate the increased expression of *Zosma04g26100*. *Zosma05g29470*, identified as a potential target for NOVEL056, displayed a predicted cutting site that is not located near the peak of degraded fragments (Supplementary Figure S5). The homologous gene *athPAL1* (*AT2G37040*) of *Zosma05g29470* is implicated in the biosynthesis of lignin and flavonoid (Olsen et al., 2008), suggesting

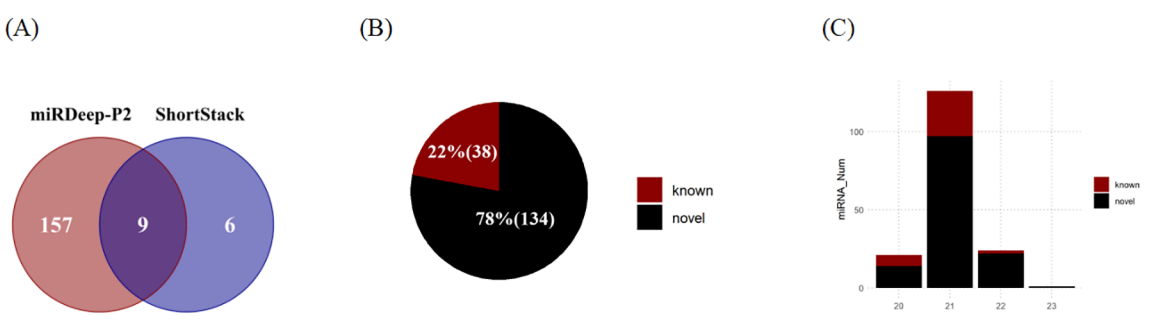


FIGURE 4
Identification of microRNAs in eelgrass. **(A)** The number of MIRNAs identified by ShortStack and miRDeep-P2. **(B)** The number of identified MIRNAs belonging to known and novel families. **(C)** The number of miRNAs (mature sequence) of different lengths.

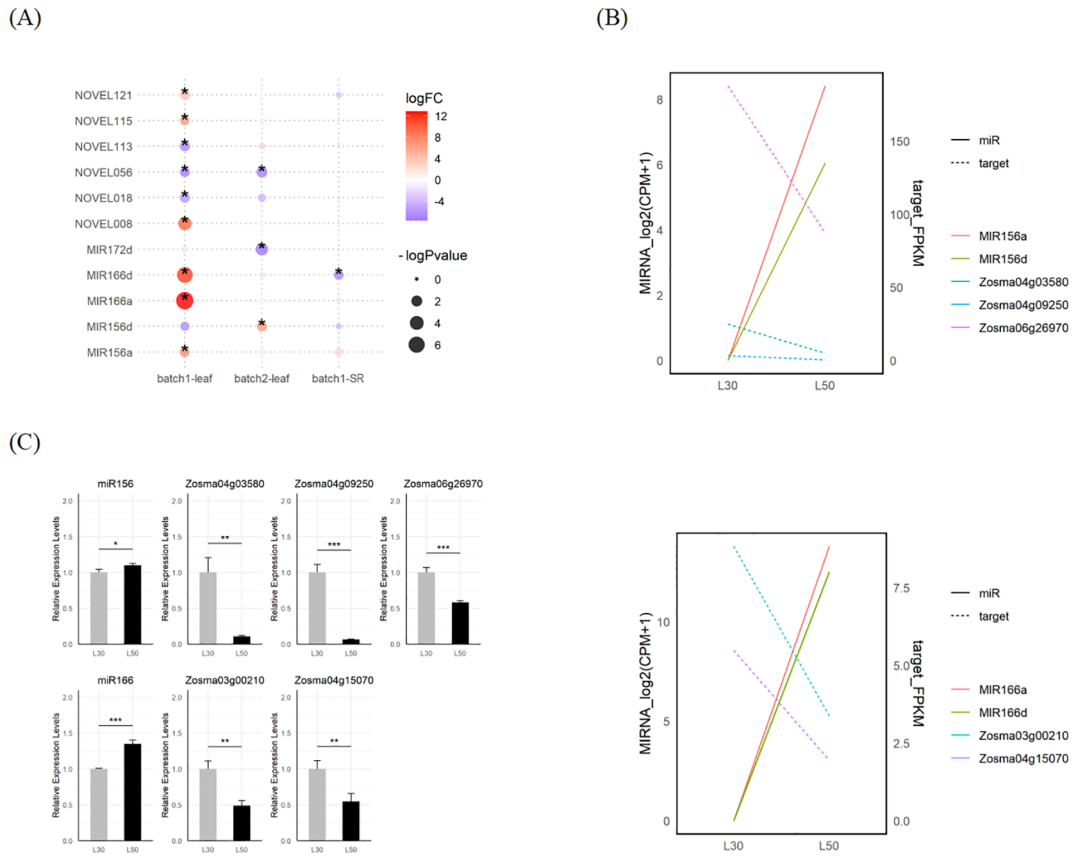


FIGURE 5
DEmicroRNAs and their potential targets in eelgrass. **(A)** The DEmiRNAs in response to salt stress in eelgrass identified by edgeR. **(B)** The expression of MIR156, MIR166 and their predicted targets in L30 and L50. **(C)** Validated expression of MIR156a/d and MIR166a/d mature sequences as well as their predicted targets using qRT-PCR. The gray bar stands for L30, while the black bar stands for L50. The star marks on statistical charts represent the statistical significance: "*" stands for $P < 0.05$, "**" stands for $P < 0.01$, "***" stands for $P < 0.001$.

that the down-regulation of *Zosma05g29470* could adversely affect related metabolic functions.

Although some genes did not exhibit obvious responses to salt stress, they were potentially regulated by microRNAs, as indicated by the degradome data and previous studies (Figure 6). For instance, the target gene of miRNA156, *Zosma05g09900*, is a member of the SPL family, of which homologous gene has been implicated in various processes such as plant morphogenesis (Ferreira e Silva et al., 2014), secondary metabolism (Gou et al., 2011), and signal transduction (Barrera-Rojas et al., 2023). *Zosma05g02470* and *Zosma03g23770*, both belonging to the HD-ZIP family (Supplementary Figure S5), are predicted target genes of miR166. Their homologous genes in *A. thaliana* play crucial roles in regulating vascular development (Kim et al., 2005). Moreover, the degradome data provided evidence for additional miRNA-target pairs, including miR396-GRF (*Zosma02g02440*/*Zosma01g12870*), miR393-TIR (*Zosma01g13700*/*Zosma02g25510*), miR167-ARF (*Zosma01g35720*), miR319-TCP (*Zosma03g04610*), and miR164-NAC (*Zosma05g19590*) (Supplementary Figure S5), which have been reported to function in other plant species (Guo et al., 2005; Gutierrez et al., 2009; Liang et al., 2014; Koyama, 2017; Wang et al., 2018). The miRNA cleavage sites identified by the degradome are speculative and require future verification.

# 4 Discussion

## 4.1 Osmosis homeostasis at high salinity

The enriched GO-term "response to water deprivation" suggests that eelgrass may experience osmotic stress similar to drought conditions in high salt environment. Most DEGs within this GO-term are significantly up-regulated in leaf, including *Zosma01g16060*, *Zosma03g14850*, *Zosma03g23560*, *Zosma03g33910*, *Zosma03g37150*, *Zosma05g03710* and *Zosma05g33490*. Among these genes, *Zosma01g16060* is a member of the PP2C family, of which homolog in *A. thaliana*, *HAI2* (*AT1G07430*), whose mutant has been documented to enhance drought resistance by regulating proline and osmoregulatory solute accumulation (Bhaskara et al., 2012). The other two DEGs *Zosma05g03710* and *Zosma03g14850* in GO term of "response to water deprivation" also appear to be involved in salt stress. The homolog (*AT1G01470*) of *Zosma05g03710* has been reported to exhibit significant protective effects under salt stress (Jia et al., 2014), while the homolog *RCI2B* (*AT3G05890*) of *Zosma03g14850* is responsive to abiotic stresses such as low temperature and water scarcity, with its expression induced by ABA (Capel et al., 1997). *Zosma05g33490* and *Zosma03g37150* belong to the *AP2/ERF* family. The homologous gene *DREB1A* (*AT4G25480*)

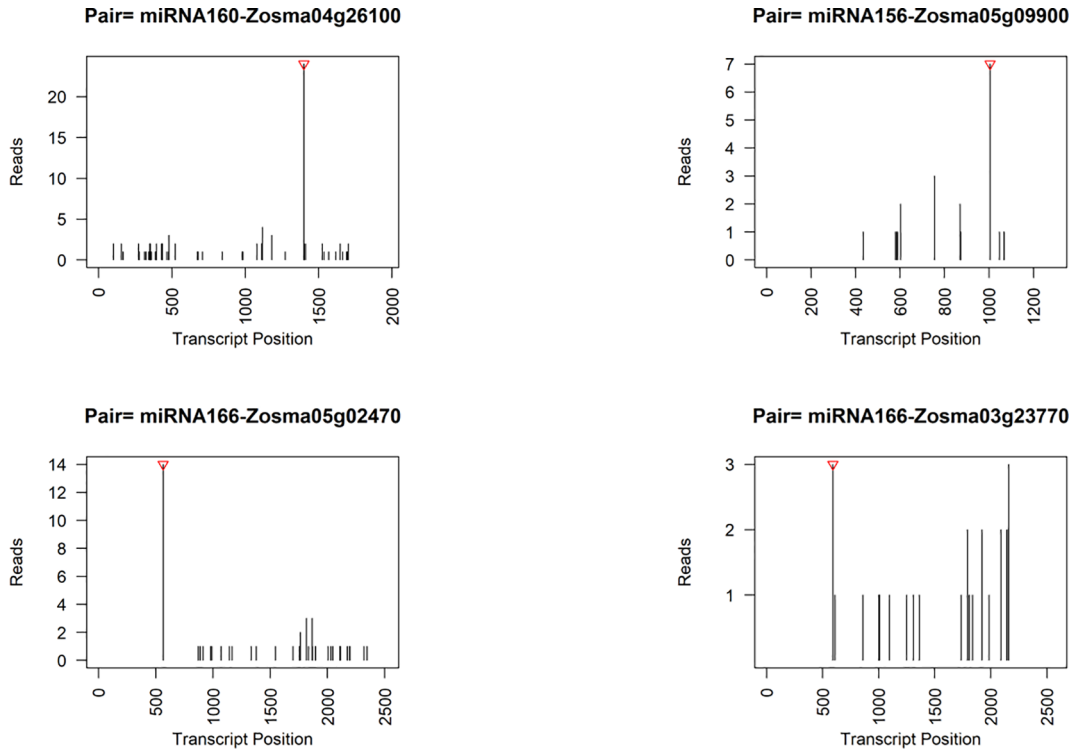


FIGURE 6
Representative target plots (t-plot) depicting categories of the cleaved mRNAs confirmed by degradome sequencing. The red triangle at the top represents the predicted cleavage location.

of *Zosma05g33490* has been implicated in the response to abiotic stresses, including drought, across various plant species (Polizel et al., 2011; Ravikumar et al., 2014). Meanwhile, the homolog of *Zosma03g37150* is known to participate in gene expression related to dehydration and cold stress (Sakuma et al., 2002). Besides, the collinear genes of *Zosma01g16060*, *Zosma05g33490*, and *Zosma05g03710* in rice and maize also exhibit responses to salt stress, suggesting a conserved role among these "response to water deprivation" genes (Supplementary Data S10; Supplementary Figure S6). By comparing the enriched go-terms, we observed that the biological process "response to water deprivation" is conserved in three species (Supplementary Figure S6C). Within this go-term, some gene families, such as AP2, PP2C, and Annexin, are present in both eelgrass and rice, suggesting similarities in how marine and terrestrial plants respond to high salinity stress.

Aquaporins are the key regulators for regulating osmotic homeostasis in plants (Ren et al., 2021). Previous studies in other seagrass have suggested that aquaporins contribute to the adaptation in hypersaline environments (Sandoval-Gil et al., 2023), and one of the studies has shown that aquaporins are involved in the maintenance of osmotic balance (Serra et al., 2013). In this study, we identified a total of 25 aquaporins in eelgrass (Supplementary Data S11). The gene expression profile revealed that several aquaporin members, including *Zosma01g17610*, *Zosma01g27210*, *Zosma02g03080*, *Zosma02g23130*, and *Zosma03g25250*, exhibited high expression levels across multiple organs (Supplementary Figure S7A). The phylogenetic analysis (Supplementary Figure S7B) indicates that *Zosma01g17610* belongs to the TIP branch, while *Zosma01g27210*, *Zosma02g23130*, and *Zosma02g03080* belong to the SIP branch, and *Zosma03g25250* is part of the NIP branch. Members of the TIP branch have been associated with the promotion of new lateral root primordia (Reinhardt et al., 2016), whereas SIP branch members are primarily localized in the endoplasmic reticulum, functioning as channels for water, small molecules, and ions (Ishikawa et al., 2005). Additionally, NIP branch members are implicated in the absorption of certain mineral ions and can influence hydrogen peroxide ($H_2O_2$) levels (Kamiya et al., 2009; Kamiya and Fujiwara, 2009; Wang et al., 2017). The widespread expression of these genes may facilitate the transport of water and small solutes across cell membranes in eelgrass. Simultaneously, we observed that three aquaporins (*Zosma03g21300*, *Zosma01g24240*, and *Zosma03g27440*) exhibited significantly down-regulated expression levels under high salt conditions. The phylogenetic tree reveals that *Zosma01g24240* belongs to the PIP1 branch, *Zosma03g21300* to the PIP2 branch, and *Zosma03g27440* to the TIP branch. Members of the PIP1 branch are reported to be involved in water transport and immune responses (Postaire et al., 2010; Tian et al., 2016), while those in the PIP2 branch are associated with drought resistance (Chen et al., 2021, 2022) and the transport of $H_2O_2$ (Rodrigues et al., 2017; Wang et al., 2020). *Zosma03g27440* and *Zosma01g17610* share the same branch, suggesting potential functional redundancy. Furthermore, a number of their homologous genes in rice and maize, such as *Zm00001eb096680*, also exhibit reduced expression at high salinity (Supplementary Figure S7C). In terrestrial plants, drought or salt

stress can suppress the expression of certain aquaporins such as PIPs, thereby reducing root hydraulic conductivity by limiting water loss (Yepes-Molina et al., 2020). The down-regulation of aquaporins in eelgrass might reflect a conserved character in plants responding to salt stress.

## 4.2 Ion homeostasis at high salinity

Plant adaptation to high-salinity environments depends in part on the maintenance of cell ion homeostasis, a process significantly facilitated by ion transporters (Malakar and Chattopadhyay, 2021). In this study, we identified several key ion transporter families in eelgrass, including five Na(+)/H(+) exchangers (NHX), five K(+) efflux antiporters (KEA), fifteen cation/H(+) exchangers (CHX), and eleven sodium/calcium exchanger proteins belonging to CAX family (Supplementary Data S11). The gene expression profile (Supplementary Figure S8A) indicates that most NHX and KEA genes are broadly expressed across multiple organs, with the exception of one NHX member (*Zosma01g13710*), which exhibits specific expression in floral organs. In contrast, the expression of CHX family exhibits organ specificity, particularly with higher expression levels in male flowers, suggesting a potential role in reproductive development. Approximately half of the CAX members are also widely expressed in various organs, including *Zosma02g20240*, which shows significant accumulation under high salt stress. While alterations in calcium levels are critical in the SOS pathway (Ali et al., 2023), there is currently no evidence linking CAX family members to this process. Previous research has indicated that certain CAX family members, such as *athNCL* (*AT1G53210*), contribute to plant salt tolerance (Wang et al., 2012). The genes of eelgrass in the same branch of *athNCL* include *Zosma01g22450* and *Zosma06g26160* (Supplementary Figure S8B), while *Zosma02g20240* is positioned on a separate branch, indicating the need for further investigation into their roles in salt tolerance. Additionally, comparative analysis reveals that, unlike eelgrass, many ion channel protein genes in rice and maize respond to salt stress (Supplementary Figure S8C), highlighting the differences in ion regulation mechanisms between terrestrial and marine plants.

## 4.3 Activation of antioxidant system and secondary metabolic pathways

Osmotic stress and ionic stress induced by salt stress can lead to the production of ROS in plants (Hasanuzzaman et al., 2021). To mitigate the effects of ROS, plants can accumulate osmotic products and enhance the activity of antioxidant enzymes, thereby improving their tolerance to salt stress (Yang and Guo, 2018). In this study, several antioxidant enzymes were identified in eelgrass, including SOD, CAT, GPX, and APX (Supplementary Data S11). Gene expression profiles revealed that, while most antioxidant enzymes did not show a significant response to salt stress, they were highly expressed across multiple organs (Supplementary Figure S9A). Zhang et al. (2023) also discovered the upregulation of SOD, peroxidase and other antioxidant enzyme genes in germination of eelgrass, but with no significant difference. Olsen et al. (2016) reported many stress-resistance genes in eelgrass. The salinity and temperature fluctuation are usually gradual in coastal environments, we speculate that high constitutive expression of antioxidant enzyme genes in eelgrass might be the adaptation mechanism to reduce the ROS during the gradual change of abiotic stress. Notably, *Zosma06g29150*, a member of the GPX family, exhibited significant up-regulation in the leaf, indicating that this enzyme may function in reducing $H_2O_2$ by oxidizing glutathione (GSH) (Das and Roychoudhury, 2014), thereby enhancing salt tolerance. GPX was also reported as the most abundant DEGs and proteins in eelgrass under low salinity stimulation during germination (Zhang Y. et al., 2023), which is coincident with the result of our study. It indicated that GPX family is the main antioxidant enzyme for scavenging ROS in eelgrass. Furthermore, homologous genes of *Zosma41g01010* in rice and maize, such as *Os02g0664000* and *Zm00001eb016270*, also respond to salt stress (Supplementary Figures S9B, C).

Salt stress induces secondary metabolic changes in plants, especially the accumulation of phenolic compounds, including lignin (Dabravolski and Isayenkov, 2023) and flavonoids (Shomali et al., 2022). Lignin fortifies plant cell walls, thereby protecting membrane integrity under salt stress. Flavonoids play a role in reducing ROS accumulation to enhance plant resistance to adverse conditions (Li et al., 2018). The biosynthesis of many phenolic compounds occurs via the phenylpropanoid pathway (Salam et al., 2023). Transcriptional analysis in this study revealed that several genes associated with phenylpropanoid and flavonoid synthesis were responsive to high salt stress. This suggests that the synthesis of phenolic compounds in eelgrass is highly active under such conditions. Furthermore, homologous genes in rice and maize exhibited significant up-regulation (Supplementary Figure S10), supporting the conserved secondary metabolic responses to salt stress across plant species.

## 4.4 Activation of phytohormone signaling pathway

Plant hormones are important participants in the salt tolerance of plants (Yu et al., 2020). In eelgrass, we identified a series of hormone-related genes responding to salt stress, suggesting high salinity stimulates the activation of phytohormone signaling pathway.

We have mentioned in the result that the ABA synthesis gene, *Zosma04g22590*, a member of the NCED family, was consistently up-regulated across three comparisons. However, another NCED family member, *Zosma01g20220*, exhibited down-regulation. In rice and maize, most members of this family are up-regulated (Supplementary Figure S11), suggesting the conservation of ABA signaling in plant salt responses. This viewpoint is further supported by several potential downstream genes of the ABA signaling pathway, including dehydrin family protein (*Zosma03g27730*), protein kinases (*Zosma03g25920*), and PP2C family members (*Zosma01g41250*, *Zosma02g21670*). Their expressions were up-regulated at high salinity and homologous genes have been

reported to be induced by ABA (Supplementary Figure S11). *RAB18* is the homolog of *Zosma03g27730* and reported to interact with *PIP2B* (Hernández-Sánchez et al., 2019), which suggests the regulation of aquaporin genes by ABA signaling. *Zosma01g41250* and *Zosma02g21670* are members of the PP2C family. Phylogenetic tree analysis shows that *Zosma01g41250* is located on the branch with *HAI1* and *HAI2*, while *Zosma02g21670* is located on the branch with *PP2C5* and *AP2C1*(Supplementary Figure S11). It is reported that HAI PP2C mutants had enhanced proline and osmoregulatory solute accumulation at low water potential (Bhaskara et al., 2012). Both *PP2C5* and *AP2C1* function as MAPK phosphatases, which are important to ABA signaling (Brock et al., 2010; Schweighofer et al., 2007). The up-regulation of PP2C members seems to be a conserved character under salt stress, as many homologous genes in rice and maize also show similar responses (Supplementary Figure S11). Terrestrial plants typically respond to osmotic stress caused by high salinity by regulating stomatal opening and closing via ABA (Hedrich and Shabala, 2018; Komatsu, 2020). Since eelgrass lacks stomata (Olsen et al., 2016), how ABA helps eelgrass cope with high-salinity environments needs further investigation.

In addition, JA, auxin, brassinosteroid (BR), cytokinin (CK) and gibberellin (GA) are also potential regulatory factors in the salt stress response of eelgrass. Research indicates that JA signaling in terrestrial plants is activated in response to salt stress, thereby enhancing salinity tolerance (Valenzuela et al., 2016; Zhao et al., 2014). Among the DEGs identified in eelgrass, *Zosma01g30620*, *Zosma05g15520*, and *Zosma06g28020* are associated with JA signaling and down-regulated at high salinity. The homologous gene of *Zosma01g30620*, lipoxygenases (LOX3) is involved in JA synthesis (López-Cruz et al., 2014). The homolog of *Zosma05g15520*, jasmonic acid carboxyl methyltransferase (JMT) is a carboxyl methyltransferase that catalyzes the formation of methyl jasmonate from jasmonate (Seo et al., 2001). *Zosma06g28020* is homologous to the jasmonic acid receptor *COI1* (Song et al., 2021). Furthermore, we found that auxin-related genes *Zosma03g17780* and *Zosma05g12790* were down-regulated under high salt stress. The homolog of *Zosma03g17780*, *PGP4* encodes an auxin effector transmembrane transporter, which is involved in auxin transport and inhibits root hair elongation (Cho et al., 2007). The homolog of *Zosma05g12790*, *ARA-2* plays a role in the auxin signaling pathway and inhibits lateral root development (Koh et al., 2009). Exogenous application of BR can enhance the salt tolerance of terrestrial plants, indicating that BR may be involved in salt tolerance (Fu and Yang, 2023). *Zosma03g35130* and *Zosma03g30090* are identified as BR-related genes. Overexpression of the *BKI1*, a homolog of *Zosma03g35130*, leads to a salt-tolerant phenotype (Zhang et al., 2017). *DOGT1*, a homolog of *Zosma03g30090*, encodes a don-glucosyltransferase that regulates BR activity (Poppenberger et al., 2005). Moreover, *Zosma06g28530* and *Zosma01g36380*, family members of two-component response regulator *ARR-A*, are associated with CK (Li et al., 2013; Ishida et al., 2008). These two genes are down-regulated at high salinity in eelgrass, most of which homologous genes in maize exhibited similar responses (Supplementary Figure S11). Among the down-regulated DEGs in SR tissue, we identified one gene related to gibberellin synthesis, *Zosma06g07970* (ent-kaurene oxidase), suggesting that hypersalinity may regulate gibberellin levels in eelgrass.

In terrestrial plants, the actions of different phytohormones are interconnected. For instance, the key regulator jasmonate ZIM-domain proteins (JAZ) in JA could be regulated by the PYL6-MYC2 module of ABA (Aleman et al., 2016). CK receptor kinase significantly regulates ABA levels (Nishiyama et al., 2013). The interplay between ABA and GA signaling under abiotic stress conditions is significantly influenced by DELLA proteins (Aizaz et al., 2024). In the future, we aim to reveal the reasons for these transcriptional changes by studying the hormone content in eelgrass. Furthermore, exploring the potential interactions of phytohormones under salt stress in eelgrass will be valuable.

## 4.5 SOS and MAPK signaling pathway in eelgrass

The SOS pathway is crucial for plant salt tolerance. Its core components include SOS1 (sodium-proton exchanger), SOS2 (CBL-interacting protein kinase), SOS3 (calcium-binding EF-hand family protein), and SCaBP8 (SOS3-like calcium-binding protein). Additional components associated with SOS pathway, such as *HIS1-3*, *MPK4*, *PLATZ2*, *RSA1* at the transcriptional level, and *UBC*, as well as *14-3-3*, *BIN2*, *CIPK8*, *GI*, *PKS5*, and *PP2C* at the post-transcriptional level, were also identified for plant salt tolerance (Ali et al., 2023). In our study, we utilized OrthoFinder (Supplementary Data S11) to identify SOS pathway genes in eelgrass. We found that none of these genes exhibited a significant response to salt stress, which was different from the findings in rice and maize (Supplementary Figure S12). Unlike terrestrial plants, which only have their roots in direct contact with soil salinity change, the whole plant of seagrass is exposed to the hypersalinity. The SOS pathway genes show high expression levels in various organs in eelgrass (Supplementary Figure S12A), which may provide a foundation for the protein-level responses of SOS pathway. Furthermore, several genes including *Zosma01g22480* (*SCaBP*), *Zosma05g05710* (*14-3-3*), and *Zosma01g41780* (*BIN2*), were specifically expressed in floral organs, indicating their potential involvement in the reproductive development of eelgrass.

Salt stress can activate the MAPK signaling cascade, which involves protein kinases that phosphorylate various substrates (Taj et al., 2010). In this study, we observed that the expression of two MAPKKK genes, *Zosma03g00830* and *Zosma03g00810*, was down-regulated under high salt conditions in leaf. Their *A. thaliana* homolog *MAPKKK18* (*AT1G05100*) is induced by ABA and promotes leaf senescence (Matsuoka et al., 2015). This suggests that eelgrass may enhance its salinity tolerance by reducing the accumulation of these MAPKKK genes, thereby avoiding senescence. Additionally, the colinear gene *Os05g0545300*, corresponding to *Zosma03g00810*, also responded to salt stress, although it exhibited down-regulation in only one comparison (Supplementary Figure S13).

## 4.6 miRNA and their potential targets in eelgrass

We identified a total of 172 MIRNA loci using small RNA-seq data. The mature sequences derived from these MIRNAs were predominantly 21 nucleotides in length. 83 (71.6%) of these microRNAs had uracil (U) as the first base at the 5' end. Previous studies have demonstrated that the presence of uracil at the 5' end can enhance the binding of microRNAs to the AGO1 protein (Mi et al., 2008). Based on the similarity of mature miRNAs, we identified 38 MIRNA belonging to known families, which is far fewer than the 93 known conserved miRNAs predicted genome-wide by Ma et al. (2021). The limited number of known miRNAs might be attributed to the restrictions in the plant tissues or RNA extraction method. The same kits for total RNA extraction were used for both mRNA and small RNA sequencing, as they have been employed in other researches (Zhang M. et al., 2023; Hu et al., 2021). In order to prove the accuracy of our study, we have experimentally validated the response of some DEmiRNAs using qRT-PCR. The results proved the existence of those miRNAs and the expression pattern of them was the same as the result from library construction.

Differential expression analysis of miRNAs revealed multiple miRNAs response to salt stress, including miR156, miR166, miR172, and a number of *de novo* miRNAs. miR156 has been reported to participate in salt tolerance across different plant species such as apple (Ma Y. et al., 2021), tobacco (Kang et al., 2019) and Alfalfa (Arshad et al., 2017). Similarly, miR166 has been shown to respond to salt stress in plants such as *Hemerocallis fulva* (Zhou et al., 2023), sugar beet (Zhang Z. et al., 2023), and potato (Kitazumi et al., 2015). It also plays a regulatory role in other abiotic stresses, including drought (Zhao et al., 2024) and low potassium conditions (Lei et al., 2023). In cereal crops, miR172 contributes to salt tolerance by maintaining ROS homeostasis (Cheng et al., 2021). Based on expression correlation analysis, we hypothesize that miR156 and miR166 are key regulators of the salt stress response in eelgrass. Specifically, miR156 was significantly up-regulated in leaf, while three of its target genes, WRKY family member *Zosma06g26970*, cellulose synthase *Zosma04g03580*, and heavy metal-related domain protein *Zosma04g09250*, were significantly down-regulated. Similarly, miR166 exhibited significant up-regulation in leaf, with two of its target genes, HD-ZIP family member *Zosma03g00210* and S-locus lectin protein kinase family protein *Zosma04g15070*, also showing significant down-regulation. This negative correlation in expression patterns suggests the potential existence of miRNA-target modules involved in the salt stress response. Meanwhile, the degradome data predicted additional miRNA-target pairs (Figure 5; Supplementary Figure S5), which require further verification of their function in eelgrass.

Several microRNAs, including miR160 (Tang et al., 2022), miR164 (Lu et al., 2017), miR167 (Ye et al., 2020), miR172 (Cheng et al., 2021), miR319 (Zhou et al., 2013), miR390 (Chu et al., 2022), miR393 (Denver and Ullah, 2019), miR396 (Pegler et al., 2021), miR398 (He et al., 2021), miR399 (Pegler et al., 2020), and miR528 (Wang et al., 2021), have been reported to respond to salt stress or contribute to salt tolerance in various plant species. Although these miRNAs were identified in eelgrass, their expression levels did not exhibit significant differences under salt stress. However, some target genes of these miRNAs are responsive to salt stress (Supplementary Data S7), such as *Zosma01g26740*, a predictive target gene for miR167, and *Zosma03g30130*, a predictive target gene for miR319. *Zosma01g26740* belongs to the *ARF* family and shows significantly reduced transcription levels under salt stress. *ARF8* (*AT5G37020*), which is homologous to *Zosma01g26740*, has been reported to be regulated by miR167 and involved in root development (Gutierrez et al., 2009; Liao et al., 2023). Similarly, *Zosma03g30130*, a member of MYB family, exhibits down-regulated transcription levels under salt stress. *MYB33* (*AT5G06100*), which is homologous to *Zosma03g30130*, is reported to be regulated by miR319 and specifically down-regulated in roots treated with ethylene, thereby influencing root growth (Zhang et al., 2016). The interaction between these prediction targets and miRNAs is worthy of further exploration in eelgrass.

## 4.7 Essential roles of TFs in the response to salt stress

The results revealed that 81% of salt-responsive TFs were distributed in eight modules: M1, M2, M3, M4, M5, M6, M7, and M9. A homologous analysis of these TFs indicated that several homologous genes from the bHLH, ERF, and MYB families in rice and maize exhibited similar expression patterns under high salt stress (Supplementary Figure S14). For instance, the bHLH family member *Zosma03g02210*, *Os04g0300600*, *Os04g0301500*, and *Zm00001eb086370* are grouped in a branch. Similarly, ERF family members *Zosma03g37150* and *Os06g0166400* are found in the same branch, while ERF family members *Zosma02g05080* and *Os12g0168100* are collinear genes in one branch. Additionally, MYB family members *Zosma06g17610*, *Zosma06g17660*, *Os03g0720800*, *Os11g0207600*, and *Zm00001eb168720* are grouped together in a branch. The consistent up-regulation of these genes suggests that they may function as conserved TFs involved in response to high salinity.

We focused on TFs that potentially regulate enriched biological processes and pathways, including GO:0009414 (response to water deprivation), map04016 (MAPK signaling pathway - plant), map00940 (phenylpropanoid biosynthesis), and map01110 (biosynthesis of secondary metabolites). To evaluate the expression correlation between DEGs, we calculated the Pearson correlation coefficient, considering values of ≥0.8 as indicative of similarity. The results revealed the potential regulatory roles of several TFs (Supplementary Figure S15). For instance, *Zosma04g22590* (NCED) and *Zosma02g25150* (arogenate/prephenate dehydratase) may be targeted by the ERF family member *Zosma05g04820*. *Zosma03g22300* (phenylalanine ammonia-lyase) may be regulated by MYB family members *Zosma06g17610* and *Zosma06g17660*. Furthermore, numerous potential binding sites for TFs are located in the upstream regions of microRNAs that respond to salt stress (Supplementary Figure S4). Further research is needed to determine whether these TFs can effectively regulate microRNA expression.

### 4.8 Summary

In this study, we performed a comprehensive analysis to reveal the response of eelgrass to high salt using transcriptome and degradome, and compared the result with other transcriptomes obtained from NCBI. In total, 14 DEmiRNAs and 691 DEGs including 53 TFs were identified. We further predicted the interactions between TFs, miRNAs, and their potential target genes. For instance, the up-regulated ERF members in the leaf may function by regulating the ABA synthase NCED, while MYB members might affect secondary metabolism by regulating PAL. Additionally, miRNA156-WRKY and miRNA166-HD-ZIP are supposed to be regulatory modules influencing the response on the post-transcriptional level.

Through the identification of homologous genes and expression profiling, we obtained a series of conserved responsive genes in eelgrass and two terrestrial plants rice and maize. The osmotic response related to the go-term "response to water deprivation" seems to be conserved in three species. Besides, we identified other conserved responses between rice and maize (Supplementary Figure S16), which suggest potential differences between terrestrial plants and marine plants in response to salt stress, such as the "gibberellin biosynthetic process". Moreover, eelgrass exhibits specific responses to high salinity, as evidenced by the enriched go-terms such as fucose biosynthesis and vacuolar protein processing. These findings enhance our understanding of the molecular-level adaptability of seagrass to marine environments. In the future, we aim to validate the functions of these genes and their homologs in model organisms through experiments such as constructing overexpression plants. The conserved and specific responsive genes can serve as potential genetic resources for improving the salt tolerance of crops.

## Data availability statement

The RNA-seq, small RNA-seq and degradome data used in this study has been deposited into CNCB database (https://www.cncb.ac.cn/) with the accession number of CRA020957 (BioProject: PRJCA031998). The other datasets for detailed analysis were provided in supporting information files.

## Ethics statement

All methods were performed in accordance with the relevant Chinese national guidelines. All experimental studies on plants complied with relevant institutional, national, and international guidelines and legislation.

## Author contributions

HZ: Writing – original draft, Writing – review & editing, Funding acquisition. CL: Writing – original draft, Writing – review & editing, Funding acquisition. XD: Writing – original draft. DY: Writing – review & editing. QG: Writing – original draft. PL: Writing – original draft.

## Funding

The author(s) declare financial support was received for the research, authorship, and/or publication of this article. This work was mainly supported by the Fund of Educational Department of Liaoning Province (LJKQZ20222354, LJ212410158026, 2024JBYBZ003).

## Acknowledgments

We are very grateful to Professor Peidong Zhang's research group for providing the resources of eelgrass plants for this work.

## Conflict of interest

The authors declare that the research was conducted in the absence of any commercial or financial relationships that could be construed as a potential conflict of interest.

## Publisher's note



## Supplementary material

The Supplementary Material for this article can be found online at: https://www.frontiersin.org/articles/10.3389/fpls.2025.1497064/full#supplementary-material

## References

Aizaz, M., Lubna null Jan, R., Asaf, S., Bilal, S., Kim, K.-M., et al. (2024). Regulatory dynamics of plant hormones and transcription factors under salt stress. *Biology* 13, 673. doi: 10.3390/biology13090673

Aleman, F., Yazaki, J., Lee, M., Takahashi, Y., Kim, A. Y., Li, Z., et al. (2016). An ABA-increased interaction of the PYL6 ABA receptor with MYC2 Transcription

Factor: A putative link of ABA and JA signaling. *Sci. Rep.* 6, 28941. doi: 10.1038/srep28941

Ali, A., Petrov, V., Yun, D.-J., and Gechev, T. (2023). Revisiting plant salt tolerance: novel components of the SOS pathway. *Trends Plant Sci.* 28, 1060–1069. doi: 10.1016/j.tplants.2023.04.003

Altmann, M., Altmann, S., Rodriguez, P. A., Weller, B., Elorduy Vergara, L., Palme, J., et al. (2020). Extensive signal integration by the phytohormone protein network. *Nature* 583, 271–276. doi: 10.1038/s41586-020-2460-0

Arshad, M., Gruber, M. Y., Wall, K., and Hannoufa, A. (2017). An Insight into microRNA156 Role in Salinity Stress Responses of Alfalfa. *Front. Plant Sci.* 8, 356. doi: 10.3389/fpls.2017.00356

Bai, Q., Wang, X., Chen, X., Shi, G., Liu, Z., Guo, C., et al. (2018). Wheat miRNA TaemiR408 Acts as an Essential Mediator in Plant Tolerance to Pi Deprivation and Salt Stress via Modulating Stress-Associated Physiological Processes. *Front. Plant Sci.* 9, 499. doi: 10.3389/fpls.2018.00499

Barajas-Lopez, J. D., Tiwari, A., Zarza, X., Shaw, M. W., Pascual, J. S., Punkkinen, M., et al. (2021). EARLY RESPONSE TO DEHYDRATION 7 remodels cell membrane lipid composition during cold stress in arabidopsis. *Plant Cell Physiol.* 62, 80–91. doi: 10.1093/pcp/pcaa139

Barrera-Rojas, C. H., Vicente, M. H., Pinheiro Brito, D. A., Silva, E. M., Lopez, A. M., Ferigolo, L. F., et al. (2023). Tomato miR156-targeted SlSBP15 represses shoot branching by modulating hormone dynamics and interacting with GOBLET and BRANCHED1b. *J. Exp. Bot.* 74, 5124–5139. doi: 10.1093/jxb/erad238

Bascom, C. (2023). Hormone synergy: Auxin and jasmonate boost abscisic acid signaling via ARF10 and ARF16. *Plant Cell* 35, 971–972. doi: 10.1093/plcell/koad012

Begum, Y. (2022). Regulatory role of microRNAs (miRNAs) in the recent development of abiotic stress tolerance of plants. *Gene* 821, 146283. doi: 10.1016/j.gene.2022.146283

Bhaskara, G. B., Nguyen, T. T., and Verslues, P. E. (2012). Unique drought resistance functions of the highly ABA-induced clade A protein phosphatase 2Cs. *Plant Physiol.* 160, 379–395. doi: 10.1104/pp.112.202408

Brock, A. K., Willmann, R., Kolb, D., Grefen, L., Lajunen, H. M., Bethke, G., et al. (2010). The Arabidopsis mitogen-activated protein kinase phosphatase PP2C5 affects seed germination, stomatal aperture, and abscisic acid-inducible gene expression. *Plant Physiol.* 153, 1098–1111. doi: 10.1104/pp.110.156109

Cambridge, M. L., Zavala-Perez, A., Cawthray, G. R., Statton, J., Mondon, J., and Kendrick, G. A. (2019). Effects of desalination brine and seawater with the same elevated salinity on growth, physiology and seedling development of the seagrass *Posidonia australis*. *Mar. pollut. Bull.* 140, 462–471. doi: 10.1016/j.marpolbul.2019.02.001

Capel, J., Jarillo, J. A., Salinas, J., and Martínez-Zapater, J. M. (1997). Two homologous low-temperature-inducible genes from *Arabidopsis* encode highly hydrophobic proteins. *Plant Physiol.* 115, 569–576. doi: 10.1104/pp.115.2.569

Chen, Q., Liu, R., Wu, Y., Wei, S., Wang, Q., Zheng, Y., et al. (2021). ERAD-related E2 and E3 enzymes modulate the drought response by regulating the stability of PIP2 aquaporins. *Plant Cell* 33, 2883–2898. doi: 10.1093/plcell/koab141

Chen, S., Xu, K., Kong, D., Wu, L., Chen, Q., Ma, X., et al. (2022). Ubiquitin ligase OsRINGzf1 regulates drought resistance by controlling the turnover of OsPIP2;1. *Plant Biotechnol. J.* 20, 1743–1755. doi: 10.1111/pbi.13857

Chen, H. C., Huang, S.-C., Chen, Y.-F., Kuo, C.-W., Chen, Y.-H., and Chang, M.-C. (2023). Overexpression of OsERF106MZ promotes parental root growth in rice seedlings by relieving the ABA-mediated inhibition of root growth under salinity stress conditions. *BMC Plant Biol.* 23, 144. doi: 10.1186/s12870-023-04136-8

Cheng, X., He, Q., Tang, S., Wang, H., Zhang, X., Lv, M., et al. (2021). The miR172/IDS1 signaling module confers salt tolerance through maintaining ROS homeostasis in cereal crops. *New Phytol.* 230, 1017–1033. doi: 10.1111/nph.17211

Cho, M., Lee, S. H., and Cho, H.-T. (2007). P-glycoprotein4 displays auxin efflux transporter-like action in *Arabidopsis* root hair cells and tobacco cells. *Plant Cell* 19, 3930–3943. doi: 10.1105/tpc.107.054288

Chu, Y., Bai, W., Wang, P., Li, F., Zhan, J., and Ge, X. (2022). The mir390-GhCEPR2 module confers salt tolerance in cotton and *Arabidopsis*. *Ind. Crops Prod.* 190, 115865. doi: 10.1016/j.indcrop.2022.115865

Cui, M. H., Yoo, K. S., Hyoung, S., Nguyen, H. T. K., Kim, Y. Y., Kim, H. J., et al. (2013). An Arabidopsis R2R3-MYB transcription factor, AtMYB20, negatively regulates type 2C serine/threonine protein phosphatases to enhance salt tolerance. *FEBS Lett.* 587, 1773–1778. doi: 10.1016/j.febslet.2013.04.028

Dabravolski, S. A., and Isayenkov, S. V. (2023). The regulation of plant cell wall organisation under salt stress. *Front. Plant Sci.* 14. doi: 10.3389/fpls.2023.1118313

Das, K., and Roychoudhury, A. (2014). Reactive oxygen species (ROS) and response of antioxidants as ROS-scavengers during environmental stress in plants. *Front. Environ. Sci.* 2. doi: 10.3389/fenvs.2014.00053

Denver, J. B., and Ullah, H. (2019). miR393s regulate salt stress response pathway in *Arabidopsis thaliana* through scaffold protein RACK1A mediated ABA signaling pathways. *Plant Signaling Behav.* 14, 1600394. doi: 10.1080/15592324.2019.1600394

Emery, L., Whelan, S., Hirschi, K. D., and Pittman, J. K. (2012). Protein Phylogenetic Analysis of Ca(2+)/cation Antiporters and Insights into their Evolution in Plants. *Front. Plant Sci.* 3. doi: 10.3389/fpls.2012.00001

Ferreira e Silva, G. F., Silva, E. M., Azevedo da, M. S., Guivin, M. A. C., Ramiro, D. A., Figueiredo, C. R., et al. (2014). microRNA156-targeted SPL/SBP box transcription factors regulate tomato ovary and fruit development. *Plant Journal: For Cell Mol. Biol.* 78, 604–618. doi: 10.1111/tpj.12493

Fu, H., and Yang, Y. (2023). How plants tolerate salt stress. *Curr. Issues Mol. Biol.* 45, 5914–5934. doi: 10.3390/cimb45070374

Gao, X., Cong, Y., Yue, J., Xing, Z., Wang, Y., and Chai, X. (2019). Small RNA, transcriptome, and degradome sequencing to identify salinity stress responsive miRNAs and target genes in *Dunaliella salina*. *J. Appl. Phycol.* 31, 1175–1183. doi: 10.1007/s10811-018-1612-1

Gou, J.-Y., Felippes, F. F., Liu, C.-J., Weigel, D., and Wang, J.-W. (2011). Negative regulation of anthocyanin biosynthesis in *Arabidopsis* by a miR156-targeted SPL transcription factor. *Plant Cell* 23, 1512–1522. doi: 10.1105/tpc.111.084525

Guo, H. S., Xie, Q., Fei, J.-F., and Chua, N.-H. (2005). MicroRNA directs mRNA cleavage of the transcription factor NAC1 to downregulate auxin signals for arabidopsis lateral root development. *Plant Cell* 17, 1376–1386. doi: 10.1105/tpc.105.030841

Gutierrez, L., Bussell, J. D., Pacurar, D. I., Schwambach, J., Pacurar, M., and Bellini, C. (2009). Phenotypic plasticity of adventitious rooting in *Arabidopsis* is controlled by complex regulation of AUXIN RESPONSE FACTOR transcripts and microRNA abundance. *Plant Cell* 21, 3119–3132. doi: 10.1105/tpc.108.064758

Hasanuzzaman, M., Raihan, M. R. H., Masud, A. A. C., Rahman, K., Nowroz, F., Rahman, M., et al. (2021). Regulation of reactive oxygen species and antioxidant defense in plants under salinity. *Int. J. Mol. Sci.* 22, 9326. doi: 10.3390/ijms22179326

He, Y., Zhou, J., Hu, Y., Fang, C., Yu, Y., Yang, J., et al. (2021). Overexpression of sly-miR398b increased salt sensitivity likely via regulating antioxidant system and photosynthesis in tomato. *Environ. Exp. Bot.* 181, 104273. doi: 10.1016/j.envexpbot.2020.104273

Hedrich, R., and Shabala, S. (2018). Stomata in a saline world. *Curr. Opin. Plant Biol.* 46, 87–95. doi: 10.1016/j.pbi.2018.07.015

Hernández-Sánchez, I. E., Maruri-López, I., Molphe-Balch, E. P., Becerra-Flora, A., Jaimes-Miranda, F., and Jiménez-Bremont, J. F. (2019). Evidence for *in vivo* interactions between dehydrins and the aquaporin AtPIP2B. *Biochem. Biophys. Res. Commun.* 510, 545–550. doi: 10.1016/j.bbrc.2019.01.095

Hu, Z., Nie, Z., Yan, C., Huang, H., Ma, X., Wang, Y., et al. (2021). Transcriptome and Degradome Profiling Reveals a Role of miR530 in the Circadian Regulation of Gene Expression in Kalanchoë marnieriana. *Cells* 10, 1526. doi: 10.3390/cells10061526

Ishida, K., Yamashino, T., and Mizuno, T. (2008). Expression of the cytokinin-induced type-A response regulator gene ARR9 is regulated by the circadian clock in *Arabidopsis thaliana*. *Biosci. Biotechnol. Biochem.* 72, 3025–3029. doi: 10.1271/bbb.80402

Ishikawa, F., Suga, S., Uemura, T., Sato, M. H., and Maeshima, M. (2005). Novel type aquaporin SIPs are mainly localized to the ER membrane and show cell-specific expression in *Arabidopsis thaliana*. *FEBS Lett.* 579, 5814–5820. doi: 10.1016/j.febslet.2005.09.076

Iuchi, S., Kobayashi, M., Taji, T., Naramoto, M., Seki, M., Kato, T., et al. (2001). Regulation of drought tolerance by gene manipulation of 9-cis-epoxycarotenoid dioxygenase, a key enzyme in abscisic acid biosynthesis in *Arabidopsis*. *Plant Journal: For Cell Mol. Biol.* 27, 325–333. doi: 10.1046/j.1365-313x.2001.01096.x

Jia, F., Qi, S., Li, H., Liu, P., Li, P., Wu, C., et al. (2014). Overexpression of Late Embryogenesis Abundant 14 enhances *Arabidopsis* salt stress tolerance. *Biochem. Biophys. Res. Commun.* 454, 505–511. doi: 10.1016/j.bbrc.2014.10.136

Jiang, Y., and Deyholos, M. K. (2009). Functional characterization of Arabidopsis NaCl-inducible WRKY25 and WRKY33 transcription factors in abiotic stresses. *Plant Mol. Biol.* 69, 91–105. doi: 10.1007/s11103-008-9408-3

Kamiya, T., and Fujiwara, T. (2009). NIP1;1, an aquaporin homolog, determines the arsenite sensitivity of *Arabidopsis thaliana*. *J. Biol. Chem.* 284, 2114–2120. doi: 10.1074/jbc.M806881200

Kamiya, T., and Fujiwara, T. (2009). Arabidopsis NIP1;1 transports antimonite and determines antimonite sensitivity. *Plant Cell Physiol.* 50, 1977–1981. doi: 10.1093/pcp/pcp130

Kang, C., He, S., Zhai, H., Li, R., Zhao, N., and Liu, Q. (2018). A sweetpotato auxin response factor gene (IbARF5) is involved in carotenoid biosynthesis and salt and drought tolerance in transgenic *arabidopsis*. *Front. Plant Sci.* 9. doi: 10.3389/fpls.2018.01307

Kang, T., Yu, C.-Y., Liu, Y., Song, W.-M., Bao, Y., Guo, X.-T., et al. (2019). Subtly manipulated expression of zmmiR156 in tobacco improves drought and salt tolerance without changing the architecture of transgenic plants. *Front. Plant Sci.* 10. doi: 10.3389/fpls.2019.01664

Kim, J., Jung, J.-H., Reyes, J. L., Kim, Y.-S., Kim, S.-Y., Chung, K.-S., et al. (2005). microRNA-directed cleavage of ATHB15 mRNA regulates vascular development in *Arabidopsis* inflorescence stems. *Plant Journal: For Cell Mol. Biol.* 42, 84–94. doi: 10.1111/j.1365-313X.2005.02354.x

Kitazumi, A., Kawahara, Y., Onda, T. S., De Koeyer, D., and de los Reyes, B. G. (2015). Implications of miR166 and miR159 induction to the basal response mechanisms of an andigena potato (*Solanum tuberosum* subsp. andigena) to salinity stress, predicted from network models in *Arabidopsis*. *Genome* 58, 13–24. doi: 10.1139/gen-2015-0011

Koch, M. S., Schopmeyer, S. A., Holmer, M., Madden, C. J., and Kyhn-Hansen, C. (2007). Thalassia testudinum response to the interactive stressors hypersalinity, sulfide and hypoxia. *Aquat. Bot.* 87, 104–110. doi: 10.1016/j.aquabot.2007.03.004

Koh, E. J., Kwon, Y.-R., Kim, K.-I., Hong, S.-W., and Lee, H. (2009). Altered ARA2 (RABA1a) expression in *Arabidopsis* reveals the involvement of a Rab/YPT family member in auxin-mediated responses. *Plant Mol. Biol.* 70, 113–122. doi: 10.1007/s11103-009-9460-7

Komatsu, K. (2020). Decoding ABA and osmostress signalling in plants from an evolutionary point of view. *Plant Cell Environ.* 43, 2894–2911. doi: 10.1111/pce.13869

Koyama, T. (2017). Roles of miR319 and TCP transcription factors in leaf development. *Plant Physiol.* 175, 874–885. doi: 10.1104/pp.17.00732

Lei, X., Chen, M., Xu, K., Sun, R., Zhao, S., and Wu, N. (2023). The miR166d/TaCPK7-D Signaling Module is a Critical Mediator of Wheat (*Triticum aestivum* L.) Tolerance to K+ Deficiency. *Int. J. Mol. Sci.* 24, 7926. doi: 10.3390/ijms24097926

Li, Y., Kurepa, J., and Smalle, J. (2013). AXR1 promotes the *Arabidopsis* cytokinin response by facilitating ARR5 proteolysis. *Plant Journal: For Cell Mol. Biol.* 74, 13–24. doi: 10.1111/tpj.12098

Li, Q., Yu, H.-M., Meng, X.-F., Lin, J.-S., Li, Y.-J., and Hou, B.-K. (2018). Ectopic expression of glycosyltransferase UGT76E11 increases flavonoid accumulation and enhances abiotic stress tolerance in *Arabidopsis*. *Plant Biol. (Stuttgart Germany)* 20, 10–19. doi: 10.1111/plb.12627

Liang, G., He, H., Li, Y., Wang, F., and Yu, D. (2014). Molecular mechanism of microRNA396 mediating pistil development in *Arabidopsis*. *Plant Physiol.* 164, 249–258. doi: 10.1104/pp.113.225144

Liao, R., Wei, X., Zhao, Y., Xie, Z., Nath, U. K., Yang, S., et al. (2023). bra-miR167a Targets ARF8 and Negatively Regulates *Arabidopsis thaliana* Immunity against *Plasmodiophora brassicae*. *Int. J. Mol. Sci.* 24, 11850. doi: 10.3390/ijms241411850

Liu, J., Wang, H., Su, M., Li, Q., Xu, H., Song, J., et al. (2023). A Transcription Factor SlNAC4 Gene of Suaeda liaotungensis Enhances Salt and Drought Tolerance through Regulating ABA Synthesis. *Plants (Basel)* 12, 2951. doi: 10.3390/plants12162951

Liu, R., Meng, J.-H., Zuo, W.-T., Jin, W.-M., Wang, L.-Q., and Sun, T.-T. (2024). The phloem protein 2 (PP2) is positively regulated by ThNAC13 that enhances salt tolerance of *Tamarix*. *Environ. Exp. Bot.* 224, 105784. doi: 10.1016/j.envexpbot.2024.105784

Liu, Z., Wang, P., Wang, Z., Wang, C., and Wang, Y. (2024). Birch WRKY transcription factor, BpWRKY32, confers salt tolerance by mediating stomatal closing, proline accumulation, and reactive oxygen species scavenging. *Plant Physiol. biochem.: PPB* 210, 108599. doi: 10.1016/j.plaphy.2024.108599

López-Cruz, J., Finiti, I., Fernández-Crespo, E., Crespo-Salvador, O., García-Agustín, P., and González-Bosch, C. (2014). Absence of endo-1,4-β-glucanase KOR1 alters the jasmonate-dependent defence response to *Pseudomonas syringae* in *Arabidopsis*. *J. Plant Physiol.* 171, 1524–1532. doi: 10.1016/j.jplph.2014.07.006

Lu, X., Dun, H., Lian, C., Zhang, X., Yin, W., and Xia, X. (2017). The role of peu-miR164 and its target PeNAC genes in response to abiotic stress in *Populus euphratica*. *Plant Physiol. biochem.: PPB* 115, 418–438. doi: 10.1016/j.plaphy.2017.04.009

Ma, X., Olsen, J. L., Reusch, T. B.H., Procaccini, G., Kudrna, D., Williams, M., et al. (2021). Improved chromosome-level genome assembly and annotation of the seagrass, *Zostera marina* (eelgrass). *F1000Research* 10, 289. doi: 10.12688/f1000research.38156.1

Ma, Y., Xue, H., Zhang, F., Jiang, Q., Yang, S., Yue, P., et al. (2021). The miR156/SPL module regulates apple salt stress tolerance by activating MdWRKY100 expression. *Plant Biotechnol. J.* 19, 311–323. doi: 10.1111/pbi.13464

Malakar,, and Chattopadhyay, D. (2021). Adaptation of plants to salt stress: the role of the ion transporters. *J. Plant Biochem. Biotechnol.* 30, 668–683. doi: 10.1007/s13562-021-00741-6

Matsuoka, D., Yasufuku, T., Furuya, T., and Nanmori, T. (2015). An abscisic acid inducible Arabidopsis MAPKKK, MAPKKK18 regulates leaf senescence via its kinase activity. *Plant Mol. Biol.* 87, 565–575. doi: 10.1007/s11103-015-0295-0

Mi, S., Cai, T., Hu, Y., Chen, Y., Hodges, E., Ni, F., et al. (2008). Sorting of small RNAs into *Arabidopsis* argonaute complexes is directed by the 5' terminal nucleotide. *Cell* 133, 116–127. doi: 10.1016/j.cell.2008.02.034

Nishiyama, R., Watanabe, Y., Leyva-Gonzalez, M. A., Ha, C. V., Fujita, Y., Tanaka, M., et al. (2013). *Arabidopsis* AHP2, AHP3, and AHP5 histidine phosphotransfer proteins function as redundant negative regulators of drought stress response. *Proc. Natl. Acad. Sci. United States America* 110, 4840–4845. doi: 10.1073/pnas.1302265110

Olsen, K. M., Lea, U. S., Slimestad, R., Verheul, M., and Lillo, C. (2008). Differential expression of four *Arabidopsis* PAL genes; PAL1 and PAL2 have functional specialization in abiotic environmental-triggered flavonoid synthesis. *J. Plant Physiol.* 165, 1491–1499. doi: 10.1016/j.jplph.2007.11.005

Olsen, J. L., Rouzé, P., Verhelst, B., Lin, Y.-C., Bayer, T., Collen, J., et al. (2016). The genome of the seagrass *Zostera marina* reveals angiosperm adaptation to the sea. *Nature* 530, 331–335. doi: 10.1038/nature16548

Pegler, J. L., Oultram, J. M. J., Grof, C. P. L., and Eamens, A. L. (2020). Molecular Manipulation of the miR399/PHO2 Expression Module Alters the Salt Stress Response of *Arabidopsis thaliana*. *Plants (Basel Switzerland)* 10, 73. doi: 10.3390/plants10010073

Pegler, J. L., Nguyen, D. Q., Oultram, J. M. J., Grof, C. P. L., and Eamens, A. L. (2021). Molecular manipulation of the miR396/GRF expression module alters the salt stress response of *arabidopsis thaliana*. *Agronomy* 11, 1751. doi: 10.3390/agronomy11091751

Polizel, A. M., Medri, M. E., Nakashima, K., Yamanaka, N., Farias, J. R. B., De Oliveira, M. C. N., et al. (2011). Molecular, anatomical and physiological properties of a genetically modified soybean line transformed with rd29A:AtDREB1A for the improvement of drought tolerance. *Genet. Mol. Res.* 10, 3641–3656. doi: 10.4238/2011.October.21.4

Poppenberger, B., Fujioka, S., Soeno, K., George, G. L., Vaistij, F. E., Hiranuma, S., et al. (2005). The UGT73C5 of *Arabidopsis thaliana* glucosylates brassinosteroids. *Proc. Natl. Acad. Sci. United States America* 102, 15253–15258. doi: 10.1073/pnas.0504279102

Postaire, O., Tournaire-Roux, C., Grondin, A., Boursiac, Y., Morillon, R., Schäffner, A. R., et al. (2010). A PIP1 aquaporin contributes to hydrostatic pressure-induced water transport in both the root and rosette of *Arabidopsis*. *Plant Physiol.* 152, 1418–1430. doi: 10.1104/pp.109.145326

Qin, X., and Zeevaart, J. A. (1999). The 9-cis-epoxycarotenoid cleavage reaction is the key regulatory step of abscisic acid biosynthesis in water-stressed bean. *Proc. Natl. Acad. Sci. United States America* 96, 15354–15361. doi: 10.1073/pnas.96.26.15354

Ravikumar, G., Manimaran, P., Voleti, S. R., Subrahmanyam, D., Sundaram, R. M., Bansal, K. C., et al. (2014). Stress-inducible expression of AtDREB1A transcription factor greatly improves drought stress tolerance in transgenic indica rice. *Transgenic Res.* 23, 421–439. doi: 10.1007/s11248-013-9776-6

Reinhardt, H., Hachez, C., Bienert, M. D., Beebo, A., Swarup, K., Voß, U., et al. (2016). Tonoplast aquaporins facilitate lateral root emergence. *Plant Physiol.* 170, 1640–1654. doi: 10.1104/pp.15.01635

Ren, J., Yang, X., Ma, C., Wang, Y., Zhao, J., and Kang, L. (2021). Meta-analysis of the effect of the overexpression of aquaporin family genes on the drought stress response. *Plant Biotechnol. Rep.* 15, 139–150. doi: 10.1007/s11816-021-00666-5

Rodrigues, O., Reshetnyak, G., Grondin, A., Saijo, Y., Leonhardt, N., Maurel, C., et al. (2017). Aquaporins facilitate hydrogen peroxide entry into guard cells to mediate ABA- and pathogen-triggered stomatal closure. *Proc. Natl. Acad. Sci. United States America* 114, 9200–9205. doi: 10.1073/pnas.1704754114

Rubio, L., Belver, A., Venema, K., Jesús García-Sánchez, M., and Fernández, J. A. (2011). Evidence for a sodium efflux mechanism in the leaf cells of the seagrass *Zostera marina* L. *J. Exp. Mar. Biol. Ecol.* 402, 56–64. doi: 10.1016/j.jembe.2011.03.016

Sakuma, Y., Liu, Q., Dubouzet, J. G., Abe, H., Shinozaki, K., and Yamaguchi-Shinozaki, K. (2002). DNA-binding specificity of the ERF/AP2 domain of *Arabidopsis* DREBs, transcription factors involved in dehydration- and cold-inducible gene expression. *Biochem. Biophys. Res. Commun.* 290, 998–1009. doi: 10.1006/bbrc.2001.6299

Salam, U., Ullah, S., Tang, Z.-H., Elateeq, A. A., Khan, Y., Khan, J., et al. (2023). Plant metabolomics: an overview of the role of primary and secondary metabolites against different environmental stress factors. *Life (Basel Switzerland)* 13, 706. doi: 10.3390/life13030706

Sandoval-Gil, J. M., Ruiz, J. M., and Marín-Guirao, L. (2023). Advances in understanding multilevel responses of seagrasses to hypersalinity. *Mar. Environ. Res.* 183, 105809. doi: 10.1016/j.marenvres.2022.105809

Schweighofer, A., Kazanaviciute, V., Scheikl, E., Teige, M., Doczi, R., Hirt, H., et al. (2007). The PP2C-type phosphatase AP2C1, which negatively regulates MPK4 and MPK6, modulates innate immunity, jasmonic acid, and ethylene levels in *Arabidopsis*. *Plant Cell* 19, 2213–2224. doi: 10.1105/tpc.106.049585

Seo, H. S., Song, J. T., Cheong, J. J., Lee, Y. H., Lee, Y. W., Hwang, I., et al. (2001). Jasmonic acid carboxyl methyltransferase: a key enzyme for jasmonate-regulated plant responses. *Proc. Natl. Acad. Sci. United States America* 98, 4788–4793. doi: 10.1073/pnas.081557298

Serra, I. A., Nicastro, S., Mazzuca, S., Natali, L., Cavallini, A., and Innocenti, A. M. (2013). Response to salt stress in seagrasses: PIP1;1 aquaporin antibody localization in *Posidonia oceanica* leaves. *Aquat. Bot.* 104, 213–219. doi: 10.1016/j.aquabot.2011.05.008

Shivaraj, S. M., Deshmukh, R., Bhat, J. A., Sonah, H., and Bélanger, R. R. (2017). Understanding aquaporin transport system in eelgrass (*Zostera marina* L.), an aquatic plant species. *Front. Plant Sci.* 8. doi: 10.3389/fpls.2017.01334

Shomali, A., Das, S., Arif, N., Sarraf, M., Zahra, N., Yadav, V., et al. (2022). Diverse physiological roles of flavonoids in plant environmental stress responses and tolerance. *Plants (Basel Switzerland)* 11, 3158. doi: 10.3390/plants11223158

Song, S., Liu, B., Zhai, J., Zhang, Y., Wang, K., and Qi, T. (2021). The intragenic suppressor mutation Leu59Phe compensates for the effect of detrimental mutations in the jasmonate receptor COI1. *Plant Journal: For Cell Mol. Biol.* 108, 690–704. doi: 10.1111/tpj.15464

Taj, G., Agarwal, P., Grant, M., and Kumar, A. (2010). MAPK machinery in plants: recognition and response to different stresses through multiple signal transduction pathways. *Plant Signaling Behav.* 5, 1370–1378. doi: 10.4161/psb.5.11.13020

Tang, Y., Du, G., Xiang, J., Hu, C., Li, X., Wang, W., et al. (2022). Genome-wide identification of auxin response factor (ARF) gene family and the miR160-ARF18-mediated response to salt stress in peanut (*Arachis hypogaea* L.). *Genomics* 114, 171–184. doi: 10.1016/j.ygeno.2021.12.015

Tian, S., Wang, X., Li, P., Wang, H., Ji, H., Xie, J., et al. (2016). Plant aquaporin atPIP1;4 links apoplastic $H_2O_2$ induction to disease immunity pathways. *Plant Physiol.* 171, 1635–1650. doi: 10.1104/pp.15.01237

Tomasello, A., Di Maida, G., Calvo, S., Pirrotta, M., Borra, M., and Procaccini, G. (2009). Seagrass meadows at the extreme of environmental tolerance: the case of

*Posidonia oceanica* in a semi-enclosed coastal lagoon. *Mar. Ecol.* 30, 288–300. doi: 10.1111/j.1439-0485.2009.00285.x

Valenzuela, C. E., Acevedo-Acevedo, O., Miranda, G. S., Vergara-Barros, P., Holuigue, L., Figueroa, C. R., et al. (2016). Salt stress response triggers activation of the jasmonate signaling pathway leading to inhibition of cell elongation in *Arabidopsis* primary root. *J. Exp. Bot.* 67, 4209–4220. doi: 10.1093/jxb/erw202

Verma, D., Jalmi, S. K., Bhagat, P. K., Verma, N., and Sinha, A. K. (2020). A bHLH transcription factor, MYC2, imparts salt intolerance by regulating proline biosynthesis in *Arabidopsis*. *FEBS J.* 287, 2560–2576. doi: 10.1111/febs.15157

Wang, J. W., Wang, L.-J., Mao, Y.-B., Cai, W.-J., Xue, H.-W., and Chen, X.-Y. (2005). Control of root cap formation by MicroRNA-targeted auxin response factors in *Arabidopsis*. *Plant Cell* 17, 2204–2216. doi: 10.1105/tpc.105.033076

Wang, P., Li, Z., Wei, J., Zhao, Z., Sun, D., and Cui, S. (2012). A Na+/Ca2+ exchanger-like protein (AtNCL) involved in salt stress in *Arabidopsis*. *J. Biol. Chem.* 287, 44062–44070. doi: 10.1074/jbc.M112.351643

Wang, Y., Li, R., Li, D., Jia, X., Zhou, D., Li, J., et al. (2017). NIP1;2 is a plasma membrane-localized transporter mediating aluminum uptake, translocation, and tolerance in *Arabidopsis*. *Proc. Natl. Acad. Sci. United States America* 114, 5047–5052. doi: 10.1073/pnas.1618557114

Wang, L., Liu, Z., Qiao, M., and Xiang, F. (2018). miR393 inhibits *in vitro* shoot regeneration in *Arabidopsis thaliana* via repressing TIR1. *Plant Sci.: Int. J. Exp. Plant Biol.* 266, 1–8. doi: 10.1016/j.plantsci.2017.10.009

Wang, H., Schoebel, S., Schmitz, F., Dong, H., and Hedfalk, K. (2020). Characterization of aquaporin-driven hydrogen peroxide transport. *Biochim. Et Biophys. Acta Biomembr.* 1862, 183065. doi: 10.1016/j.bbamem.2019.183065

Wang, M., Guo, W., Li, J., Pan, X., Pan, L., Zhao, J., et al. (2021). The miR528-AO module confers enhanced salt tolerance in rice by modulating the ascorbic acid and abscisic acid metabolism and ROS scavenging. *J. Agric. Food Chem.* 69, 8634–8648. doi: 10.1021/acs.jafc.1c01096

Wang, C., Li, X., Zhuang, Y., Sun, W., Cao, H., Xu, R., et al. (2024). A novel miR160a-GmARF16-GmMYC2 module determines soybean salt tolerance and adaptation. *New Phytol.* 241, 2176–2192. doi: 10.1111/nph.19503

Wang, S., Jiang, R., Feng, J., Zou, H., Han, X., Xie, X., et al. (2024). Overexpression of transcription factor FaMYB63 enhances salt tolerance by directly binding to the SOS1 promoter in *Arabidopsis thaliana*. *Plant Mol. Biol.* 114, 32. doi: 10.1007/s11103-024-01431-2

Wang, X., Wang, T., Yu, P., Li, Y., and Lv, X. (2024). NO enhances the adaptability to high-salt environments by regulating osmotic balance, antioxidant defense, and ion homeostasis in eelgrass based on transcriptome and metabolome analysis. *Front. Plant Sci.* 15, 1343154. doi: 10.3389/fpls.2024.1343154

Wissler, L., Codoñer, F. M., Gu, J., Reusch, T. B., Olsen, J. L., Procaccini, G., et al. (2011). Back to the sea twice: identifying candidate plant genes for molecular evolution to marine life. *BMC Evolution. Biol.* 11, 8. doi: 10.1186/1471-2148-11-8

Xu, Q., Niu, S., Zhang, P., Zhang, X., and Fang, C. (2015). Salinity suitability of Zostera marina seedlings. *Chinese Journal of Ecology* 34(11), 3146–3150. doi: 10.13292/j.1000-4890.20151023.013

Yadav, A., Kumar, S., Verma, R., Lata, C., Sanyal, I., and Rai, S. P. (2021). microRNA 166: an evolutionarily conserved stress biomarker in land plants targeting HD-ZIP family. *Physiol. Mol. Biol. Plants* 27, 2471–2485. doi: 10.1007/s12298-021-01096-x

Yang, Y., and Guo, Y. (2018). Elucidating the molecular mechanisms mediating plant salt-stress responses. *New Phytol.* 217, 523–539. doi: 10.1111/nph.14920

Ye, Y., Wang, J., Wang, W., and Xu, L.-A. (2020). ARF family identification in Tamarix chinensis reveals the salt responsive expression of TcARF6 targeted by miR167. *PeerJ* 8, e8829. doi: 10.7717/peerj.8829

Yepes-Molina, L., Bárzana, G., and Carvajal, M. (2020). Controversial regulation of gene expression and protein transduction of aquaporins under drought and salinity stress. *Plants (Basel Switzerland)* 9, 1662. doi: 10.3390/plants9121662

Yoon, Y., Seo, D. H., Shin, H., Kim, H. J., Kim, C. M., and Jang, G. (2020). The role of stress-responsive transcription factors in modulating abiotic stress tolerance in plants. *Agronomy* 10, 788. doi: 10.3390/agronomy10060788

Yu, Z., Duan, X., Luo, L., Dai, S., Ding, Z., and Xia, G. (2020). How plant hormones mediate salt stress responses. *Trends Plant Sci.* 25, 1117–1130. doi: 10.1016/j.tplants.2020.06.008

Zhang, F., Wang, L., Lim, J. Y., Kim, T., Pyo, Y., Sung, S., et al. (2016). Phosphorylation of CBP20 links microRNA to root growth in the ethylene response. *PloS Genet.* 12, e1006437. doi: 10.1371/journal.pgen.1006437

Zhang, M., Zhao, J., Li, L., Gao, Y., Zhao, L., Patil, S. B., et al. (2017). The *Arabidopsis* U-box E3 ubiquitin ligase PUB30 negatively regulates salt tolerance by facilitating BRI1 kinase inhibitor 1 (BKI1) degradation. *Plant Cell Environ.* 40, 2831–2843. doi: 10.1111/pce.13064

Zhang, Y.-H., Li, J.-D., Yan, W.-J., Luo, F.-S., Wang, L., Zuo, L.-M., et al. (2023). The combined effect of seawater salinity and duration on the survival and growth of eelgrass Zostera marina. *Aquatic Botany* 187. doi: 10.1016/j.aquabot.2023.103652

Zhang, Y., Yue, S., Liu, M., Wang, X., Xu, S., Zhang, X., et al. (2023). Combined transcriptome and proteome analysis reveal the key physiological processes in seed germination stimulated by decreased salinity in the seagrass *Zostera marina* L. *BMC Plant Biol.* 23, 605. doi: 10.1186/s12870-023-04616-x

Zhang, Z., Fu, Z., Chen, W., Wang, L., Zhao, S., Yuanyuan, E., et al. (2023). Salt Stress Induces Complicated miRNA Responses of Sugar Beet (*Beta vulgaris* L.). *Sugar Tech.* 26, 1297–1305. doi: 10.1007/s12355-023-01341-5

Zhang, M., Zhang, X., Wang, R., Zang, R., Guo, L., Qi, T., et al. (2023). Heat-responsive microRNAs participate in regulating the pollen fertility stability of CMS-D2 restorer line under high-temperature stress. *Biol Res* 56, 58. doi: 10.1186/s40659-023-00465-y

Zhao, Y., Dong, W., Zhang, N., Ai, X., Wang, M., Huang, Z., et al. (2014). A wheat allene oxide cyclase gene enhances salinity tolerance via jasmonate signaling. *Plant Physiol.* 164, 1068–1076. doi: 10.1104/pp.113.227595

Zhao, X., Wang, X., Li, F., Dahlgren, R. A., and Wang, H. (2016). Identification of microRNA-size sRNAs Related to Salt Tolerance in *Spirulina platensis*. *Plant Mol. Biol. Rep.* 34, 539–555. doi: 10.1007/s11105-015-0938-y

Zhao, C., Ma, J., Yan, C., Jiang, Y., Zhang, Y., Lu, Y., et al. (2024). Drought-triggered repression of miR166 promotes drought tolerance in soybean. *Crop J.* 12, 154–163. doi: 10.1016/j.cj.2023.12.005

Zhou, M., Li, D., Li, Z., Hu, Q., Yang, C., Zhu, L., et al. (2013). Constitutive expression of a miR319 gene alters plant development and enhances salt and drought tolerance in transgenic creeping bentgrass. *Plant Physiol.* 161, 1375–1391. doi: 10.1104/pp.112.208702

Zhou, B., Gao, X., and Zhao, F. (2023). Integration of mRNA and miRNA Analysis Reveals the Post-Transcriptional Regulation of Salt Stress Response in *Hemerocallis fulva*. *Int. J. Mol. Sci.* 24, 7290. doi: 10.3390/ijms24087290

Zhu, J., Wei, X., Yin, C., Zhou, H., Yan, J., He, W., et al. (2023). ZmEREB57 regulates OPDA synthesis and enhances salt stress tolerance through two distinct signalling pathways in *Zea mays*. *Plant Cell Environ.* 46, 2867–2883. doi: 10.1111/pce.14644

Zou, P., Lu, X., Zhao, H., Yuan, Y., Meng, L., Zhang, C., et al. (2019). Polysaccharides derived from the brown algae lessonia nigrescens enhance salt stress tolerance to wheat seedlings by enhancing the antioxidant system and modulating intracellular ion concentration. *Front. Plant Sci.* 10, 48. doi: 10.3389/fpls.2019.00048

# Frontiers in
# Plant Science

**Cultivates the science of plant biology and its applications**

The most cited plant science journal, which advances our understanding of plant biology for sustainable food security, functional ecosystems and human health.

---

## Discover the latest Research Topics

See more →

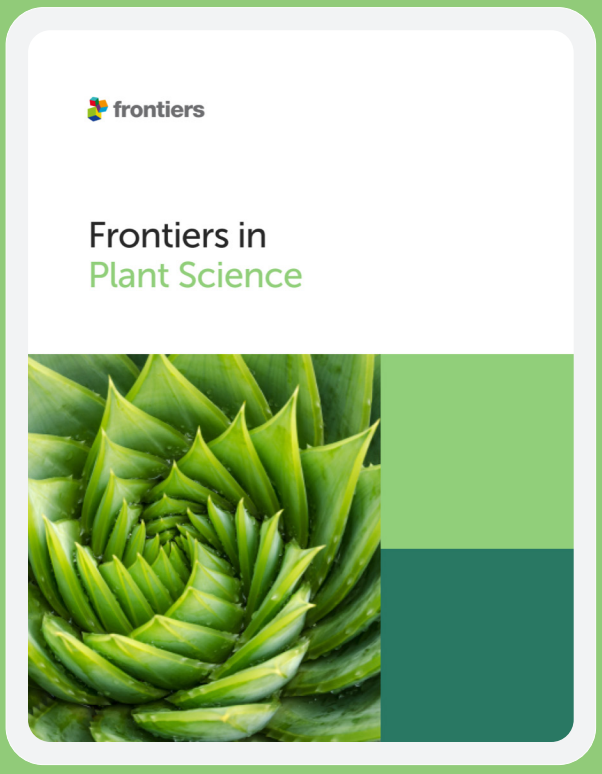


**Frontiers**

Avenue du Tribunal-Fédéral 34
1005 Lausanne, Switzerland
frontiersin.org

**Contact us**

+41 (0)21 510 17 00
frontiersin.org/about/contact